

AD A121909

AFWAL-TR-82-4075

ULTRASONIC TEST BED FOR QUANTITATIVE NDE



R.C. Addison  
Rockwell International Science Center  
1049 Camino Dos Rios  
Thousand Oaks, CA 91360

July 1982

FINAL REPORT FOR PERIOD 22 MAY 1978 - 31 MARCH 1981

Approved for Public Release; Distribution Unlimited

DTIC  
ELECTE  
NOV 26 1982  
S D  
E

Materials Laboratory  
AF Wright Aeronautical Laboratories  
Air Force Systems Command  
Wright-Patterson AFB, Ohio 45433

DTIC FILE COPY

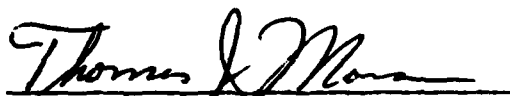
82 11 26 041

# NOTICE

When Government drawings, specifications, or other data are used for any purpose other than in connection with a definitely related Government procurement operation, the United States Government thereby incurs no responsibility nor any obligation whatsoever; and the fact that the government may have formulated, furnished, or in any way supplied the said drawings, specifications, or other data, is not to be regarded by implication or otherwise as in any manner licensing the holder or any other person or corporation, or conveying any rights or permission to manufacture use, or sell any patented invention that may in any way be related thereto.

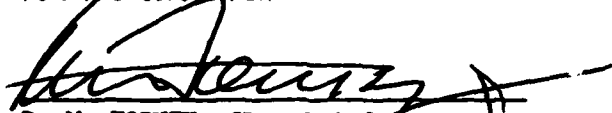
This report has been reviewed by the Office of Public Affairs (ASD/PA) and is releasable to the National Technical Information Service (NTIS). At NTIS, it will be available to the general public, including foreign nations.

This technical report has been reviewed and is approved for publication.



THOMAS J. MORAN  
Project Engineer  
Nondestructive Evaluation Branch  
Materials Laboratory

FOR THE COMMANDER



D. M. FORNEY, JR., Chief  
Nondestructive Evaluation Branch  
Metals and Ceramics Division  
Materials Laboratory

"If your address has changed, if you wish to be removed from our mailing list, or if the addressee is no longer employed by your organization please notify AFMIL/MLLP, W-PAPB, OH 45433 to help us maintain a current mailing list."

Copies of this report should not be returned unless return is required by security considerations, contractual obligations, or notice on a specific document.

UNCLASSIFIED

SECURITY CLASSIFICATION OF THIS PAGE (When Data Entered)

REPORT DOCUMENTATION PAGE		READ INSTRUCTIONS BEFORE COMPLETING FORM
1. REPORT NUMBER AFWAL-TR-82-4075	2. GOVT ACCESSION NO. <b>AD-A222 909</b>	3. RECIPIENT'S CATALOG NUMBER
4. TITLE (and Subtitle)  ULTRASONIC TEST BED FOR QUANTITATIVE NDE	5. TYPE OF REPORT & PERIOD COVERED Final Report for Period 22 May 78 - 31 Mar 81	
7. AUTHOR(s)  R.C. Addison	6. PERFORMING ORG. REPORT NUMBER SC5164.45FR	
9. PERFORMING ORGANIZATION NAME AND ADDRESS Rockwell International Science Center 1049 Camino Dos Rios Thousand Oaks, CA 91360	8. CONTRACT OR GRANT NUMBER(s)  F33615-78-C-5164	
11. CONTROLLING OFFICE NAME AND ADDRESS Materials Laboratory (AFWAL/MLLP) Air Force Wright Aeronautical Laboratories (AFSC) Wright-Patterson Air Force Base, Ohio 45433	10. PROGRAM ELEMENT, PROJECT, TASK AREA & WORK UNIT NUMBERS  3556/00/00	
12. REPORT DATE July 1982	13. NUMBER OF PAGES 213	
14. MONITORING AGENCY NAME & ADDRESS (if different from Controlling Office)	15. SECURITY CLASS. (of this report)  Unclassified	
16. DECLASSIFICATION/DOWNGRADING SCHEDULE		
17. DISTRIBUTION STATEMENT (of this Report)  Approved for Public Release; Distribution Unlimited		
18. DISTRIBUTION STATEMENT (of the abstract entered in Block 20, if different from Report)		
19. SUPPLEMENTARY NOTES		
20. KEY WORDS (Continue on reverse side if necessary and identify by block number)  Nondestructive evaluation, quantitative flaw evaluation, contour follow- ing system, ultrasonic array, simulated flaws, ultrasonic test bed.		
21. ABSTRACT (Continue on reverse side if necessary and identify by block number)  The primary objective of the Test Bed program was to bridge the gap between the fundamental studies and the application efforts relating to ultrasonic NDE. The program consisted of three phases. The first phase consisted of the system design, assembly and shakedown. This phase en- compassed the construction of the self contained unit comprising the physical Test Bed, as well as the fabrication of the ultrasonic phased array system. The second phase involved the reduction to practice of		

DD FORM 1 JAN 79 1473

EDITION OF 1 NOV 65 IS OBSOLETE

UNCLASSIFIED

SECURITY CLASSIFICATION OF THIS PAGE (When Data Entered)

UNCLASSIFIED

SECURITY CLASSIFICATION OF THIS PAGE(When Data Entered)

quantitative NDE techniques. The techniques that were implemented consisted of a subset of the defect classification and imaging techniques that were developed in the Interdisciplinary Program for Quantitative Flaw Definition. The third phase consisted of a detailed system evaluation on real and simulated problems.

The work with the quantitative inversion techniques demonstrated the feasibility of combining data obtained from low, medium and high frequency portions of the flaw spectrum to obtain an accurate estimate of the size, shape orientation and composition of the flaw. The Born Inversion technique for classification of defects was studied extensively. The effects on the accuracy of the Born Inversion due to signal-to-noise ratio, bandwidth, and geometry were all investigated. This work culminated in a successful demonstration with a naturally occurring flaw in a nickel based alloy supplied by Rolls-Royce Ltd.

The phased array system utilizes two, 32 element transducer arrays operating at 2.25 MHz. It features parallel processing of the 16 receiving channels, an array processor for "beam-forming", and mini-computer control of the system. A custom hybrid pulser/receiver was designed and fabricated specifically for this system. The system has been used for imaging known flaws in metal parts and for obtaining scattering data from these flaws.

The Test Bed program has addressed a wide range of topics that are important to a quantitative NDE program. It has successfully demonstrated that quantitative NDE techniques can be applied to naturally occurring flaws. It provides a sound technological base for the extension of these techniques to practical NDE applications. ←

UNCLASSIFIED

SECURITY CLASSIFICATION OF THIS PAGE(When Data Entered)



## PREFACE

This final Technical Report, covering the period from 22 May 1978 to 31 March 1981, was prepared by the Rockwell International Science Center under Air Force Contract F33615-78-C-5164. This program was sponsored by the Materials Sciences Office of Defense Advanced Research Projects Agency (DARPA) under ARPA order No. 3556. The DARPA Program Manager was Dr. M.J. Buckley. The work was administered under the technical direction of Dr. T.J. Moran of the Air Force Wright Aeronautical Laboratories/Materials Laboratory, Wright-Patterson Air Force Base, Ohio 45433.

The Program Manager was initially Dr. R.B. Thompson, Manager, Ultrasonic Applications Group. He was succeeded by Dr. R.C. Addison, Jr. who also served as Principal Investigator throughout the program. Other major contributors to the program were Dr. J.F. Martin, Dr. R.K. Elsley, R.B. Houston, C.C. Ruokangas, W.E. Peterson, J. Liska, H.E. Feathers and V. Nance.

<b>Accession For</b>	
NTIS GRA&I	<input checked="" type="checkbox"/>
DTIC TAB	<input type="checkbox"/>
Unannounced	<input type="checkbox"/>
Justification	
By	
Distribution/	
Availability Codes	
Dist	Avail and/or Special
A	



## TABLE OF CONTENTS

	<u>Page</u>
1.0 INTRODUCTION.....	1
1.1 Objective.....	1
1.2 Conceptual Design.....	2
1.3 Structure of Report.....	4
2.0 TEST BED SYSTEM.....	7
2.1 Overview.....	7
2.2 Scanning System.....	10
2.2.1 Hardware.....	10
2.2.2 Multiaxis Controller.....	11
2.3 Display Processor.....	19
2.4 Data Acquisition System.....	20
2.5 Minicomputer System.....	22
3.0 INSPECTION PROCEDURES.....	43
3.1 System Protocol.....	43
3.1.1 Search Mode.....	45
3.1.2 Detailed Examination Mode.....	45
3.2 Quantitative Flaw Sizing Techniques.....	48
3.2.1 Signal Preprocessing Techniques.....	49
3.2.2 Born Inversion.....	53
3.2.3 Testing of the Algorithm.....	56
3.2.4 Experimental Results.....	72
4.0 PHASED ARRAY SYSTEM.....	89
4.1 Concept and Purpose.....	89
4.2 Description of System.....	91
4.2.1 Transducers.....	96
4.2.2 Pulser/Receivers.....	97
4.2.3 Multiplexer.....	103
4.2.4 Signal Conditioning Circuitry.....	113
4.2.5 Array Digitizing Electronics.....	116
4.2.6 S/200 Software Utilized for Control of Array and AP400.....	121
4.2.7 Array Processor Control and Operation.....	129
4.2.8 Display of Data.....	132
4.2.9 Packaging of Array Subsystems.....	137

## TABLE OF CONTENTS

	<u>Page</u>
4.3 Operation of Phased Array System.....	139
4.3.1 Array Radiation Pattern Characteristics.....	139
4.3.2 Imaging of Flaws in Metals.....	143
4.3.3 Born Inversion of Array Data.....	145
5.0 SUMMARY.....	151
6.0 REFERENCES.....	157
APPENDIX A DIFFUSION BONDED SAMPLE DOCUMENTED.....	A-1
APPENDIX B DOCUMENTATION FOR PHASED ARRAY HARDWARE.....	B-1

## LIST OF FIGURES

<u>Figure</u>	<u>Page</u>
2.1 Photograph of Test Bed lab.....	8
2.2 Block diagram of test bed system.....	9
2.3 Block diagram of multiaxis controller with sample profile.....	12
2.4 Interpretation of data block command.....	14
2.5 Block diagram of data acquisition system.....	21
2.6 A schematic of the pattern of moves followed in an X-Y raster scan.....	24
2.7 User terminal display after operation of RASTER and RAST MAG. User inputs are delineated by boxes.....	25
2.8 User terminal display after operating PROFILE. User inputs are delineated by boxes.....	27
2.9 An example of a profile requiring contour moves. (a) Sketch of profile, (b) the resulting data blocks are shown.....	28
2.10 User terminal display during operation of PROPLOT. User inputs are delineated by boxes.....	29
2.11 Output display of PROPLOT showing part profile, transducer path and pivot point path.....	30
2.12 User terminal display during operation of TBCON. User inputs are delineated by boxes.....	32
2.13 A schematic of the refraction of the acoustic beam at the surface of the sample.....	36
2.14 User terminal display after operation of TBDISC. User inputs are delineated by boxes.....	39
2.15 Images resulting from the display of data taken in mode I of TBCON.....	41
3.1 Inspection protocol.....	44

## LIST OF FIGURES

<u>Figure</u>		<u>Page</u>
3.2	Preprocessing of acquired flaw signal.....	50
3.3	Illustration of one dimensional Born inversion.....	54
3.4	Experimental and simulated flaw waveforms including grain scattering noise.....	59
3.5	Radius estimates for ensembles of noisy flaw waveforms vs signal-to-noise ratio for a 200 $\mu\text{m}$ radius spherical void.....	60
3.6	Radius estimates for ensembles of noisy flaw waveforms vs signal-to-noise ratio for a 400 $\mu\text{m}$ radius spherical void.....	61
3.7	Radius estimates for ensembles of noisy flaw waveforms vs signal-to-noise ratio for a 600 $\mu\text{m}$ radius spherical void.....	62
3.8	Magnitude spectrum for a spherical void.....	64
3.9	Effect of limited bandwidth on the accuracy of the Born inversion.....	66
3.10	Normalized calibration curves for the Born inversion algorithm with different bandwidths and center frequencies.....	67
3.11	Calibration curves to be used when the flaw radius is not known.....	69
3.12	Born inversion estimates of flaw radii vs time shifts of the flaw response relative to its centroid.....	76
3.13	Transducer placement patterns for interrogation of (a) 1200 $\mu\text{m}$ diameter flaw and (b) 800 $\mu\text{m}$ diameter flaw.....	78
3.14	Results of Born inversion algorithm analyses of scattering data from a 1200 $\mu\text{m}$ spherical void.....	79
3.15	Results of Born inversion algorithm analysis of scattering data from a 400 $\mu\text{m}$ $\times$ 800 $\mu\text{m}$ oblate ellipsoidal void.....	82
3.16	Rolls-Royce sample made of powder metallurgy nickel based superalloy material.....	84
3.17	(a) C-scan image of flaw in Rolls-Royce sample.....	85

## LIST OF FIGURES

<u>Figure</u>	<u>Page</u>
3.17 (b) B-scan image of flaw in Rolls-Royce sample.....	85
3.18 Results of metallographic sectioning of flaw.....	87
4.1 Contour scanning mode.....	90
4.2 Contour scanning - 2 arrays.....	92
4.3 Scattering data acquisition mode - 2 arrays.....	93
4.4 Ultrasonic phased array system block diagram.....	95
4.5 Duration of transient response for transducer array.....	98
4.6 Transducer array.....	99
4.7 Pulser/receiver schematic.....	101
4.8 Comparison of hybrid pulser excitation of commercial transducer with commercial pulser excitation.....	102
4.9 Frequency response of hybrid receiver.....	104
4.10 Photograph of hybrid pulser/receiver.....	105
4.11 Coding scheme for multiplexer.....	106
4.12 Partitioning and interconnection of multiplexer.....	108
4.13 Photograph of multiplexer board.....	109
4.14 Schematic block diagram of multiplexer.....	110
4.15 (a) Schematic of signal conditioning circuitry: main amplifier, attenuator, and clipper.....	114
4.15 (b) Schematic of signal conditioning circuitry: filter, dc level shifter, and buffer amplifier.....	115
4.16 Schematic of control memory.....	118
4.17 Transmit trigger delays.....	120

## LIST OF FIGURES

<u>Figure</u>	<u>Page</u>
4.18 Conversion delay generator and address generator.....	122
4.19 Block diagram of digitizer.....	123
4.20 Sample screen display for ARRAY.....	126
4.21 Ultrasonic beam formed by a 2.5 MHz array with Hanning amplitude weighting. (a) No time delay quantization (b) 50 ns time delay quantization.....	131
4.22 Computational time requirements for beam synthesis.....	133
4.23 Sector scanning pattern.....	135
4.24 Illustration of a sector scan transmitted through a water/metal interface.....	136
4.25 Multiplexer, pulser/receiver and transducer assembly mounted on Test Bed scanning bridge.....	138
4.26 Array radiation function illustrating single element factor and array factor.....	140
4.27 Array radiation pattern for uniform excitation of 16 elements.....	142
4.28 Polar plot of radiation pattern within a metal part when there is a 50 mm water path.....	144
4.29 Unprocessed image obtained from a titanium part with a flat front surface.....	146
4.30 Differential image of a 1200 $\mu$ m spherical void in a titanium disk.....	147
4.31 B-scan of 1200 $\mu$ m spherical void obtained with a single element transducer having the same aperture as the array.....	148

# LIST OF TABLES

<u>Table</u>		<u>Page</u>
2.1	Command characters for multiaxis controller.....	15
2.2	Commands recognized by Task 1 of TBCON.....	33
2.3	Library of display processor routines.....	38
3.1	Results of Born Inversion analysis of an 800 $\mu$ m diameter spherical void.....	80
3.2	Results of examination of Rolls-Royce sample.....	86
3.3	Comparison of Test Bed results and metallographic examination results.....	88
4.1	XMT/RCV segment select codes.....	111
4.2	Host command codes.....	117
4.3	Primary ARRAY modules.....	124
4.4	Commands to ARRAY.....	125
4.5	Range and interpretation of octal data codes for host commands.....	129



## 1.0 INTRODUCTION

### 1.1 Objective

The primary objective of this program was to bridge the gap between the fundamental studies and the application efforts relating to ultrasonic NDE. To accomplish this objective, the program created a test facility containing state-of-the-art ultrasonics equipment that is sufficiently flexible to allow the implementation and evaluation of new techniques and equipment. This evaluation has been done using both simulated and real defects which occur in laboratory and real aircraft samples. The facility is accessible to researchers not associated with the contractor to facilitate the development of new NDE methods and techniques.

Interested parties may use the facility at a nominal cost. For information regarding procedures for accessing the facility and business arrangements, contact:

P.H. Milham  
Director of Contracts and Pricing  
Rockwell International Science Center  
1049 Camino Dos Rios  
Thousand Oaks, CA 91360  
PH (805) 498-4545

Inquiries concerning technical capabilities should be directed to R.C. Addison, Jr., at the same address.

The program was composed of three phases. The first phase consisted of the system design, assembly and shakedown. This phase encompassed the construction of the self contained unit comprising the physical Test Bed, as well as the fabrication of an ultrasonic phased array system. The second phase involved the reduction to practice of quantitative NDE techniques. The techniques that were implemented consisted of a subset of the long wavelength,

defect classification and imaging techniques that were developed in the Interdisciplinary Program for Quantitative Flaw Definition.<sup>1</sup> The third phase consisted of a detailed system evaluation on real and simulated problems.

## 1.2 Conceptual Design

The Ultrasonic Test Bed program was initiated to complement the AF/DARPA Interdisciplinary Program for Quantitative Flaw Definition.<sup>1</sup> This interdisciplinary program has fostered the development of a variety of new techniques for the quantitative characterization of flaws. The program was and is currently concerned with characterization methods encompassing both ultrasonic and electromagnetic techniques. A major thrust of the program has been directed towards the development of ultrasonic inversion techniques. These techniques permit the characterization of a flaw based on the measurement of the ultrasonic fields incident on and scattered by the flaw. The utility of these techniques has been categorized according to the ratio of a representative flaw dimension to the wavelength of the ultrasound. For convenience this ratio is referred to in terms of the dimensionless quantity  $ka$ , where  $k = \frac{2\pi}{\lambda}$  and  $a$  is a representative radius of the flaw. Thus the inversion technique commonly referred to as imaging is useful at large  $ka$  values in the regime where the flaw size is larger than the wavelength. In the medium  $ka$  range where  $0.5 < ka < 6$ , the flaw size is less than or comparable to the wavelength. Techniques applicable in this  $ka$  range are herein referred to as model-based reconstruction techniques. The low  $ka$  range refers to values of  $ka$  less than 0.5. The inversion methods used in this region are simply called long wavelength techniques.

At the inception of the Ultrasonic Test Bed program the variety of techniques that had been developed to operate in each of these three regimes had been shown to work theoretically and in some cases experiments with idealized geometries had been conducted. What was needed was some means to test these inversion algorithms under conditions that were representative of those found in real parts and to integrate those algorithms that were suitable

into a coherent system that could collect data over the entire range of  $ka$  values.

The Ultrasonic Test Bed program was designed to carry out these tasks. The Test Bed program was specifically concerned with the ultrasonic techniques and of those available it has concentrated on the subsets that are useful in characterizing internal flaws such as voids and inclusions. It is important to note that the procedure for testing these techniques proved to be a lengthier task than had been initially estimated. This resulted in a selection of the available techniques to produce a flaw analysis capability that extended over all wavelength ranges and yet permitted the program to be completed within the available time frame. As an example, a long wavelength technique for accurately locating the center of a flaw was implemented because it was useful in improving the accuracy of the model-based reconstruction technique known as the inverse Born approximation. However the long wavelength technique for measuring the flaw related parameter known as  $A_2$  was not implemented.

The work statement specifically mentioned that the defect classification technique that utilized nonlinear networks was to be implemented. This technique was not included among those that were tested. A preliminary investigation of this technique revealed that the applicable  $ka$  range for these networks is  $1 < ka < 3$ . The range of applicability of the inverse Born approximation completely overlaps this range. Further, the nonlinear networks require measurements of the flaw to be made from a minimum of 12 different angles with 19 independent measurements being preferred. This is an impractically large number of measurements to characterize a single flaw. In addition to the time required to acquire the data, the geometry of most real parts would restrict the spatial window to a relatively few measurement directions. Despite these drawbacks there was still interest in testing the utility of the networks. The software for using the non-linear networks did not arrive until the program for analyzing flaws was well advanced and much of the available time had already been allocated. When the software was received it was not

compatible with the computer used for the Test Bed. A significant effort would have been required to correct the software so that it would run on the Test Bed computer. Given the other drawbacks of this particular technique, a decision was made to omit this technique from consideration.

A useful function of the Test Bed program has been to communicate information back to the interdisciplinary program concerning areas where practical constraints degraded the results and further fundamental work was required.

To achieve these goals, the Test Bed was built as a self-contained unit, complete with a large ultrasonic water tank, transducer array, mechanical positioning devices, analog and digital signal generation and processing circuitry, dedicated minicomputer for control and data interpretation, and display units. Fundamental to the system is the capability to scan transducers over parts and acquire data. Important differences between the Test Bed and many of the conventional systems are that the multiaxis scanning system is controlled by a microprocessor system and is capable of contour following modes of scanning. The data acquisition techniques differ in that entire waveforms are digitized and stored on the disk memory of the minicomputer. The chief distinction of the Test Bed system, however, is the presence of algorithms within the minicomputer for carrying out the inversion techniques outlined above. The capabilities of the Test Bed for imaging studies are enhanced by an ultrasonic phased array system that was constructed at the Science Center as part of the program.

### 1.3 Structure of Report

This report covering the activities and accomplishments of the Test Bed program is divided into three major sections. The first of these, the Test Bed System, provides a description of the various hardware subsystems that are interconnected to form the physical system. The major hardware items covered are the scanning system, the data acquisition device, the display processor, and the minicomputer system. The software for controlling the

operation of this system is also detailed. This software includes the main multitasking program, as well as the specific programs for directing the multiaxis controller and for displaying data via the display processor.

The next section describes the inspection procedures. A thorough explanation is given of the protocol used in examining a part. The operation of the one-dimensional Born inversion algorithm is explained and the procedures used in testing the algorithm are presented in conjunction with the results of these tests. Finally experimental results with known flaws and unknown flaws in various specimens are provided.

The final major section details the design, fabrication and testing of the ultrasonic phased array system. All of the major subsystems are described from the transducers to the array processor. The general aspects of phased array operation and the fundamental advantages and limitations are discussed. Results obtained with the system for flaws within metal parts are presented, for both inversion methods involving imaging and Born inversion techniques.

The report ends with a section providing conclusions and recommendations for future work in the area encompassed by the Test Bed program.

## 2.0 TEST BED SYSTEM

### 2.1 Overview

The Test Bed is a multifaceted system with many of its unique capabilities residing in especially written algorithms and signal processing techniques. There is, however, a significant amount of hardware that comprises the physical portion of the system. The photograph of the Test Bed laboratory in Fig. 2.1 shows most of this hardware and the block diagram in Fig. 2.2 shows how it is interconnected. The major component of the system is the six-axis scanning system and the large water tank that dominate the foreground. Closely associated with this is the microprocessor based multi-axis controller shown to the right of the water tank. In the background, the Data General ECLIPSE S/200 minicomputer can be seen. The color raster-scan image display unit (TV monitor) associated with the Genisco display processor is shown to the left of the S/200. Adjacent to it is one of the Tektronix 4006 terminals associated with the system. Behind the terminal can be seen the Data General disk memory unit. Not visible in the photograph are the Biomation 8100 A/D converter used for data acquisition, the pulser/ receiver, and the Tektronix 453A oscilloscope used with the system. There are also two hard copy units available, a Versatec unit for the computer terminals and an Image Resources Videoprint 500 for the image display unit.

This hardware provides a capability of scanning rotationally symmetric parts using a contour scanning technique as well as flat parts using a raster scanning technique. The pulser/receiver is a unit made by Panametrics that satisfies the needs of this system. The received waveforms are digitized with a Biomation data acquisition unit and stored on the disk memory of the Data General minicomputer. With the possible exception of the waveform digitization, these tasks are accomplished using procedures that are widespread and to a large extent can be considered as conventional.

The system has the capability of displaying the conventional C-scan and B-scan images using a variety of amplitude coding schemes involving the

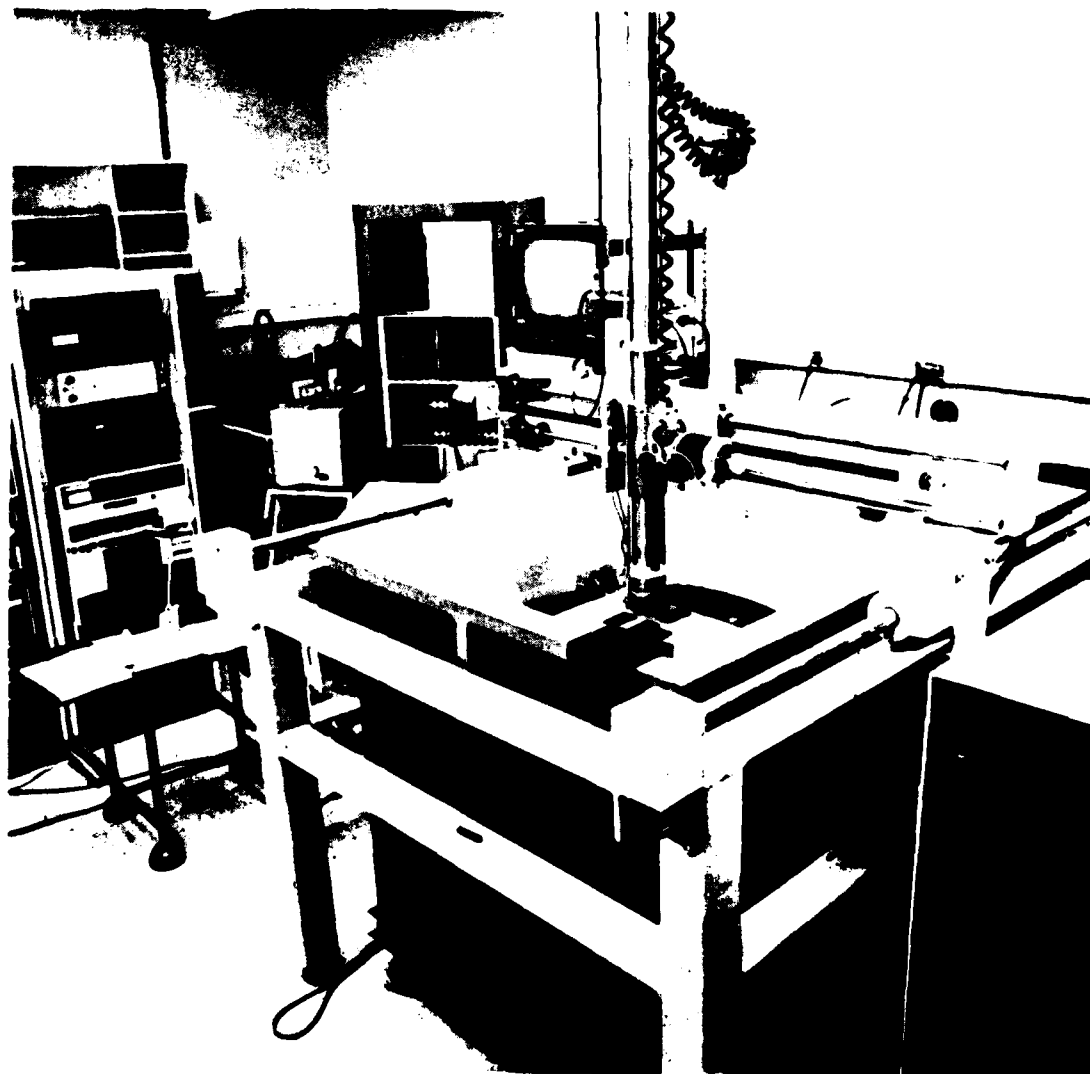


Fig. 2.1 Photograph of Test Bed lab.

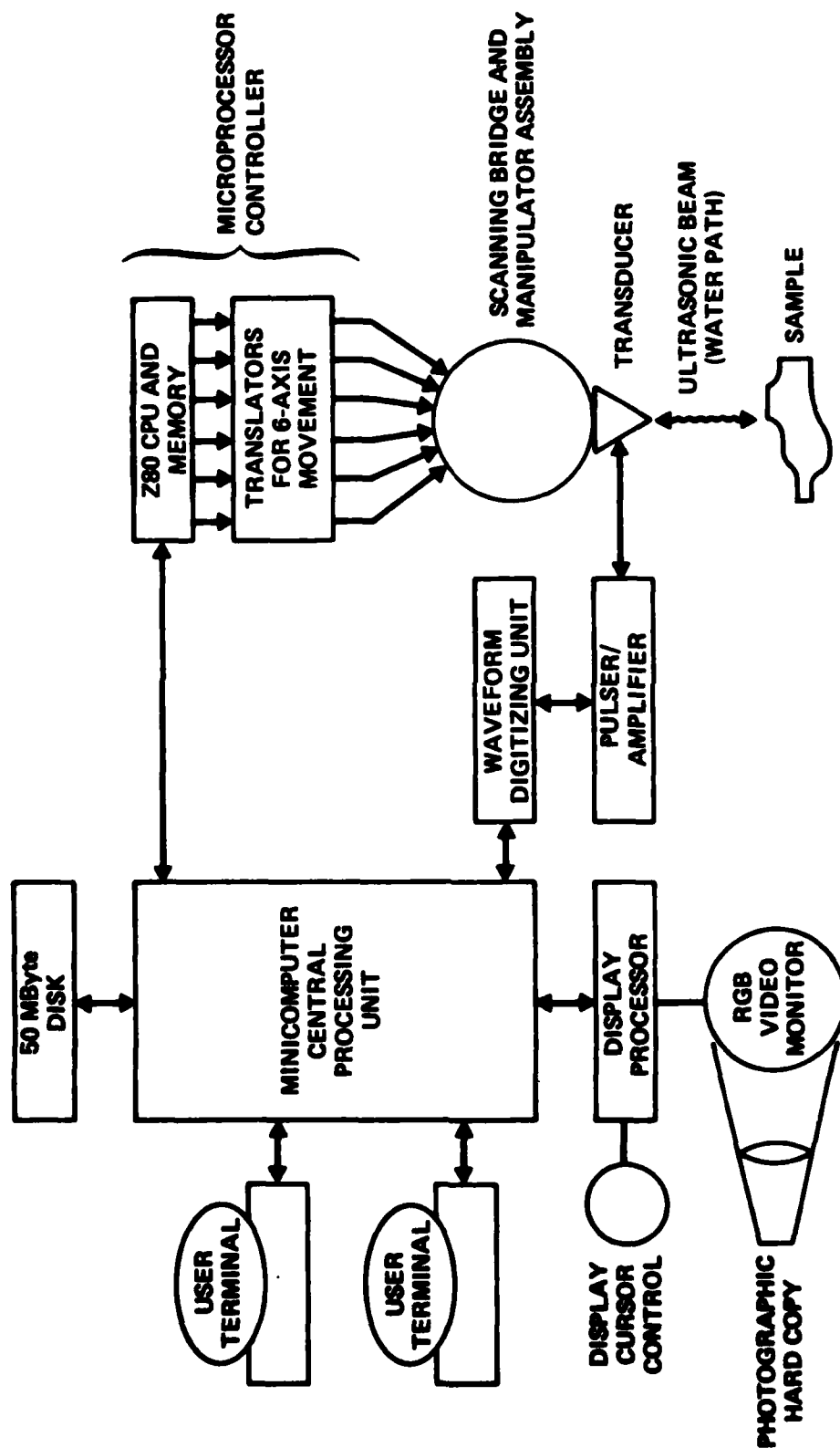


Fig. 2.2 Block diagram of Test Bed system.



gray scale or pseudo-color rendition of the data. These techniques are not generally available in conventional inspection systems but significantly enhance the information content conveyed by the images.

The unique capabilities of the system reside in its ability to manipulate the data with the minicomputer. This permits an array of signal - processing techniques including time gating, frequency filtering, and transducer deconvolution. These techniques are frequently used to prepare signals for processing by algorithms designed to characterize detected flaws in terms of their size, shape, orientation, and composition.

## 2.2 Scanning System

### 2.2.1 Hardware

The scanning system for the Test Bed provides five degrees of freedom for the transducer plus a turntable that can be used to rotate circularly symmetric parts. The X and Y motions are based on an assembly that existed at the Science Center prior to the Test Bed program. This assembly was upgraded so that the bridge could support a manipulator arm and the frame work would fit around the water tank. Although no special efforts were made to assure precise mechanical positioning accuracies, the rigidity is probably adequate to insure an accuracy of about 0.040 inches over the entire range of motion. The X and Y axes are driven by stepping motors having 200 steps/revolution via ball screws that provide a linear precision of 0.001 inches/step. The relative accuracy over short distances of less than 10 inches is about 0.010 inches. The maximum speed of the X or Y axis is 2 inches per second if the motor is ramped up to the maximum speed. Without ramping the maximum speed is 0.3 inches per second.

The Z axis motion and the two gimbal axes are provided by a manipulator that is available commercially from Automation Industries. The Z axis has a maximum travel distance of 48 inches. It is driven by a stepping motor that provides a linear precision of 0.001 inches/step. The accuracy for the full

travel range is specified to be 0.010 inches. The angular motions are provided by a primary and secondary gimbal that are driven by stepping motors. The primary gimbal rotates about an axis that is parallel to the Y axis of the system and is designated the B axis. Similarly the secondary gimbal rotates about an axis that is orthogonal to the B axis and is designated the A axis. The primary gimbal can travel over a total angular range of  $300^\circ$  with a precision of  $0.1^\circ$  per step. The secondary gimbal can travel over a total angular range of  $\pm 40^\circ$  with the same precision. The accuracy of these axes has not been determined but appears to be significantly worse than the precision and is affected by an interaction between the axes. The inaccuracies in these axes are the chief sources of error in the overall pointing accuracy of the system.

The sixth degree of freedom is provided by a turntable that is available commercially from Automation Industries. The turntable has a three-jaw chuck capable of holding parts with diameters up to 30 inches. The unit is driven by a stepping motor with a precision of  $0.1^\circ$  per step and a maximum speed of 15 rpm.

The scanning assembly is built around a water tank with overall dimensions of 5 feet long  $\times$  3.25 feet wide  $\times$  3.5 feet deep. The tank is made of mild steel with a PVC liner. There is a recirculating pump and filters for keeping the water clean.

### 2.2.2 Multiaxis Controller

The multiaxis controller is a microprocessor based unit that controls the movements of each of the six axes. A block diagram of the unit is shown in Fig. 2.3. The system is capable of scanning a transducer over a two-dimensional profile while maintaining an angle of incidence perpendicular to the surface and maintaining a constant water path distance. The system can also be used to scan a transducer in a raster pattern for generating C-scan images.

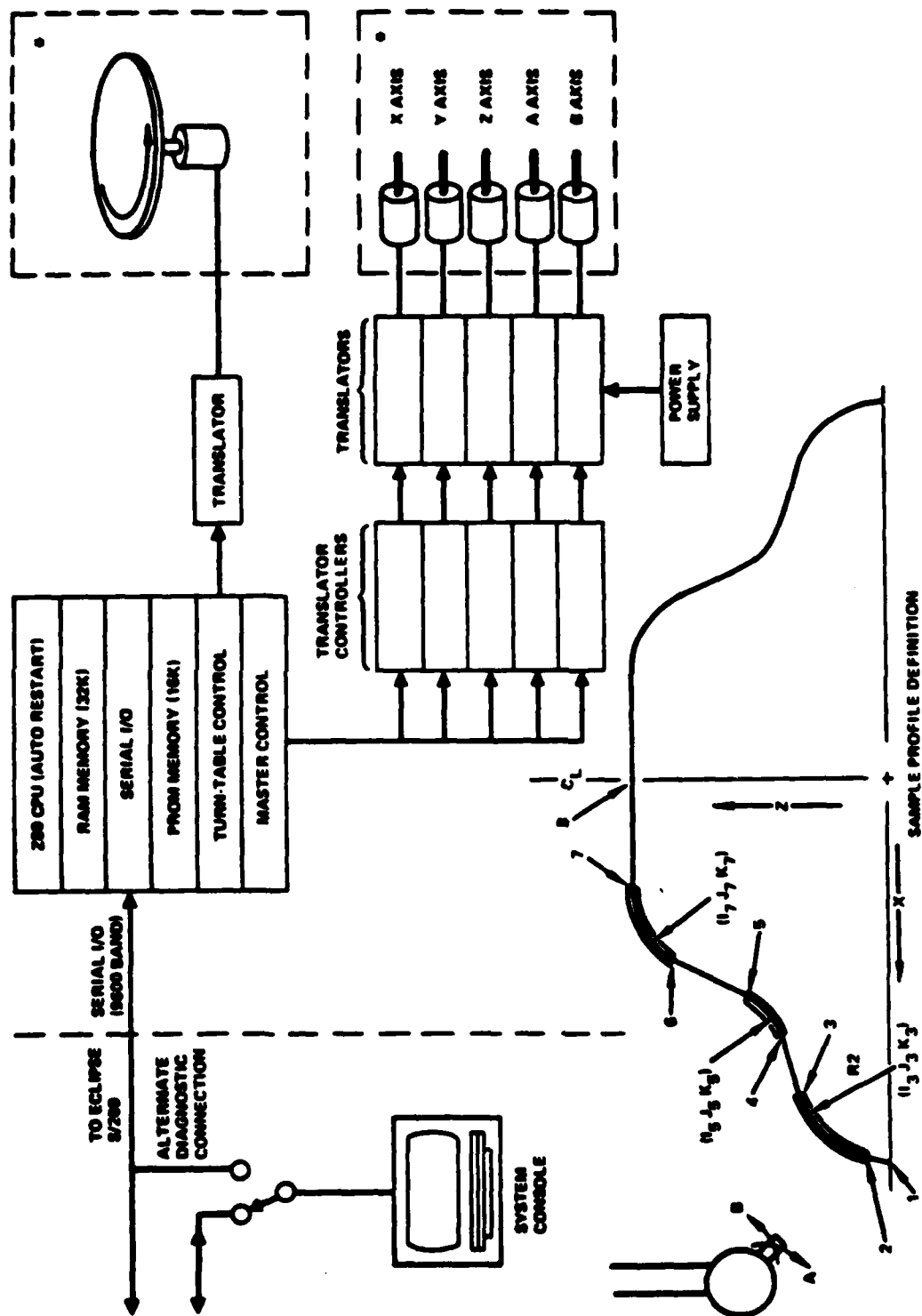


Fig. 2.3 Block diagram of multiaxis controller with sample profile.

The software for the microprocessor-based manipulator control subsystem was created by that unit's manufacturer. It is resident in an EPROM, and is therefore relatively easily changed. The function of this software is to receive command characters and data strings from the minicomputer, and translate these into pulses to the stepping motors and/or responses to the minicomputer. There are 13 command characters recognized by the Z80 software, and 13 response characters which it generates, some of which are followed by signed integers. Table 2.1 shows a list of these 26 characters with a description of their meanings. Data is passed to the Z80 in a sequence of ASCII characters called a data block. An example of this is "N5F10X10Y1000B910" which is interpreted in Fig. 2.4 and can be read "on the fifth move go from the present position to  $X = 0.010$  inches,  $Y = 1.000$  inches, with a  $B$  angle of  $91^\circ$  at a speed of 10% of the maximum (although the actual maximum speed of the axis is limited by the motor to 2 inches/second), the maximum repetition rate of the pulser driving the motors is 3 KHz corresponding to a speed of 3 inches/second. It is this maximum of 3 inches/second that is referred to as 100% of maximum speed.) The data block is decoded and stored in a RAM memory until it is time for execution of the move. Up to 256 separate data blocks may be stored, if necessary, before movement is initiated with an "I" character. Execution consists of calculating the distance required in each coordinate, converting it into stepping motor pulses for the axes involved, and sending out the pulses to each axis, appropriately interleaved to provide maximum accuracy in following the contour of the move.

The Z80 also may receive input from the "joystick," the handheld manual control unit, if no data block move is in progress. In this mode, it is possible to reposition any of the 6 axes by closing a toggle switch on this unit for a period of time. Then a "G" command from the minicomputer to the Z80 will return the correct new position of the 6 axis system. However, it is necessary after one or more such manual moves, to send to the Z80 a special "M" data block in order to update the memory of the Z80.

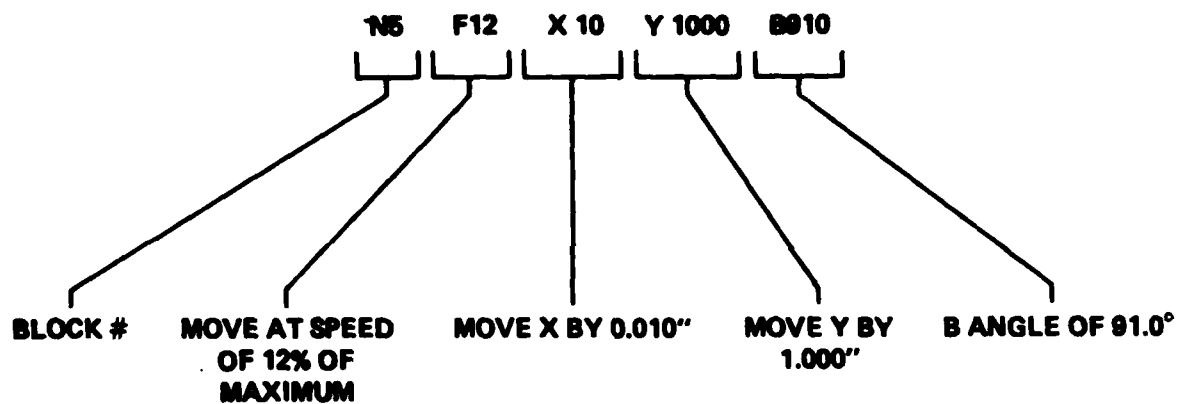


Fig. 2.4 Interpretation of data block command.

Table 2.1  
Command Characters for Multiaxis Controller

Name	To μP	From μP	Description
HOLD	D	---	Halt existing processes
CONTINUE	E	---	Continue halted process
GET X	X	---	Request X position
GET Y	Y	---	Request Y position
GET Z	Z	---	Request Z position
GET A	A	---	Request A position
GET B	B	---	Request B position
GET TT	T	---	Request TT position
X RESPONSE	---	X	Response header (sign and 5 digits)
Y RESPONSE	---	Y	Response header (sign and 5 digits)
Z RESPONSE	---	Z	Response header (sign and 5 digits)
A RESPONSE	---	A	Response header (sign and 5 digits)
B RESPONSE	---	B	Response header (sign and 5 digits)
TT RESPONSE	---	T	Response header (sign and 5 digits)
GET ALL	G	---	Get all axis positions
DATA	N	---	Data block to follow
STATUS	S	---	Request status of microprocessor
STATUS RESPONSE	---	M	Returned status
FAULT RESPONSE	---	V	Non-solicited hardware error
BLOCK DATA REQUEST RESPONSE	---	W	Non-solicited request for data
START	I	---	Commence movement at block 0000
DATA VALID RESPONSE	---	Q	Non-solicited, good data field
DATA NON-VALID RESPONSE	---	R	Non-solicited, ignore data until data valid command received
ERROR RESPONSE	U	U	Unrecognized message, arguments may or may not exist
INITIALIZE	0	---	Initialize to reference switches
ACKNOWLEDGE RESPONSE	---	K	Acknowledge receipt of command

A number of problems have been encountered with the operation of this system which require more operator patience and skill than is desired. Many of these items have reputedly been corrected on newer versions of the controller. In view of the growing acceptance of such systems by the NDE community, it seems appropriate to list some of the items that are sources of error or frustration so that others who need to select or specify similar systems can avoid the same pitfalls.

A. Problems relating to limit switches:

1. When the system activates a limit switch under manual control it does not stop.
2. When the system activates a limit switch under computer control, it stops but the system has to be reset before it can be driven out of the limit under manual control.
3. When the system activates a limit switch it does not keep a count of how far it moved beyond the limit.
4. The limit switches on the manipulator do not work well and inhibit the operation of the manipulator for some applications. They have been removed from our system.

B. Problems relating to the reset switch:

1. The reset switch has to be activated twice to ensure that the system is completely initialized.
2. When the reset switch is activated, the axes tend to move a distance corresponding to about one stepping motor step.

C. Problems related to the manual control:

1. If an NØ block has been executed and an initiate (I) command has been given, the system will keep track of its position accurately as long as it is driven under computer control. However, if the manual control is used to move the system, the Z-80 is not updated at the end of the move and further moves under computer control do not account for the manual moves that have occurred.
2. The speed of an axis move with the "fast" manual control is too slow for moves greater than about 1 in. It would be preferable to be able to obtain maximum speeds while under manual control.
3. There are no position encoders to monitor the motion of the axis making it necessary to query the computer to determine position when moving the transducer with manual control.
4. There is no on-line display of position.

D. Problems related to turntable:

1. The turntable cannot be moved to a specific position under computer control.

E. Problems related to passing blocks from minicomputer to micro:

1. Carriage returns during data block sending are not always recognized. Systematic interruptions occur approximately every 8 or 16 blocks, although the events seem to be aperiodic.



F. Problems related to contour following mode of operation:

1. Curvilinear moves are inaccurate. The stepping motors for the involved axes do not always interleave the pulses properly. For instance, the X and B axes will reach their terminal positions while Z is continuing to move to reach its final position. This means the final position is correct, but the path followed to reach it is not correct.
2. Curvilinear moves cannot cross 90° quadrant boundaries. Furthermore, for moves that have to cross such boundaries, it is necessary to insert a block that produces a linear move between the curvilinear moves on each side of the boundary.
3. It is necessary for the coordinates of a curvilinear move to be provided to the precision of the machine otherwise confusion results and the machine moves totally incorrectly. The machine has no way of checking data and indicating that a problem exists. Thus the system is not robust to operator error.

G. Problems related to error messages:

1. There are a variety of situations in which the system fails to function or will function incorrectly but there is no error message that would tell the operator that he has made an error.

H. Problems related to initialization of system:

1. Home values are stored in an EPROM and the EPROM has to be reprogrammed to change them.

- I. Problems related to C-scans and "data dropout":

1. There are no trigger pulses available that can be used to gauge the distance that the transducer has moved and thus synchronize a pulser.

The personnel who have used the system believe that the most pressing need is robustness in the face of operator error and better diagnostics when errors are encountered.

## 2.3 Display Processor

The Genisco display processor is specifically intended to accept command and data strings sent from the minicomputer and to translate these into arrangements of pixels in a  $480 \times 512$  RAM memory. The 8 bit word associated with each pixel can be coded as one of 16 levels of gray or as one of 256 different colors and displayed on the Conrac color raster-scan image display unit (hereafter referred to as the TV monitor). The TV monitor displays a 525 line raster on a cathode ray tube (CRT) measuring 11.4 inches high  $\times$  15.5 inches wide.

The software in the display processor was created by Genisco and is for all practical purposes hardwired and unchangeable. Twenty basic commands are defined. A complete description of them is beyond the scope of this text, but they include these functions:

1. Display of alphanumeric characters with any combination of four different orientations and four different character sizes;
2. Replacement of the bit pattern describing any pixel;

3. Display of a general rectangle;
4. Display of a vector drawn between any two points;
5. Cursor display and control;
6. Return to minicomputer of data, such as the position of the cursor;
7. Hardware zoom and scroll;
8. Replacement of the video look-up table which provides the correspondence between bit pattern and displayed color.

Communication between the Genisco unit and the Data General minicomputer takes place over the I/O bus of the minicomputer at instantaneous data rates in excess of 4 megabits per second.

#### 2.4 Data Acquisition System

The data acquisition system is composed of a number of interconnected units shown in Fig. 2.5. The transducers used with the system span the frequency range of approximately 1 to 25 MHz. Typically these are wideband units that provide short transient responses. Both focused and unfocused units are used. The pulser/receiver is a commercially available unit from Panametrics. None of its functions can be computer controlled but it produces a short pulse and the receiver can provide up to 40 dB of gain. The receiver recovers from saturation quickly and an internal attenuator can provide up to 68 dB of attenuation. It has functioned well for the applications encountered with the Test Bed. The output of the receiver goes to a Tektronix 453A oscilloscope used to observe the received waveforms. The output also goes to a waveform acquisition unit made by Biomation that digitizes selected portions of the received signals. It contains a nominal 8 bit analog to digital converter

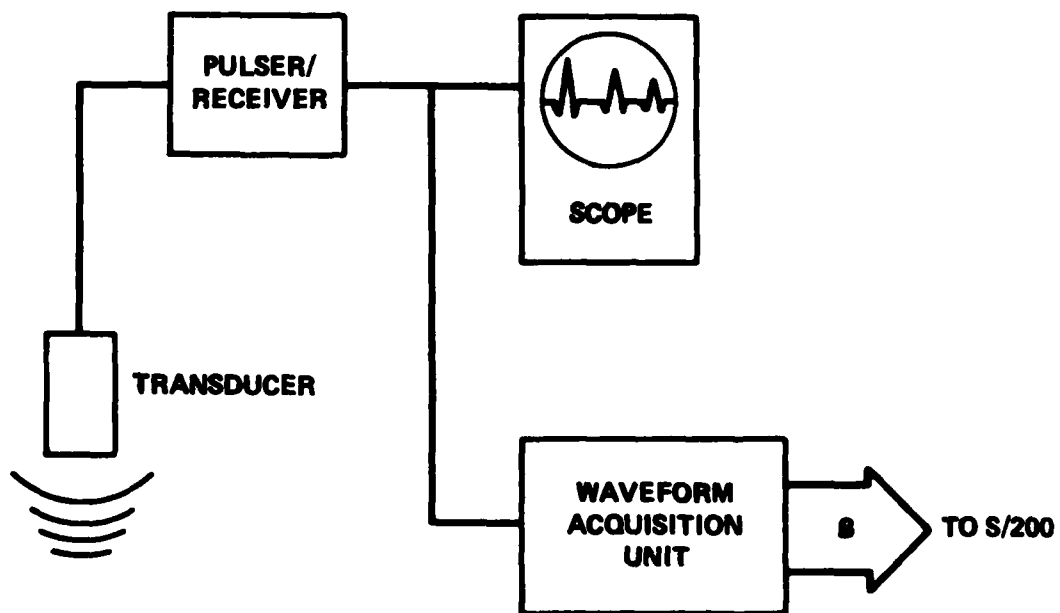


Fig. 2.5 Block diagram of data acquisition system.

with a maximum sampling rate of 100 MHz. Tests of this unit show that its accuracy decreases with increasing frequency at frequencies above 500 kHz. In order to obtain sufficient accuracy in the sampled data, a signal averaging technique<sup>2</sup> was used. This technique involved averaging multiple acquisitions of the waveform while varying the dc offset of the instrument between acquisitions. A typical procedure which provided more than adequate accuracy consisted of averaging 250 waveforms in groups of 10 at each of 25 different dc offsets.

Some special software has been designed for interfacing the waveform acquisition unit to the minicomputer. This code which is partially in assembly language, arms the unit, waits for a trigger, collects the waveform and then processes the waveform in a manner which is specified by the operator. Although the inherent speed of the Biomation unit will permit 500 waveforms of 1024 samples each to be acquired each second, this rate has never been achieved in practice. A more typical waveform acquisition rate is about 100 per second.

The ultrasonic phased array system is also used for data acquisition. This system will be fully described in Section 4.0.

## 2.5 Minicomputer System

The minicomputer for the Test Bed is a Data General Eclipse S/200. The unit contains a 162 K byte memory and can be partitioned to allow operators at two separate terminals to access it. It has been equipped with a 50 M byte disk memory and 9 track magnetic tape unit.

The software for the minicomputer has been written entirely at the Science Center. It is largely in Fortran, although certain portions which access the Biomation A/D converter are in assembly language. It includes four different categories of programs, all of which operate interactively with the user. The categories are listed below:

1. programs for generating and checking disk files of data blocks which may be interpreted by the Z80;
2. multitasking control programs for managing the manipulator, data acquisition, and storage on disk;
3. programs for displaying the data in color or black and white via the Genisco display processor;
4. ISP, a signal processing and display program of enormous flexibility.

All but ISP have been created for the Test Bed project. A brief description of each of the categories of minicomputer programs with the exception of ISP follows.

In category (1) there are two kinds of programs for generating disk files of data blocks. One kind which generates a file corresponding to a raster pattern in X & Y contains two slightly different programs. In each program the pattern of moves illustrated in Fig. 2.6 is generated. The pattern begins with the move (AB, BC) and then repeats the pair (CD, DE) until the area within the dashed lines is traversed. One program, RASTER, is completely flexible and allows any number of CD moves, and any length of DE and CD. Figure 2.7a shows the user terminal screen display which occurs during operation of RASTER with both prompts from the minicomputer and user inputs. User inputs are outlined with boxes. The other program, RASTMAG, is limited to creating one of seven raster patterns. Each of these patterns has 125 (CD, DE) moves. The pattern is exactly square and may have one of seven different edge lengths 0.25 inches, 0.50 inches, 1.0 inches, 2.5 inches, 5 inches, 10 inches, and 25 inches. This represents a variation of  $10^4$  in area in order to service parts or samples ranging in size from a transistor assembly to a turbine disk. Figure 2.7b shows the screen display for operation of RASTMAG.

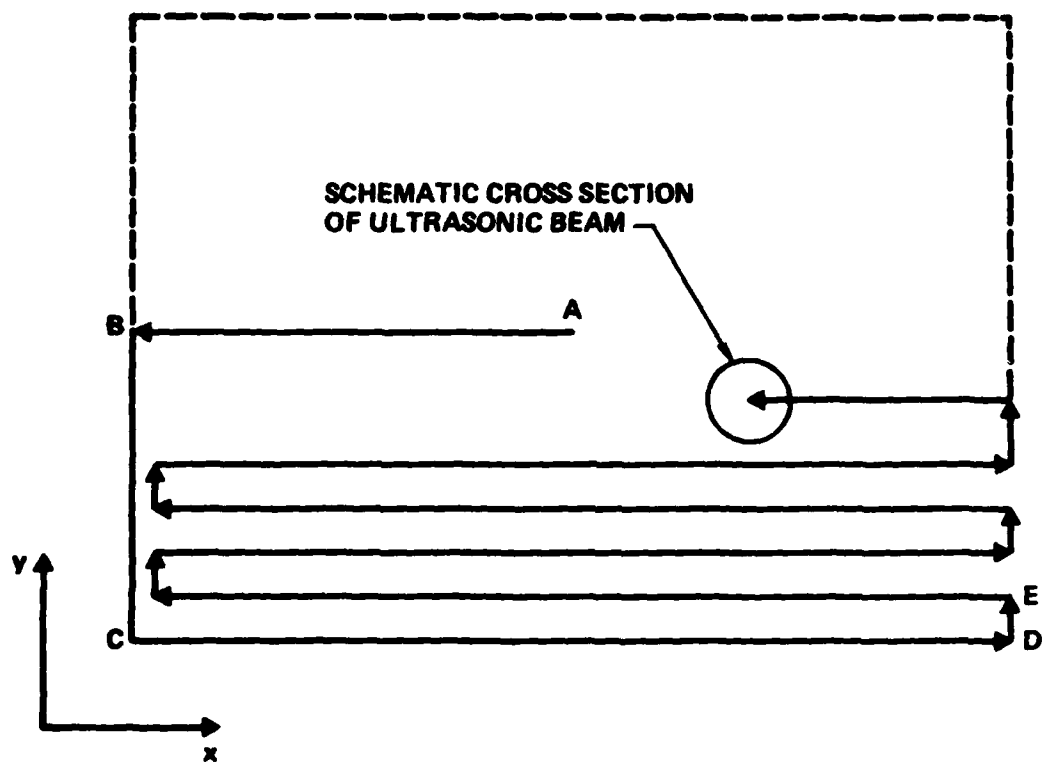


Fig. 2.6 A schematic of the pattern of moves followed in an X-Y raster scan.

**RASTER**

ENTER STARTING X, Y:

ENTER FINAL X, Y:

NUMBER OF RASTERS (I.E. # OF X-SCANS):

ENTER NAME OF NEW DISK FILE: (7 CHAR).DB

R

(a)

**RASTMAG**

FOR SQUARE OF      25.00    10.00    5.00    2.50    1.00    00.50    00.25 INCHES

MAGNIFICATION =    00.40    1.00    2.00    4.00    10.00    20.00    40.00

(b)

PLEASE ENTER MAGNIFICATION DESIRED:

PLEASE ENTER RASTER CENTER IN X, Y:

ENTER NAME OF NEW DISK FILE: (7 CHAR).DB

R

Fig. 2.7 User terminal display after operation of RASTER and RAST MAG. User inputs are delineated by boxes.



The second kind of data block generation program is represented by PROFILE, which is primarily for creation of data blocks corresponding to the profile of a complex part shape with rotational symmetry such as a turbine disk. Figure 2.8 shows the screen display for operation of PROFILE to create a disk file corresponding to the contour shown in Fig. 2.9a. The resulting disk file is shown in Fig. 2.9b. At a few points in the contour, it is necessary to change the entry angle of the acoustic beam without changing the entry point on the part surface. During this change, it may be important not to record data. Ordinarily, as execution of each data block is begun, an "R" is sent from the micro, rapidly followed by a "Q" after the final speed has been reached. However, if "M60" has been specified in the data block, the "Q" is never sent and data is not taken during that move. Notice that PROFILE has automatically inserted non-data-taking moves at the appropriate places. These can be easily modified to omit the "M60" if data-taking is desired during those moves. The arc centers "I" and "K" are specified if a circular contour must be followed during the move.

In order to provide a check on the data blocks generated with PROFILE, a program named PROPLOT has been coded that, for any given contour scan, makes a plot of the part profile and two paths associated with the transducer manipulator. It needs as input from the operator only the name of the data file containing the data blocks and the length of the transducer. One path is the path the center of the transducer face makes during the scan; the other is the path made by the manipulator pivot point. Figure 2.10 shows one example of the user-computer interaction with user inputs shown in boxes. Data non-valid moves are flagged and the values of two internal variables are displayed for diagnostic purposes.

The lower half of Figure 2.11 shows the result of executing PROPLOT; the part profile appears with the two paths of interest. Use of color allows an operator to make an easy check for interference: the part profile is white, the pivot point path is red, and the transducer path is green. For purposes of illustration, the data blocks used to generate the graphic display

# **PROFILE**

PLEASE TYPE IN NAME OF NEW DISK FILE: (7 CHAR).DB

TESTCON.DB

TYPE 1 IF AP WILL BE CHANGED DURING PROFILE

MODE, TRANSDUCER OFFSET, FEED RATE, TURNABLE SPEED : 21.4.0.5.25

ENTER INITIAL X,Y,Z,A,B :

0.0,0.0,13.7

FOR NEW SEGMENT, 8

ENTER L FOR LINEAR, C FOR CIRCULAR SEGMENT, AND E FOR END DATA BLOCK

X,Y,Z OF THE END POINT OF THIS SEGMENT: 1.0,0.4

FOR NEW SEGMENT, 8

ENTER L FOR LINEAR, C FOR CIRCULAR SEGMENT, AND E FOR END DATA BLOCK

X,Y,Z OF THE END POINT OF THIS SEGMENT: 1.2,0.1.5

RADIUS OF THIS SEGMENT : 1.5

CI, CK ARE : 1.55692 4.308110E-02

DATA NON-VALID SEGMENT GENERATED 2

FOR NEW SEGMENT, 8

ENTER L FOR LINEAR, C FOR CIRCULAR SEGMENT, AND E FOR END DATA BLOCK

X,Y,Z OF THE END POINT OF THIS SEGMENT: 2.1,0.1.8

FOR NEW SEGMENT, 8

ENTER L FOR LINEAR, C FOR CIRCULAR SEGMENT, AND E FOR END DATA BLOCK

X,Y,Z OF THE END POINT OF THIS SEGMENT: 2.8,0.2.3

RADIUS OF THIS SEGMENT : -1.5

CI, CK ARE : 1.61475 3.21934

DATA NON-VALID SEGMENT GENERATED 5

FOR NEW SEGMENT, 8

ENTER L FOR LINEAR, C FOR CIRCULAR SEGMENT, AND E FOR END DATA BLOCK

X,Y,Z OF THE END POINT OF THIS SEGMENT: 3.4,0.3.6

FOR NEW SEGMENT, 8

ENTER L FOR LINEAR, C FOR CIRCULAR SEGMENT, AND E FOR END DATA BLOCK

X,Y,Z OF THE END POINT OF THIS SEGMENT: 4.6,0.4.2

RADIUS OF THIS SEGMENT : 2.0

CI, CK ARE : 4.84261 2.21477

DATA NON-VALID SEGMENT GENERATED 8

FOR NEW SEGMENT, 8

ENTER L FOR LINEAR, C FOR CIRCULAR SEGMENT, AND E FOR END DATA BLOCK

X,Y,Z OF THE END POINT OF THIS SEGMENT: 6.4,0.4.2

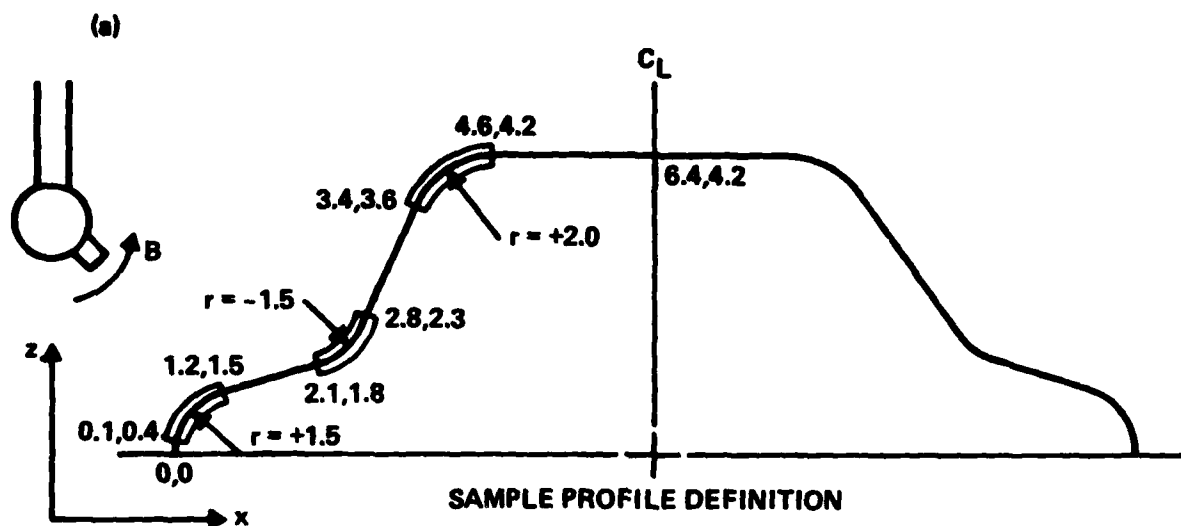
FOR NEW SEGMENT, 8

ENTER L FOR LINEAR, C FOR CIRCULAR SEGMENT, AND E FOR END DATA BLOCK

OK, DISK FILE IS READY TO USE:

TESTCON.DB

Fig. 2.8 User terminal display after operating PROFILE. User inputs are delineated by boxes.



(b)

TYPE	TESTCON.	DB								
N	01	21X	01	02	00	00	-126T	4000F	00	25
N	10	00A	00	-140						
N	1X	100Y	02	300A	00	-140				
N	00	00A	00	127						
N	0X	1570Y	02	1543A	00	004I	1550K	43		
N	0X	1543Y	02	1543A	00	005				
N	3X	1100Y	02	1500A	00	1312I	1550K	43		
N	00	00A	00	1004						
N	4X	2100Y	02	1200A	00	1004				
N	00	00A	00	1002						
N	0X	000Y	02	2300A	00	1402I	1614K	3210		
N	7X	00A	00	1052						
N	7X	2300Y	02	2000A	00	1052				
N	00	00A	00	430						
N	0X	4000Y	02	4100A	00	40I	4040K	2214		
N	10	00A	00	0						
N	10X	0300Y	02	4100A	00	0				
N	11	00	0							

Fig. 2.9 An example of a profile requiring contour moves. (a) Sketch of profile, (b) the resulting data blocks are shown.

**PROPLOT**

PLEASE TYPE IN NAME OF DISK FILE OF DATA BLOCKS:

**TSTCURVE.DB**

TYPE 1 IF YOU WANT A PAUSE AFTER EACH MOVE

DATA NON-VALID MOVE

DATA NON-VALID MOVE

ENTER TRANSDUCER LENGTH: **0.45**

BP. THETAS	(2)	=	90 . 0000	0.000000
BP. THETAS	(2)	=	90 . 0000	0.000000
BP. THETAS	(2)	=	126 . 900	0.644023
BP. THETAS	(2)	=	89 . 5000	- 8.72660E-03
BP. THETAS	(2)	=	90 . 0000	0.000000
BP. THETAS	(2)	=	90 . 0000	0.000000
BP. THETAS	(2)	=	126 . 900	0.644023
BP. THETAS	(2)	=	89 . 5000	- 8.72660E-03

END OF DISK FILE

STOP

R

Fig. 2.10 User terminal display during operation of PROPLOT. User inputs are delineated by boxes.

```

N0 M11 G99 S2 F5 T1000 X0 Y0 Z0
N1 M60 A0 B900
N2 X1500
N3 M60 B1269
N4 X2978 Z500 B905 I3000 K-2000
N5 X3022 B895
N6 X4500 Z0 B531 I3000 K-2000
N7 M2 S0

```

```

(B) _____
(C) _____
(A) _____

```

```

PART PROFILE (A)
PIVOT POINT PATH (B)
TRANSDUCER PATH (C)
TSTCURVE.DB

```

Fig. 2.11 Output display of PROPLOT showing part profile, transducer path and pivot point path.

have been added to the upper half of this monitor photograph; this information does not normally appear. The labels under the drawing, however, are standard for this display.

In category 2) we have the multitasking control program, named TBCON, which manages the manipulator, data acquisition, and storage on disk. It maintains three tasks. Task 1 communicates with the operator via the user terminal; its standard prompt is "WAITING FOR CONTROL WORD." It allows one to send characters directly to the Z80 to construct and send data blocks, to start and stop data-taking, or to perform other useful tasks such as calculating the refraction of the acoustic beam through a flat part surface. Task 2, which has priority over all the other tasks, reads and interprets response characters from the Z80. Task 3 operates the Biomation A/D converter as described in Section 2.4, and stores, at intervals, pertinent data on disk for later access by display programs. Communication between tasks is via an area of memory common to all three. Table 2.2 shows a list of the commands recognized by Task 1 along with their functions. The commands "RI" and "RF" are explained later. The command "TW" calls a subroutine which varies the angles A and B separately over a small range and picks the values which yield the maximum signal. That is, it "tweaks up" A and B. TBCON provides the user with three modes of acquisition which are detailed separately below, and correspond to C-scans, B-scans, and A-scans. B- and C-scans are performed in a raster fashion, either rectangular or circular, i.e., in increments of X and Y of a cartesian coordinate system, or increments of radius and angle of a polar coordinate system. If the user specifies a circular scan, additional position information is stored on disk in Task 3.

MODE 1: C-scan. During a scan, only the minimum and maximum peak amplitudes of each waveform are actually stored on disk; this provides a rapid scan of a horizontal plane of an entire sample. Figure 2.12 shows a typical C-scan start-up for TBCON, with user inputs outlined by boxes. In this case, the user chose to take data with one of the seven pre-determined rectangular raster patterns. After sending over the data blocks contained in MGNF010.DB,

### EXAMPLE OF PROGRAM

**TBCON**

TYPE 1 IF SEARCH SCAN **0**

CALCULATE X, Y (Y = 1) **1**

TYPE 0 IF YOU PLAN TO ACQUIRE DATA WITH ISP: **1**

ENTER 1 FOR XY OR 2 FOR RT **1**

NUMBER OF SAMPLE INTERVALS **100**

ENTER DESIRED SPEED AND # OF SAMPLES PER INCH: **20,250**

TYPE IN NAME OF DATA STORAGE FILE: (UP TO 12 CHAR.)

**P159TST1.T1**

OK, TASKS ARE STARTED

WAITING FOR A CONTROL WORD

**DB**

PLEASE ENTER DATA BLOCK:

**N0M21F28T1X0Z0**

WAITING FOR A CONTROL WORD

W

K

**DF**

TYPE IN NAME OF DATA BLOCK FILE: (7 CHAR) DB

**MGNF010.DB**

TYPE 1 TO TRANSFER ONLY 1 BLOCK AT A TIME: **0**

NEW BLOCK:      N              1X      -5000

W

K

NEW BLOCK:      N              1Y      -4960

W

K

NEW BLOCK:      N              2X      5000

W

K

•

• (AND SO ON)

•

Fig. 2.12 User terminal display during operation of TBCON. User inputs are delineated by boxes.

Table 2.2  
Commands Recognized by Task 1 of TBCON

User Command	Task 1 Response
Any single letter: A, B, etc.	Sends that character directly to the Z80
DB	Allows entry of a data block for transmission to the Z80.
DF	Reads a file of data blocks from disk and sends them to the Z80.
BE	Starts Task 3, plus sends "I" to Z80.
HA	Suspends Task 3, sends "D" to Z80.
CO	Restarts Task 3, plus sends "E" to Z80.
FI	Suspends Task 3, sends "D," closes the output file.
CH	Allows a change in threshold while data taking and movement are momentarily halted
RI, RF	See text
TW	See text
NØ	Gets current position of axes; returns a data block beginning with NØ with current position specified. This updates the Z80's memory after a joystick move.
X+1ØØØ, or Y-1232, or Z-5Ø, etc.	This type of command constructs a data block consisting of N1X1ØØØ or N1Y-1232 or N1Z-5Ø and sends it to the Z80.
XX	Closes output file and suspends all tasks, effectively ending the program.



the standard prompt recurs, and the user types in "BE." From there on, the scan is automatic and the presence of an operator is not necessary until the data is ready for display. For this program, start-up takes less than five minutes and a scan of a 5 inch by 5 inch area with 125 raster lines takes about 20 minutes.

While sending the data blocks to the Z80, Task 1 is also storing them in the output file (on disk). When movement begins, Task 2 goes into a continuous loop which is broken only by occasional disk storage activities. The rate of this loop is set by the Panametrics Pulser/Receiver which provides the trigger for the digitizer unit. All the data pairs for a given CD move (See Fig. 2.6) are stored in a sequence on the disk. In this manner, the resulting data output file has as many data pair sequences as it has CD data blocks.

This rectangular scan is the fastest possible way of obtaining a full image or C-scan because it does not query the Z80 after movement is initiated. The current data-taking rate in this mode can be as high as 150 Hz, which corresponds to a part sampling rate of 417 points per inch at the normal scan speed of 0.36 inches per second. A circular scan queries the Z80 and stores position information for each waveform. Although its maximum data-taking rate is only 80 Hz, this mode lends itself to more complicated scans with other than pure raster moves. For example, this is used during scans involving rotation of the turntable.

In C-scan operation, a further option allows the user to specify an amplitude threshold whose value can vary as a function of depth below the surface of the part. The amplitude of a waveform is only stored if it exceeds the threshold value. A varying threshold permits adjustment of the detection sensitivity to compensate for material attenuation, focusing effects, front surface "ring-down", etc.

MODE 2: B-scan. During a scan, information about the entire waveform is kept, as opposed to only the maximum and minimum values that are kept in a C-scan. Scans may be performed in either a rectangular or circular fashion. Data storage occurs more frequently than during the C-scan mode, and includes

position and amplitude information, identified by X, Y, and Z coordinates where Z represents the position in time of a point within the waveform.

The speed of a B-scan decreases proportional to the amount of data recorded. As in the previous mode, the user may specify a time-varying threshold which must be exceeded before the data will be stored. The threshold may be described as constant or exponentially decaying. This option provides the capability of storing only portions of waveforms and thus increases the data acquisition speed.

MODE 3: A-scan. The third mode of operation involves using TBCON as a sub-task of ISP. In this mode, TBCON provides position control and calculates the Fresnel reflection loss at the water/metal interface. ISP performs data acquisition and analysis of the data. This mode is employed when it is necessary to record entire waveforms for the detailed examination of a flaw. In the course of such an examination, it is desirable to acquire data from arbitrary angles relative to the surface of the part. Figure 2.13 shows the refraction of the acoustic beam at the surface of the sample. The angle of incidence is designated  $\theta_e$  and the angle of refraction is designated  $\theta_i$ . The TBCON commands "RI" and "RF" are used to call a subroutine which:

1. calculates the position of the pivot point in X, Y, and Z,
2. calculates the gimbal angles A and B,
3. sends the appropriate data block to the Z80,
4. calculates the Fresnel reflection loss at the water/metal interface.

Then data is acquired at that angle with ISP and can be stored on a disk file for further analysis.

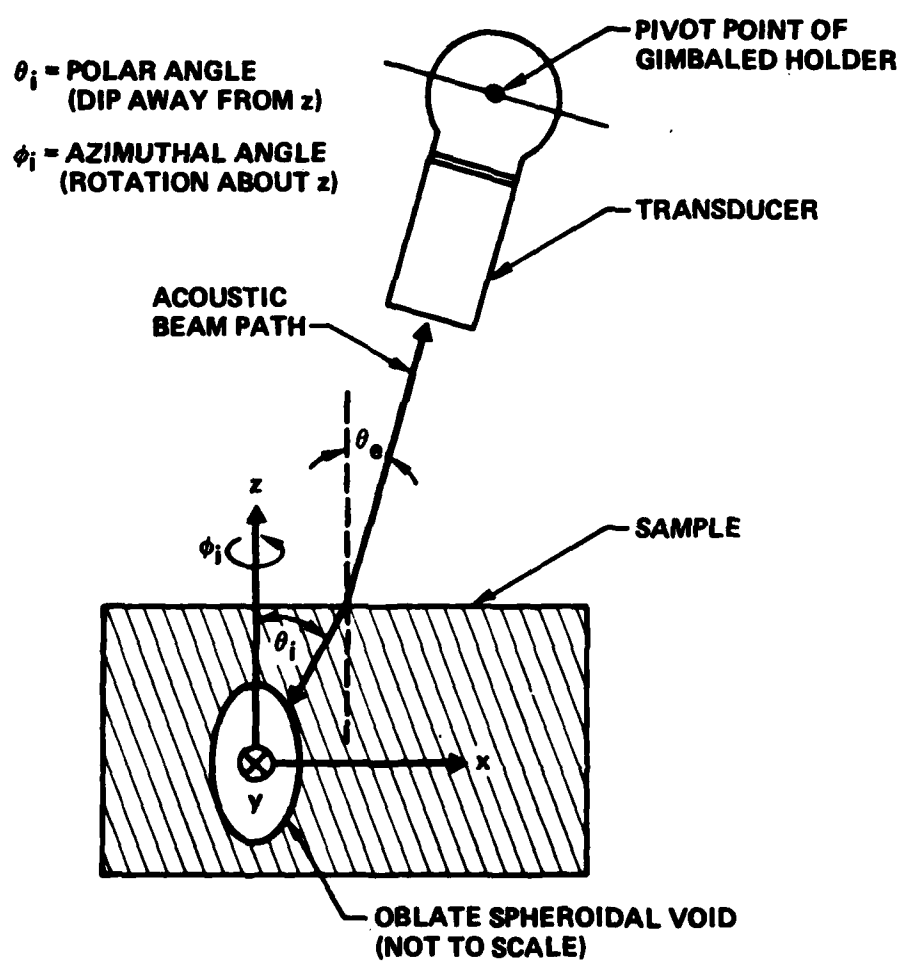


Fig. 2.13 A schematic of the refraction of the acoustic beam at the surface of the sample.

The third category of programs comprise the routines that have been written so the S/200 can control the Genisco display processor. Twenty of them are basic to the display functions and are gathered into a library, PGP.LB, which is listed in Table 2.3. Two programs have been written to display the results of the first two data-taking modes of TBCON. C-scan data obtained in MODE 1 is displayed by TBDISC, while MODE 2 B-scan data is displayed by TBDISZ. The two programs are very similar and an explanation of the operation of TBDISC should suffice for both programs.

The interaction between the user and computer to obtain the display of a C-scan image is shown in Fig. 2.14; user inputs are outlined with boxes. The program has a number of options including:

1. Clearing or not clearing the monitor;
2. Rectangular raster or spiral format data;
3. Choice of seven magnifications;
4. Arbitrary reference point to establish an absolute coordinate system;
5. Use of most positive or most negative signal acquired;
6. Relative sizing options such that more than one image may be displayed at once (up to nine);
7. Alteration of the contrast and brightness from the calculated values;
8. Offset of alternate rasters in the X direction;

Table 2.3  
Library of Display Processor Routines

PGP.LB Function Name	Description of Function
VLGGS	Generates a gray scale and updates the VLT with it.
VLGNS	Generates a blue, green, red, white scale and updates the VLT with it.
COLOR	Allows selection of color to apply to other functions, with optional pre-empt.
WRSTR	Sends an alphanumeric string to the display processor for display on the monitor
XYZOO	Zooms display in a region centered at an arbitrary X, Y, to one of four factors: 1, 2, 4, or 8.
CUREN	Enables a cursor of any color combined with four different shapes.
WRZRA	Writes a raster of data.
WRVEC	Writes a vector given beginning and end points
CURDI	Disables a previously enabled cursor.
CURTR	Allows user to track with cursor to a desired position and returns X, Y coordinates to minicomputer.
SETPL	Turn on selected memory planes.
SCROL	Scrolls display in X and Y.
WRREC	Writes a cartesian rectangle at an arbitrary X, Y with optional color fill.
SETUP	Clears all parameters to their default values.
WRVLT	Writes a user defined video lookup table to the display processor.
LENGT	Function returning the length of an alpha numeric array.
ZOOM	Zooms top left area of screen to desired factor.
CLRPL	Clears selected memory planes.
ARGCN	Counts the number of arguments in a subroutine call.
PGPDR	Interface between minicomputer CPU and display processor.

TBDISC

TYPE 1 FOR CLEAR PGP : ☐ 1  
DFLAW

ENTER FILENAME

☐ P103TST5.Y1

RASTER (0) OR SPIRAL (1) : ☐ 0

FOR SQUARE OF 25.00 10.00 5.00 2.50 1.00 .50 .25 INCHES

MAGNIFICATION = .40 1.00 2.00 4.00 10.00 20.00 40.00

PLEASE ENTER MAGNIFICATION DESIRED : ☐ 20

PLEASE ENTER RASTER CENTER IN X,Y : ☐ 0,0

AUG # PTS/INCH = 218.506

TOTAL #PTS, #INCHES 13734 62.8548

POS RANGE IS : 3.00000 119.000

NEG RANGE IS : -121 -1

DISPLAY BASED ON POS(1) OR NEG(2) PEAK ☐ 2

FILE HAS BEEN READ AND REOPENED

HOW MANY IMAGES AT ONCE? (1, 4 OR 9) ☐ 1

OLD CONTRAST, BRIGHTNESS = 1.00000

-2.01667

NEW CONTRAST, BRIGHTNESS = ☐ 1,0

X OFFSET TO CORRECT ZIGZAG : ☐ -2

IER ROBLK 9

DONE, RE-MAP COLORS? (1 FOR YES) ☐ 0

CHANGE ULT? ☐ 1

OPTIONS: 0 = GRAY SCALE, 1 = NORMAL

ENTER OPTION: ☐ 1

DONE, RE-MAP COLORS? (1 FOR YES) ☐ 0

CHANGE ULT? ☐ 0

USE CURSOR? ☐ 1

ENTER ZOOM FACTOR AND TRACK TO DESIRED POINT ☐ 0

X,Y= -1.06667E-02 6.80000E-02

ENTER ZOOM FACTOR AND TRACK TO DESIRED POINT ☐ 1

X,Y= -1.06667E-02 6.80000E-02

ENTER ZOOM FACTOR AND TRACK TO DESIRED POINT ☐ 0

STOP

R

Fig. 2.14 User terminal display after operation of TBDISC. User inputs are delineated by boxes.

9. Alteration of VLT;

10. Use of cursor to zoom any portion and measure any point in absolute coordinates.

Two examples of images resulting from the display of MODE 1 data are shown in Fig. 2.15. It displays the amplitude of reflected sound from two different voids in titanium, translated into a gray scale video display. The transducer was a focused beam piezoelectric unit operating at 5 MHz. The image on the left is from a 0.50 inch by 0.50 inch region centered on a spherical void of 800 micron diameter;  $\theta_i$  was  $0^\circ$ . The image on the right is from a 0.25 inch by 0.25 inch region centered on an oblate spheroid, 250 microns by 800 microns (see Fig. 2.13). The internal angle,  $\theta_i$ , was  $60^\circ$ . The file name and the key to the color vs intensity code or video look up table (VLT) are displayed automatically at the bottom of the image.

In addition, a large variety of display software has been created for testing various subroutines, for displaying data in 3D perspective, for changing the VLT, for using the cursor, for labeling, and other auxiliary functions.

The software that is used for processing the signals acquired during the investigation of a particular flaw is known as the Interpretive Signal Processing (ISP) program. This software was created at the Science Center separately from the Test Bed program and is unique in the field of NDE. ISP is a large multitasking program that runs on the S/200 under the command of an external terminal. It can be used to string together a number of signal processing operations in a group that is designated a "procedure". There are over 40 distinct operations that can be used in a "procedure". Those operations pertinent to the Test Bed include:

1. Waveform acquisition (in conjunction with an A/D converter).

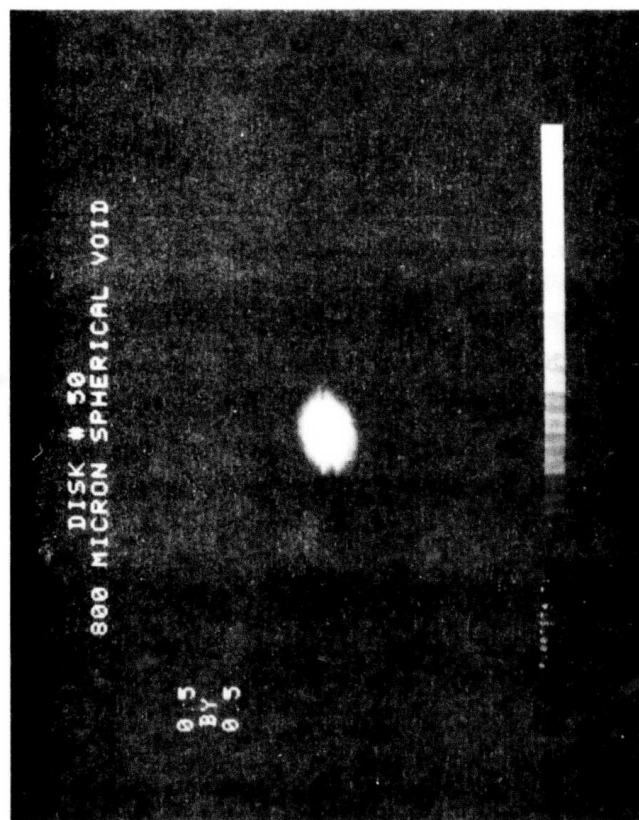


Fig. 2.15 Images resulting from the display of data taken in mode I of TBCON.



2. Waveform transformation including: addition, subtraction, Fourier transforming, time shifting, multiplication, division, etc.
3. Feature extraction including: maxima, minima centroids, energy, statistical data, etc.
4. Display of data including: automatic scaling, linear plots, log plots, etc.
5. Position control by calling TBCON as a sub-task.

The "procedures" employing these operations can read single or multiple record files from the disk memory of the S/200 and modify them with sequential processing operations. There can also be internal looping within a "procedure". The algorithms used for the inversion technique to be described in Section 3.0 are designed using the ISP procedures to take advantage of the flexibility and ease of use. Once the utility of an algorithm has been established, the required element of ISP can be abstracted and incorporated into a stand-alone software routine.

In the case of the Born Inversion algorithm, a combination of three ISP procedures entailing over 100 separate operations was constructed and employed for inversion measurements under this contract. Afterwards, in a separately funded effort,<sup>3</sup> the required ISP functions were extracted and incorporated into a new program called BIP which is an interactive stand-alone program.

### 3.0 INSPECTION PROCEDURES

#### 3.1 System Protocol

The protocol for the system is designed to permit the acquisition of data from a part in a logical fashion that will permit the outputs of the available analysis techniques to be combined to produce the best estimate of the flaw characteristics. In other words the goal is to maximize the synergism that can be obtained from the available analysis techniques.

There is a hierarchy associated with these analysis techniques. The fundamental inversion techniques each use a specific portion of the flaw's frequency spectrum to extract estimates of various flaw characteristics such as size, shape, orientation and composition. These characteristics are then combined using a universal inversion algorithm. This algorithm also uses a priori information such as the probabilities of having particular flaw types, noise levels, etc. The output is a probabilistic estimate of the flaw characteristics that is based on all the data available from that flaw. This estimate is then used as an input to a fracture mechanics based accept/reject criteria to decide whether the part is acceptable.

Although the general structure for the protocol is generic in nature and can be applied to many different systems and flaw types, the Test Bed has been specifically applied to the ultrasonic examination of bulk flaws in materials. Consequently the protocol has been adapted to these specific needs. The technique consists of a search mode for the detection of tentative flaw indications followed by a detailed examination of these tentative flaws to extract as much quantitative information about them as possible. A diagram outlining the protocol is shown in Fig. 3.1.

The description of the protocol is logically coherent only when taken as a whole. Although as many features of the protocol have been implemented as time permitted, all features have not been implemented. The descriptions contained in the following sections point out the current state of implementation of a particular technique or procedures.

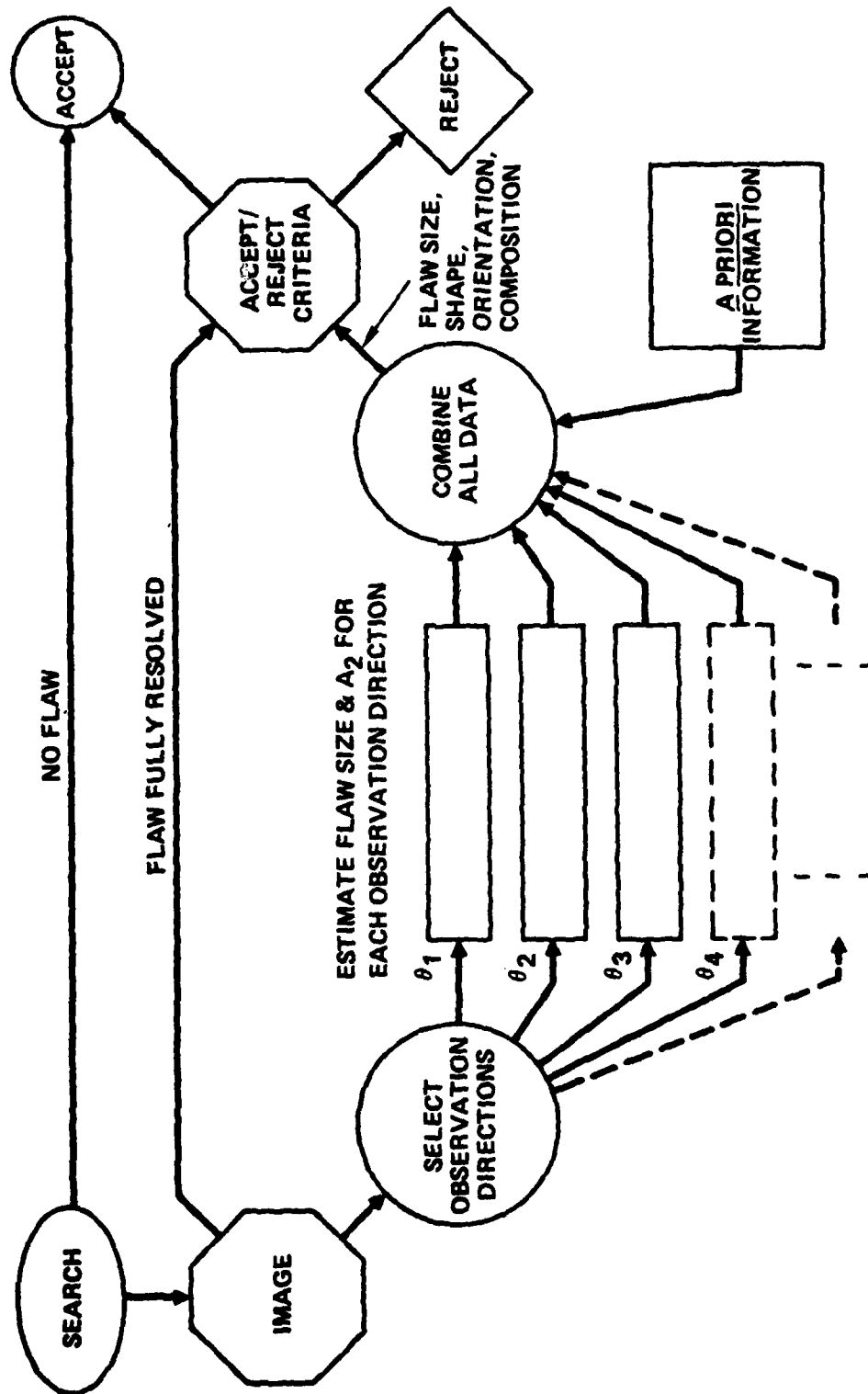


Fig. 3.1 Inspection protocol.

### 3.1.1 Search Mode

The search mode is implemented by scanning a transducer over the part in some regular pattern. For a flat part this can be a back and forth raster pattern. In the case of a shaped disk, the transducer follows the contour of the disk as it moves radially. The disk is mounted on the turntable and rotates beneath it to produce a concentric circle pattern. The transducer used for this inspection is either unfocused or weakly focused to provide complete coverage of a part with a coarse scanning pattern. A tentative flaw indication is identified as any signal that exceeds a preset threshold. When a flaw indication is detected its location is stored in memory so that a detailed inspection of each tentative flaw can be made at the conclusion of the search mode scan.

The transducer selected for the search mode depends on the nature of the part that is to be inspected, the types of flaws that are anticipated, and the required speed of the inspection. The transducer frequency depends on the thickness of the part and the attenuation of the material. The focusing properties of the transducer depend on the depth range over which flaw indications must be detected as well as the expected size of the flaws and the time allotted for the scan.

### 3.1.2 Detailed Examination Mode

At the conclusion of the search mode, each site of a tentative flaw is returned to in turn and a detailed examination of that flaw signal is performed. The detailed examination utilizes several techniques that have validity in different spectral regions or for different ranges of  $ka$  where  $a$  is a representative dimension of the flaw and  $k$  is the wavenumber ( $2\pi/\lambda$ ) in the material. The short wavelength region or high  $ka$  range is covered by imaging techniques which produce B- and C-scan displays. The medium wavelengths are covered by model based reconstruction techniques. The Test Bed has implemented the particular technique known as the one dimensional inverse Born algorithm for obtaining flaw information in this domain. The

long wavelength technique provides information about the location of the center of the flaw as well as the coefficient of the  $\omega^2$  term in the expansion of the scattering spectrum of the flaw which is commonly designated  $A_2$ . The location of the flaw center is essential as an input for the inverse Born technique and the coefficient  $A_2$  can provide information about the composition of the flaw. The determination of  $A_2$  has not been implemented.

#### 3.1.2.1 Imaging

The detailed inspection begins with the imaging of a localized region surrounding the flaw site. Either a single element focused transducer or a multielement phased array transducer can be used. If a single element focused transducer selected, it should operate at the highest frequency that is consistent with the required penetration depth and the transducer availability. In practice the focal length of the transducer is limited by the finite number of available transducers. However given the availability of suitable transducers the focal length should be determined by the expected size and depth of the flaws as well as by the depth of focus required for the inspection. At the present time, no provision is made for imaging through curved surfaces. Cylindrically curved and spherically curved surfaces could be compensated for by fitting the transducer with auxiliary lenses but no efforts have been made to do this. This localized scan can provide either a C-scan with an operator selectable depth slice displayed on the monitor or a B-scan corresponding to a single scan line passing through the flaw indication. If a multielement phased array transducer is selected, it will be able to rapidly scan an ultrasonic beam to acquire B-scan data. It will be able to change the focus of the beam in one dimension. This will permit the accommodation of various curvatures in a cylindrical surface.

The results of the imaging inspection can be classified according to the completeness with which the flaw is resolved. If the flaw is sufficiently large that it is completely resolved by the focal spot of the scanning transducer then the image can provide a complete description of the flaw's

size, shape, and orientation. The protocol would then move directly to the accept/reject criteria to determine the suitability of the part for additional usage. It may only be possible to resolve selected dimensions of the flaw, in which case the rough shape of the flaw and its orientation can still be determined from the image and used in the next step of the protocol. If none of the flaw dimensions are resolvable, then the image can still provide a mapping function to determine how many individual flaws are represented by the one flaw indication. Since the inversion techniques involving medium and long wavelengths only work with isolated flaws, it is essential to have this information before applying them.

#### 3.1.2.2 Selection of Observation Directions and Estimation of Flaw Size

To obtain an image it is necessary to acquire many waveforms but these are acquired with very regular spacing of the transducer positions and the data is obtained quickly. Some of the model based reconstruction techniques also require a large number of waveforms. However these waveforms usually have to sample a sphere or hemisphere surrounding the flaw in a very specific way to insure a good inversion. When the spatial window available to inspect the flaw is restricted by the geometry of the part, these techniques incur large errors or fail to work altogether. In contrast, the Born inversion technique requires only a single waveform to obtain a single size estimate corresponding to the projection of the flaw along the propagation direction. Although a reasonably detailed image of a flaw can be obtained by using the Born inversion technique with waveforms taken at many different angles, this is unlikely to be done in a practical situation. The size of the flaw along two or three critical directions is probably all that will be required. These directions are selected on the basis of the C- and B-scan images as well as the available spatial windows allowing access to the flaw.

Once the observation directions are selected, waveforms are acquired from the flaw with transducers whose bandwidths encompass both the long and medium wavelength regime. These waveforms are then processed to obtain the

flaw size for each observation direction. The exact procedure for doing this currently requires some iteration of the measurements and the judgment of an operator. The prospects for making this procedure completely automatic are favorable but will require additional development.

### 3.1.2.3 Combination of All Data

After these flaw parameters are determined, all of the available information about the flaw including any a priori information is combined using an algorithm that produces an estimate of the flaw size, shape, orientation, and composition.

The Test Bed program has been chiefly concerned with the imaging techniques and with the one-dimensional Born inversion technique for estimating flaw sizes. The long wavelength portion of the spectrum provides information about the location of the center of the flaw and the long wavelength scattering coefficient  $A_2$ . The information about the center of the flaw has been used extensively in conjunction with the Born inversion algorithm but little work has been done to measure  $A_2$ . The algorithms for combining the data to obtain a probabilistic answer for the flaw size, shape and composition has been incorporated into the Test Bed software resident in the mini-computer. Because complete input data was not available for any of the flaws that were examined i.e.,  $A_2$ , signal to noise data for the signals, and probabilistic data concerning different flaw compositions, the algorithm was not utilized. An informal approach has been used to combine data from the imaging technique, the Born inversion and data obtained about the impedance of the flaw relative to the host material. From this size, shape orientation and some information about the flaw's composition was deduced. Additional information on this experiment is presented in 3.2.4.4.

## 3.2 Quantitative Flaw Sizing Techniques

The inversion technique required for the estimation of flaw size encompasses the medium wavelength regime as defined above. The flaw sizing

technique is the one-dimensional Born inversion algorithm which requires an input from the long wavelength measurement regarding the location of the center of the flaw. This technique is strictly valid only for ellipsoidal, weakly scattering flaws; however, in practice it appears to work reasonably well for nonellipsoidal strongly scattering flaws that have a convex shape. This particular algorithm has been found to be robust in the presence of low signal to noise ratio and limited transducer bandwidth. Before using the algorithm it is necessary to ascertain if the bandwidth of the transducer encompasses the appropriate spectral region of the flaw being examined. This is a transducer selection problem that is solved by examining the experimentally measured spectrum of the flaw. The spectrum is obtained by sequentially acquiring signals from the flaw with transducers having successively lower center frequencies. The transducer characteristics are deconvolved from the measured flaw signals and the magnitude spectrum is examined for peaks. Below some frequency there will be no additional peaks in the spectrum but only an  $f^2$  dependence of the spectral magnitude. The transducer whose bandwidth encompasses the lowest peak of the magnitude spectrum is the appropriate one to use for acquiring Born inversion data.

### 3.2.1 Signal Preprocessing Techniques

There is some pre-processing required for the signals acquired from the flaw and this is diagramed in the flow chart shown in Fig. 3.2. The main objective of this pre-processing is to isolate the flaw signal, and force the signal spectrum to zero in those regions where the transducer has insufficient energy. To accomplish this a reference signal is acquired from the backface of the sample or from a flat surface on a piece of similar material. This signal is taken to be the impulse response of the transducer system in the absence of a flaw. The portion of the acquired waveform containing the flaw signal is separated by multiplying the waveform by a rectangular window whose length and position are selected by the operator. The resulting waveform is then shifted in time so that  $t = 0$  occurs at the centroid of the pulse. This eliminates the excess phase that is associated with a pulse that is located



### Preprocessing of Acquired Flaw Signal

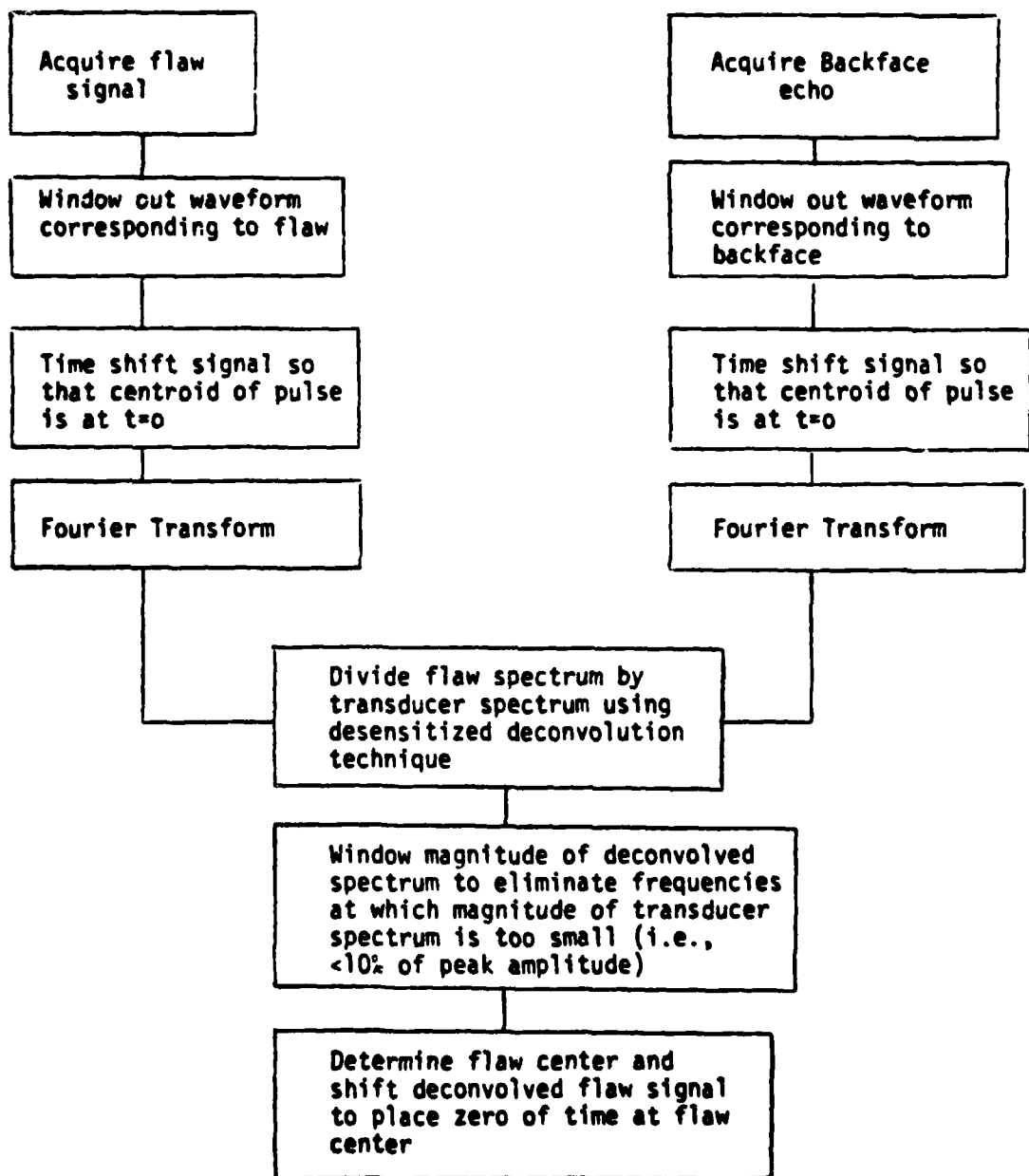


Fig. 3.2 Preprocessing of acquired flaw signal.

far from  $t = 0$ . This waveform is then Fourier transformed to obtain the frequency spectrum of the measured flaw signal. The reference (transducer) spectrum signal is obtained in a similar manner.

The measured flaw spectrum is equal to the product of the flaw spectrum and the transducer spectrum, plus various sources of noise. The flaw spectrum is obtained by dividing the measured spectrum by the transducer spectrum. The division is a noise vulnerable operation. The energy in the transducer spectrum is only above the noise level over a certain bandwidth. Outside of this bandwidth a straight forward division would produce a result that was dependent on the noise and had undefined portions because of division by zero. To avoid problems caused by the noise, a desensitized division technique is used. This is essentially the same as the Wiener filtering technique described by Murakami et al.<sup>4</sup> This technique forces the quotient of the two spectra to zero when the amplitude of the transducer spectra becomes comparable to that of the noise associated with the transducer spectra. The Wiener filter has a bandpass amplitude that is near one over most of the bandwidth of the transducer. At the band edges it decreases smoothly to zero. It is essentially zero at a bandwidth corresponding to the -20 dB bandwidth of the transducer for the transducer spectra used in the Test Bed work.

The result of this division is an estimate of the complex spectral back scattering amplitude of the flaw alone. Frequently there are small artifact signals produced outside the -20 dB bandwidth of the transducer and these are eliminated by replacing those portions of the waveform's spectral magnitude that lie below the transducer's bandwidth with a parabolic curve that passes through zero at zero frequency and coincides with the flaw spectral magnitude at approximately the low frequency -20 dB level. Those artifacts occurring above the bandwidth of the transducer are suppressed by multiplying the spectral magnitude by a cosine-squared function (Hann window) that is centered at zero frequency and goes to zero at a frequency that is operator selected but usually corresponds to a frequency that is 20-30% higher than the high frequency -20 dB level of the transducer bandwidth function.

The exact value is not critical since the Born inversion algorithm tends to suppress high frequency data.

The complex frequency spectrum that results from these calculations is essentially ready to be input to the Born inversion algorithm once it has been time shifted so that the centroid of the flaw is at  $t = 0$ . This requires shifting the signal by an amount  $\tau$  equal to the difference between the centroid of the pulse and the centroid of the flaw. This quantity can best be determined by examining the long wavelength data obtained from the flaw. The value of  $\tau$  can then be found from the slope of the phase in the long wavelength region. This slope is found approximately by using the a priori information that the phase intercept at zero frequency must be an integral multiple of 180 degrees. The slope is found by fitting a straight line to the long wavelength portion of the phase curve of the deconvolved frequency spectrum and having the zero frequency intercept be an integral multiple of 180 degrees. Since the slope of the phase curve can be directly related to a time shift in the time domain, the time shift required to reduce the slope to zero can be calculated. Generally this is done iteratively to produce the best estimate of the required time shift.

In some cases, the transducer used to acquire the data may not have sufficient bandwidth to cover the long wavelength region. In these cases a lower frequency transducer may be used to acquire the required long wavelength data. An empirical technique has also been found which works with good accuracy when the bandwidth available is suitably broad and is well centered on the first peak of the magnitude spectrum. This technique which depends on certain features of the characteristic function produced by the Born inversion is an iterative technique that is more easily explained after the Born inversion algorithm has been described and will therefore be postponed until this algorithm is presented.

### 3.2.2 Born Inversion

The particular Born inversion technique that is referred to in this report is the one-dimensional inverse Born approximation algorithm that was developed by Rose<sup>5</sup> as part of the Interdisciplinary Program for Quantitative NDE. It has been theoretically investigated by a number of people<sup>6</sup> and its operation has been examined in both the frequency domain<sup>7</sup> and the time domain.<sup>8</sup> The operation is most easily explained in the time domain and this will be done here. The particular algorithm that has been used experimentally performs the same processing on the data, but for reasons of computational convenience performs them in the frequency domain.

The theory of the Born inversion is strictly valid only for weakly scattering or singly scattering objects. In practice it works for many strongly scattering objects such as voids and inclusions in metals and inclusions in ceramics. The operation is illustrated in Fig. 3.3. Consider an ultrasonic wave that is propagating toward a weakly scattering ellipsoidal object as shown at the top of Fig. 3.3. The band-limited impulse response of this object can be shown to be a function like that in the center of Fig. 3.3 with a small constant positive amplitude over the region corresponding to the interior of the object and two negative going peaks of short duration at each edge of the object. The one-dimensional inverse Born algorithm generates a characteristic function by integrating this impulse response in a particular way. The integral extends over a window that is symmetrically located about the center of the object. This center point is taken as the  $t = 0$  point. As the integration window expands, it produces a function of time (or distance since the two are related through the velocity of sound in the medium). This characteristic function is shown schematically in the lower portion of Fig. 3.3. The function has zero slope at the origin and then decreases to zero amplitude smoothly as the window expands. The size of the object along the propagation direction of the incoming wave is given by the distance from the center of the scatterer to the edge of the characteristic function.

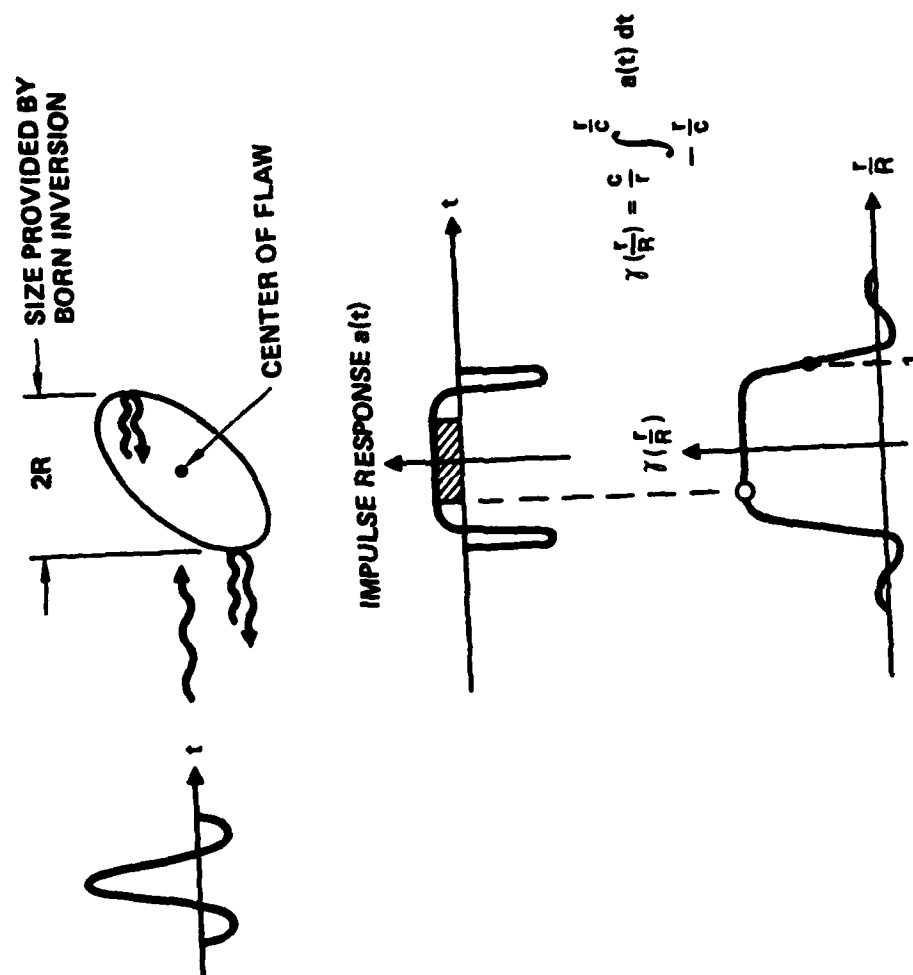


Fig. 3.3 Illustration of one dimensional Born inversion.

The algorithm used in the Test Bed operates in the frequency domain but performs all of the equivalent functions described for the time domain version. The expression for the characteristic function is given by:

$$\gamma(t) = \frac{c}{r} \int_{-\infty}^{\infty} \frac{1}{\omega} A(\omega) \sin \omega t d\omega \quad (3.1)$$

where  $A(\omega)$  is the conditioned input spectrum obtained from the flaw. The key steps in the algorithm are listed below:

1. Divide spectrum by frequency:  $A'(\omega) = \frac{A(\omega)}{\omega}$ .
2. Obtain inverse transform of  $A'(\omega)$  designated  $\gamma'(t)$ .

$$\gamma'(t) = \int_{-\infty}^{\infty} A'(\omega) \sin \omega(t) d\omega$$

3. Rescale the resulting time axis by (acoustic velocity)/2 to convert the time units to distance units measured from the center of the flaw. This radius coordinate is designated  $r$ .
4. Divide the resulting function by  $r$ . A linear extrapolation of the two data points closest to  $r = 0$  is used to obtain the undefined point at  $r = 0$ . The resulting function is the characteristic function.
5. The radius estimate is obtained by calculating the area under the characteristic function and dividing it by its peak height. This has been found to work better than a variety of other radius estimators which were investigated.

6. In the curves that are plotted, the characteristic function is normalized through division by the value of the peak amplitude point. Further, since the curve is symmetric about  $r = 0$ , only one half is plotted.

### 3.2.3 Testing of the Algorithm

Much of our time has been occupied with the testing and refining of the Born inversion algorithm. First the effect of several parameters on the accuracy of the algorithm was investigated. The parameters that have been identified as being of interest include:

1. the signal to noise ratio of the measured flaw signal,
2. the ratio of the mid-band wavelength of the transducer to the radius of the flaw,
3. the bandwidth of the transducer,
4. the curvature of the wavefronts incident on the flaw,
5. the geometric shape of the flaw.

To minimize the effects of unknown or unwanted parameters, the theoretical scattering spectrum from a flaw was used as an input signal and the effects of the desired parametric changes on the predicted flaw radius were noted.

To test the sensitivity of the Born inversion to the presence of noise in the data, simulated experimental waveforms were synthesized. These waveforms consisted of the calculated scattering signal from a spherical void with a noise signal added. The noise signal was designed to simulate the scattering of ultrasound by grains in the host material. This type of noise has a power spectrum proportional to  $f^4$  ( $f$  = frequency) and the noise waveform spectrum is given by:

$$N_g(f) = \left(\frac{f}{f_0}\right)^4 N(f) \quad , \quad (3.2)$$

were  $f_0$  is a reference frequency and  $N(f)$  is a complex valued, white, Gaussian noise spectrum consisting of samples of a Gaussian random variable,  $v(f)$ , for which

$$E[v(f) v(f')^*] = \sigma_f^2 \delta_{ff'} \quad . \quad (3.3)$$

Where  $E$  represents the operation of averaging over the members of the ensemble,  $v(f)$  is one member of the noise ensemble,  $\sigma_f^2$  is the variance of  $v(f)$  and  $\delta_{ff'}$  is the Kronecker delta. The parameter  $f_0$  is chosen arbitrarily to be the maximum frequency of the sampled waveform. The mean energy in  $N_g$  is therefore

$$U_g = \Delta f \sum_{f=-f_0}^{f_0} \sigma_f^2 \left( \frac{f}{f_0} \right)^4 \quad . \quad (3.4)$$

The energy in the simulated signal is

$$U_s = \Delta f \sum_{f=-f_0}^{f_0} |A(f)|^2 \quad , \quad (3.5)$$

where  $A(f)$  is the calculated spectrum of the signal. The signal-to-noise ratio of the simulated experimental waveforms is defined to be

$$(S/N)^2 = \frac{\text{energy in flaw signal}}{\text{mean energy in noise signal}} \quad (3.6)$$

$$(S/N)^2 = \frac{U_s}{U_g} \quad , \quad (3.7)$$

where the bandwidth extends from 0 to  $f_0$ .



The simulated waveforms are calculated in the frequency domain, then multiplied by the measured spectrum of an ultrasonic transducer and finally put into the time domain. These operations can be written in the form

$$a_x(t) = \mathcal{F}^{-1} \{X(f) \cdot [A(f) + N_g(f)]\} \quad 3.8$$

where  $a_x(t)$  is the simulated flaw waveform,  $A(f)$  is the calculated spectrum of the signal,  $N_g(f)$  is the spectrum of the grain scattering noise,  $X(f)$  is the transducer spectrum and  $\mathcal{F}^{-1}$  refers to a Fourier transform from frequency to time domains. The Born inversion algorithm is then applied to the waveforms in the same way that it is applied to experimental signals.

Figure 3.4 shows simulated and experimental flaw waveforms. The upper curve is an experimental waveform recorded for an 800  $\mu\text{m}$  diameter spherical void. The middle and lower curves are simulated flaw waveforms. The middle curve contains no noise and the lower curve contains enough noise to produce a signal to noise ratio of 0 dB as defined in Eq. 3.6. The similarity between the simulated and the measured waveforms demonstrates the accuracy of the model used to create the simulated waveforms.

The transducer  $X(f)$  used in Eq. 3.8 was assumed to be a cosine-squared function that was centered at 5 MHz and had zero amplitude at below  $f = 0$  and above 10 MHz. The calculated spectrum was always that of a spherical void. Three different sizes of spheres were used. The different sized spheres have different portions of their spectrum within the 0-10 MHz bandwidth of the transducer; thus providing a test of the sensitivity of the Born inversion algorithm to the combined effects of noise and limited bandwidth. The radius estimates obtained for ensembles of noisy signals as a function of signal-to-noise ratio are shown in Figs. 3.5, 3.6 and 3.7. Both the average radius and the 95% confidence limits are shown for spheres having diameters of 400  $\mu\text{m}$ , 800  $\mu\text{m}$  and 1200  $\mu\text{m}$ . Each radius represents the average of 100 signals each composed of the calculated scattering amplitude and an

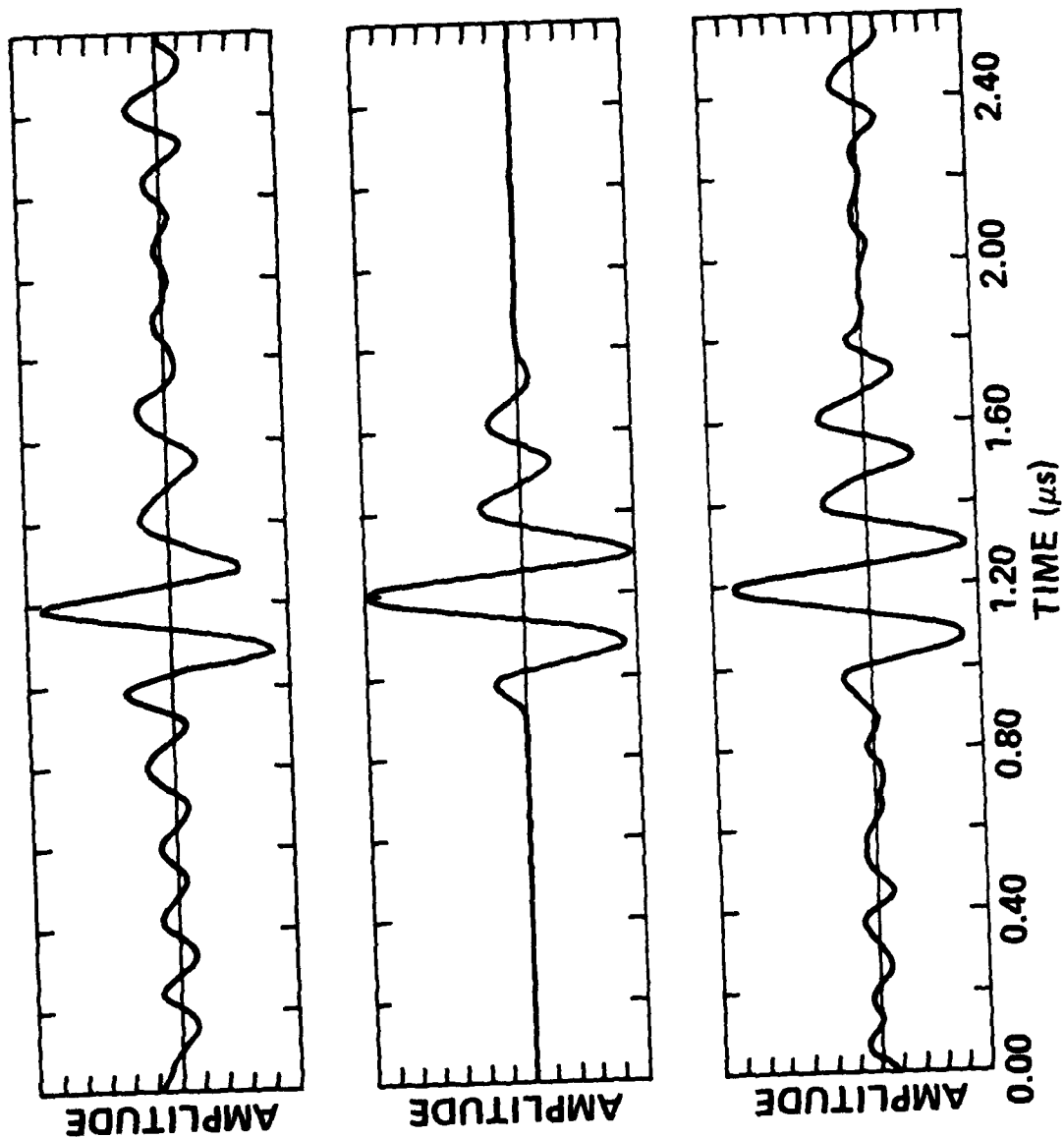


Fig. 3.4 Experimental and simulated flaw waveforms including grain scattering noise.

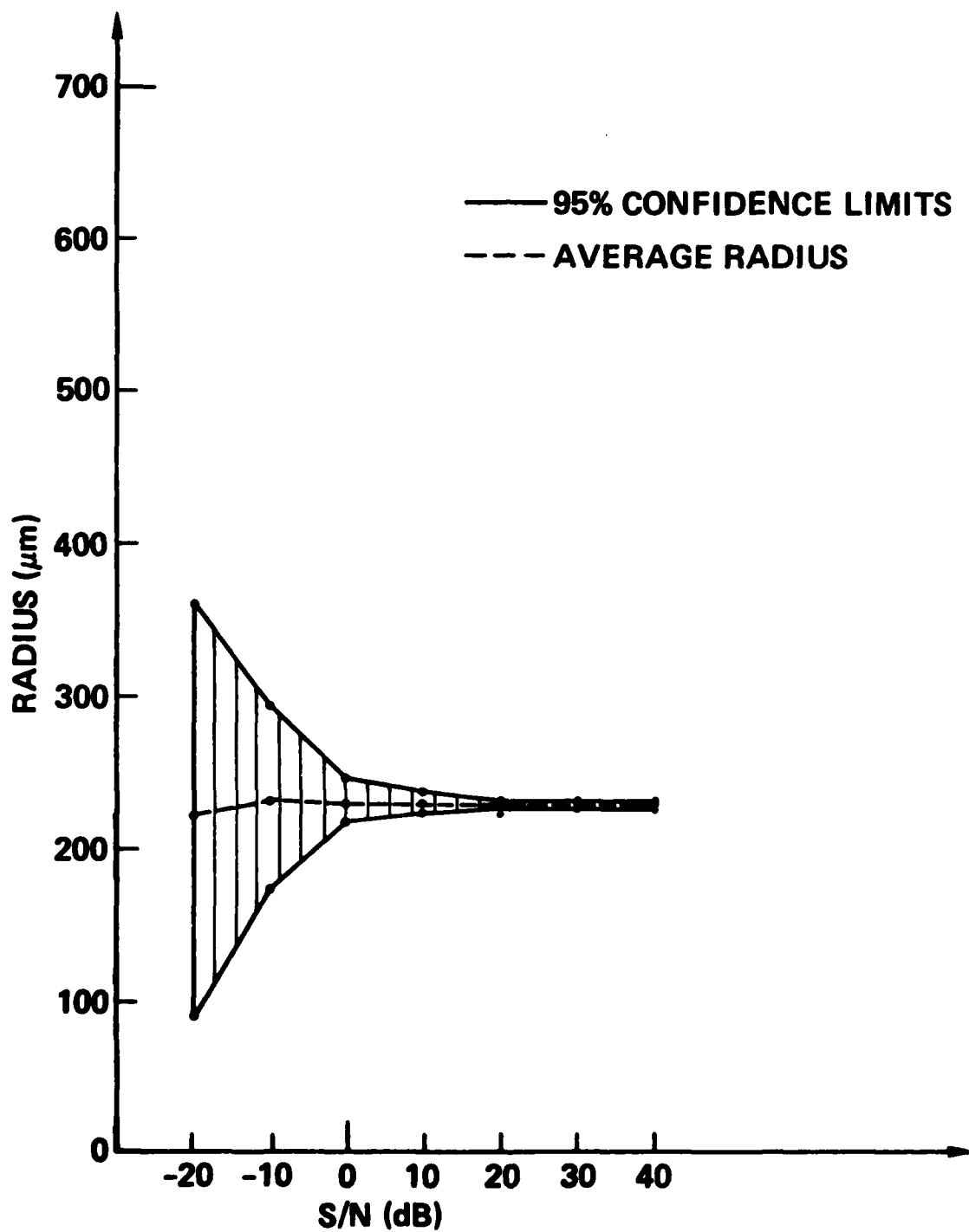


Fig. 3.5 Radius estimates for ensembles of noisy flaw waveforms vs signal-to-noise ratio for a 200  $\mu\text{m}$  radius spherical void.

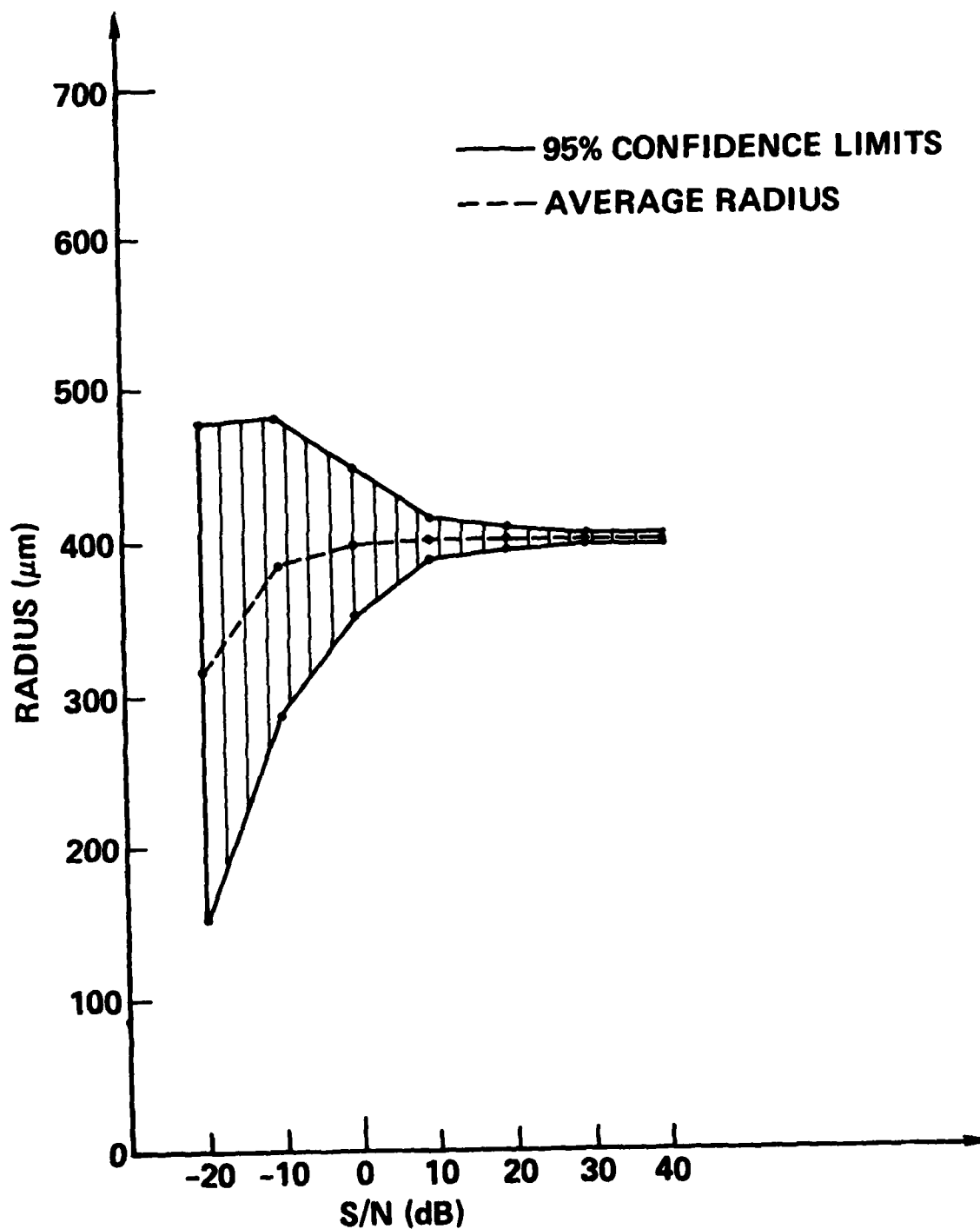


Fig. 3.6 Radius estimates for ensembles of noisy flaw waveforms vs signal-to-noise ratio for a 400  $\mu\text{m}$  radius spherical void.

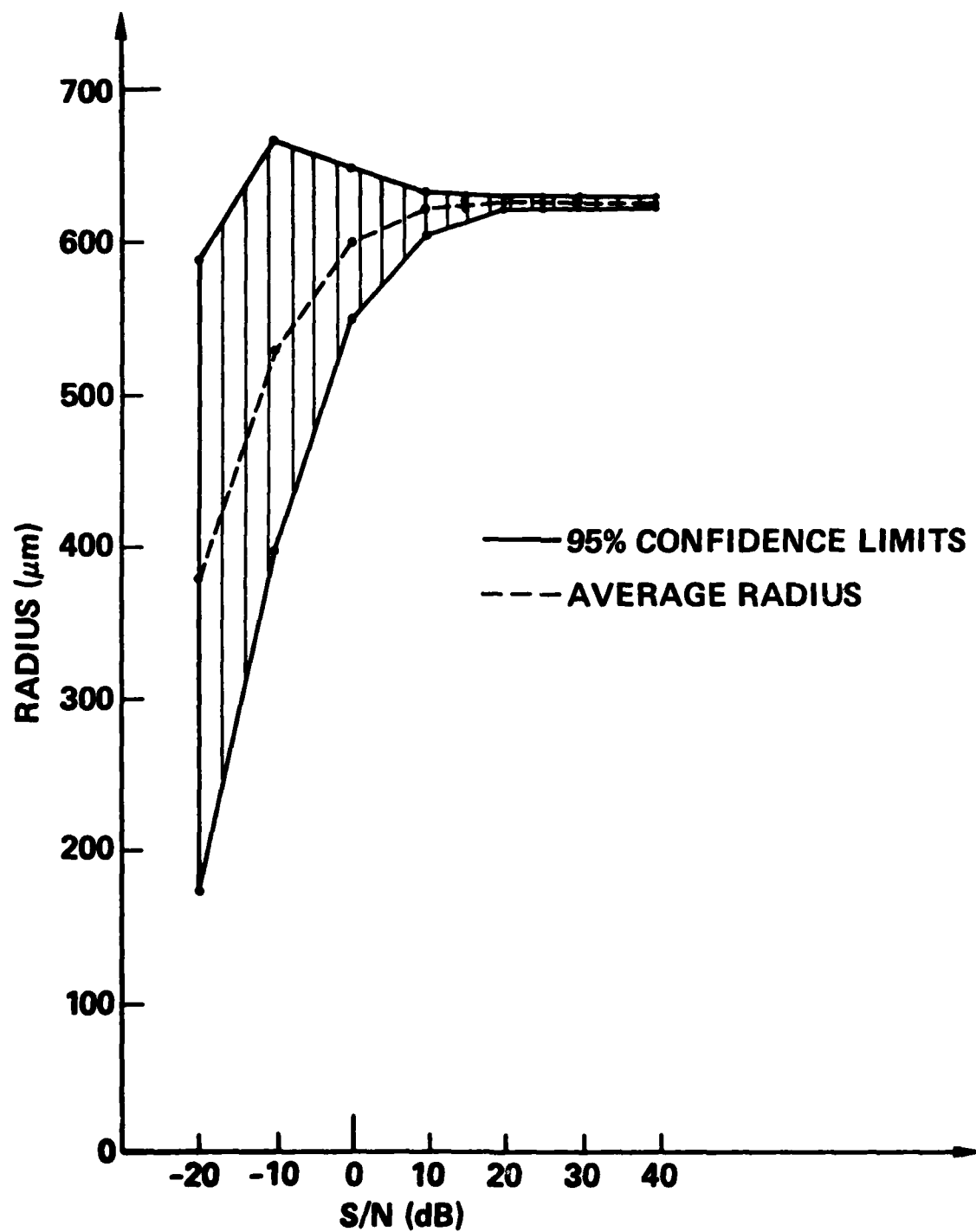


Fig. 3.7 Radius estimates for ensembles of noisy flaw waveforms vs signal-to-noise ratio for a 600  $\mu\text{m}$  radius spherical void.

independent noise waveform from the ensemble. Each of the noise waveforms has the same mean energy. In Fig. 3.5, 3.6 and 3.7, the dashed curve shows the mean radius estimate vs signal-to-noise ratio. The solid curves show the 95% confidence levels for the ensemble. As the signal-to-noise ratio decreases, the uncertainty of the estimates increases and the mean of the estimates eventually becomes inaccurate too. Note that the 95% confidence level is within  $\pm 10\%$  of the correct answer for signal-to-noise ratios as low as 0 dB. Examples of signals in the presence of this level of grain scattering noise are shown in Fig. 3.4. The systematic decrease in the mean value is conjectured to be related to the method of estimating the radius from the characteristic function described above. The area under the characteristic function is probably not significantly affected by the noise, but it is likely that the peak height is increased by the noise and causes the radius estimate to be decreased. The values of the mean estimates for high signal-to-noise ratios are close to the correct answer for the 800  $\mu\text{m}$  and 1200  $\mu\text{m}$  diameter spheres where the bandwidth of the transducer is encompassing the appropriate portion of the sphere scattering spectrum. For the 400  $\mu\text{m}$  diameter sphere, the mean radius estimate is becoming too large and reflects the lack of adequate high frequency data. The reason for this will be explained below.

The effect of transducer center frequency and bandwidth on the radius predictions provided by the Born inversion can be significant. A suitable technique for selecting a transducer was previously outlined in the protocol section. To understand how the bandwidth affects the results, it is helpful to consider the magnitude of the scattering spectrum from an ellipsoidal flaw. The spectrum for a spherical void is shown in Fig. 3.8 where the amplitude is plotted vs  $ka$ . The details of the spectrum will change as the material properties of the host material and the flaw are varied; however, certain major features will remain essentially unchanged. In the low  $ka$  region the amplitude of the scattering always increases in proportion to the square of the frequency. The first peak generally occurs at approximately  $ka = 1$ ; although for certain inclusion types, it can get as high as  $ka = 2$ . Finally this first peak is always followed by many other peaks that are not,

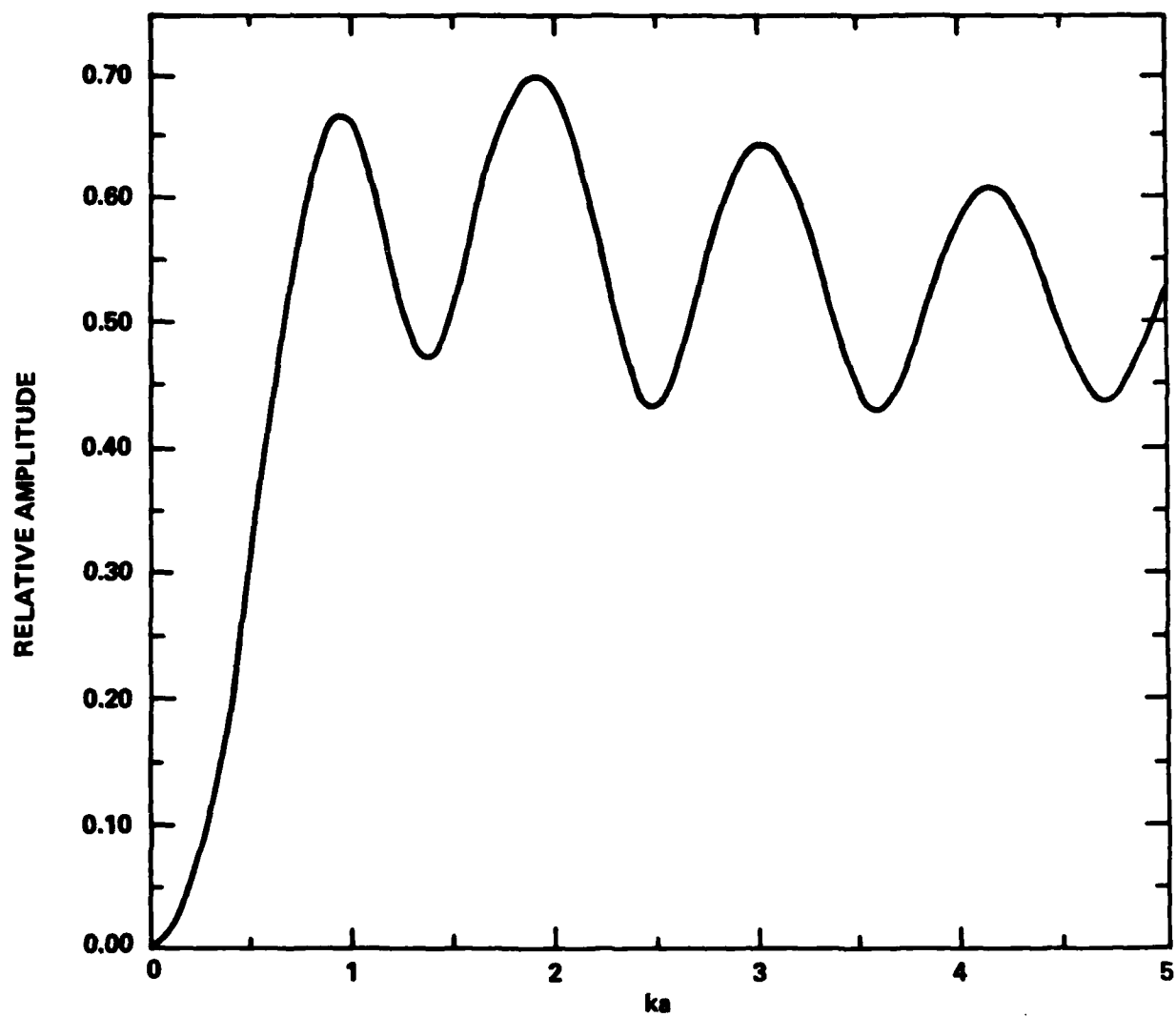


Fig. 3.8 Magnitude spectrum for a spherical void.

in general, equally spaced nor do their amplitudes have any simple relationship to one another. The Born inversion technique is sensitive to the portion of the spectrum that includes the first peak. It is therefore essential that the bandwidth of the transducer used to obtain data for the Born inversion encompass this first peak. This requirement can become severe for ellipsoidal flaws with a factor of two or more difference in the lengths of the major and minor axes. It is sometimes necessary to resort to the use of two or more transducers in these cases.

Figure 3.9 shows radius estimates obtained using calculated scattering data for a spherical void when the bandwidth is limited. The dashed curve shows the effects of raising the minimum  $ka$  value present in the data. The result is an underestimate of greater than 20% when  $ka_{\min} > 0.5$ . The solid curve shows the effect of lowering the maximum  $ka$  value present in the data. The result is an overestimate of greater than 20% when  $ka_{\max} < 2$ . From this somewhat simplified analysis one can conclude that the bandwidth required to obtain radius estimates accurate to 20% must extend from  $ka = 0.5$  to  $ka = 2$ . If insufficient low frequency data is available, then an underestimate is obtained and if insufficient high frequency data is available, an overestimate is obtained.

An ultrasonic transducer limits both the high and low frequencies. Figure 3.10 illustrates the effect of having both limits on the radius estimates. The curves shown in Fig. 3.10 are calibration curves obtained for a particular type of bandpass window that corresponds to the windows used to generate Fig. 3.9. The high frequency limit was provided by a cosine squared window centered at  $f = 0$  and decreasing to zero at  $f_{\max}$ . The low frequency window was a rectangular window that truncated the calculated scattering data at  $f_{\min}$ . For this particular case the results show that as the center frequency of the transducer decreases all of the calibration curves coalesce into one curve that overestimates the radius of the flaw. As the center frequency of the transducer increases, the calibration curve tends to first run parallel to a line of constant radius and then decrease. An analysis of



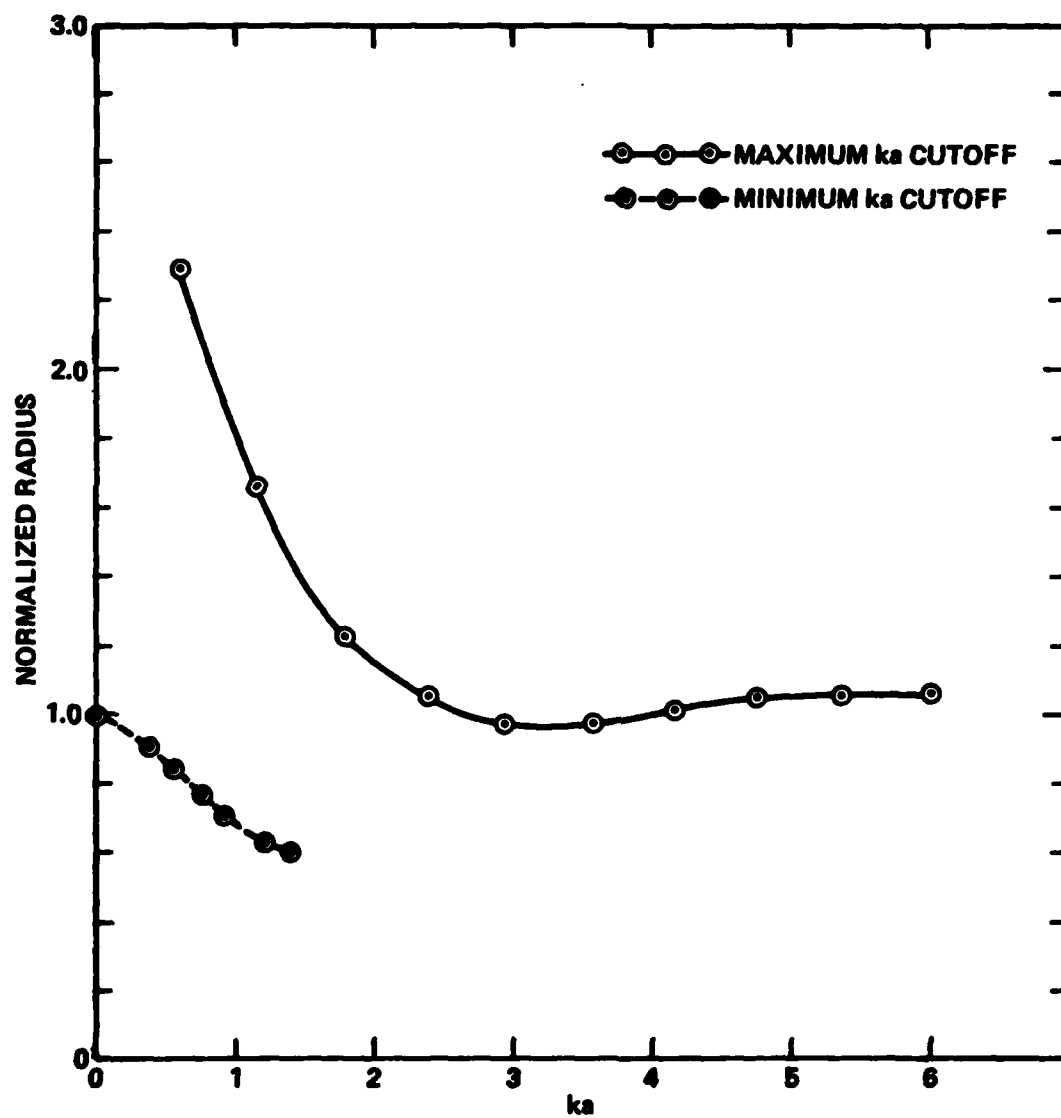


Fig. 3.9 Effect of limited bandwidth on the accuracy of the Born inversion.

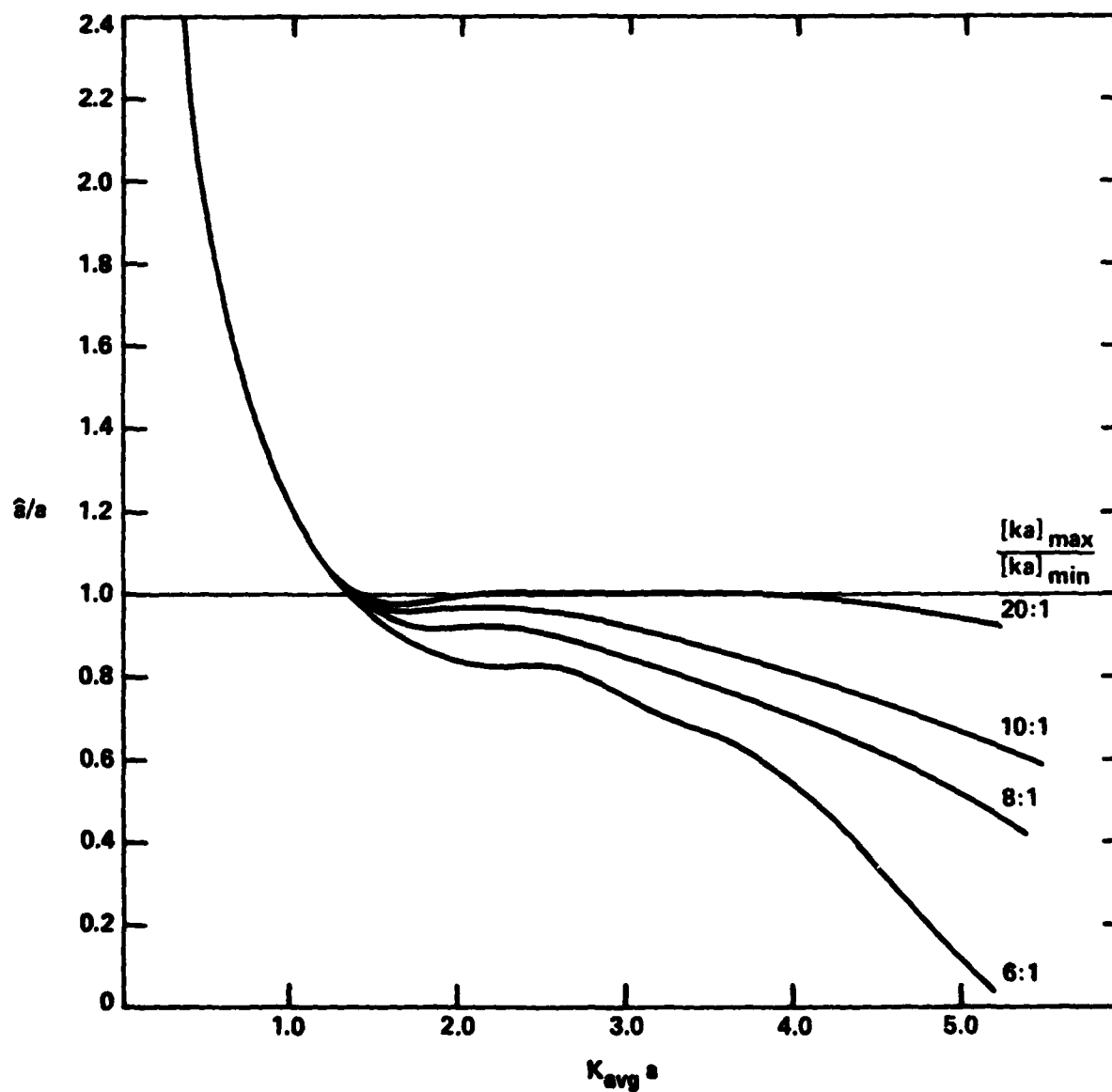


Fig. 3.10 Normalized calibration curves for the Born inversion algorithm with different bandwidths and center frequencies.

the curves shows that they decrease below 80% of the true radius when the low frequency end of the transducer bandwidth as defined above exceeds a frequency corresponding to  $ka \approx 0.75$ . The curves increase above 120% of the true radius when the high frequency end of the transducer bandwidth defined above is reduced below a frequency corresponding to  $ka \approx 1.8$ . Thus for a simulated transducer we obtain requirements for  $ka_{\min}$  and  $ka_{\max}$  that are not too different from the crude estimates that were made above. One should use caution in applying these results to an experimental situation since the particular bandpass characteristics associated with the transducer and the desensitized deconvolution function must be known. When these characteristics are known a calibration curve can be calculated. This curve can be used to correct the estimate obtained from the Born inversion for the errors caused by a lack of bandwidth or because the center frequency of the transducer is too high or too low.

In situations where the true radius of a scatterer is unknown, a set of normalized curves like those shown in Fig. 3.10 are not too useful. Note, however, that these curves can be replotted in the form shown in Fig. 3.11. In this case, it is only necessary to know the bandwidth and center frequency of the transducer. The entry point on the vertical axis is obtained from the radius predicted by the Born inversion. The actual radius can be found by drawing a horizontal line from the entry point to the particular transducer curve that is relevant to the experimental situation, and then drawing a vertical line from this intersection to the horizontal axis. If the intersection with the calibration curve occurs in the region where the curves have coalesced, the center frequency of the transducer should be increased. Although it is not shown in Fig. 3.11, the curves all bend over and drop to low values for sufficiently high transducer center frequencies. This apparently occurs because the minimum frequency of the transducer is no longer encompassing the lowest peak in the magnitude scattering spectrum of the flaw. The Born inversion algorithm is beginning to interpret the second peak as if it were the first peak. Presumably, the calibration curves will be cyclic as the center frequency of the transducer is raised. From an experimental viewpoint, it is this aspect of the Born inversion algorithm's

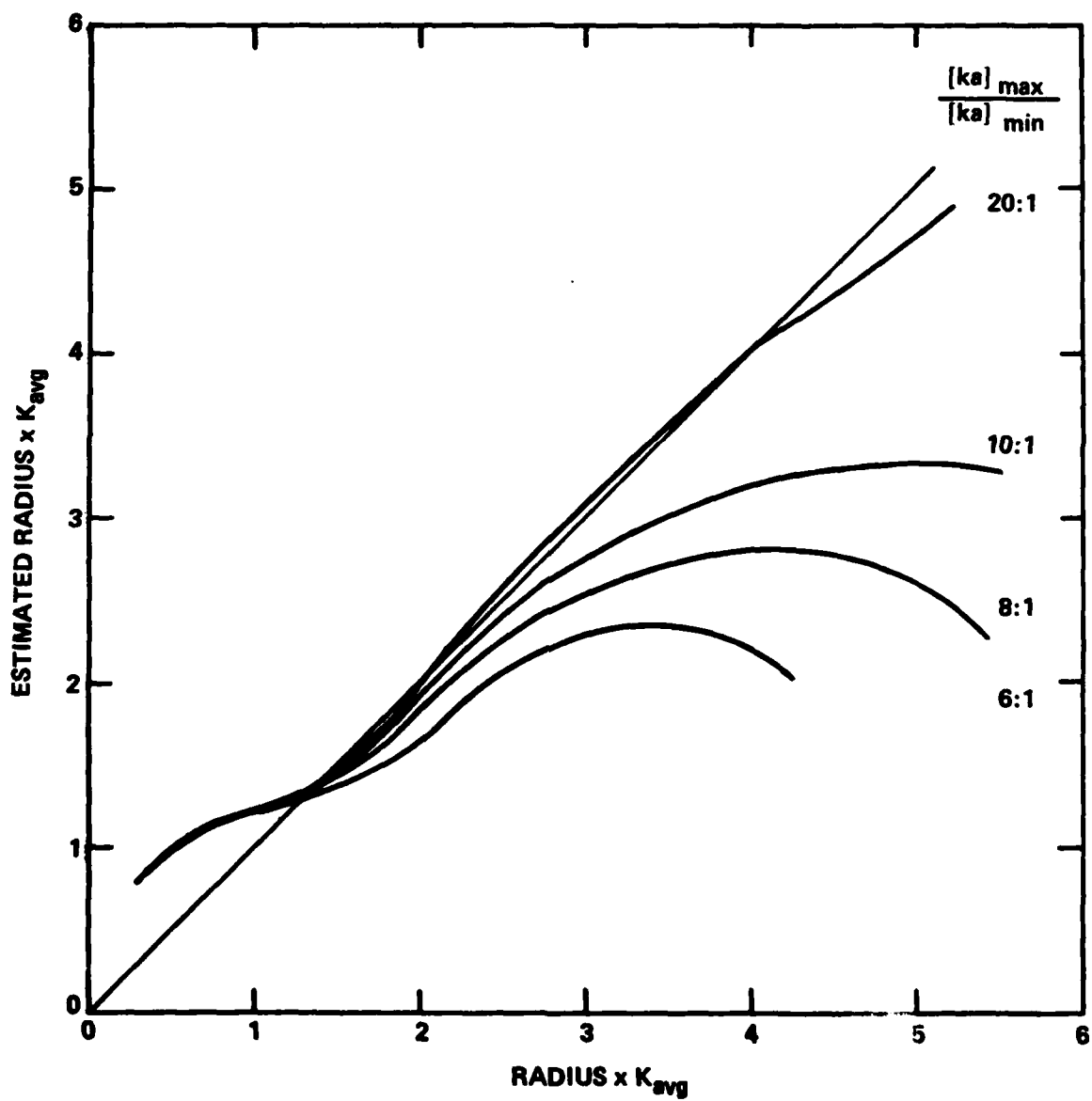


Fig. 3.11 Calibration curves to be used when the flaw radius is not known.

operation that requires a preliminary look at the magnitude spectrum of the flaw to insure that the bandwidth of the transducer is encompassing the first peak. If this is not true, the radius estimates provided by the algorithm are likely to be in error by a factor equal to the ratio between the frequencies of the second and first peak of the scattering spectrum.

From this investigation, it can be concluded that the bandwidth requirements of the Born inversion are not very severe. The required ratio of the maximum to minimum frequencies is between 2.4:1 and 4:1 depending on the exact nature of the transducer bandshape. Since many commercially available transducers have bandwidths with  $f_{\max}/f_{\min} = 8$ , they can be used for acquiring scattering data. A single transducer can be used for obtaining accurate radius estimates of flaws with radii variations of 3.3:1 to 2:1 if it has the appropriate center frequency. As an example, a transducer with a center frequency of 5 MHz,  $f_{\min} = 1.1$  MHz and  $f_{\max} = 8.9$  MHz would be capable of measuring flaw radii in titanium with maximum values ranging from 460  $\mu\text{m}$  to 690  $\mu\text{m}$  and minimum values ranging from 205  $\mu\text{m}$  to 230  $\mu\text{m}$ . The exact range would of course depend on the detailed shape of the transducer bandpass and the signal-to-noise ratio.

The next area of concern about the performance of the Born inversion technique involves the distortion of the incident wave by the entry surface of the part. This can occur when flaws are located below curved surfaces or when the incident wave must propagate obliquely through a flaw surface. There are two potential problems involved. First, the theory for the Born inversion assumes that a plane wave is incident on the flaw. It is not known how the accuracy is affected if this wavefront becomes curved or otherwise distorted. Second, the deconvolution technique uses a reflection off a flat surface as a reference. In the first case, the focusing or distortion of the wave at the flaw can in principle be removed via a backward wave propagation technique; although in practice, this is not done. In the second case, the consequences of the deviation of the wavefront from a plane wave on the character of the deconvolved waveform are not known.

The errors caused by these wavefront distortions can be calculated for specific geometries and experimental situations, but this was beyond the scope of this program. Furthermore, this calculation did not seem essential to the primary goal of determining how the inversion technique would work in practical situations. In lieu of a theoretical calculation, an empirical approach has been used to evaluate errors that are encountered with some common geometries. The reference waveform is typically the signal obtained from reflection at normal incidence of a wave from the backface of the specimen being examined. In the cases that have been tried, the backface is about 10 to 20 wavelengths further along the path of propagation than the flaw. In a few cases, a backface echo from a separate specimen made of the same material has been used as a reference. The signal waveforms back-scattered from the flaw have been obtained using both waves that are incident normally on the front surface of the specimen and waves that are incident at various angles, with the maximum angle corresponding to an internal refraction angle of  $60^\circ$ . In all cases, the deconvolution has been computed using the backface echo obtained from the normally incident wave. Both the backface and the flaw were in the far field of the transducer. A number of flaws having known sizes were examined and the data was analysed using the Born inversion algorithm. There was no evidence that there were any errors being generated via the deconvolution that could be attributed to wavefront distortion. Some backscattered signals have also been acquired through a concave cylindrically curved interface with a radius of curvature of 3.5 inches. The data has not been exhaustively tested but the initial indications are that an underestimate of between 10% and 25% is obtained. Although these errors are not considered significant, the possibility that curved wavefronts could cause systematic errors should be considered when using the Born inversion. In these tests, the reference waveform was obtained from a flat surface. No investigation was made of the effect of focused beams on the accuracy of the Born inversion.

### 3.2.4 Experimental Results

Experiments involving the acquisition of data from flaws and requiring the use of various aspects of the protocol have been conducted concurrently with the other investigations. Most of the experiments have been conducted using known flaw types that have been machined into titanium pieces which were subsequently diffusion bonded. This procedure<sup>9</sup> for fabricating samples with known defects was developed at the Science Center and has been extensively used to produce a variety of flaw types including:

1. Ellipsoidal voids
2. Spherical inclusions
3. Simulated fatigue cracks.

A set of samples were specifically prepared for this program that were designed to simulate turbine bore samples. These samples are described in Appendix A. A sample was also obtained from Rolls-Royce Ltd. that contained a naturally occurring flaw. This sample provided an example of the performance of the Born inversion algorithm when the characteristics of the flaw were unknown.

#### 3.2.4.1 Description of Experiments

Much of the data was acquired from spherical flaws located in titanium disks. The disks are 4 in. in diameter and 1 in. thick. They are made from extruded titanium bar stock. The apparent grain size looking along the extrusion direction is relatively small and creates a low amplitude ultrasonic grain scattering noise. In the transverse direction, the grains are considerably larger and the grain scattering noise level is significant compared to the signal levels.

Experimentally the first problem is the detection of the flaw. Although there are a variety of techniques for enhancing the reliability of detection through detailed analysis of a tentative flaw indication, the first

task is to determine that there is something present in the waveform to be analyzed. This means that the signal-to-noise ratio must be sufficiently high that the amplitude of the signal is above the noise for part of the time that it is present. Therefore the initial detection is accomplished using an amplitude threshold technique.

It is desirable to obtain as high a signal to noise ratio as possible. This can be achieved by either increasing the signal level or decreasing the noise level. The major noise sources are either thermal noise generated in the electronic amplifier, grain scattering noise in the material being investigated, or residual transducer "ring down" signals from the front face of the part. The thermal noise can be reduced through the time averaging of multiple signals. The grain scattering noise can in principle be reduced through the spatial averaging of multiple signals, but this has not been achieved in practice. The transducer "ring-down" noise can be reduced by subtracting two signals acquired from different spatial regions of the part but having identical front surface echos. For the Test Bed work, the time averaging of waveforms and subtraction have been used where necessary to reduce thermal and "ring-down" noise below the level of the grain scattering noise. Subtraction has been able to suppress front surface "ring-down" noise by 25-30 dB. This makes the grain scattering noise the dominant source of noise in most of the experimental work. The strength of this noise source increases as the square of the frequency and this must be considered when selecting a transducer.

The other approach to enhancing the signal-to-noise ratio is to increase the signal level. If grain scattering noise is dominant, simply increasing the output of the transducer will not help, since the amplitude of the grain scattering noise rises in proportion to the strength of the incident signal. The signal level can be increased by focusing the transducer provided the size of the defect is less than the focal spot size of the beam. A decrease of the spot size diameter by a factor of two increases the signal-to-noise ratio by 12 dB. Since the minimum spot size is dependent on the



wavelength, higher frequency transducers will produce smaller spots and correspondingly higher signals. Note that this frequency dependence and that of the grain scattering tend to cancel. In some cases the flaw is oriented in an unfavorable way and the backscattered signal amplitude is weak. The situation can sometimes be improved by tilting the transducer relative to the flaw and thereby obtaining a larger backscattered signal.

The four inch diameter titanium disk samples allow high signal to noise ratio signals to be obtained. Consequently, the samples containing 400  $\mu\text{m}$ , 800  $\mu\text{m}$  and 1200  $\mu\text{m}$  diameter spherical voids have been extensively used to investigate experimentally the effects of transducer bandwidth on the accuracy of the Born Inversion. Although the flaw location in these samples is known, a search mode with a C-scan image output was employed using the techniques outlined above to enhance flaw detectability. An example of one of these is shown in Fig. 2.15.

As explained in Section 3.2.1, the signals for the Born inversion are deconvolved to remove the transducer dependent components. In principle the reference signal used in the deconvolution should be obtained from a plane surface that is the same distance from the front face of the part as the flaw. In practice, it has been determined that a reference signal from the back face of the part or from a plane surface in another part made from the same material works satisfactorily. This allows a single reference signal to be used for the deconvolution of signals acquired at different angles relative to the flaw. There is some question about the problem that may occur for flaws located below curved surfaces; i.e., is it necessary to obtain a reference signal from a plane below the same curved surface? For modest curvatures the errors introduced appear to be small; however, an extensive study of the effect was not conducted.

When the Born inversion algorithm is used to obtain the size of a flaw, the location of the center of the flaw has to be precisely determined. The centroid of the pulse that is backscattered from the flaw is used as an initial estimate of the center of the flaw and is sufficiently accurate to

obtain a deconvolved waveform during the pre-processing of the signal as indicated in Section 3.2.1. Two techniques have been used to obtain a more precise estimate of the flaw center. The first technique requires that the characteristic function, defined in Section 3.2.2, have a flat top when it intersects the axis at  $r = 0$ . This is an empirical technique that does not have a strong theoretical basis. It does provide accurate answers in cases where the bandwidth of the transducer is centered on the portion of the flaw scattering spectrum containing the first peak. There are two steps involved in obtaining the time shift. First the data is analysed using the Born inversion algorithm with a range of time shifts both positive and negative relative to the centroid of the pulse. This results in a curve of the type shown in Fig. 3.12. The fact that some of the excursions of the curve are positive and some are negative is not relevant. The sign is dependent on the pre-processing of the signal and either sign is acceptable. The important characteristic of this curve is the shape. Note that in the region from  $t \approx -0.05$  to  $\approx 0.15$ , the curve has a sharp minima, a broad local maxima, and a second minima that is less sharp than the first. This shape forms a recognizable signature and it is known that the center of the flaw is located near the second minima and displaced to the left of it. The exact location is determined by generating a sequence of characteristic functions for time shifts ranging from  $t = 0$  to  $t = 0.1$  and recording which curve has a maximally flat top at the origin. The radius estimate associated with this curve is taken as the radius of the flaw. The curve in Fig. 3.12 was generated using data obtained from an 800  $\mu\text{m}$  diameter spherical void with a nominal 5 MHz transducer. Note that the radius estimates between the broad local maxima and the second minima range from  $\approx 270 \mu\text{m}$  to  $\approx 390 \mu\text{m}$ . Since the correct value is 400  $\mu\text{m}$ , the lowest estimate is only in error by about 32%. For many applications this may be acceptable, in which case the determination of the maximally flat characteristic function is unnecessary. Some caution should be used with this latter approach since the variation of the maximum error as the flaw spectrum shifts within the transducer bandwidth has not been investigated. Furthermore, inclusions and other flaw types may produce different results.

The second technique for determining the center of the flaw is rigorously correct. It involves the use of long wavelength data to determine

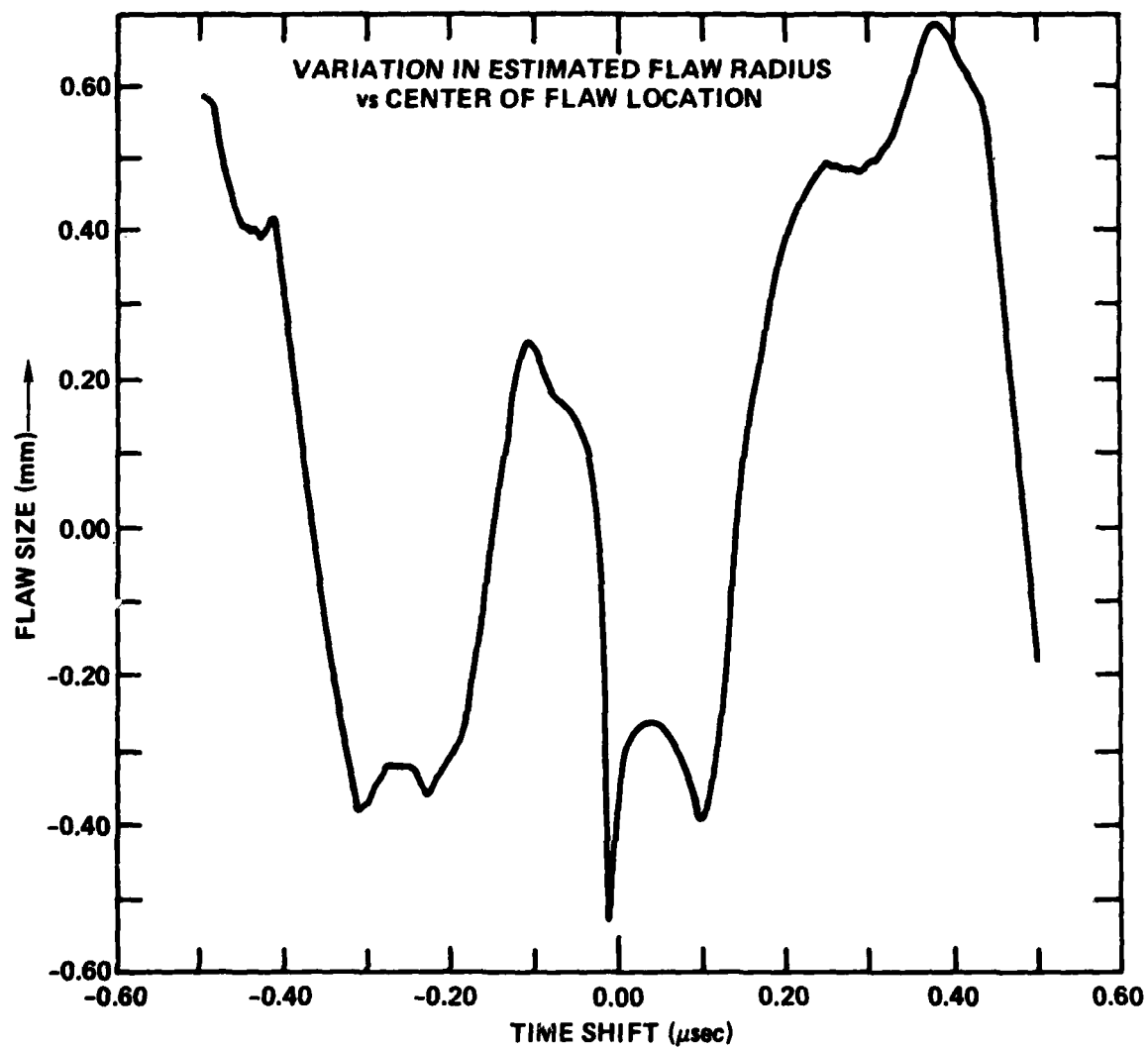


Fig. 3.12 Born inversion estimates of flaw radii vs time shifts of the flaw response relative to its centroid.

the phase of the deconvolved flaw signal. When the time corresponding to the center of the flaw is correctly chosen, the phase at low frequencies (corresponding to  $ka < 0.5$ ) is constant and has a value that is an integral multiple of  $\pi$ . This method was described in Section 3.2.1

#### 3.2.4.2 Spherical Flaws

Experimental data was acquired from the spherical voids on many occasions and using several different transducers. There are two sets of data that will serve to summarize the results. One set of data was acquired from an 800  $\mu\text{m}$  diameter spherical void using the transducer placement pattern shown in Fig. 3.13b. The geometry and definition of the angles  $\theta_i$  and  $\phi_i$  are shown in Fig. 2.13. Note that the angles specified in Fig. 3.13b are internal angles. The signals were acquired using a 5 MHz transducer with a -20 dB full bandwidth of 5.50 MHz. The results are given in Table 3.1. The mean diameter is 390  $\mu\text{m}$  and the error bars to the 95% confidence level extend  $\pm 30 \mu\text{m}$  about this mean.

The second set of data was acquired from a 1200  $\mu\text{m}$  diameter spherical void using the transducer placement pattern shown in Fig. 3.13a. The geometry and definition of the angles are the same as for the 800  $\mu\text{m}$  void. In this case the signals were acquired using a 2.25 MHz transducer with a -20 dB full bandwidth of 2.65 MHz. The three plots shown in Fig. 3.14 summarize the results. The Born inversion assumes that the object measured has inversion symmetry. This implies that the diameter is being measured; thus each measurement produces two points on the polar plots in Fig. 3.14. To show a full cross section, the data obtained for two values of  $\phi_i$  are combined in each of the diagrams. Thus the first cross section includes data acquired at  $\phi_i = 0^\circ$  and  $180^\circ$  for  $\theta_i = 0, 30^\circ, 45^\circ$ , and  $60^\circ$ . Similarly the data at  $\phi_i = 120^\circ$  and  $300^\circ$  is combined in the second cross section and that for  $\phi_i = 60^\circ$  and  $240^\circ$  in the third. The cross sections shown correspond to  $\phi_i = 0, 60^\circ$  and  $120^\circ$  and  $\theta_i = 0^\circ, \pm 30^\circ, \pm 45^\circ$ , and  $\pm 60^\circ$ . The mean diameter is 1320  $\mu\text{m}$  and the error bars to the 95% confidence level extend  $\pm 210 \mu\text{m}$  about this mean. The mean diameter is approximately 10% high. About half of this error can be attributed to the bandpass of the transducer being centered somewhat below the optimum frequency, while the

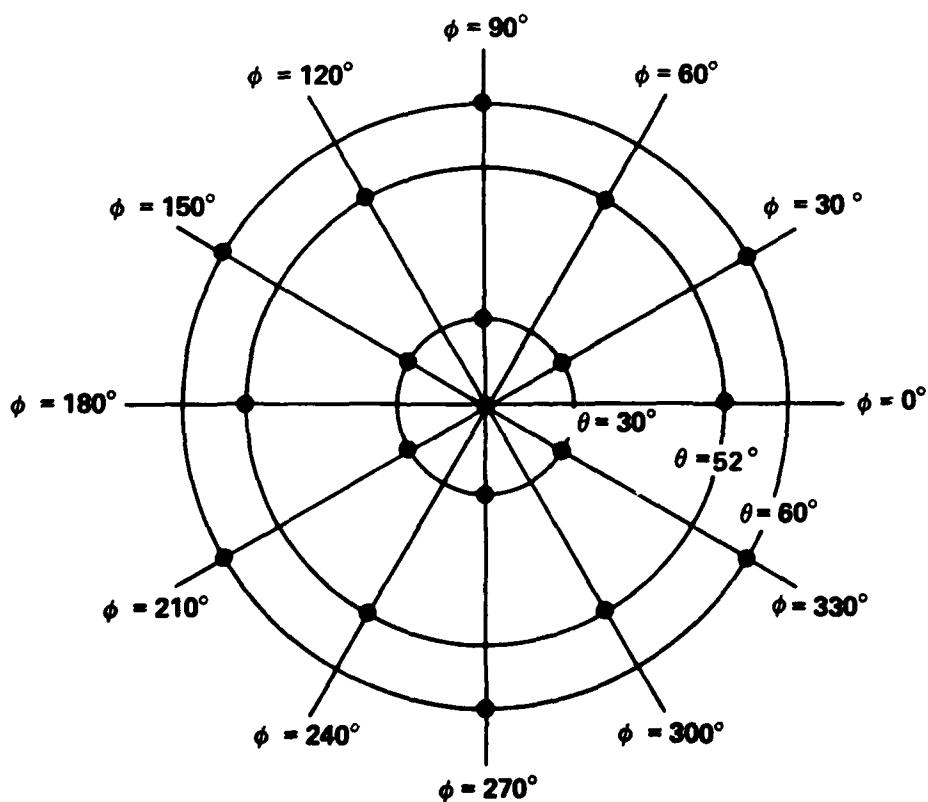
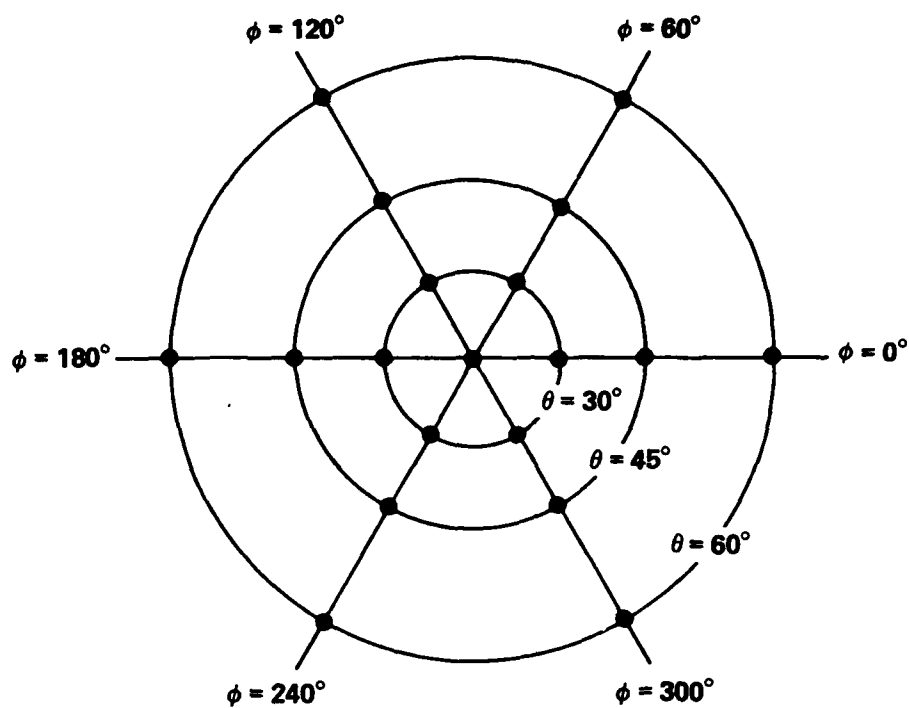


Fig. 3.13 Transducer placement patterns for interrogation of (a) 1200  $\mu\text{m}$  diameter flaw and (b) 800  $\mu\text{m}$  diameter flaw.

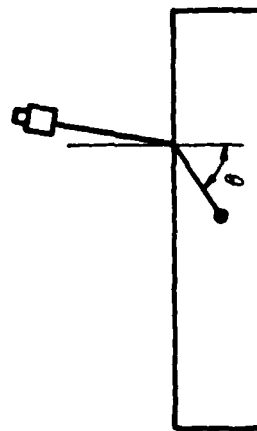
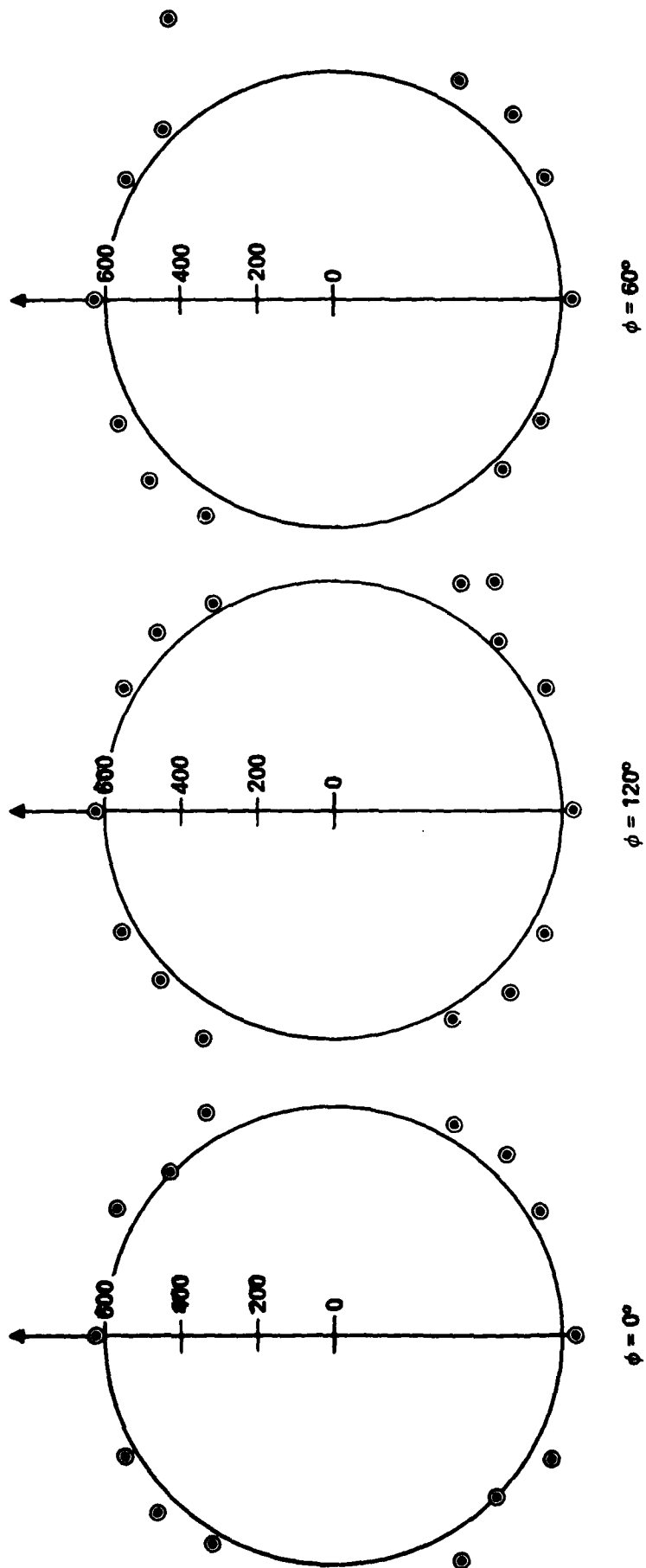


Fig. 3.14 Results of Born inversion algorithm analyses of scattering data from a 1200  $\mu\text{m}$  spherical void.

Table 3.1  
Results of Born Inversion Analysis of An  
800  $\mu\text{m}$  Diameter Spherical Void

$\theta_i$ (degrees)	$\phi_i$ (degrees)	Estimated Radius ( $\mu\text{m}$ )
0	0	390
30	30	390
30	90	390
30	150	390
30	210	390
30	270	390
30	330	380
52	0	420
52	60	380
52	120	390
52	180	390
52	240	440

remaining error can be accounted for by uncertainties in the actual size and shape of the defect.

#### 3.2.4.3 Oblate Spheroids

A test of the Born inversion algorithm with an ellipsoidal void was more difficult because of the wide bandwidth required and the need to acquire data with two transducers having different center frequencies. Several attempts were made to acquire data from ellipsoidal voids in samples with flat entry surfaces. These attempts were made prior to the determination of the bandwidth requirements of the Born inversion algorithm which was discussed in Section 3.2.3. Furthermore, good techniques for experimentally determining the location of the center of the flaw had not been established.

In most cases, the estimate of the size of the flaw for normal incidence of the ultrasonic beam was accurate; but for other angles the results were inaccurate. This inaccuracy is now attributed to the inadequate bandwidth in some cases and inadequate signal-to-noise ratio in others. To demonstrate that the Born inversion technique could be used with ellipsoidal flaw shapes, a somewhat simpler experimental situation was selected. A  $400\text{ }\mu\text{m} \times 800\text{ }\mu\text{m}$  oblate ellipsoid was available in a "trailer hitch" sample and the contact transducer available for use with it had a center frequency of 6.5 MHz and a -20 dB full bandwidth of 13.5 MHz. Thus a single transducer was adequate for measurements at all angles. A set of measurements was made for polar angles ranging from zero degrees to 90 degrees. The results are displayed in Fig. 3.15.

The solid curve shows the outline of the oblate ellipsoid. The dotted curve with the hourglass shape shows the results that would be produced by a true Born scatterer; i.e., the diameter obtained at each angle would be equal to the distance between two planes that were perpendicular to the direction of propagation and tangent to the near and far surfaces of the ellipsoid. The complex spectra of the backscattered signal from a 2:1 oblate ellipsoid were calculated by Opsal<sup>10</sup> at Lawrence Livermore Laboratories and furnished to the Science Center. This theoretical data was used as an input to the Born inversion algorithm and the results are given by the open circles. Note that the resulting curve is roughly elliptical in shape but is slightly larger than either the solid or dotted curves. The cause of the discrepancy has not been identified.

Finally, the experimental results are given by the open squares and open triangles. The open squares represent results obtained when the estimate of the location of the center of the ellipsoid is obtained using long wavelength techniques as explained in Section 3.2.1. The open triangles represent results obtained when the location of the center of the ellipsoid is obtained using the empirical technique of requiring the characteristic function to have a flat top at the origin as explained above. Note that these experimental results span the range of results obtained by the other



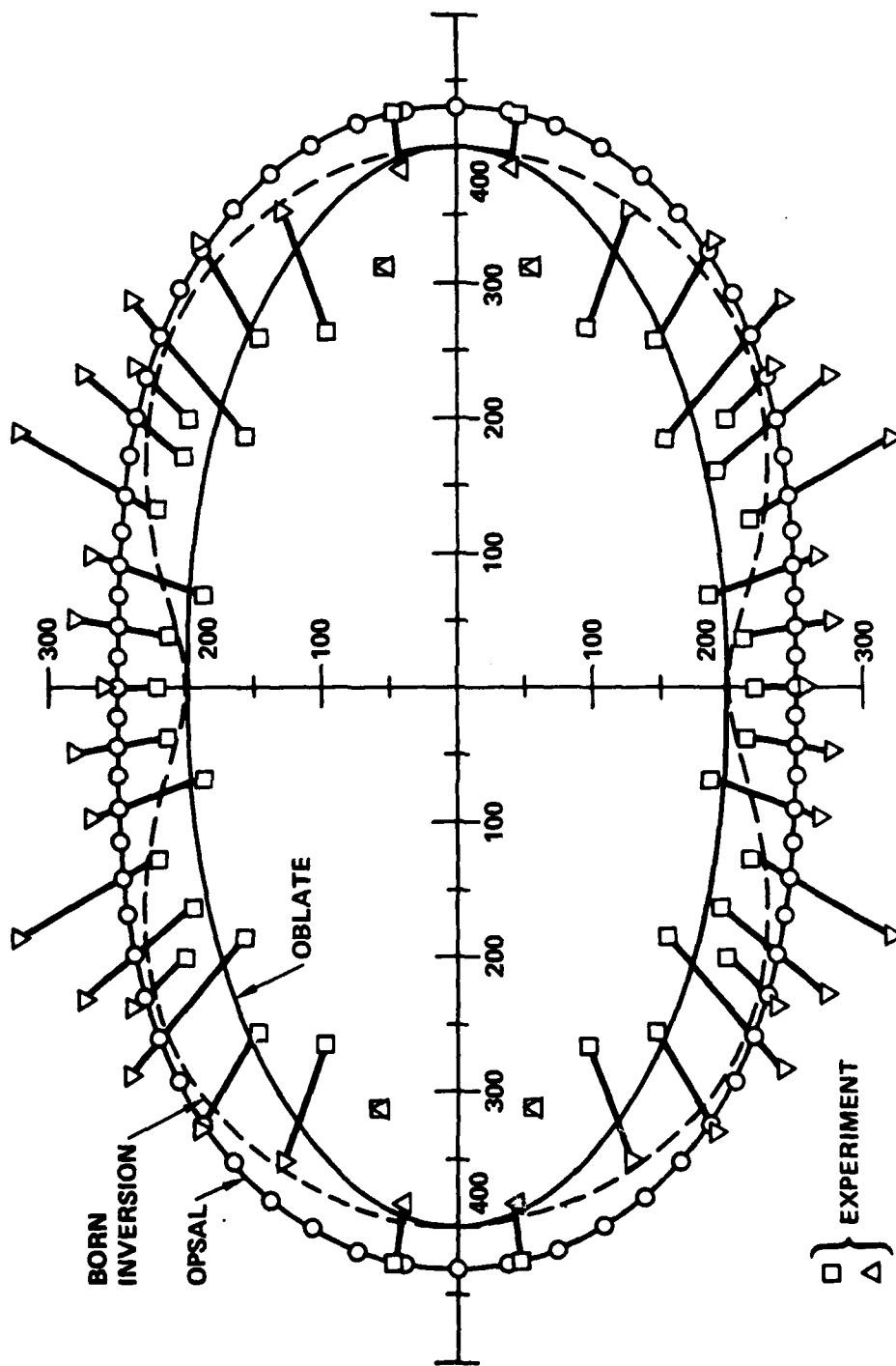


Fig. 3.15 Results of Born inversion algorithm analysis of scattering data from a  $400 \mu\text{m} \times 800 \mu\text{m}$  oblate ellipsoidal void.

techniques. The overall accuracy is good and the shape is definitely elliptical. This is believed to be the first time that extensive measurements made on an ellipsoid of revolution and used with an inversion technique have resulted in accurate size estimates of the ellipsoid.

These results demonstrate that experimental procedures have been devised to obtain accurate results with the Born inversion algorithm. No major problems are being encountered with the deconvolution procedures or other pre-processing steps. Further the results demonstrate that the Born inversion can be used to obtain the shape of the flaw. In the cases presented thus far the shape of the flaw was known a priori. To establish the validity of the technique, it is important to obtain the characteristics of a flaw whose shape is unknown before the experiment.

#### 3.2.4.4 Rolls-Royce Sample

A sample made of powder metallurgy nickel based superalloy material was obtained from Rolls-Royce Ltd. This sample is shown in Fig. 3.16. The sample was known to contain a flaw but none of the characteristics were known. The objective was to apply the full range of quantitative flaw characterization techniques to this sample and predict the characteristics of the flaw as completely as possible. Upon completion of this task, the sample was returned to Rolls-Royce, Ltd. and metallographically sectioned so that the true characteristics of the flaw could be determined.

The protocol described in Section 3.1 was used to inspect the sample. Because of the small sample size, the search mode was combined with the imaging that is required as the first step of the detailed examination. The C-scan and B-scan images obtained of the flaw are shown in Fig. 3.17. From these images, the orientation and long dimension of the flaw were determined. The images were also used to select the observation directions for the backscattering measurements that provide input data for the Born inversion analysis. This data was analysed and the short transverse dimensions of this needle-like flaw were estimated.

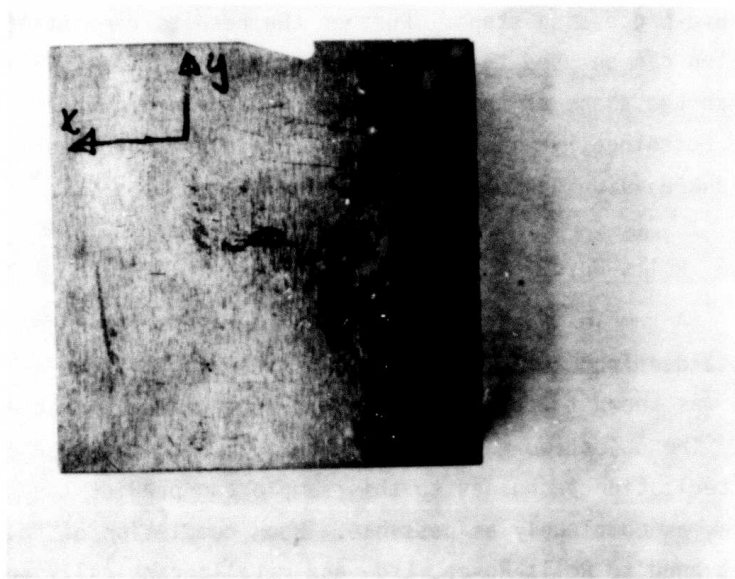


Fig. 3.16 Rolls-Royce sample made of powder metallurgy nickel based superalloy material.

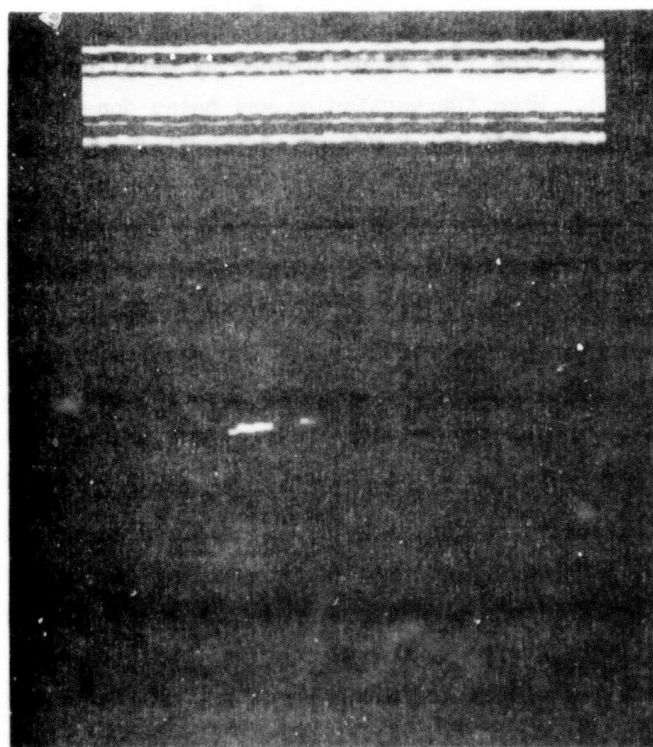
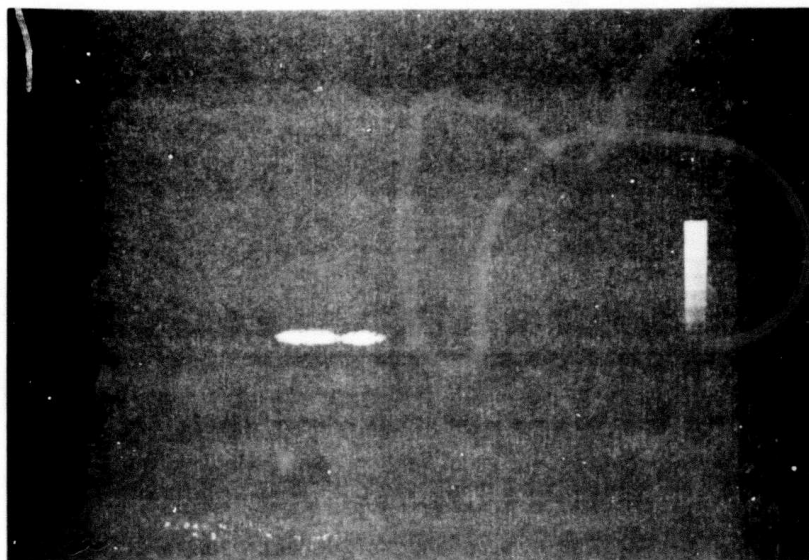


Fig. 3.17 (a) C-scan image of flaw in Rolls-Royce sample.  
 (b) B-scan image of flaw in Rolls-Royce sample.

Finally the phase of the signals returned from the flaw were examined to determine that the acoustic impedance of the flaw was greater than that of the surrounding material. These measurements, summarized in Table 3.2, were returned to Rolls Royce along with the sample.

Table 3.2  
Results of Examination of Rolls-Royce Sample

---

X Axis = 0.172 inch	(Imaging)
Y Axis = 0.007 inch	Born Inversion
Z Axis = 0.006 inch	Born Inversion
Angle to X Axis = 4.3°	
Acoustic impedance of defect	> metal

---

The shape of the flaw as determined by metallographic sectioning is shown in Fig. 3.18. When the sectioning was being done the presence of a prior particle boundary region surrounding the flaw was detected. The flaw was a calcium, silicon, aluminum, titanium rich ceramic material and the boundary region represents a ceramic/matrix reaction zone. The flaw dimensions are all specified in Fig. 3.18. Note the similarity of the flaw shape and of the C-scan image in Fig. 3.17a even though the transverse dimension is not resolved in the C-scan. The results of the quantitative NDE analysis and the metallographic sectioning are compared in Table 3.3. The agreement between the two techniques is excellent. These results are far more precise than those obtained using conventional NDE procedures.

For calibration purposes Rolls-Royce measured the amplitude of the signal returned from this flaw relative to the amplitude of the signal returned from a 0.050 inch diameter flat bottom hole. The measurement was repeated using three different transducers and two different pulser/receiver units. For each transducer and pulser/receiver combination, the measurement

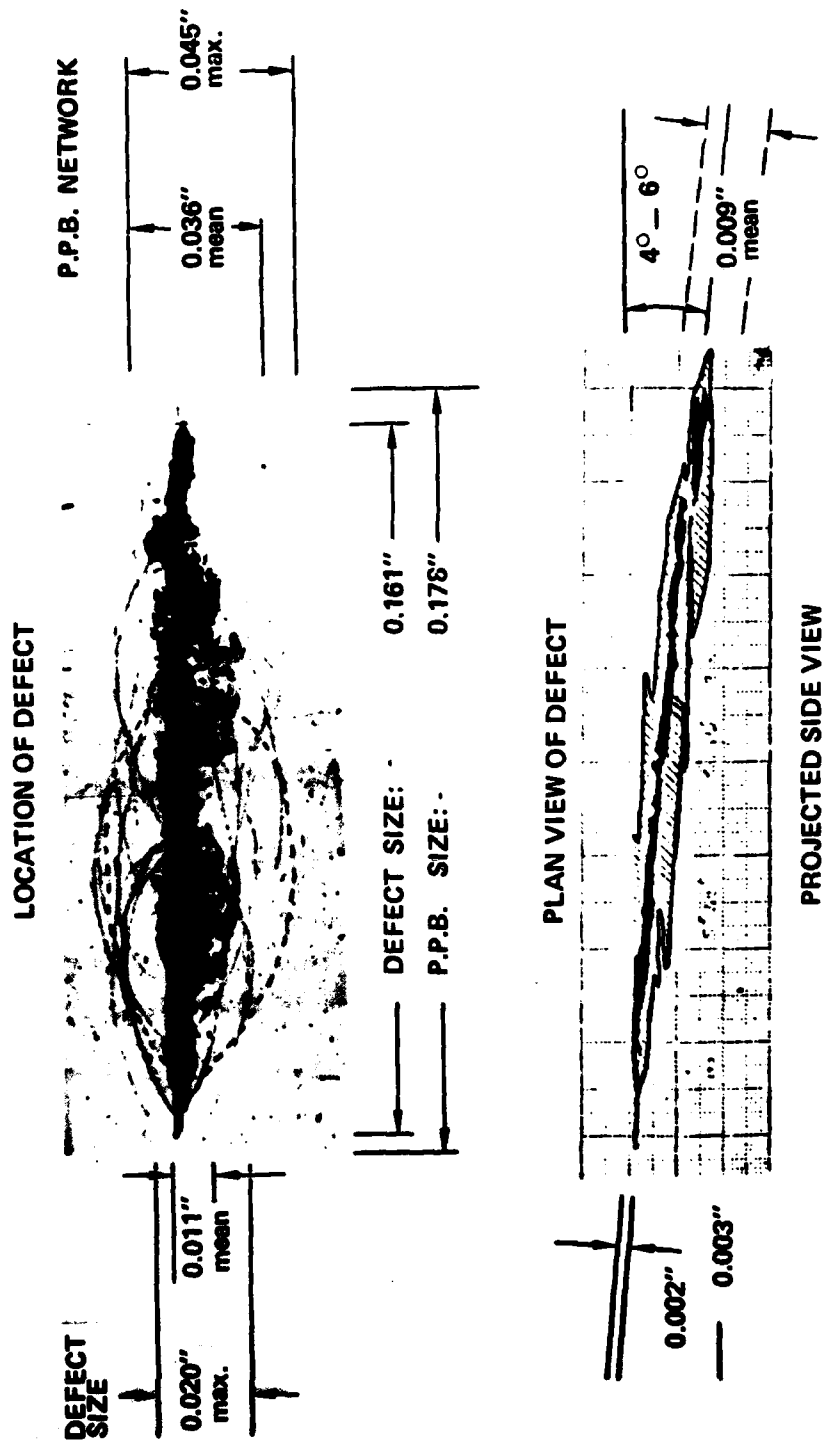


Fig. 3.18 Results of metallographic sectioning of flaw.

Table 3.3  
Comparison of Test Bed Results and Metallographic  
Examination Results

Science Center Test Bed		Rolls-Royce Sectioning	
Flaw		Flaw	Reaction Zone
X Axis	0.172 inch	0.161	0.178
Y Axis	0.007 inch	0.011	0.036
Z Axis	0.006 inch	0.002	0.009
Angle	4.3°	4° - 6°	

Acoustic impedance higher than the surrounding metal is consistent with a ceramic inclusion.

was made from each of two opposite faces of the sample. The measured amplitudes varied by 5 dB. Since the conversion factor between flaw size and scattering amplitude is dependent on flaw shape, orientation and composition as well as flaw size, one cannot precisely state the flaw size variation that would correspond to a 5 dB amplitude variation. If the shape, orientation and composition remain constant, the amplitude will be proportional to flaw size for flaws with  $ka$  greater than approximately one. Thus, the 5 dB variation would correspond to nearly a factor of two variation in flaw size.

## 4.0 PHASED ARRAY SYSTEM

### 4.1 Concept and Purpose

Even though the use of phased ultrasonic array systems is widespread in the medical community<sup>11-15</sup> there is currently little use of them for NDE applications. There is interest in using them but appropriate applications must be found. It is also important to realize that the requirements placed on an array for medical applications are quite different than those needed for NDE applications.<sup>16</sup> The intent of the design of this system is that it be useful in a number of configurations so that many different applications can be investigated. For this reason the system is not very compact. This should not be viewed as a shortcoming since the essential features for a particular application can always be abstracted to produce a compact system. The two important questions are: Is the system reaching its potential as a data acquisition device? And, how does its performance compare with alternative techniques?

The usefulness of an array for NDE applications stems from the capability of the array to rapidly scan an ultrasonic beam and to change the focus to accommodate the curved surfaces of different parts. This latter characteristic will be referred to as beam agility. At the present time, the applications of arrays in NDE are limited. These limitations are due to the current technology relating to array fabrication and to physical constraints imposed by materials that are to be inspected. A thorough discussion of this aspect of the problem has been given in the paper by Addison.<sup>16</sup>

The rapid beam scanning capability of an array can be exploited in several different ways in a quantitative NDE application. If the array is sufficiently long, it can be used in a contour scanning mode for inspecting circularly symmetric parts such as engine disks. An example of this mode of operation is shown in Fig. 4.1. Here the beam is always entering the part normal to the surface. The beam agility feature can be used to compensate for focusing effects caused by curvature of the metal surface. The tilting and



# IMAGING MODE

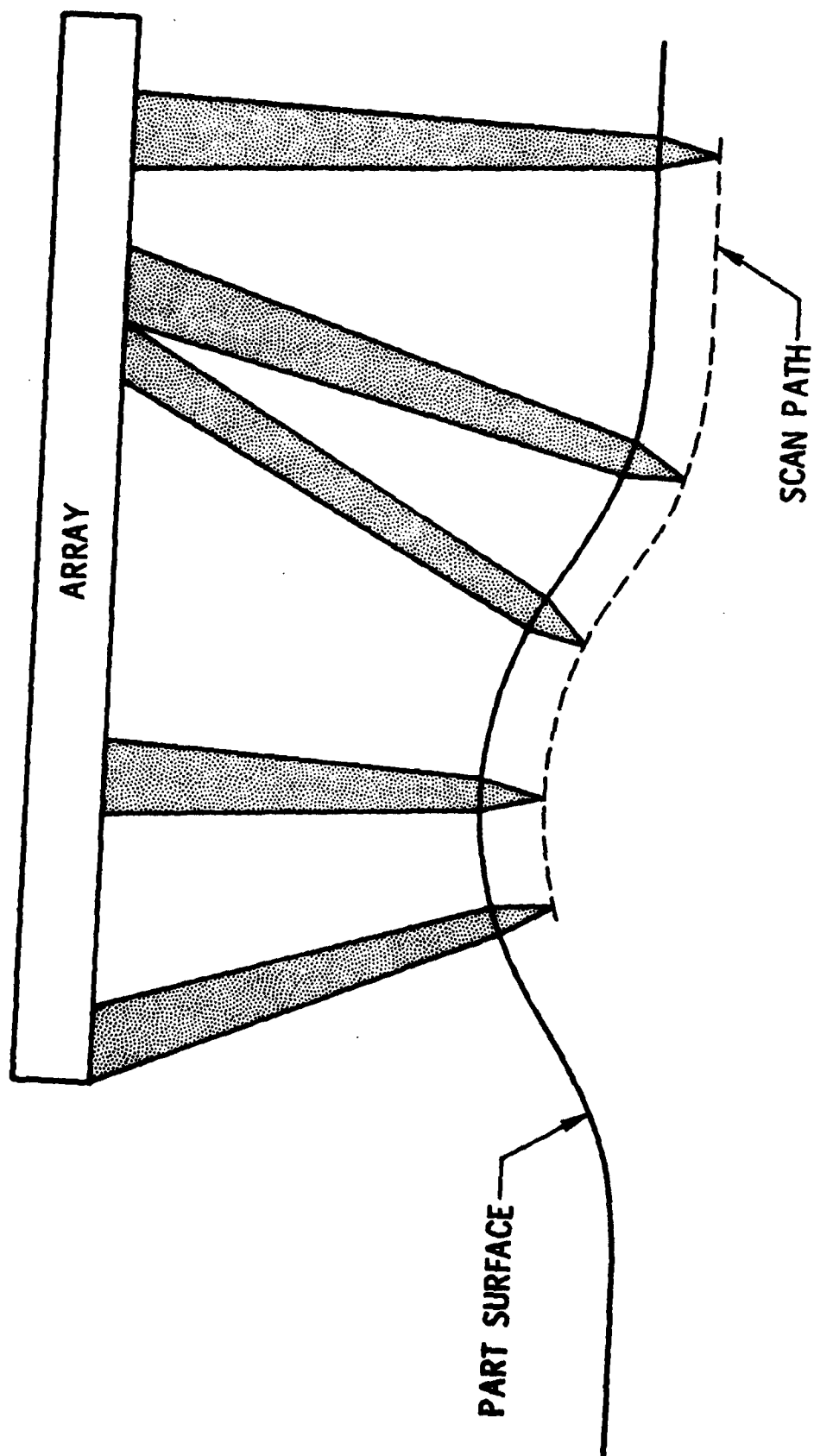


Fig. 4.1 Contour scanning mode.

## 4.0 PHASED ARRAY SYSTEM

### 4.1 Concept and Purpose

Even though the use of phased ultrasonic array systems is widespread in the medical community<sup>11-15</sup> there is currently little use of them for NDE applications. There is interest in using them but appropriate applications must be found. It is also important to realize that the requirements placed on an array for medical applications are quite different than those needed for NDE applications.<sup>16</sup> The intent of the design of this system is that it be useful in a number of configurations so that many different applications can be investigated. For this reason the system is not very compact. This should not be viewed as a shortcoming since the essential features for a particular application can always be abstracted to produce a compact system. The two important questions are: Is the system reaching its potential as a data acquisition device? And, how does its performance compare with alternative techniques?

The usefulness of an array for NDE applications stems from the capability of the array to rapidly scan an ultrasonic beam and to change the focus to accommodate the curved surfaces of different parts. This latter characteristic will be referred to as beam agility. At the present time, the applications of arrays in NDE are limited. These limitations are due to the current technology relating to array fabrication and to physical constraints imposed by materials that are to be inspected. A thorough discussion of this aspect of the problem has been given in the paper by Addison.<sup>16</sup>

The rapid beam scanning capability of an array can be exploited in several different ways in a quantitative NDE application. If the array is sufficiently long, it can be used in a contour scanning mode for inspecting circularly symmetric parts such as engine disks. An example of this mode of operation is shown in Fig. 4.1. Here the beam is always entering the part normal to the surface. The beam agility feature can be used to compensate for focusing effects caused by curvature of the metal surface. The tilting and

translation of the beam is done electronically and avoids problems with mechanical inaccuracies and backlash that are frequently encountered in mechanical drives. The technological capability for making a linear array transducer that would be long enough to scan over the entire radius of a turbine disk has not been demonstrated at this time. At the inception of this program, it appeared likely that an array transducer of length 6 inches with the performance needed for this application could be purchased. This did not prove to be the case. To assure the performance of the array, it was necessary to reduce the length to about 1/2 inch. To preserve some of the capabilities of a longer array transducer, two of the shorter array transducers are used with a mechanically variable spacing between them as shown in Fig. 4.2. Although this severely limits the use of the array system for contour following applications, it can be used to demonstrate the feasibility of the concept.

If the use of the array system in a contour following mode is considered the equivalent of a search mode for a single element transducer, then the use of the array in a sector scan mode can be considered as the equivalent of a detailed examination mode. The array can be set up to generate a fan beam to obtain a B-scan image of the flaw or it can be used to obtain scattering data from the flaw that can be used with the Born inversion or long wavelength techniques. This scattering mode, shown in Fig. 4.3, can acquire data using either a pulse-echo or a pitch-catch technique.

#### 4.2 Description of System

The electronics for driving this array have a somewhat different objective than some of the array based systems that are currently available, which acquire and display an image in as little time as possible. This system must be sufficiently flexible to be used in a wide variety of situations and be capable of operating in many different modes. It must acquire a waveform while minimizing distortion due to crosstalk or nonlinearities. It is desirable to display a single image and be able to recognize the important

## IMAGING MODE

Variable Spacing

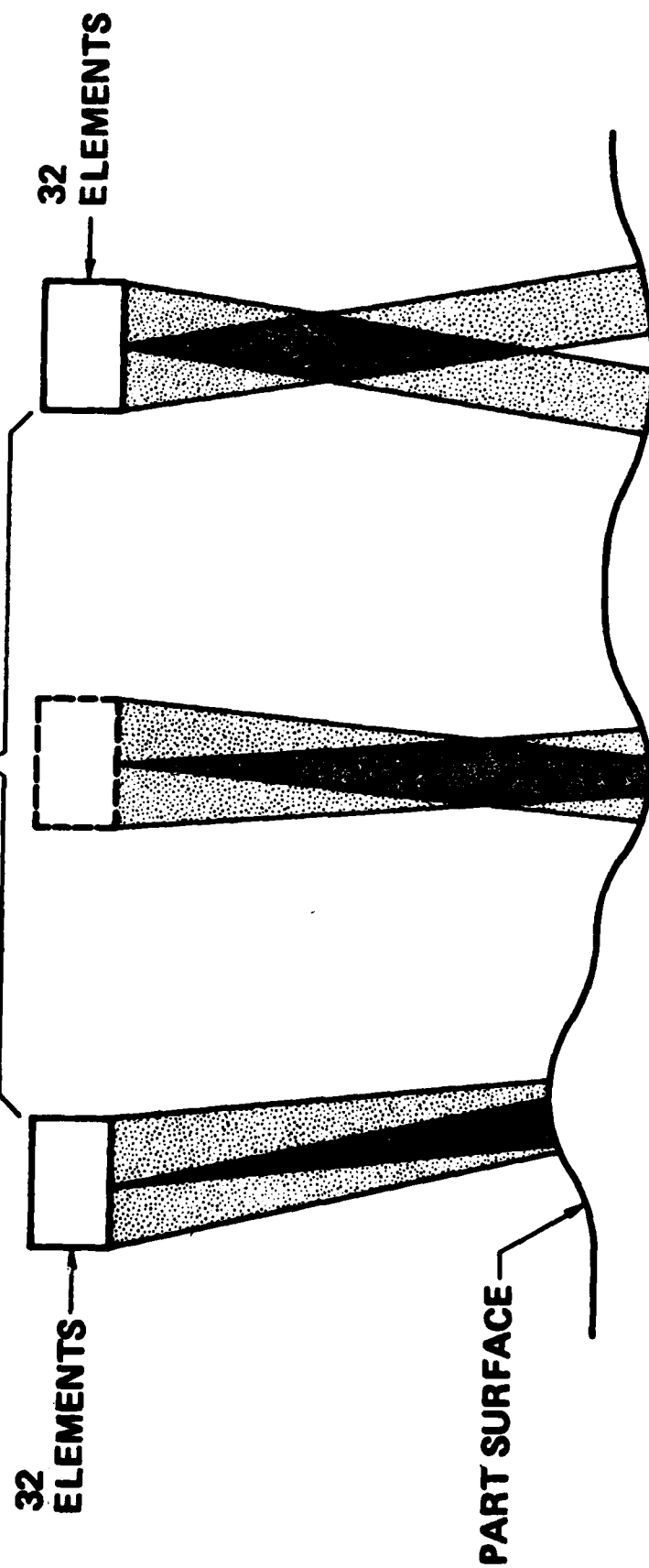


Fig. 4.2 Contour scanning - 2 arrays.

## SCATTERING MODE

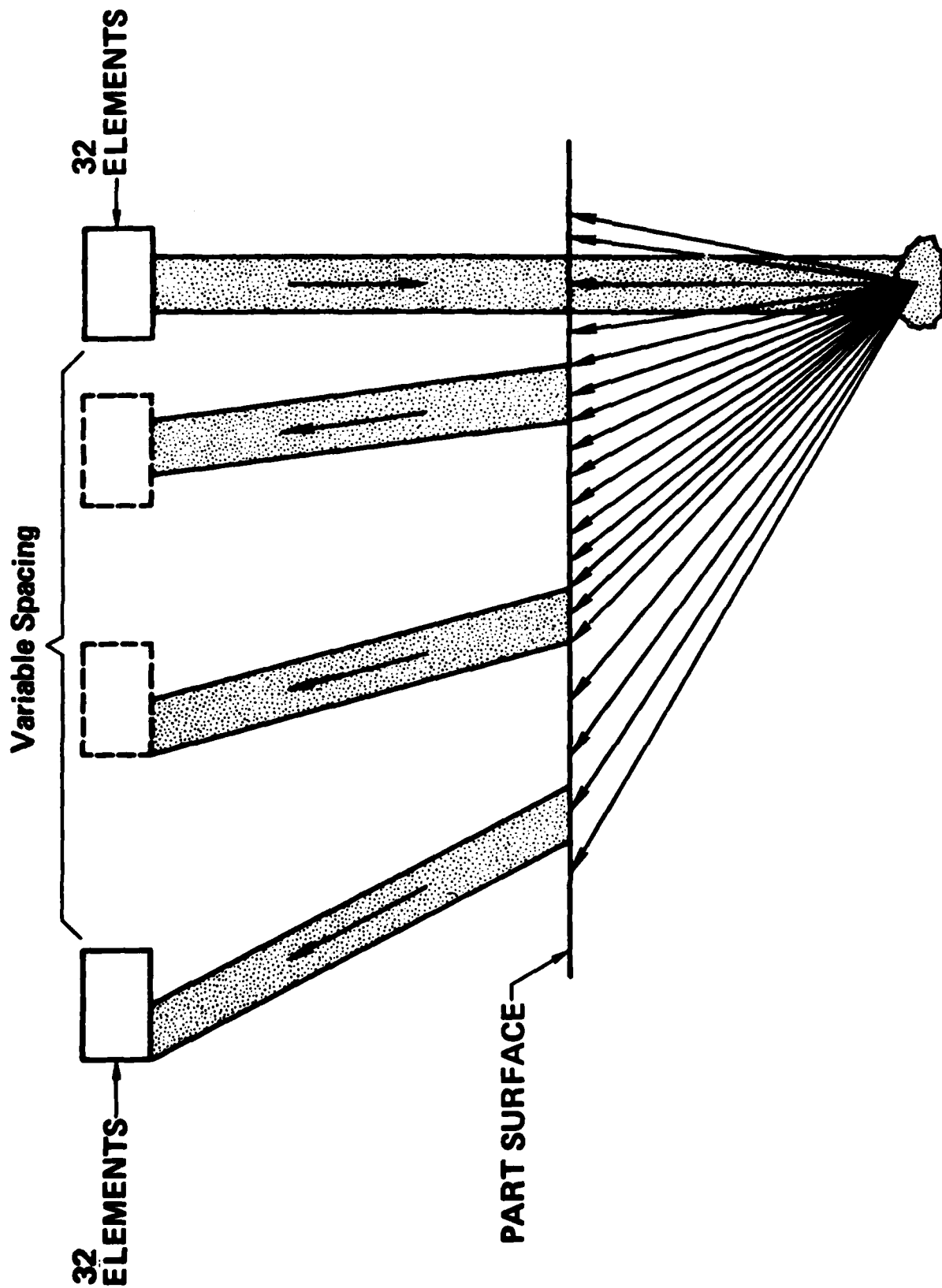


Fig. 4.3 Scattering data acquisition mode - 2 arrays.

details of the object under study. The system must process the signals with sufficiently low distortion that when scattering data is acquired, the resulting signals can be used with the various inversion techniques.

The block diagram in Fig. 4.4 delineates the major subassemblies of the array system and their functions. The S/200 minicomputer sends out a set of codes that selects the desired set of 16 transmit elements, the desired set of 16 receive elements, and the set of time delays that define the transmit beam direction. These codes are stored in the control memory. The timing and control block interprets the codes and activates the transmit and receive multiplexers so that the appropriate array elements are selected. This block also sends suitably delayed trigger signals to each of the 16 selected transmitter elements to synthesize an ultrasonic beam with the desired direction. The trigger signals, which are positive going TTL level pulses, activate the pulser and cause a 5 to 400 volt pulse to be applied to each selected transducer element. The returning ultrasonic signal from the object under investigation is received by each of the 16 selected receive elements. The received signals are each amplified 26 dB by a low noise, low distortion, hybrid preamplifier. They are then passed through the receiver multiplexer to a line driver and then to a signal conditioning circuit. The signal conditioning circuit serves as an anti-aliasing filter and adjusts the peak-to-peak amplitude of the signal as well as its dc level to make it compatible with the A/D converter. The next block is the 8 bit, 18 MHz A/D converter which digitizes the signal and loads it into an  $8 \times 1$  K bit fast random access buffer memory. All 16 of the A/D converters are started synchronously after a delay corresponding to an ultrasonic round trip time that is selected by the operator. The contents of each of the sixteen memories are sequentially clocked through the interface to the array processor at a rate compatible with the operation of the array processor and minicomputer (approximately 0.5 MHz). The array processor has the task of shifting the waveforms and summing them to synthesize a beam from a specified direction. The array processor also interpolates between data points in the waveform if the desired shift is not an integral number of clock cycles. This reduces the sidelobe

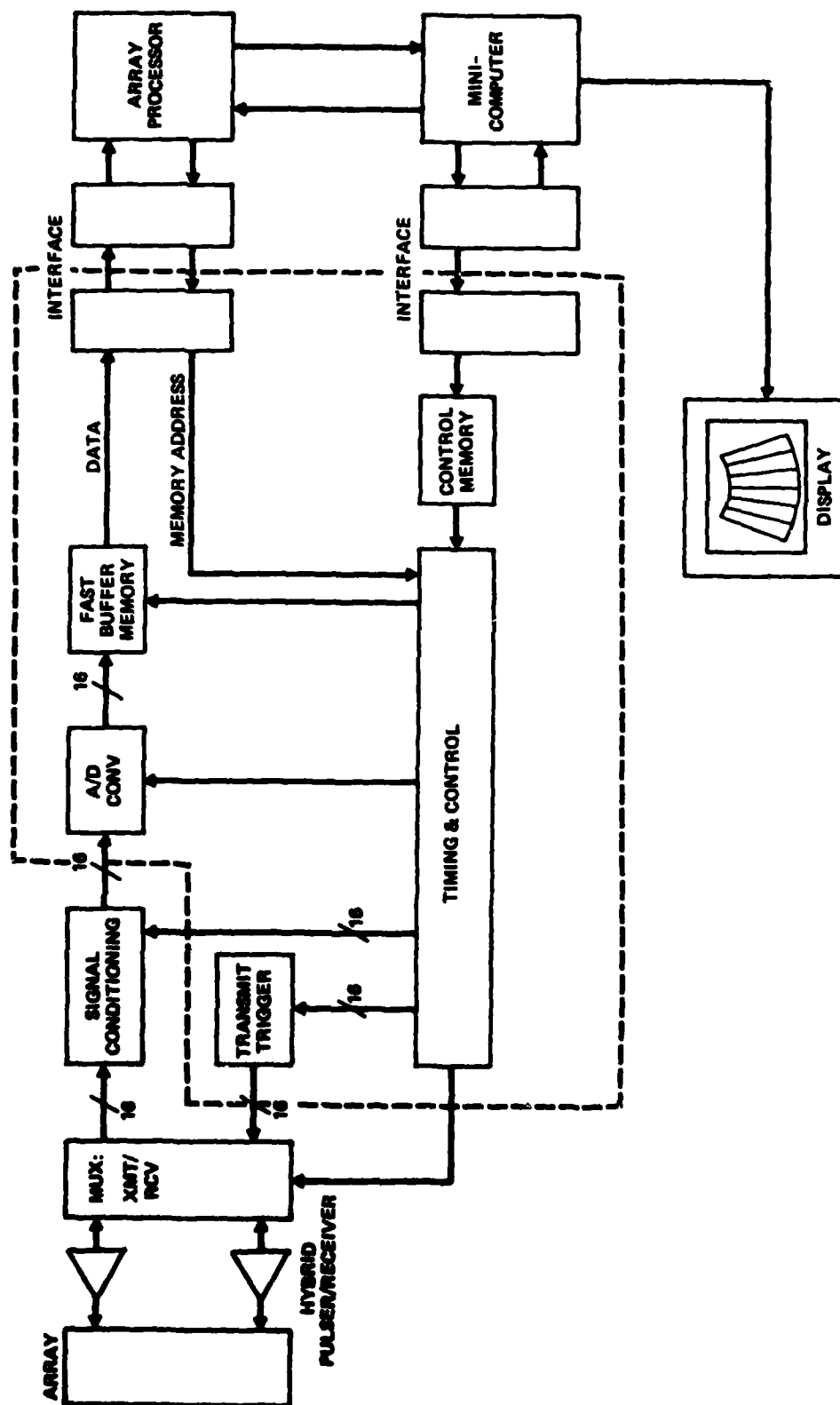


Fig. 4.4 Ultrasonic phased array system block diagram.

levels in the array response. The array processor is also used to correct for amplitude errors in the response of a particular array element. After the beam-forming operation is completed, the processed signals are sent to the S/200 minicomputer for storage on the disk memory and to be displayed on the color display. The unprocessed waveforms can also be sent to the S/200 for storage on the disk memory. The display unit can be programmed in a general way to display the data in many different formats. For image data, a B-scan display is the most useful, although C-scans can be displayed if desired. The scattering data is not displayed but only recorded for use with the inversion algorithms. Detailed schematic drawings of the circuits in the hybrid pulser/receiver, the multiplexer, the signal conditioner and the blocks contained in the dotted outline can be found in Appendix B.

#### 4.2.1 Transducers

The first major subassembly is the transducer array. Originally this was to be a 6 inch transducer containing 240 elements which could be used for contour scanning. An array of this sort must possess a sufficiently wide bandwidth and short transient response that it can be used to detect flaws below metal surfaces. This condition requires the "ring down" from the front surface echo to decay by about 20 dB before the flaw signal occurs. Furthermore the cross-talk between array elements must be about 25 dB below the direct signal.

A vendor was contacted who claimed that a custom transducer satisfying these requirements could be fabricated. A sub-contract was issued to build the array and a unit was manufactured. Preliminary testing of the unit revealed that the transient response was too long by an order of magnitude. Also the peak amplitude of the individual element responses varied by more than  $\pm 10$  dB about the average level. The vendor made several attempts to improve this performance without success. Conversations with other experts indicated that the current state of array technology is not sufficiently advanced to manufacture an array this large meeting the required specifications.



To obtain the required transducer characteristics the system was reconfigured to use two 32 element arrays. These arrays have a nominal center frequency of 2.25 MHz. While a higher frequency is desirable for NDE applications, no commercial sources of such arrays could be located. The peak amplitude and the duration of the transient response of each of the 32 elements were carefully measured. The peak amplitudes were less uniform than desired with the amplitudes of 95% of the elements being within  $\pm 37\%$  of the mean value. This variation is less than that encountered with many commercially available transducers and was accepted. The data on the duration of the transient response is summarized in Fig. 4.5. Since the exact shape of the transient response varies among transducer elements, we have measured the decay times relative to the time of the peak of the transient response. In this way the curves shown in Fig. 4.5 are obtained. The thin line represents the average decay time of the 32 elements. The thick lines form an envelope that contains the decay times of 95% of the elements. A third curve shows the theoretical decay time for a similar transducer element.<sup>17</sup> This decay time is considerably shorter than that of the array elements and is approximated by the performance of a carefully fabricated single element transducer.<sup>18</sup> The array performance is adequate for our needs and far exceeds the performance of the 240 element array that was tested early in the program. One of the transducer arrays is shown in Fig. 4.6.

#### 4.2.2 Pulser/Receivers

The next subassembly after the transducer in Fig. 4.4 is the pulser/receiver package. Several design limitations dictated that the pulser/receiver be on the array side of the multiplexer. First, a high voltage transmit pulse is required for the transducer excitation. Second, the receiving circuits require a voltage limiting transmit/receive switch. Third, the received signals have to be provided with a local low noise amplifier to overcome any low level multiplexer noise. This means that it will be necessary to have a pulser/receiver for each transducer element or a total of 64 for this system. Placing the pulser/receiver at a remote location would be prohibitive because of the

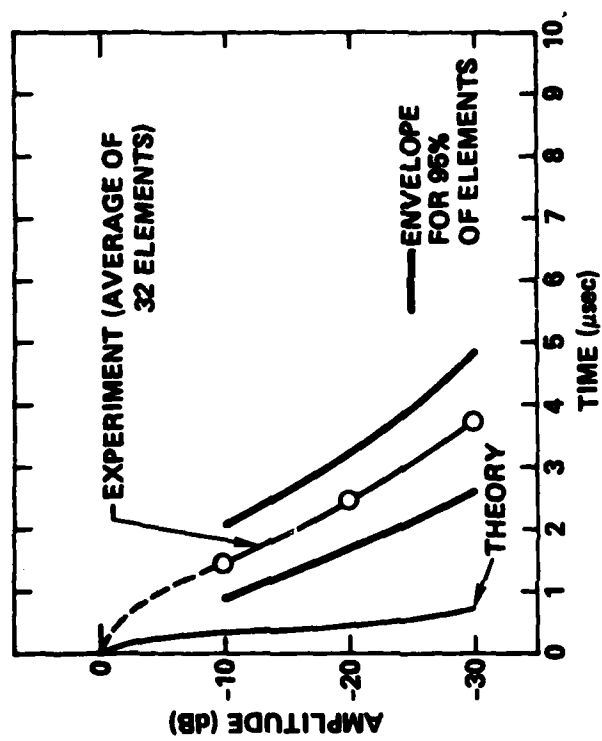


Fig. 4.5 Duration of transient response for transducer array.

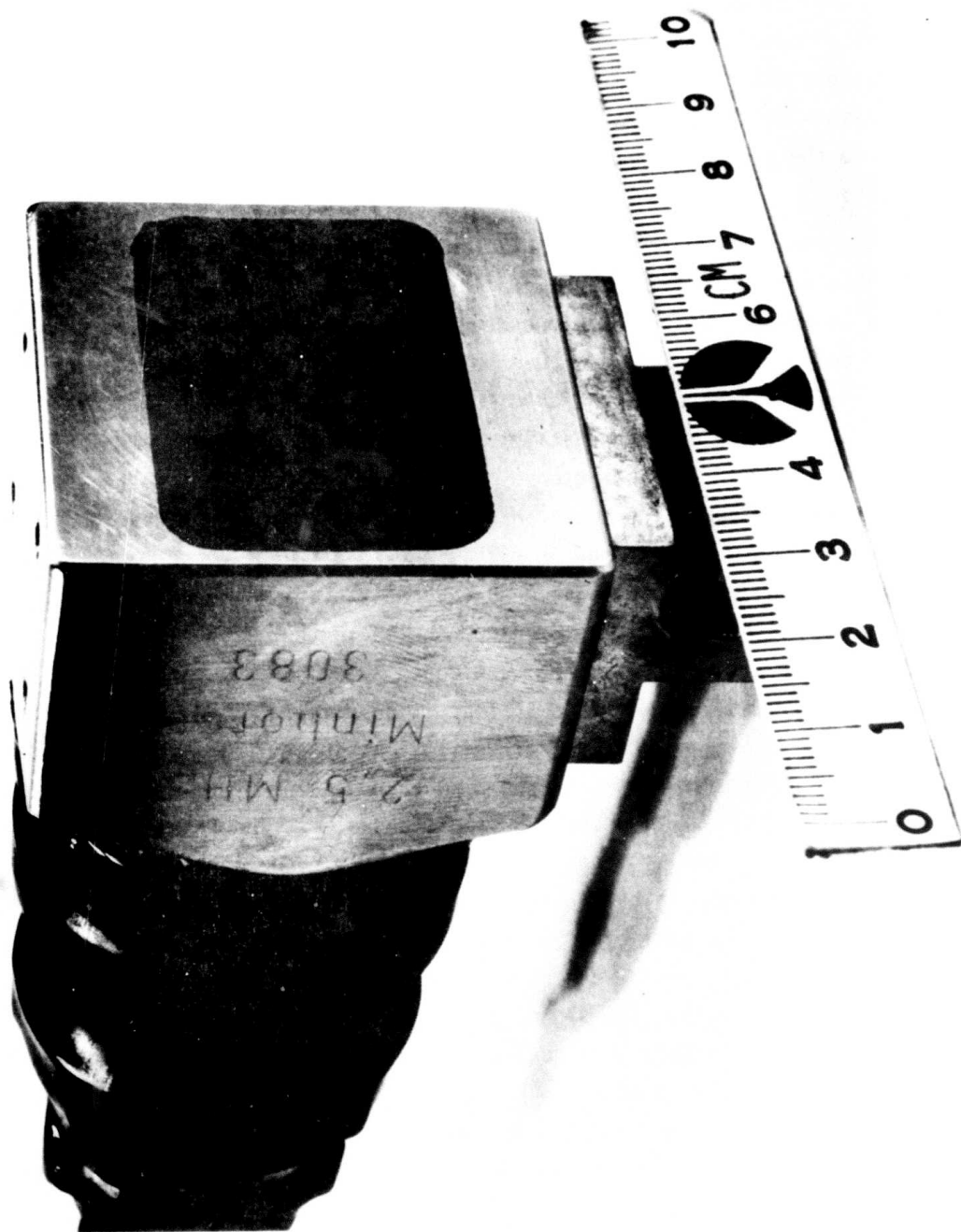


Fig. 4.6 Transducer array.

bulk of the cables that would be required for the interconnection and the possibility of severe signal degradation due to cable capacitance. These considerations led to the decision to package the pulser/receiver as compactly as possible and to build the unit as a hybrid circuit. This imposed several constraints on the circuit design relating to availability of components in chip form, to the power dissipation of the units, and to the size of the completed circuit.

The pulser circuit is shown in Fig. 4.7a. The switching element is an SCR. A number of alternatives were investigated including a transistor operated in the avalanche mode and one operated as a high voltage switching transistor. The switching transistor was found to be too slow for this application. The avalanche switching speed was more than adequate but it was difficult to obtain repeatable results with a selection of transistors. Furthermore, the units would only operate reliably over a small range of applied dc voltages. The SCR has an adequate switching speed and operates reliably over a wide range of dc voltages. This voltage range is sufficient to vary the output amplitude of the transmitted pulse by more than 30 dB. Transistor  $Q_1$  is used for shaping the current pulse produced by the TTL input pulse so that it will reliably drive the SCR (labeled D1). Transistor  $Q_5$  is used to speed up the charging rate of C2 so that the pulser can be operated at repetition rates of 1 KHz. The pulser has been used to excite a 2.25 MHz commercial transducer. The echo returned from a block of aluminum has been compared with that obtained from a commercial pulser (Panametrics Model 5052) using the same transducer. The results are compared in Fig. 4.8. It is readily seen that the transient response of the transducer is essentially the same in both cases. Thus we can conclude that the switching speed of the SCR is sufficiently fast that the spectral content of the pulse produced will fully excite the bandpass of the transducer. The receiver circuit is shown in Fig. 4.7b. The signal path is composed of transistors  $Q_2$  and  $Q_3$ , while  $Q_4$  is used to turn it on and off. The gain of the circuit is principally determined by the ratio of  $R_x$  to  $R_y$  and thus can be made relatively independent of variations in the active elements and the temperature. The gain has been set at 26 dB. The circuit is ac coupled to avoid problems with dc drift and has a

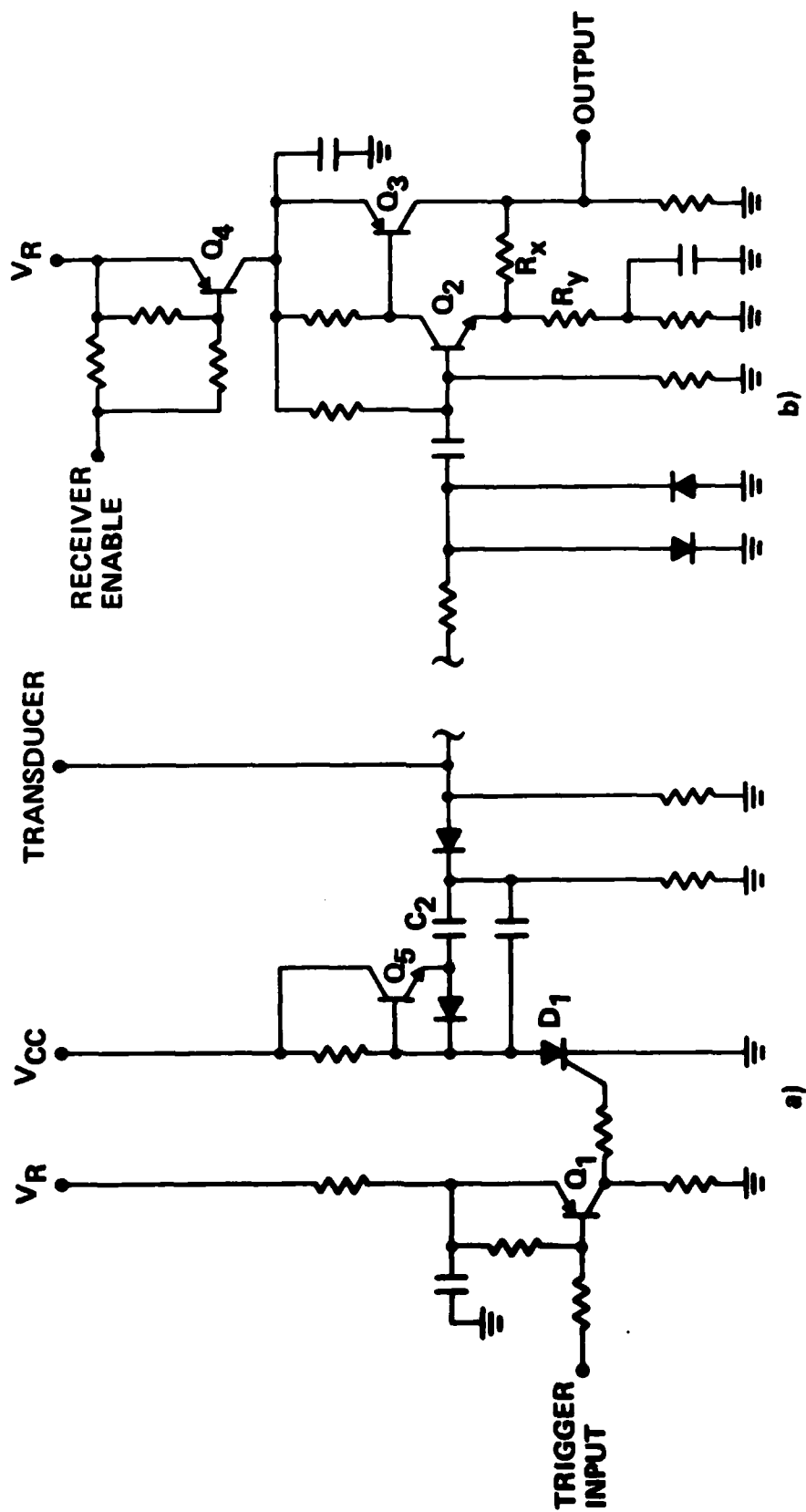
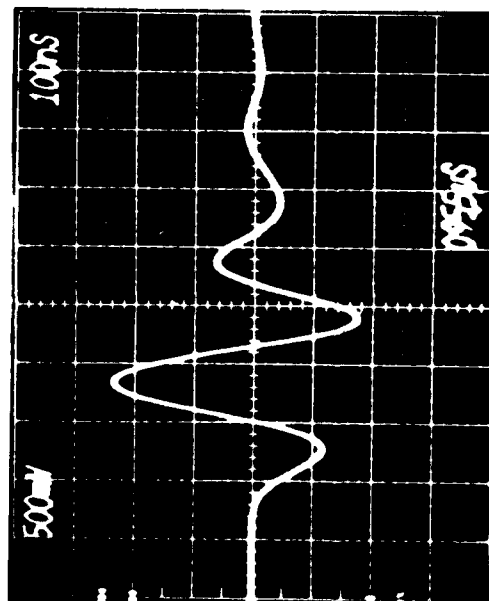
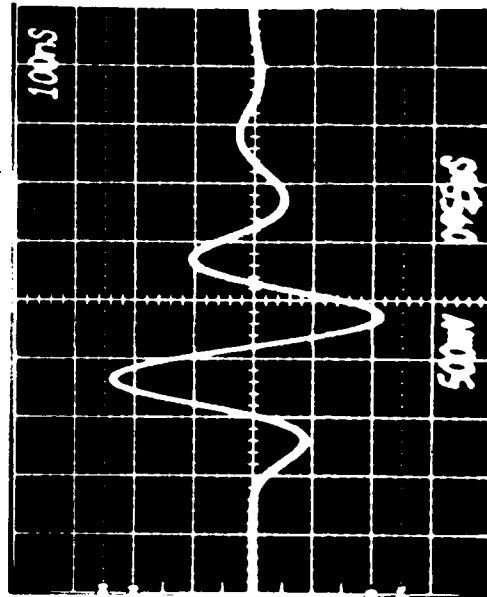


Fig. 4.7 Pulser/receiver schematic.

## ULTRASONIC ECHOES



**HYBRID PULSER/RECEIVER**



**COMMERCIAL PULSER/RECEIVER**

Fig. 4.8 Comparison of hybrid pulser excitation of commercial transducer with commercial pulser excitation.

low frequency 3 dB point of 0.7 MHz and a high frequency 3 dB point of about 30 MHz. The complete frequency response of a typical receiver is shown in Fig. 4.9. The low frequency 3 dB point is a compromise between the need to provide a sufficiently broad bandwidth to prevent phase distortion of the signals and the need to provide a rapid recovery after being driven into saturation by a high amplitude signal. The recovery time is observed to be 1  $\mu$ sec and no signal distortion can be detected when commercial transducers are used. The power dissipation of the receiver is only 70 milliwatts. The provision to turn the receiver on with a TTL pulse when it is among the 16 addressed receivers reduces the cross-talk from receivers that are not addressed.

Two complete hybrid pulser/receivers were mounted on a single substrate. This choice minimized the board complexity and kept the hybrid package from becoming unwieldy. The package shown in Fig. 4.10 is a 3.4 cm  $\times$  2 cm  $\times$  0.5 cm hermetically sealed can with 24 pins. Two voltages are needed to operate the unit: five volts for both the trigger input stage of the pulser and the receiver stage and a transducer excitation voltage that can be varied from about five volts to four hundred volts.

#### 4.2.3 Multiplexer

The multiplexer section consists of three, 64 to 16 multiplexers. The total of 64 transducer elements are grouped into segments that each contain four elements. The four elements in any one segment are switched as a unit. Thus it is possible to digitally select 13 distinct groups of 16 contiguous pulsers (four segments) from among the 64 available. Similarly and independently, 16 contiguous receivers can be selected. There are two digital multiplexers: one for supplying triggers to the selected pulsers and one for enabling the selected receivers. There is one analog multiplexer that is used to convey the output signals of the selected receivers to the 16 receive channels.

The coding scheme for the multiplexers can best be understood using the diagram in Fig. 4.11. Each of the numbered rectangles corresponds to four

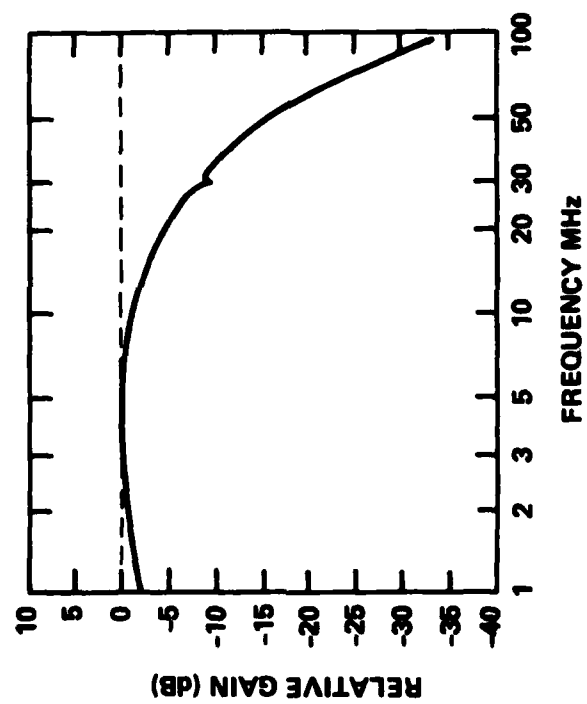


Fig. 4.9 Frequency response of hybrid receiver.



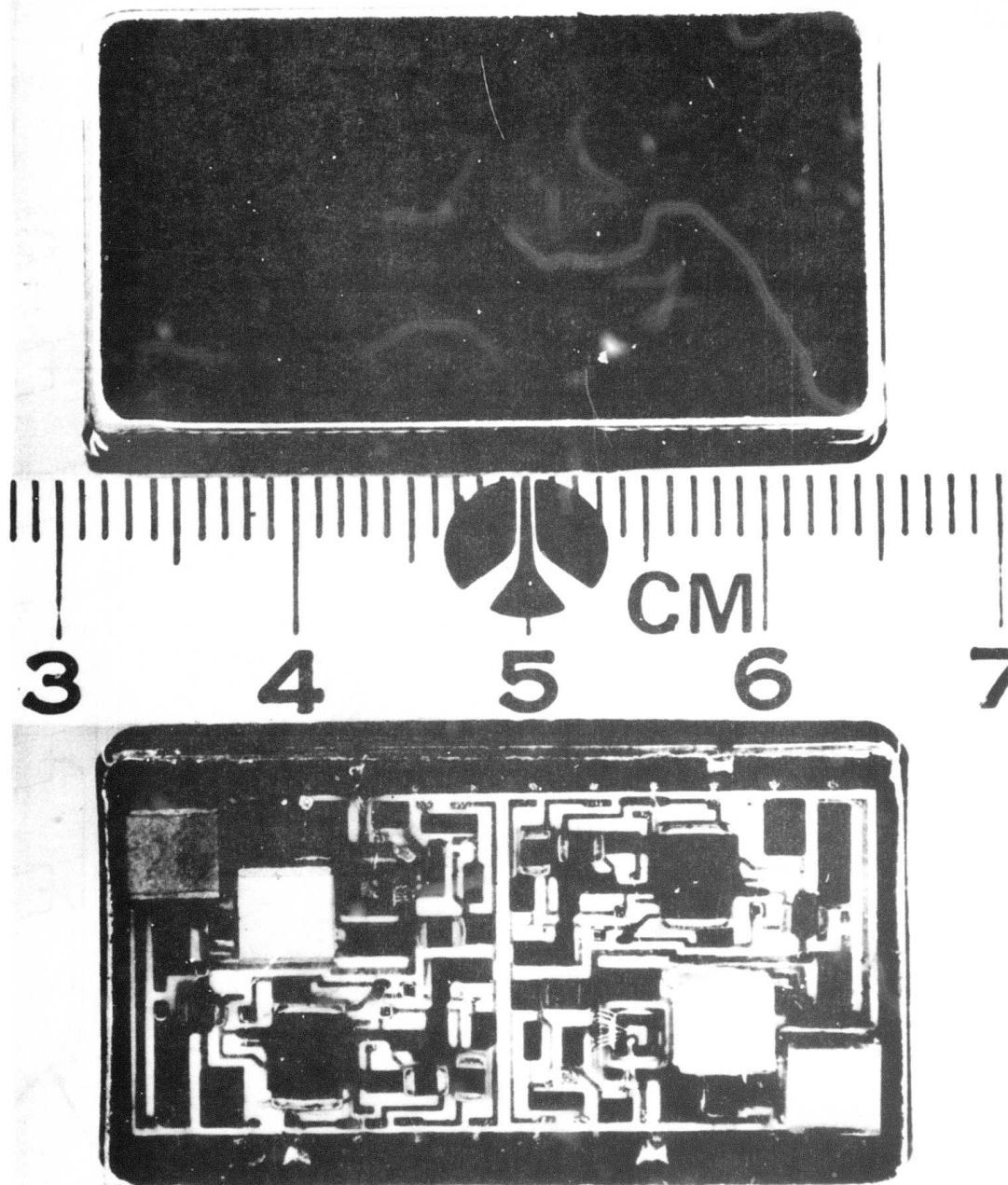


Fig. 4.10 Photograph of hybrid pulser/receiver.

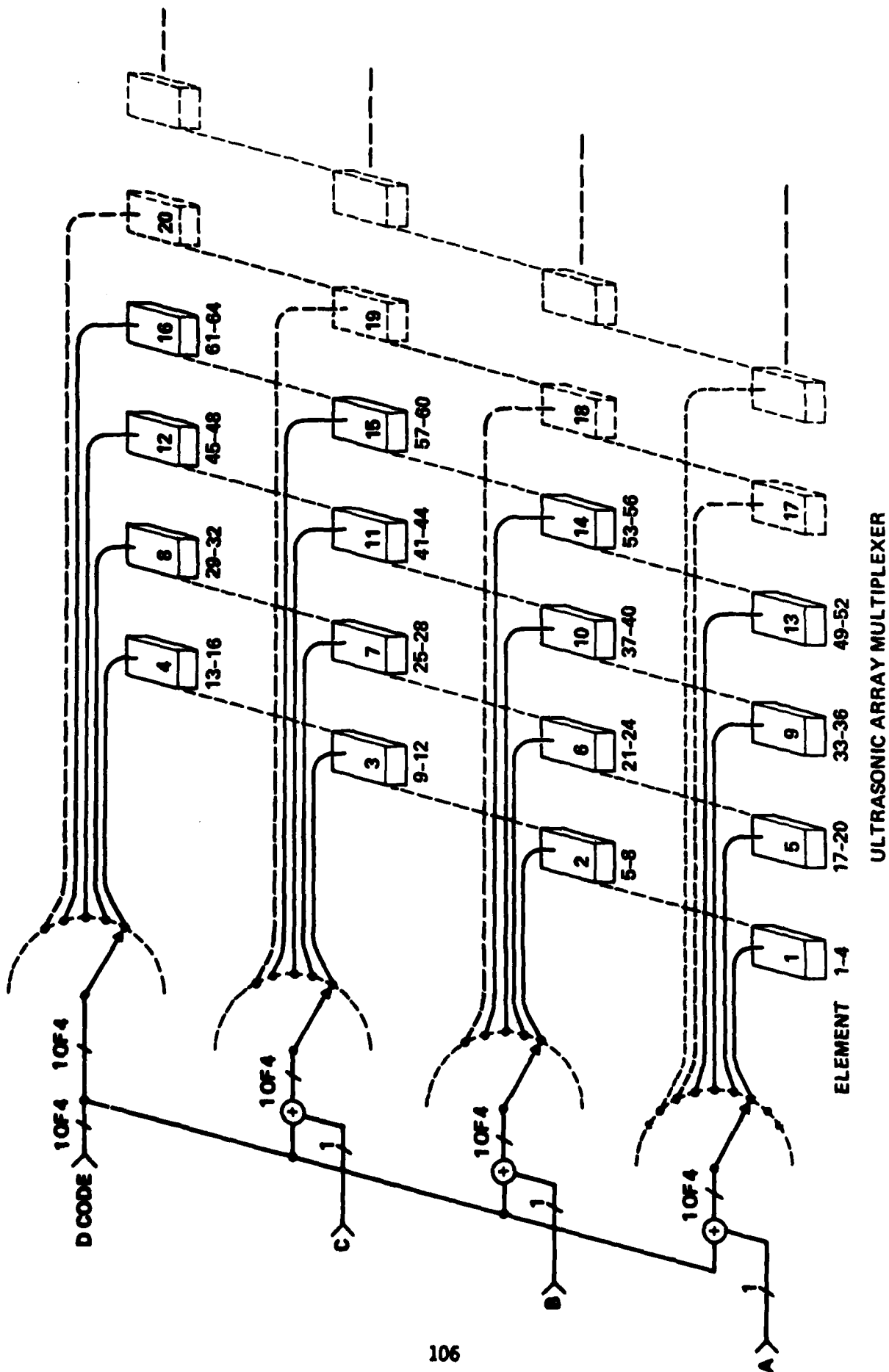


Fig. 4.11 Coding scheme for multiplexer.

elements (i.e., pulsers or receivers). In the actual hardware each of the switches has only four positions rather than the arbitrarily large number shown in Fig. 4.11. The four switch positions provide 13 distinct groups of elements that can be selected. The switching is accomplished by initially sending a master code on the line labeled D that selects the same corresponding position for each of the four switches. Note that this automatically selects four contiguous segments of elements containing a total of 16 elements. To shift the selected group of four segments by an integral multiple of four segments (16 elements), the master code is simply advanced or retarded by  $n$ , where  $n$  is the appropriate integer. For shifts of less than four segments, the auxiliary codes are used. A shift of one segment is provided by changing the "A" code by one, a shift of two segments results from changing the "A" and "B" codes by one, etc. In this way it is possible to select any group of 16 contiguous elements in groups of four segments.

The multiplexer subassembly is contained on three printed circuit boards which are partitioned and interconnected as shown in Fig. 4.12. The circuitry on board 1 serves to buffer and decode the five bit transmit and five bit receive codes that are sent from the timing and control circuitry. Also located on this board is the circuitry for generating the eight bit code that is required to control the pulser and receiver selection. The remaining two boards are identical. Each board contains half of the multiplexers and half of the pulser/receiver packages. The 64 transducer elements are arranged in a row and for the purposes of switching are divided into segments of four elements each. The 16 segments are numbered from left to right. The multiplexers and pulser/receivers corresponding to the even numbered elements are located on board 2 and those corresponding to the odd numbered elements are on board 3. Fig. 4.13 is a photograph of one of these boards and Fig. 4.14 is a block diagram of the multiplexer.

As shown in Fig. 4.14, the transmit elements are selected with the XMT code which is decoded and used to switch the XMT MUX to the desired positions. The triggers for the hybrid pulsers are then transmitted through the multiplexer

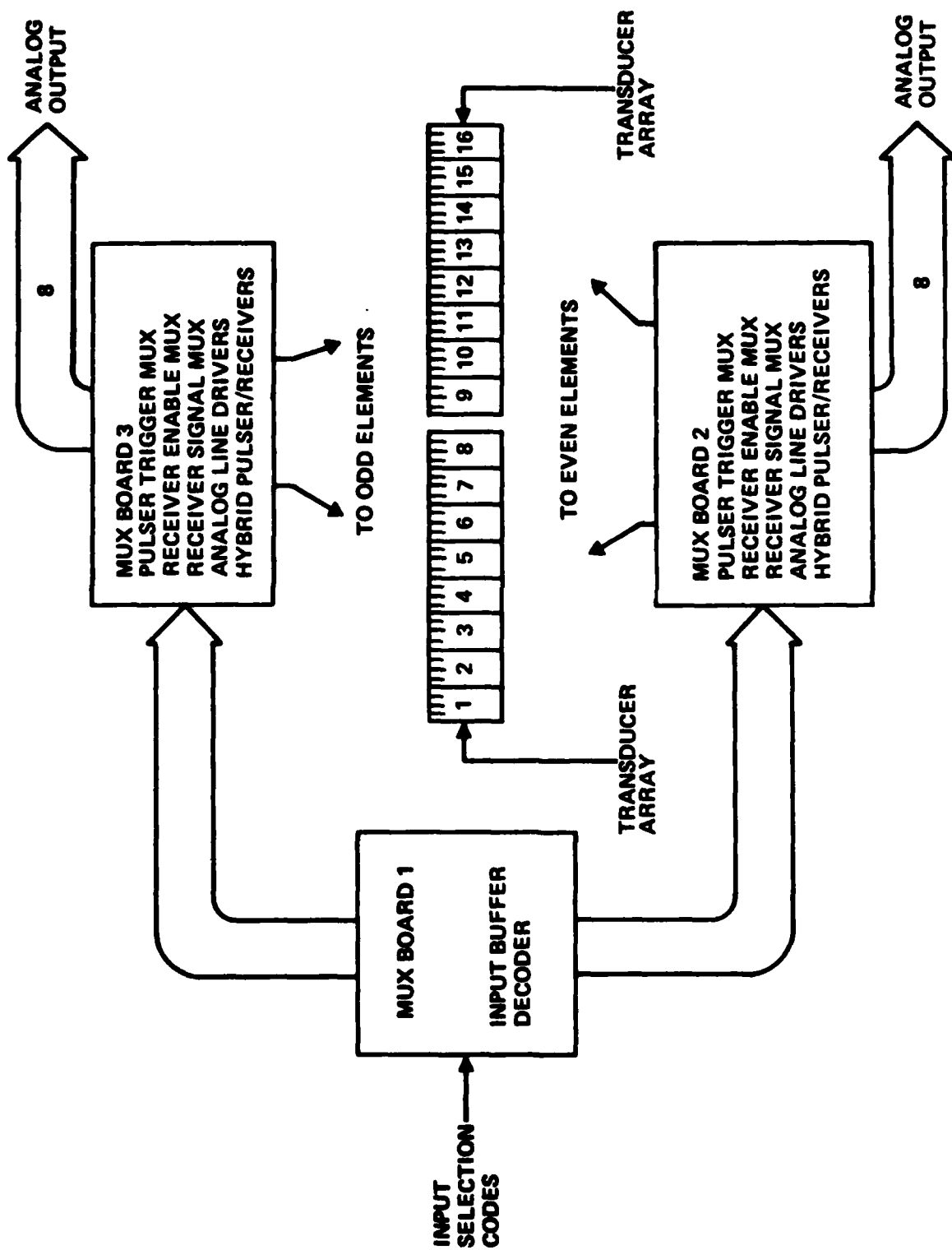


Fig. 4.12 Partitioning and interconnection of multiplexer.

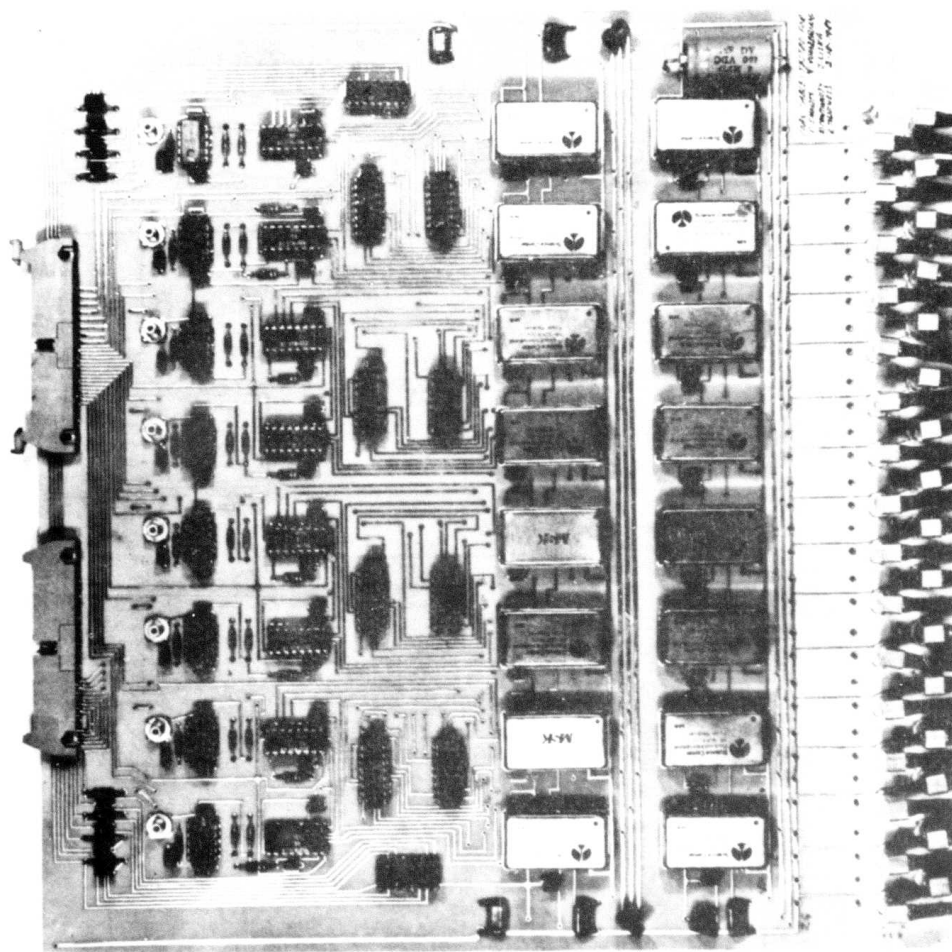


Fig. 4.13 Photograph of multiplexer board.

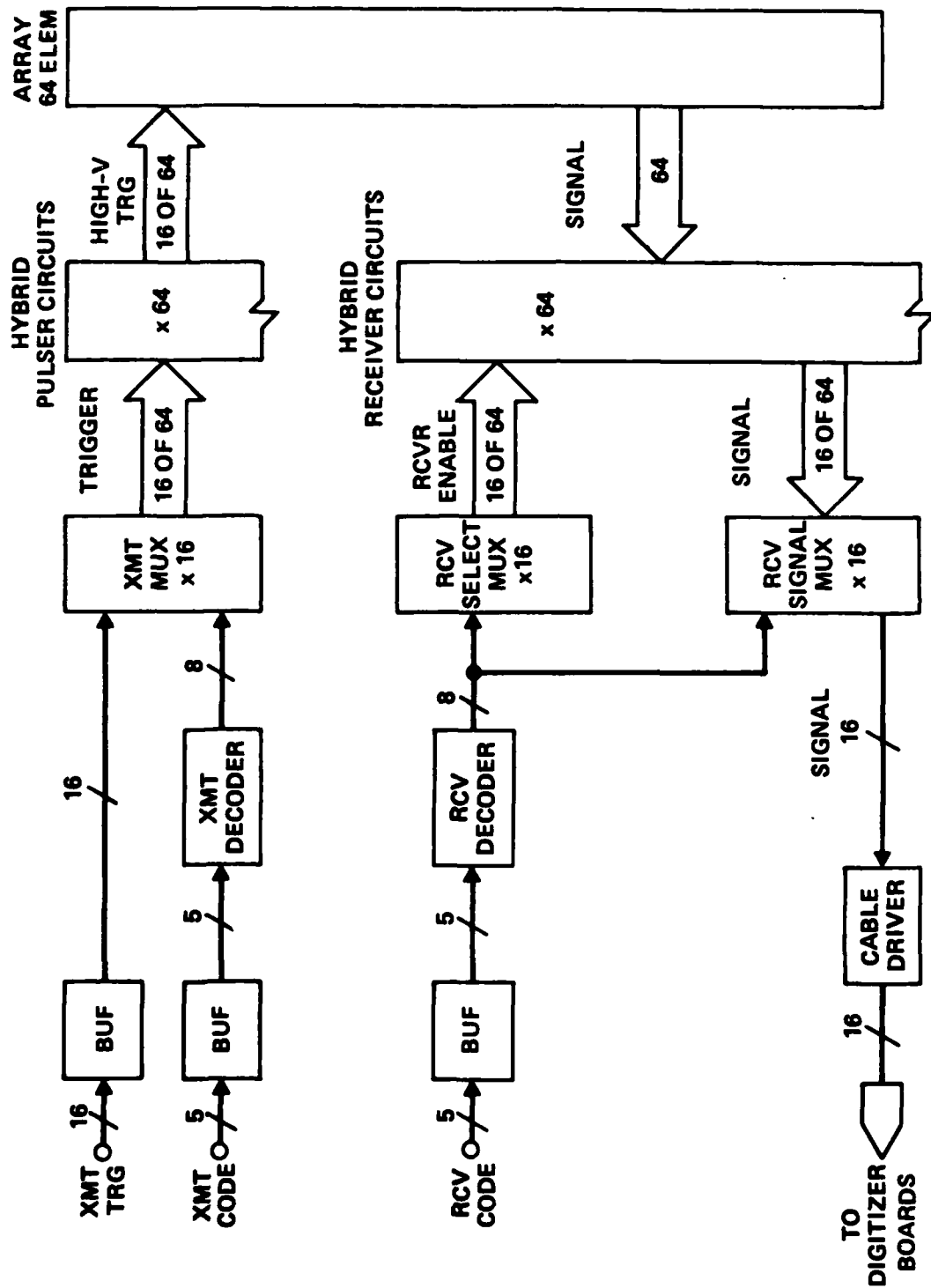


Fig. 4.14 Schematic block diagram of multiplexer.

to activate the selected transducer elements. The receiver elements are selected in an analogous way with the RCV code. In this case the code switches both the digital and the analog multiplexers. The digital unit is used to enable 16 of the receiver circuits by switching the receiver's +5 volt power path internal to each hybrid. The analog unit connects the outputs of the 16 enabled receivers to the 16 line drivers. These line drivers connect the multiplexer assembly to the signal conditioning circuitry through 75 ohm coaxial cables. The specific channels selected by each of the group codes are listed in Table 4.1.

Table 4.1  
XMT/RCV Segment Select Codes

Array Segment Selection (4 elements/segment)					Binary Code					Octal Code	
<u>MSB</u>	<u>LSB</u>	<u>C</u>	<u>B</u>	<u>A</u>							
1 thru	4				0	0	0	0	0	00	
2 thru	5				0	0	0	0	1	01	
3 thru	6				0	0	0	1	1	03	
4 thru	7				0	0	1	1	1	07	
5 thru	8				0	1	0	0	0	10	
6 thru	9				0	1	0	0	1	11	
7 thru	10				0	1	0	1	1	13	
8 thru	11				0	1	1	1	1	17	
9 thru	12				1	0	0	0	0	20	
10 thru	13				1	0	0	0	1	21	
11 thru	14				1	0	0	1	1	23	
12 thru	15				1	0	1	1	1	27	
13 thru	16				1	1	0	0	0	30	

It is essential that the analog multiplexer used for the received signals have crosstalk and feedthrough levels that are negligible compared with the direct signals. The design of the multiplexer function is such that there are 16 individual multiplexer integrated circuit packages in the analog section. Each IC connects to only one active transducer element at a time. The IC's are sufficiently well separated that the crosstalk and feedthrough between them is of no concern. It is the interactions between the four inputs of the individual IC that might cause a problem. Using a bread-board model, a known signal with a particular source resistance was applied to all the input pins except for the one pin that was connected to the output pin. This input pin was connected to ground through a 39 ohm resistor. The signal level at the output was then compared to the input signal level applied to the input pins. The output was found to be 35 dB below the input signal level. Since an 8 bit A/D converter has a dynamic range of 48 dB, this crosstalk level is not negligible. However, in the actual circuit, the receivers for the other input pins are not enabled, providing at least another 26 dB of isolation (corresponding to the receiver amplifier gain). Therefore the overall isolation of the analog output signal from signals at inactive multiplexer inputs is in excess of 60 dB. This degree of isolation is acceptable and provides a comfortable margin over the minimum signal that would affect the output of the A/D converter. The actual performance of the system will not be this good since the weak link in the effort to suppress crosstalk is the transducer array. The crosstalk of the particular array used in this system was not measured, but the level is reportedly less than 30 dB below the direct signals.

The printed circuit boards comprising the multiplexer assembly are mounted in a waterproof box with dimensions of 14 inches  $\times$  15 inches  $\times$  16 inches. This box is attached to the two transducer arrays through 64 coaxial cables. The lengths of the cables from the transducers to the connectors on the p.c. board are between 17 and 25 inches depending on the physical location of the p.c. board connector. The multiplexer box and the transducer arrays are held in place by a special frame that will be described in Section 4.2.9.



#### 4.2.4 Signal Conditioning Circuitry

The purpose of the signal conditioning circuitry is to prepare the signals for the A/D converter. The circuitry is composed of the main amplifier, a digitally controlled attenuator, a clipping circuit, a filter, a dc level shifter and a low output impedance buffer amplifier. A schematic of the circuit is shown in Fig. 4.15 a and b. (Drawing B-2 in Appendix B provides component values for this circuitry.) The main amplifier has a gain of 26 dB and a bandwidth of 10 MHz with a maximum peak to peak output voltage of 23 volts. It is based on a commercially available operational amplifier with external compensation to realize the wide bandwidth and high output voltage.

Following the amplifier is a digitally controlled attenuator. The design of the attenuator is based on a tapped constant impedance ladder network. There are 15 taps with a 3 dB change in attenuation at each tap to provide a total attenuation range of 45 dB. A 16:1 analog multiplexer is used to switch between the taps. In order to obtain the requisite bandwidth of 10 MHz and reduce feedthrough problems, it was necessary to build the multiplexer as a two stage unit with a buffer amplifier between the two stages. It also proved to be convenient to put the signal clipper composed of diodes D1 through D6 at the input to the buffer amplifier. The buffer amplifier consists of transistors, Q<sub>1</sub>, Q<sub>2</sub>, and Q<sub>3</sub>. It is a constant current biased emitter follower where the current source Q<sub>3</sub> is switched from one emitter follower to another depending on which attenuator tap is being addressed.

The signals are then passed through the filter. The filter is designed as a 6 pole, low pass, Butterworth filter with a 3 dB frequency of 6.6 MHz. This type of filter was chosen because of its sharp cutoff characteristic. It serves as an anti-aliasing filter and removes digital noise originating from the 18 MHz clocking signals. The output of the filter is ac coupled to the dc level shifting circuit (R<sub>52</sub>, R<sub>53</sub>, R<sub>54</sub>) and then coupled into the buffer amplifier. The buffer amplifier has a low output impedance that effectively suppresses transients caused by the large current pulses associated with the strobing of the A/D converter.

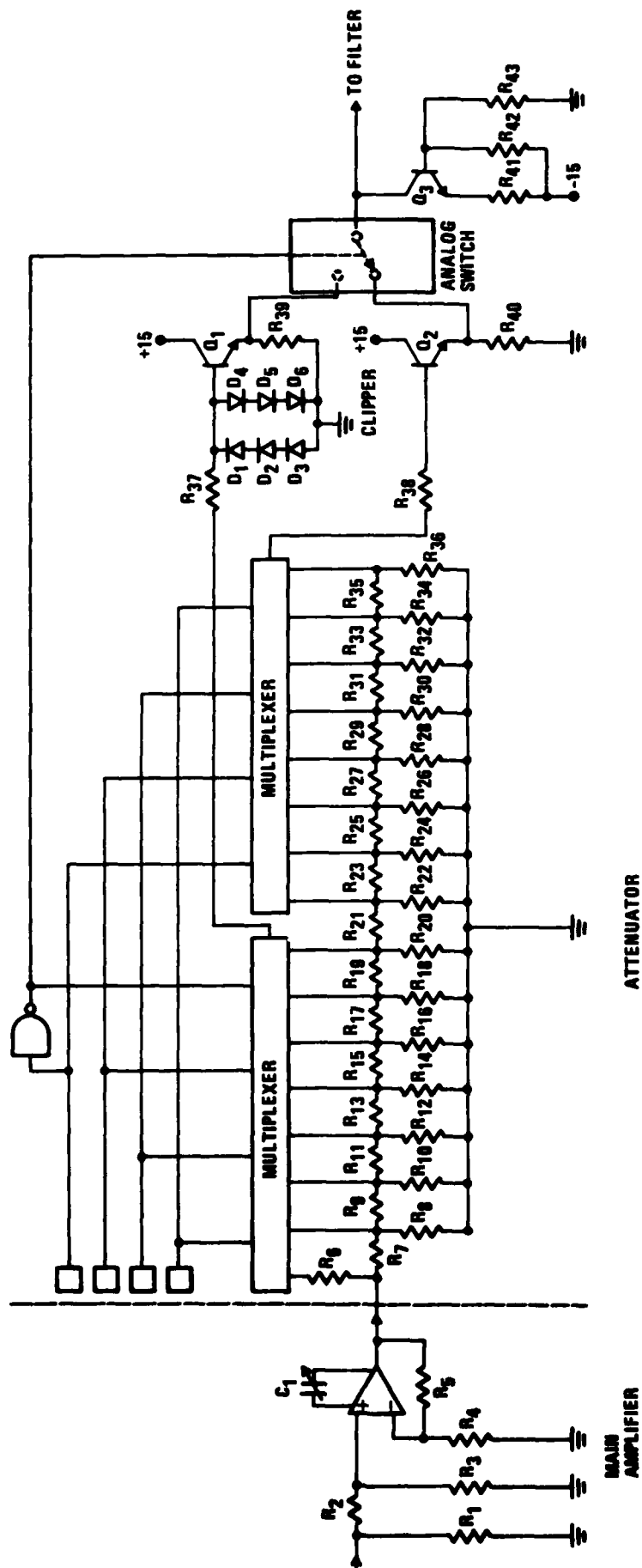


Fig. 4.15 (a) Schematic of signal conditioning circuitry: main amplifier, attenuator, and clipper.

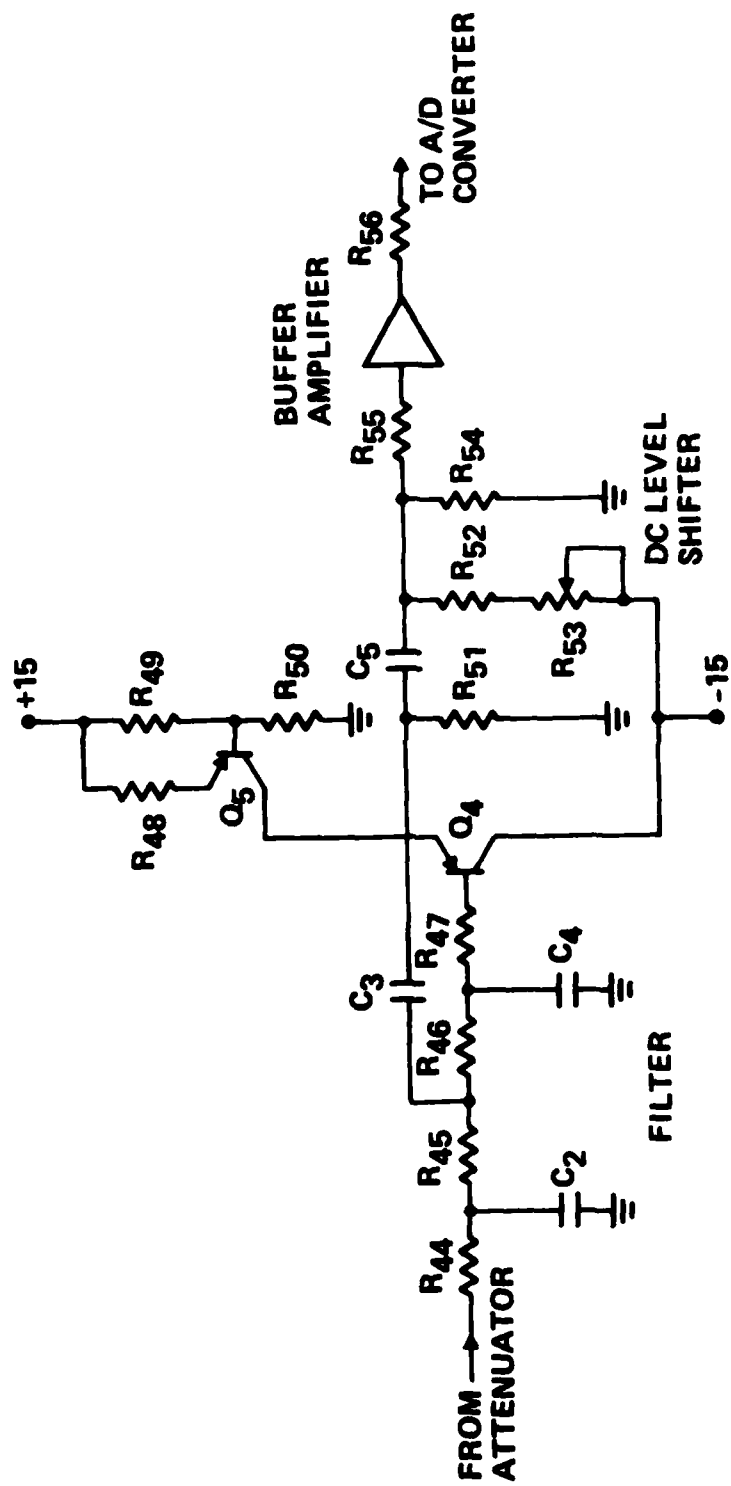


Fig. 4.15 (b) Schematic of signal conditioning circuitry: filter, dc level shifter, and buffer amplifier.

#### 4.2.5 Array Digitizing Electronics

Referring to the block diagram in Fig. 4.4, the set of blocks contained within the dotted lines comprise the Array Digitizer Electronics or ADE. These functional blocks are interconnected through a variety of lines carrying arm, trigger, clocking and data signals from the interface and the timing and control circuitry. The purposes of the ADE can be summarized as:

1. Accept and decode commands and data from the host computer.
2. Switch the multiplexer to the appropriate sets of pulsers and receivers.
3. Select the gain of each receiver channel.
4. Send trigger signals to the pulsers with the appropriate time delays.
5. Digitize the signals received after a specified delay.
6. Store the digitized signals in a buffer memory.
7. Transmit the contents of the buffer memory to the array processor.

In order to accomplish these tasks there are a total of eight command codes that are sent by the host computer and a starting memory address code that is sent by the array processor. The host computer codes are listed in Table 4.2. When the codes are received from the host computer they are immediately identified and the data associated with the command is stored in the appropriate register of the control memory, schematically illustrated in Fig. 4.16. Two of the commands, the host trigger and the host clear, are unique in that no data is associated with them and they are executed immediately after being identified.

The function of much of this circuitry can be explained by tracing the operations that take place when an array pulse and receive sequence is executed. The first command to be sent by the host computer is IO CLR. This initializes the circuits to a known state. The exact sequence of the commands following an IO CLR is not important since their function is to store data in the six registers of the control memory and this can be done in any order. A

**Table 4.2**  
**Host Command Codes**

Functions	Acronym	Command Code (Octal)	Data Field Bits
Trigger Delay Coarse	TDC 01	00	8
	TDC 02	01	
	TDC 03	02	
	TDC 04	03	
	TDC 05	04	
	TDC 06	05	
	TDC 07	06	
	TDC 08	07	
	TDC 09	10	
	TDC 10	11	
	TDC 11	12	
	TDC 12	13	
	TDC 13	14	
	TDC 14	15	
	TDC 15	16	
	TDC 16	17	
Trigger Delay Fine (2 channels merged)	TDF 1-2	20	8
	TDF 3-4	21	
	TDF 5-6	22	
	TDF 7-8	23	
	TDF 9-10	24	
	TDF 11-12	25	
	TDF 13-14	26	
	TDF 15-16	27	
Receiver Voltage Gain (2 channels merged)	RGV 1-2	30	8
	RGV 3-4	31	
	RGV 5-6	32	
	RGV 7-8	33	
	RGV 9-10	34	
	RGV 11-12	35	
	RGV 13-14	36	
	RGV 15-16	37	
Transmit Group	XMTG	40	5
Receive Group	RCVG	41	5
Host Trigger	IO TRG	42	0
Host Clear	IO CLR	43	0
Conversion Delay	CONV DLY	7 x	12

x = Part of data field

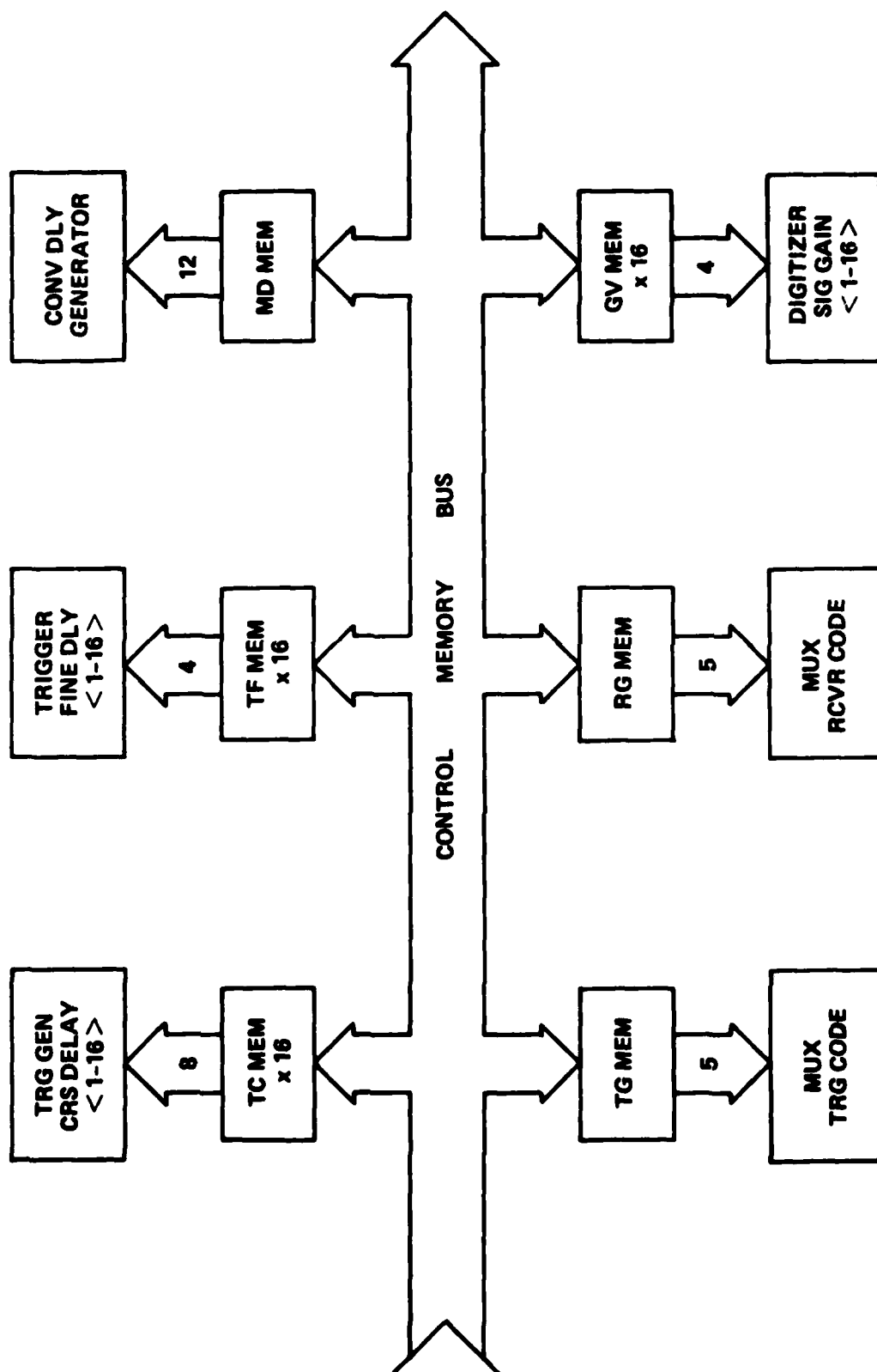


Fig. 4.16 Schematic of control memory.

typical sequence is to first send the command for selecting the set of 16 transducer array elements to be used for transmitting. The data field specifying the five bit code for the multiplexer is stored in the XMTG register of the control memory. It is then sent to the decoder board of the multiplexer where the set of transducer array elements are selected according to the scheme illustrated in Fig. 4.11. A similar procedure is followed for the selection of the 16 receiving transducer elements using the RCVG command. Next the gain of each of the 16 receiver channels is selected. The data fields specifying the four bit codes for the digital attenuator multiplexers are stored in the 16 RGV registers of the control memory. These codes are then sent to the attenuator multiplexers.

The remaining three data commands all specify delays. There are both coarse and fine delays to be specified for the transmit triggers. Also there is a delay corresponding to the ultrasonic water path transit time that is specified before starting the A/D conversion process. The procedure for processing the transmit delay commands is illustrated in Fig. 4.17. There are 16 transmit elements with delays for each one specified separately. The fine delay command, TDF, results in the four bit data field being stored in the TDF register and then being used to select the desired fine delay. The fine delay is obtained with a commercially available digitally controlled delay line. This unit is capable of selecting 16 different delays in steps of 4 nsec using a four bit input code. The fine delays are useful for reducing the quantization error associated with the specified time delays for a given steering direction and for trimming each of the channels to correct for variations in their inherent delays. The coarse delay command, TDC, results in the eight bit data field being stored in the TDC register which controls the delay generator. This delay is specified in integer multiples of a clock interval or  $\approx 55$  ns steps. After the specified number of clock pulses have been received, a trigger is sent through the fine delay circuit to the transmitter multiplexer assembly as shown in Fig. 4.17. The other delay command, known as the CONV DLY, is stored in the CONV DLY register. This data is held in the register until the main trigger is transmitted. This delay is the same for all 16 receiving channels. After this

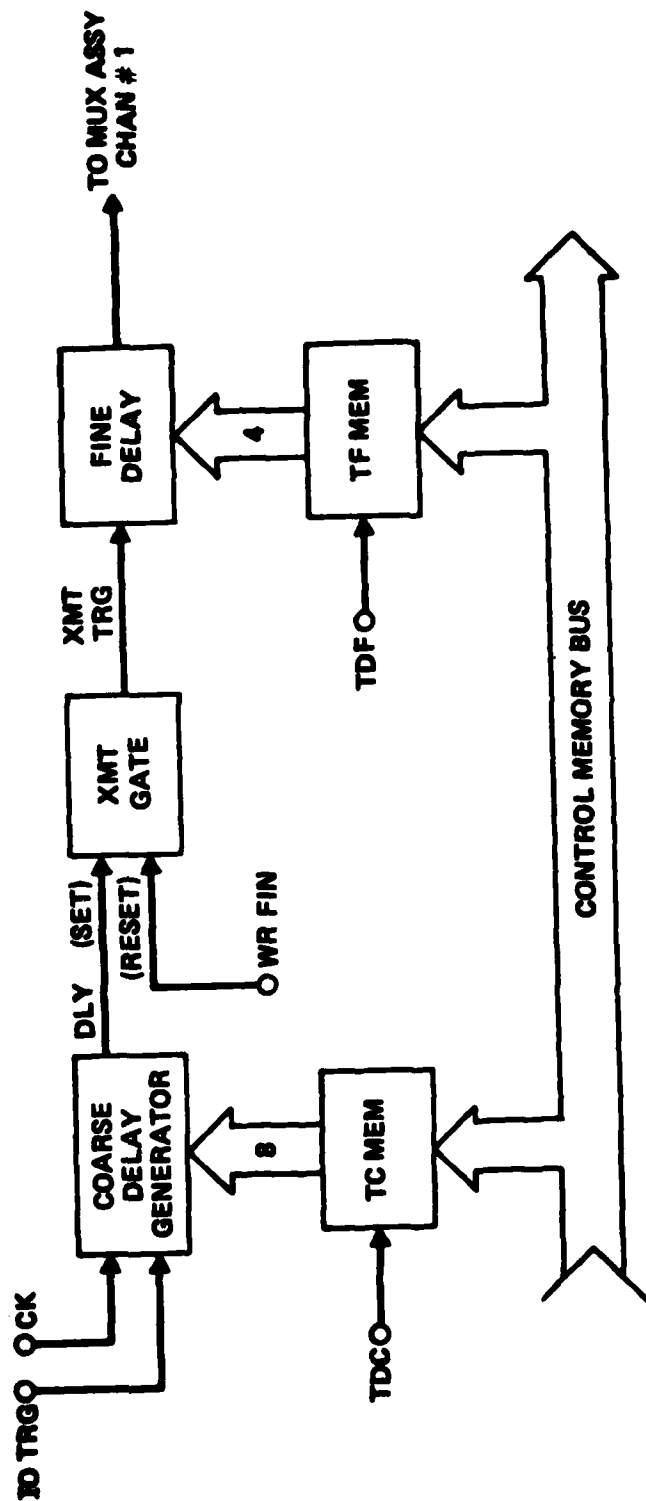


Fig. 4.17 Transmit trigger delays.



delay a gate is generated that starts the A/D converters and starts storing the waveform samples in the buffer memory as shown in Fig. 4.18.

After all six control memory registers have been filled the host command IO TRG is sent to the decoder circuit and is executed immediately. This results in the entire pulse and receive sequence being executed according to the data in the control memory. Once the digitizing process starts, it continues automatically until 1024 samples have been stored. The address generator shown in Fig. 4.18 keeps a count of the number of samples stored. When the memory is full a write finished (WR FIN) signal is generated that stops the operation of the A/D converter.

The Digitizer section is shown in Fig. 4.19. It consists of the 8 bit A/D converter (the TRW Model TDC 1007J operating at a sampling frequency of 18 MHz), a synchronizing latch, and a 1 kilobit  $\times$  8 bit RAM buffer memory. The clocking speeds being used and the close tolerances on the clocking signals dictate that all components of the digitizer be operated as a closely knit unit sharing the same p.c. board.

The next step in the operation is to transfer the contents of the 16 buffer memories to the array processor for the beam forming operation. This transfer is initiated by the array processor which places an address on the interface line as shown in Fig. 4.18. This address plus "handshake" between the ADE and the array processor will start a "memory read" operation that will transfer the contents of the memory to the array processor. The sections of the memory that are to be transferred are specified by the array processor.

#### 4.2.6 S/200 Software Utilized for Control of Array and AP400

The interactive S/200 resident software package, ARRAY, allows a user to control and coordinate the activities of both the array digitizer electronics (ADE) and the Analogic AP400 array processor (AP). The package supplies the user with the ability to easily command the acquisition of a full set of waveforms with a minimum of user input, as well as to single-step, i.e., command by single instruction, the initiation of the ADE and acquisition of data from the ADE via the AP400. The existing version of the software does not take

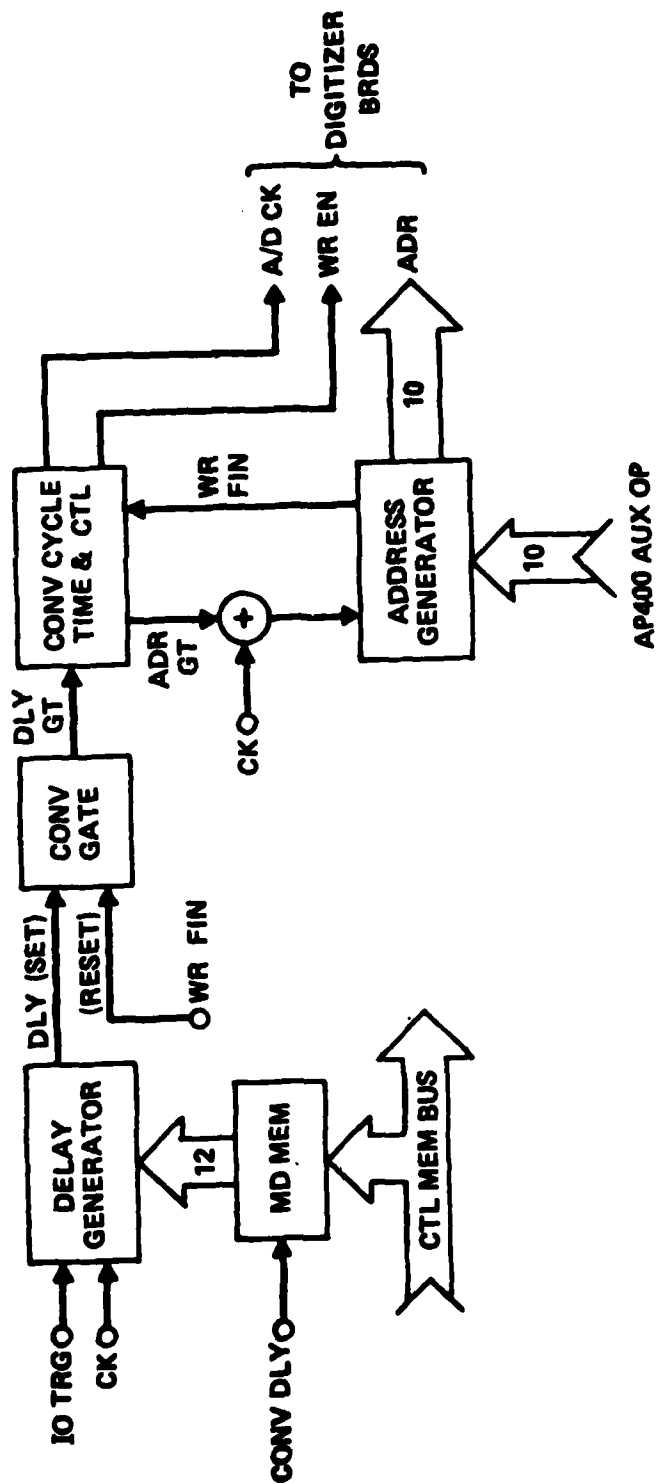


Fig. 4.18 Conversion delay generator and address generator.

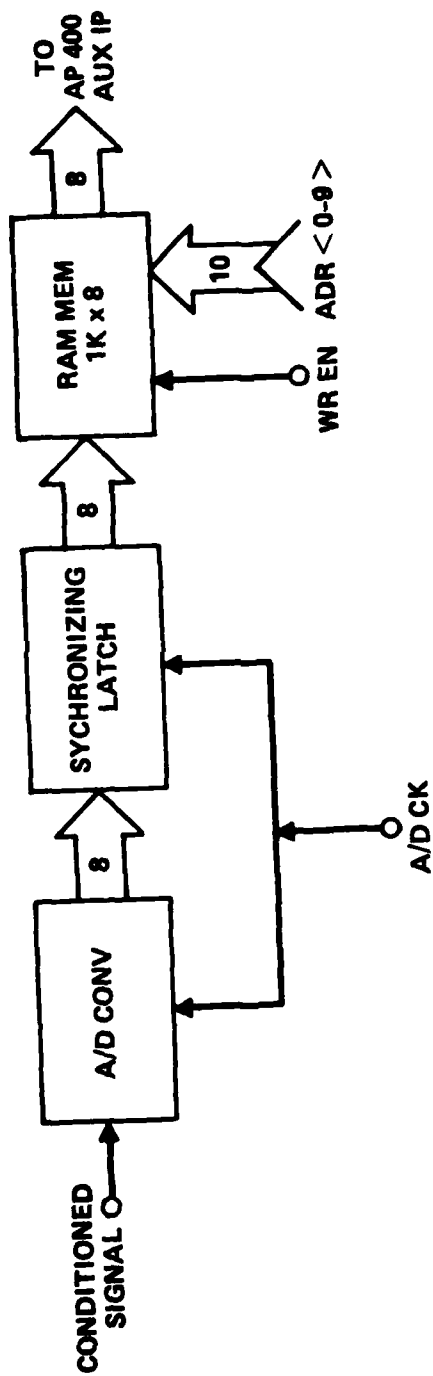


Fig. 4.19 Block diagram of digitizer.

advantage of all of the capabilities of the ADE hardware. It provides access to a subset of the hardware that will permit the generation of sector scans.

ARRAY consists of both FORTRAN 5 and assembly language modules. It was written for a Data General ECLIPSE S/200, and runs under RDOS. The modules of ARRAY are listed with their function in Table 4.3.

Table 4.3  
Primary ARRAY Modules

ARRAY.FR	System initialization, operator interface, procedure controller, and initiation of other modules.
ADEC.FR	Operator interface for direct communication to initialize the ADE.
ADE.SR	Device handler, ADE; IO is programmed.
AP400.FR	Operator interface for acquisition of a single set of data from the ADE.
DATAPLOT.FR	Plots most recently acquired waveform on TEKTRONIX screen.
WISP.FR	Writes ISP format data files.

In addition, ARRAY calls many routines supplied in the AP400 library for communication with the AP400; further information on the AP400 is included in Section 4.2.7.

Upon execution, ARRAY initializes variables as well as both the AP400 and the ADE. The ADE is initialized at this point from the perspective that it has been defined to the software. Upon execution of ARRAY, the user is presented with several options, each specified by a 2-letter mnemonic as shown in Table 4.4. Selection of options "AD", "AP", "PL", and "ST" pass control to modules ADEC, AP400, DATAPLOT, and WISP respectively; necessary user input to each of these options is detailed below.

Table 4.4  
Commands to Array

Mnemonic	Action
AD	Communicate with ADE in single command mode.
AP	Communicate with AP in single command mode.
HELP	List available options.
PL	Plot on terminal the latest waveform acquired.
PR	Initiate the procedure of acquiring a set of data.
ST	Store latest waveform acquired on disk.
XX,BYE	Exit ARRAY.

For the standard acquisition of data from a range of angles the command "PR" is specified. Upon entry to this option of ARRAY, the user is queried for sector scan definition which includes the total number of waveforms, the number of degrees in the sector, and the starting angle. In addition, the output disk file name for the storage of the waveforms, the initialization parameters for the ADE, and the number of channels to sum (1-16) must be specified. The transfer of these input parameters to the ADE, the subsequent acquisition of data, and the activities of the array processor are transparent to the user. ARRAY notifies the user of the completion of signal processing for each of the waveforms corresponding to alternate lines in the sector scan and also of the completion of the entire sector. A sample screen display for the operation of ARRAY is shown in Fig. 4.20.

The angles corresponding to the individual lines of the sector scan are used to calculate the trigger delays for each channel which are then stored in the control memory of the ADE. There are four other sets of parameters that need to be stored in the control memory before the data acquisition can begin. These consist of the specification of the group of transmitting transducer elements, the group of receiving transducer elements, the attenuator setting for each of the receiver channels, and the delay before the A/D converters start

	<u>ACTUAL SAMPLE</u>	<u>RANGE OF VALID RESPONSES</u>
	PR	
	* WFMS IN FAN, = DEG IN FAN 20.11	* WFMS: > 1 * DEGREES: > 1
	BEGIN ANGLE [-45] : [-5]	-45 < BEGIN ANGLE < +45
	FILE NAME = P01EXAM.CC	
	INIT ADE W/FILE (1) OR KB(2) 1	1 → YES, ANY OTHER RESPONSES → NO
	CHANNEL CHOICE	
	CODE CHANNELS	
	0 = 1-16	
	1 = 17-32	
	2 = 33-48	
	3 = 49-64	
	ENTER CODE FOR XMIT AND RCV 2, 2	XMIT: 0, 1, 2, 3 } INDEPENDENT RCV: 0, 1, 2, 3 }
ADE INITIATION	FOR RCVR VLTG GAIN,	
	ENTER LOW CH= OF PAIR (0,2, .14), AND 2 STEP VALS (0-15)	
	EX: 0,13,0 YIELDS 13 STEPS FOR CHO AND 0 FOR CHI	
	ENTER ICH,V1,V2 0,1,1	0 < ICH < 14 IN EVEN STEPS
	ENTER ICH,V1,V2 2,1,1	0 < V1, V2 < 15 (3dB STEPS PER UNIT)
	ENTER ICH,V1,V2 3,4,1,1	
	ENTER ICH,V1,V2 6,1,1	
	ENTER ICH,V1,V2 8,1,1	
	ENTER ICH,V1,V2 10,1,1	
	ENTER ICH,V1,V2 12,1,1	
ENTER ICH,V1,V2 14,1,1		
ENTER ICH,V1,V2 -1,0,0		
A/D DELAY (USECS): 60	0 < DELAY < 4095 (55 NS/STEP)	
* CHANS TO SUM [16] : 16	1 <= CHANS < 16	
DONE W/ANG = 2 -4.42105		
DONE W/ANG = 4 -3.26316		
DONE W/ANG = 6 -2.10526		
DONE W/ANG = 8 -0.947369		
DONE W/ANG = 10 0.210526		
DONE W/ANG = 12 1.36842		
DONE W/ANG = 14 2.52632		
DONE W/ANG = 16 3.68421		
DONE W/ANG = 18 4.84211		
DONE W/ANG = 20 6.00000		
<< ARRAY >>		

Fig. 4.20 Sample screen display for ARRAY.

operating. The specification of these parameters is termed the ADE initiation. The values of these variables may be left unchanged during subsequent passes through "PR".

The existing software only permits the selection of four groups of transmitter and receiver transducer elements rather than the sixteen that the hardware is capable of selecting. These groups represent the transducer elements 1-16, 17-32, 33-48, and 49-64 which are specified by the code numbers 0, 1, 2, and 3 respectively. For a sector scan the transmitter and receiver groups are identical.

The receiver voltage gain must initially be specified for each of the sixteen receiver channels; in subsequent passes through PR, the user may update as few as one pair. The gain is specified for two channels (one pair) on each entry in terms of attenuator steps with each step corresponding to an attenuation of 3 dB. For example the entry, "0, 1, 3" specifies the attenuation for channels 0 and 1. The first digit specifies the even number of the pair, 0, in this case. The second digit specifies the number of attenuator steps for the first or even channel of the pair. In this case 1 is specified and results in an attenuation of 3 dB for channel 0. The third digit specifies the number of attenuator steps for the second or odd channel of the pair. In this case the 3 results in an attenuation of 9 dB for channel 1. Similarly the specification, "14, 0, 0" sets the attenuator in both channels 14 and 15 to 0 dB. The user should only enter even numbers as his first channel specification; an entry of "13, 0, 0" would yield unpredictable results.

The final parameter needed to initialize the ADE is the A/D delay which is specified in microseconds, and may vary from 0 to 225  $\mu$ sec. This is the conversion delay described in Section 4.2.5 and permits an interval of time corresponding to the water path delay to elapse before digitization of the waveform begins.

After the user specifies the number of receiver channels to process, an IO TRG is automatically sent to the ADE and the data acquisition begins. After this step is completed, the data is automatically transferred to the array processor for the "beam forming" process. For sector scans the angles specified

for the receiver are the same as those for the transmitter; no additional user input is required. The details of this beam forming operation are provided in Section 4.2.7. After the beam forming operation is completed, the resulting waveform is passed back to the host, and written to disk. The user is notified as this occurs, on alternate waveforms.

Both of the commands "AD" and "AP" provide a diagnostic capability to the user. The command "AD" allows the user to send octal integer format commands directly to the ADE, while verifying their operation by use of a scope or by acquiring data by use of "AP". The commands are 5 digits in length and are of the format IIDDD where "I" represents a destination code and "D" represents data.

There are approximately 35 commands available to control the ADE. The correct ordering requires one IO CLR to precede any other commands after ADE power-up or reset. The normal sequence is then a set of codes followed by a trigger that actually activates the requests. Table 4.2 in Section 4.2.5 details the valid commands which may be used. The three octal digits representing the data field bits are appended to each of the command codes in Table 4.2 according to guidelines in Table 4.5

If desired the user may acquire data from a user-specified location in the ADE memory. The value of this option is its ability to acquire data from a particular ADE receiver channel to verify its operation. It is used in conjunction with the "AD" option. The input arguments specify the memory, offset address, and number of points to acquire. The memory is specified by a number from 0 to 15, the offset address by a number from 0 to 1023, and the number of points by a number from 1 to 1024. If the user specifies a non-zero offset, the number of points that can be acquired from that channel is 1024 minus this offset.

Finally the user may plot the most recently acquired waveform. This option is straightforward with one exception: the user must specify the vertical axis limits (YMIN, YMAX). If the user enters these two values as equal, the routine will search the data for actual minimum and maximum, and auto-scale the plot to represent the entire range of data.



Table 4.5

Range and Interpretation of Octal Data Codes for Host Commands

Functions	Range of Octal Data Codes	Interpretation
Trigger Delay Coarse	377 <sub>8</sub> -0	0 ns to 255 × 55 ns. Delay in 55 ns increments.
Trigger Delay Fine (2 channels merged)	0-377 <sub>8</sub>	The four LSB's correspond to the low channel and the four MSB's correspond to the high channel. For either channel the range is 0 ns to 15 × 4 ns. Delay in 4 ns increments.
Receiver Voltage Gain (2 channels merged)	0-377 <sub>8</sub>	The four LBS's correspond to the low channel and the four MSB's correspond to the high channel. For either channel the range is -45 dB to 0 dB. Gain in 3 dB increments.
Transmit Group	000 <sub>8</sub>	Channels 1-16
and	010 <sub>8</sub>	Channels 17-32
Receive Group	020 <sub>8</sub>	Channels 33-48
	030 <sub>8</sub>	Channels 49-64
Conversion Delay	7777 <sub>8</sub> -0	0 ns to 4095 × 55 ns. Delay in 55 ns increments.

#### 4.2.7 Array Processor Control and Operation

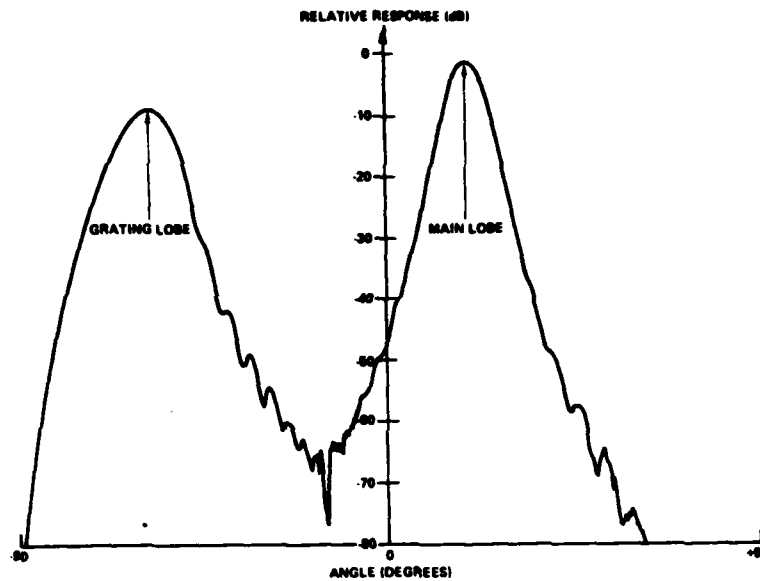
The array processor manufactured by Analogic and designated the AP400 is used for the high speed acquisition of data from the ADE and serves as the "beam-former" for the phased array system. The AP400 communicates with the S/200 minicomputer or host via the calling routine ARRAY described in Section 4.2.6. This calling routine controls the sequence of events occurring in the AP400 through a set of subroutines known as "K-calls". Most of these assembly language subroutines were provided by Analogic in the form of a library although it was necessary to modify some routines to perform specific activities. These

"K-calls" control the operations performed by the AP400 through a set of AP400 resident subroutines known as "Q-routines". The "Q-routines" were also provided by Analogic.

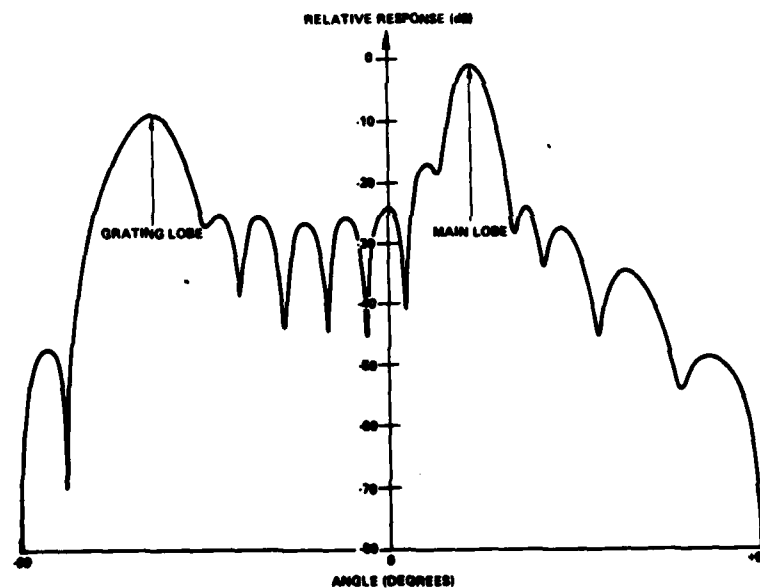
Although the array processor can be used in an interactive program which allows the user to specify, in order, each function that is to be executed, the unit is used with ARRAY in a mode that executes a set of commands specified by the "PR" section of ARRAY. This module acquires the data from each of the 16 channels of the ADE and combines them in a specific way to synthesize a beam returning from a specified angle. This synthesis is accomplished by shifting each of the waveforms by a time delay that will permit the waves to sum coherently in the direction specified. For a sector scan, this direction corresponds to that of the transmitted beam. As each waveform is shifted, it is added to a running sum until all 16 waveforms have been combined. There are several ways available to shift the waveforms. Perhaps the most straightforward technique is to shift the waveform in the time domain by an integral number of sample intervals. The sample interval for the ADE is 55 ns. When a beam is formed with this coarse quantization of the delay, the side lobe level becomes considerably higher than desired. Figure 4.21a shows a beam that has been formed from an apodized 2.5 MHz array of 16 elements with no quantization of the time delays associated with the elements. When the same array is used to form a beam with a quantization of 50 ns, the beam shown in Fig. 4.21b results. The side lobe amplitudes have increased by approximately 40 dB.

As the quantization of the time delay is decreased, the side lobe amplitudes are reduced. The best way to decrease the quantization, which implies some sort of interpolation between samples, is to perform the time shifting in the frequency domain. The signals are Fourier transformed and then multiplied by the complex phase factor  $\exp [i\omega\tau]$  where  $\tau$  is the desired time shift. The signal is then inverse Fourier transformed and summed to synthesize the beam in the desired direction.

The array processor can do the Fourier transforming operations in about the same time as the simple time shifting operations. Thus the unit permits the rapid synthesis of a beam with low sidelobes. The current algorithm completes



16 ELEMENT ARRAY  
ELEMENTS ARE 0.56λ WIDE ON 0.83λ CENTERS  
RANGE = 67λ  
HANNING AMPLITUDE WEIGHTING OF ARRAY ELEMENTS  
TIME DELAY QUANTIZATION = 0



16 ELEMENT ARRAY  
ELEMENTS ARE 0.56λ WIDE ON 0.83λ CENTERS  
RANGE = 67λ  
HANNING AMPLITUDE WEIGHTING OF ARRAY ELEMENTS  
TIME DELAY QUANTIZATION = 50 nsec

Fig. 4.21 Ultrasonic beam formed by a 2.5 MHz array with Hanning amplitude weighting. (a) No time delay quantization, (b) 50 ns time delay quantization.

the acquisition and manipulation of 16 waveforms, each with 512 sample intervals, in 400 msec. Thus for a sector scan containing 100 angles, 40 seconds are required to process the data exclusive of the time necessary to generate a display. The manner in which this time is partitioned among the various computational activities is shown in Fig. 4.22. It is believed that this time can be significantly reduced by shifting all of the computational activities to the AP400 (which requires additional data memory in the AP400) and overlaying the disk storage activities. The processing time for one angle can then be reduced to 80 msec, i.e., by a factor of five.

The operation of the AP400 under the control of the S/200's RDOS operating system had not been tried before ARRAY was written. This has permitted a much better understanding of the limitations of the AP400 with regard to:

1. Required size of program memory
2. Required size of data memory
3. Ordering of calls to perform specific functions.

There are improvements that can be made in the operation of this unit but they have only been realized as a result of having designed the first system.

#### 4.2.8 Display of Data

The general features of the Genisco display processor were described in Section 2.3. Recall that the unit contains a  $480 \times 512$  pixel memory which is mapped onto the 3:4 aspect ratio CRT of a television monitor. The memory is filled with data derived from data on the disk memory of the S/200 mini-computer. The method used to store the data in the memory of the display processor, i.e., the angles and positions of the vectors corresponding to the ultrasonic waveforms is controlled by a software routine that is specific to the application. Each of the pixels can be characterized by an 8 bit word to provide a level of gray or a color according to a code that is chosen by the operator.

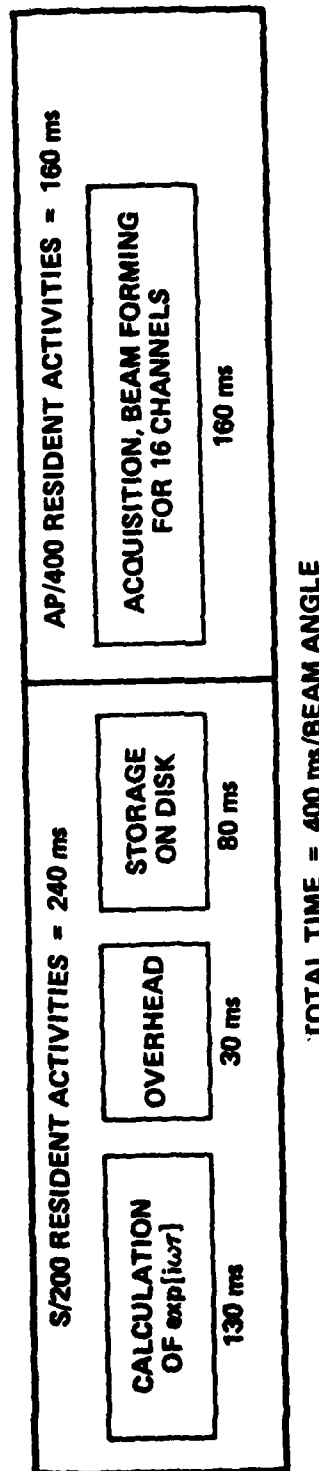


Fig. 4.22 Computational time requirements for beam synthesis.

The scan pattern of the phased array transducer is in general some sort of a compound B-scan. For the contour following mode the pattern of scan lines can become complex with some lines crossing over others. The task of displaying a B-scan of this sort has not been pursued because the 32 element arrays are not long enough to readily lend themselves to this mode of operation. For a detailed examination of a flaw using imaging, it is appropriate to use a sector scan. An example of this sort of scanning pattern is illustrated in Fig. 4.23. The data obtained with the program ARRAY can be displayed in this format by a program called WEDGE. The software for operating the array allows the operator to specify the maximum and minimum angles of the sector, the number of lines within the sector, the number of degrees in the sector, the starting angle, and the water path distance before the waveform digitization begins. This in turn implies that the size and shape of the displayed segment of the sector will change as the input variables are changed. To insure that all of the data is available for display, the sector segment is centered on the TV screen and scaled so that there is a guard band corresponding to 4% of the screen height at the top and bottom of the display as indicated in Fig. 4.23. For certain sets of input variables this scaling technique does not fill the CRT very well, so there is a provision for the operator to change the scale factor and thus magnify the image.

With metal specimens there is a significant refraction of the acoustic beam as it enters the metal. There is the possibility that the beam will not enter at all because it is incident at an angle larger than the critical angle. Once inside the metal the acoustic waves propagate faster than in the water. So, equal time increments of the waveform will correspond to different spatial distances than they did in the water. The complications that result from the refraction caused by a 4 to 1 velocity difference are illustrated in Fig. 4.24 for a sample that has a flat front face and a fan beam scanning from -10 degrees to +10 degrees. Note that the internal angles are -44 degrees to +44 degrees. A considerable distortion of the image will result if these internal angles are not properly taken into account when the data is displayed. In principle this sort of correction presents no difficulty, although in practice one must accurately know the position of the transducer relative

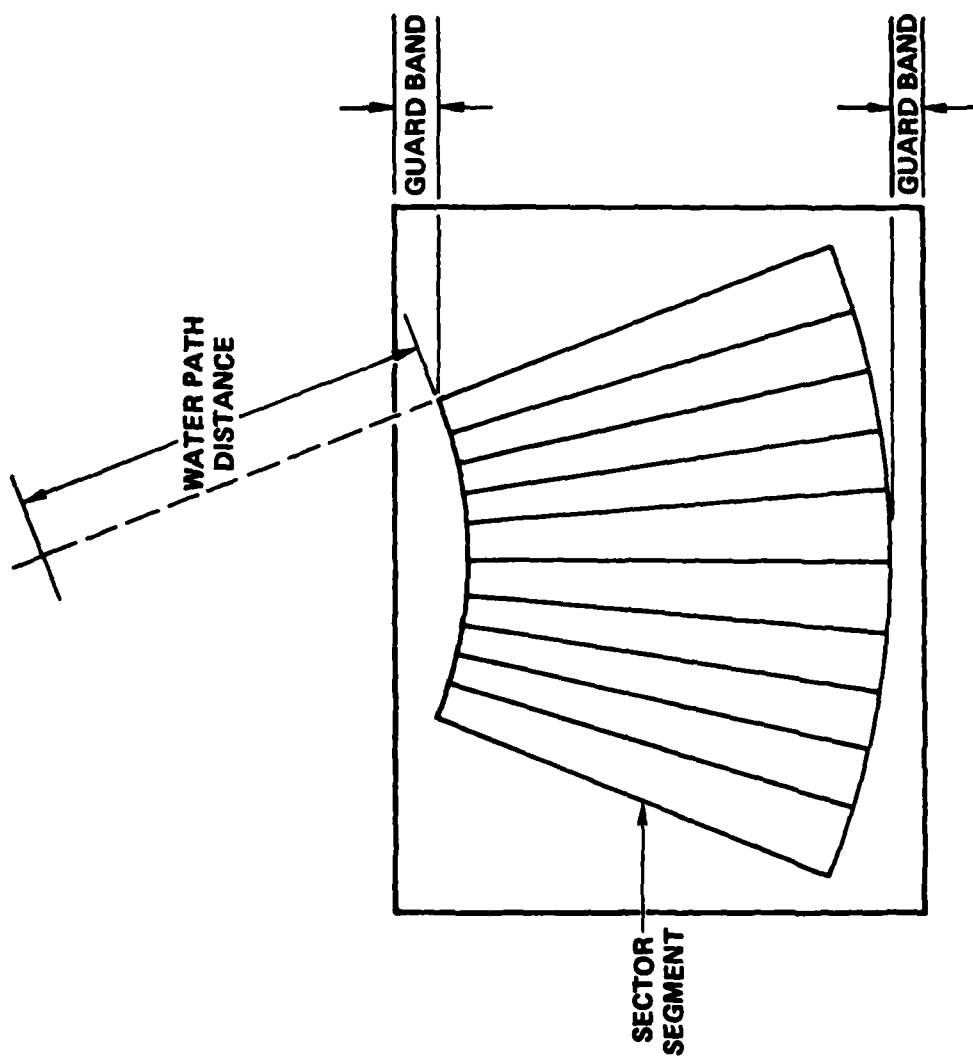


Fig. 4.23 Sector scanning pattern.

# REFRACTION OF ACOUSTIC BEAM AT WATER METAL INTERFACE

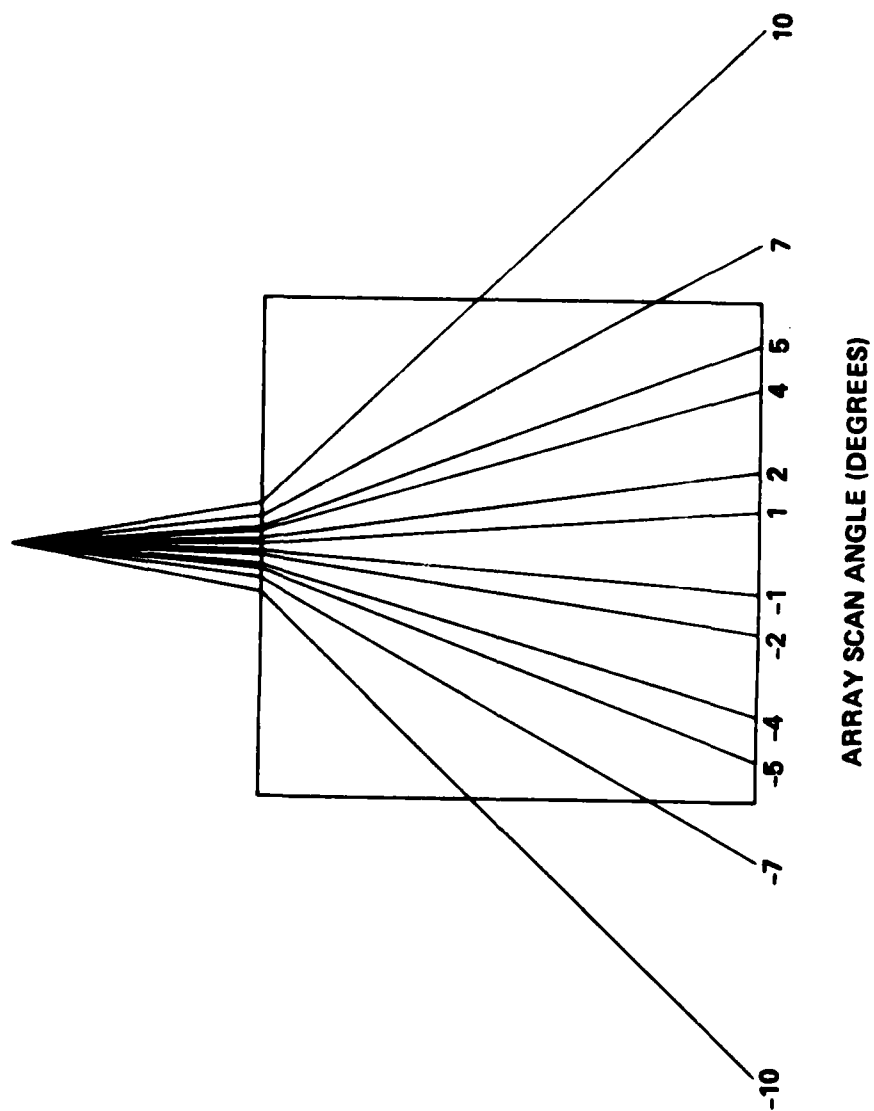


Fig. 4.24 Illustration of a sector scan transmitted through a water/metal interface.



to the surface. If the surface has some curvature this also has to be known. For an inspection task on many identical parts appropriate jigs can be fabricated to orient the part and the curvature of the surface can be programmed into the display. One of the advantages of a phased array is the ability to adjust the phases of the elements to compensate for the focusing or defocusing at a curved metal interface. To properly display the refracted beam, the operator enters the ratio of the velocity of the metal to that of the water and, for a flat surface, the perpendicular distance between the transducer and the part. The rays are then displayed as being bent at the water metal interface as shown in Fig. 4.24. To account for the change in the spatial dimension along the beam, the length of each displayed ray is stretched out by a factor equal to the ratio of the metal and water velocities.

#### 4.2.9 Packaging of Array Subsystems

The components for the phased array system are packaged in several separate groups. The minicomputer, array processor, and display processor stand by themselves. There are two custom assemblies. A relay rack which houses a card cage that contains the 16 boards for the receiver channels, the boards for the timing and control circuitry, and the boards for the control memory. Also housed in the relay rack are the power supplies for most of the system. The second custom assembly contains the multiplexers, the hybrid pulser/ receivers, and the transducers. A photograph of this unit is shown in Fig. 4.25. The circuit boards are mounted in a waterproof box made from acrylic sheet stock. The box is attached to a frame mounted on the scanning bridge of the Test Bed. The frame rides on roller bearings and is mechanically linked to the X-axis drive of the scanning system. This allows it to be moved laterally in X and Y under computer control. The box can be manually raised and lowered using a rack and pinion drive. The spacing between the two transducer array assemblies can be changed manually through a threaded drive assembly. The precision is such that one complete turn of the adjusting knob corresponds to a change in spacing of 0.100 inches. The spacing can be varied from zero inches (i.e., the array transducer housings are physically touching) to a maximum of 6 inches. The various assemblies are interconnected via a combination of ribbon cables and

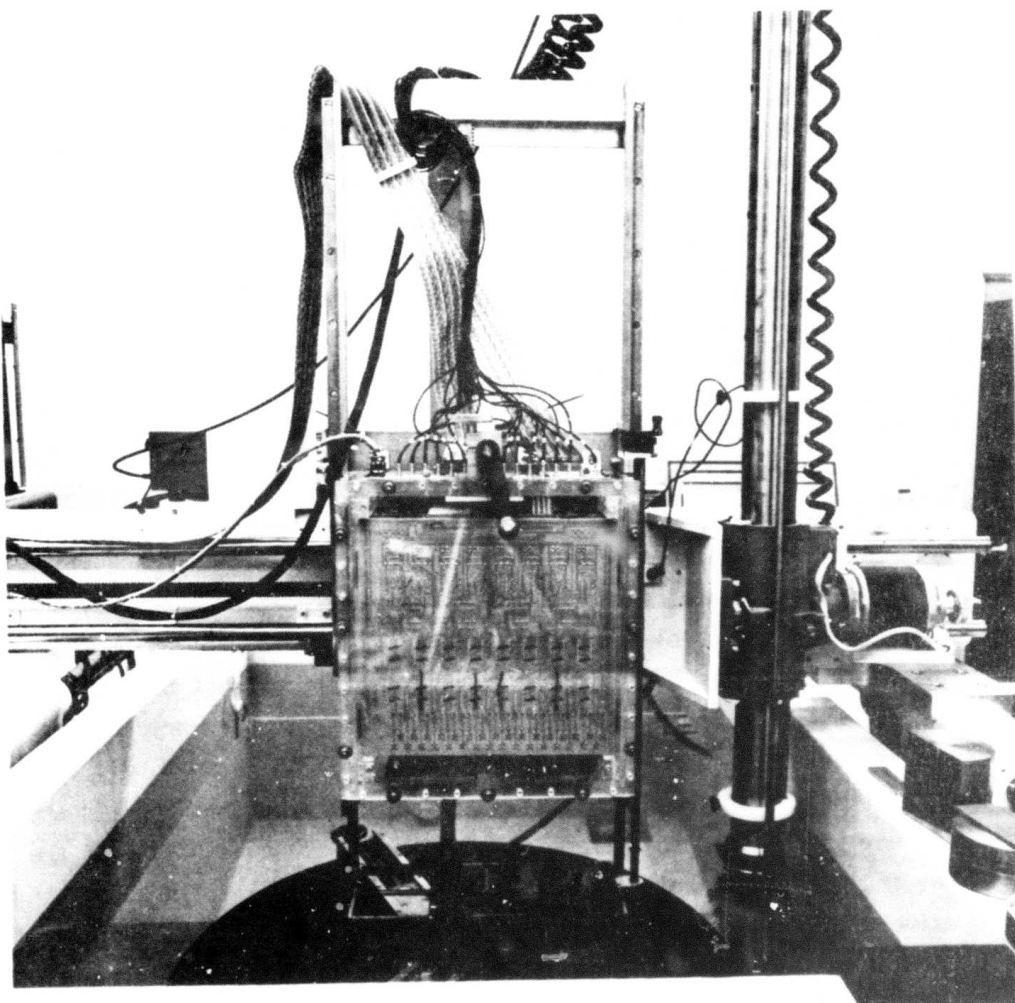


Fig. 4.25 Multiplexer, pulser/receiver and transducer assembly mounted on Test Bed scanning bridge.

coaxial cables. The ribbon cables are used for power supply voltages and digital signals. The coaxial cables have a characteristic impedance of 75 ohms and are used for transmitting the 16 analog received signals from the analog line drivers in the multiplexer box to the signal conditioning circuitry.

#### 4.3 Operation of Phased Array System

##### 4.3.1 Array Radiation Pattern Characteristics

The design of the transducer array determines the angular radiation pattern produced by the system. Of particular interest are the characteristics of the grating lobes and side lobes generated by the array. Recall that the radiation pattern or beam pattern of an array is obtained by summing the contributions of each of the elements. In the far field the sum will be the product of two factors. One factor will be the radiation pattern of the individual element and the other will be the radiation pattern of an array of point transducers. The diagram in Fig. 4.26a illustrates the distinction between the two factors. The array factor can become large in several directions other than the direction of the main beam. These are termed grating lobes and the angles at which they occur relative to the main beam are a function of the spacing between elements. If the phases of the signals applied to the elements are adjusted so that the main beam is deflected through an angle as illustrated in Fig. 4.26b, then the grating lobes are deflected through the same angle. If the array factor is considered alone, the amplitudes of the grating lobes are equal to that of the main beam. The single element factor will modify this, but it is important to realize that the amplitude of the grating lobes can become equal to or larger than that of the main beam for sufficiently large deflection angles. For a periodic array, the only ways to suppress the amplitude of the grating lobes are to make the spacing between the elements less than a half wavelength, measured in the propagating medium, at the highest frequency of interest, or to use short pulses to excite the array.

The characteristics of the side lobes associated with the main lobe (and replicated on each of the grating lobes) are determined by the overall width of the array as well as the amplitude and phase distribution applied to

# RADIATION PATTERNS

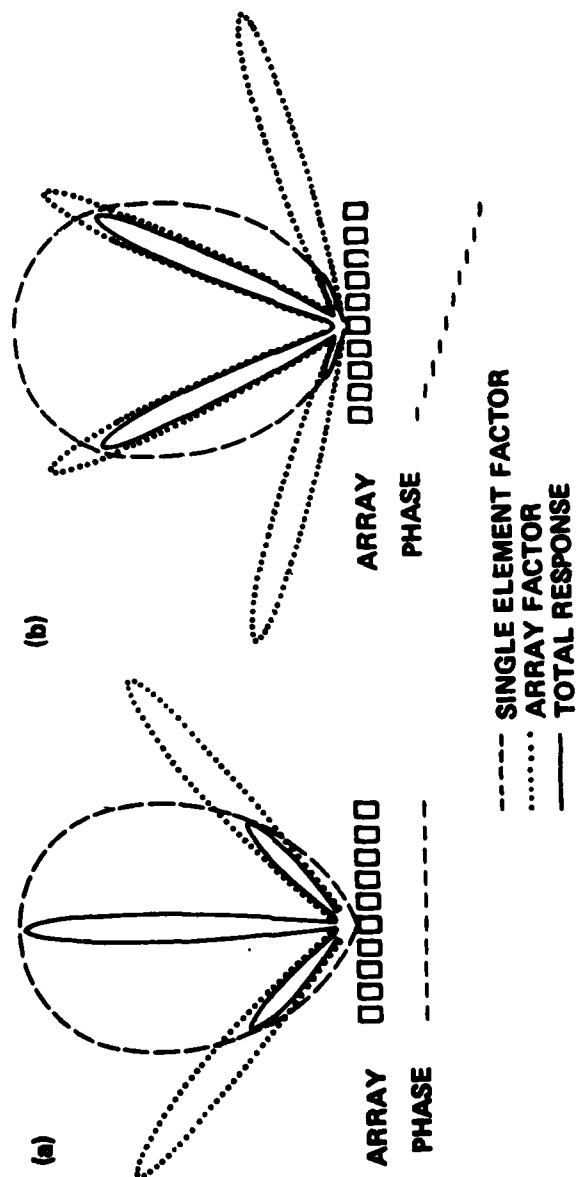


Fig. 4.26 Array radiation function illustrating single element factor and array factor.

the elements. For the Test Bed array, the width is fixed by the choice of using 16 contiguous transducer elements at a time. The phase and amplitude distributions can be varied and Fig. 4.21 is an example of changes that can be effected through altering the phase distribution. An example of the radiation pattern from the Test Bed array is shown in Fig. 4.27 for a uniform amplitude distribution. This should be compared to Fig. 4.21a where Hanning amplitude weighting is used.

The angular scanning range of an array is determined by the radiation pattern of the individual element as indicated in Fig. 4.26. The lateral extent of this radiation pattern is chiefly determined by the width of the element. For NDE applications involving flaws in metals, the critical angle at the water/metal interface is about 15 degrees. The array scanning range need not be much larger than this if only parts with flat surfaces are to be examined. If contour following is to be considered, the range of angles must be increased to accommodate the tilting of the front surface of the part. The Test Bed array transducer can scan the beam over  $\pm 45$  degrees with a decrease in beam amplitude of about 3 dB. Thus the tilting of surfaces at angles as great as 30 degrees can be accommodated and still permit a sector scan to be generated that would enter the metal part.

Although the timing of the signals transmitted or received by the array can be adjusted to obtain a focused beam, this is of no value because of the small width of the aperture formed by 16 contiguous elements (about 7.2 mm). The far field distance of an aperture of this size is about 22 mm in water. For focusing to be effective, the working distance would have to be less than this distance. It should be noted that this distance scales with the reciprocal of wavelength and would therefore be about four times shorter in a metal. Significant focusing could be obtained by combining signals from two or more 16 element groups spaced at distances of up to 150 mm at the expense of decreased angular separation between the main lobe and the grating lobes. This could well be a useful approach in situations where it has been ascertained that the grating lobes will not hit any flaws. It would effectively be a detailed examination in which the resolution was being increased via a synthetic aperture technique.

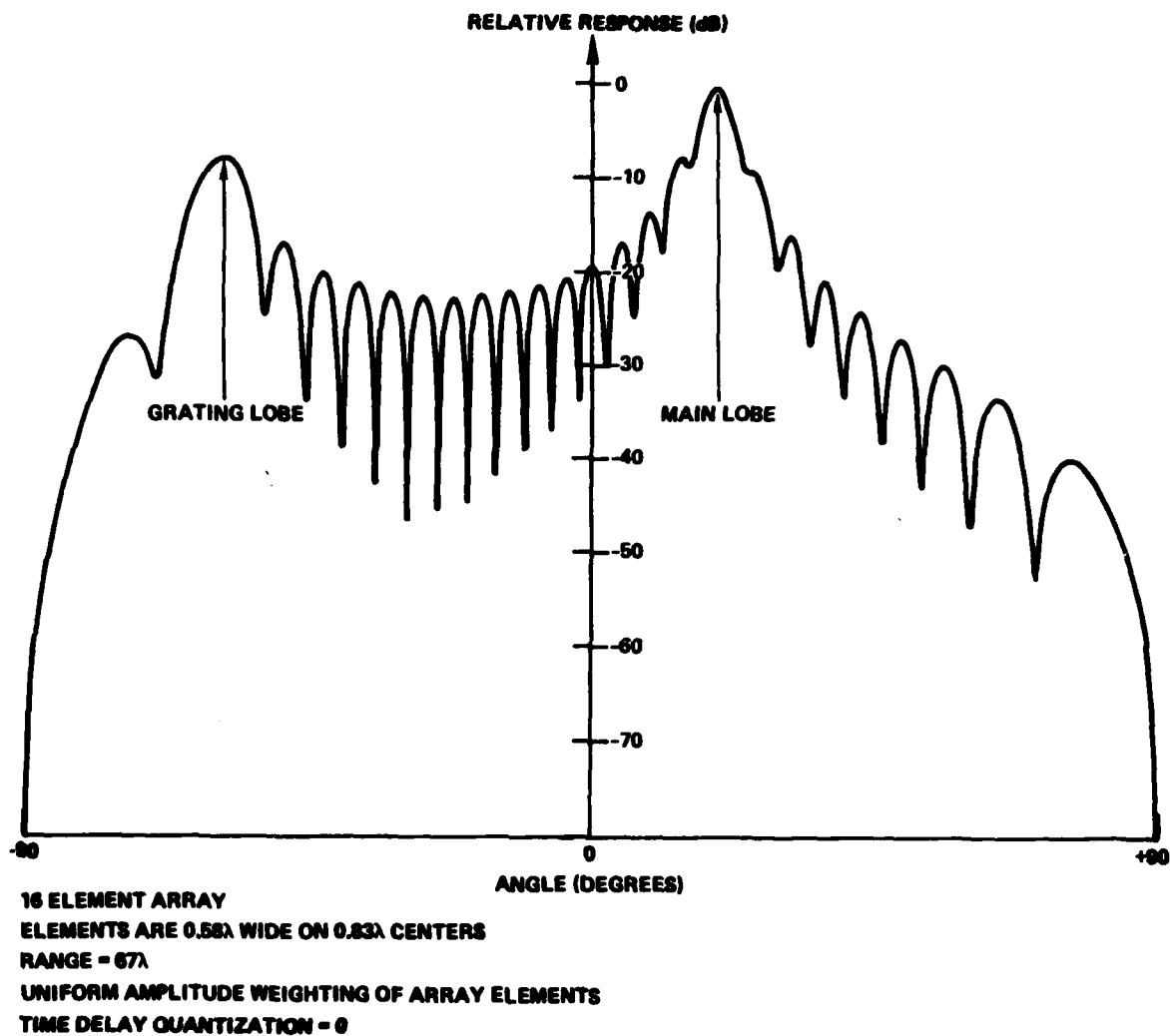


Fig. 4.27 Array radiation pattern for uniform excitation of 16 elements.

The angular width of the beam produced by the 16 element arrays is essentially the same as that produced by a single element transducer having the same aperture. For a 7.2 mm aperture, this can become rather large as indicated in Fig. 4.28. To show that this lack of resolution is the same for both an array transducer and a single element transducer, images of the same 1200  $\mu\text{m}$  flaw were made and are compared in the next section after the details of the imaging technique have been explained.

#### 4.3.2 Imaging of Flaws in Metals

The concerns associated with grating lobes, side lobes, etc. relate to the ability of the array to distinguish between targets in the lateral direction. For the imaging of flaws in metals the loss of longitudinal resolution due to the increase in velocity imposes severe constraints on the use of relatively low frequency arrays. Particularly troublesome is the low level of the flaw signal relative to the front face echo. In the case of a 1200 micrometer diameter spherical void, the front face signal must decay to a level that is 40 dB below its peak value before the flaw signal is detectable without some sort of post processing. Although the transient response measurements on the array in Fig. 4.5 do not extend to -40 dB, it can be seen that even at -30 dB the elapsed time is 4  $\mu\text{s}$  corresponding to a flaw depth of one-half inch in a metal like titanium. This severely restricts the use of real time arrays for detecting flaws in metals except in cases where the flaw signals are very strong or the flaws are located one inch or more below the surface.

One possibility for minimizing the front surface echo is to propagate through it at an oblique angle. The extent to which this is useful depends on the magnitude of the angle, whether the part can be tilted relative to the array, and the strength of the target. It has been noted that the reflection from a flat part remains reasonably strong over the entire range of  $\pm 10$  degrees that has typically been used for sector scans. This results in an imaging artifact that appears as an arc of a circle that is tangent to the surface of the part at the point where the angle of incidence of the beam is zero degrees. Since the amplitude of the backscatter from the oblique intersection of the beam with the flat surface is very small relative to a specular reflection, it is

**RADIATION PATTERN  
2.5 MHz, 16 ELEMENT TRANSDUCER**

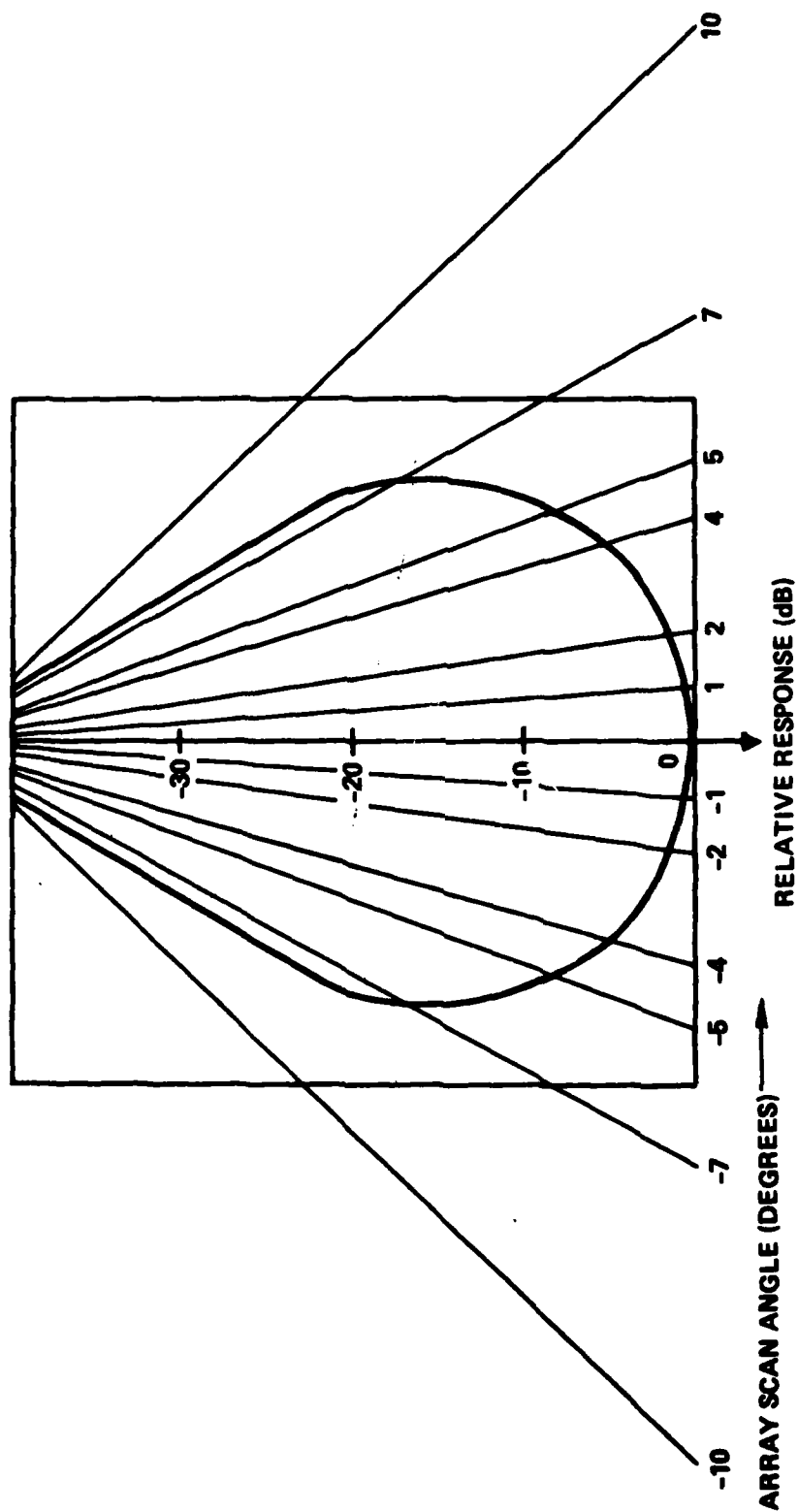


**Fig. 4.28** Polar plot of radiation pattern within a metal part when there is a 50 mm water path.



usually not visible in the image. Thus a typical image obtained from a part appears like the one shown in Fig. 4.29.

As it stands this image is not very useful. The "ring down" from the front surface echo is obscuring the flaw that is present and the artifact created by the reflection from the front surface is creating the illusion that the surface is curved. Most of these problems can be overcome by using a differential imaging technique. This means that a reference image is obtained of a region of the part that contains no flaw but has essentially the same surface reflection characteristics as the region containing the flaw. The reference image is then subtracted from the flaw image to eliminate the problems that are created by the front surface echo. When this technique is used with the image in Fig. 4.29, the differential image shown in Fig. 4.30 is obtained. The subtraction has suppressed the front surface echoes by about 25 dB and the image of the 1200  $\mu\text{m}$  spherical void stands out clearly.

The lateral extent of the flaw reflects the width of the ultrasonic beam that results from a 7.2 mm wide transducer when it propagates through a 50 mm water path and a 12.5 mm titanium path. (Some idea of the scale in Fig. 4.30 can be obtained from the fact that the distance between the front and back surface of the titanium is 25 mm). This does not result from any characteristics of the array other than its aperture. Figure 4.31 shows a B-scan image of the same flaw that was obtained using a differential imaging technique with a single element transducer whose aperture was 7.2 mm. The streaks which demonstrate the difficulty in obtaining a differential image when the transducer has to be mechanically moved, are caused by slight irregularities in the motion of the transducer. Note that the width of the flaw is about the same as in Fig. 4.30.

#### 4.3.3 Born Inversion of Array Data

A feature of the array electronics was to process the received signals with sufficiently low distortion that the array could be used for acquiring scattering data. To show that this is feasible, the zero degree waveform that makes up one line of the image in Fig. 4.30 was used as an input signal

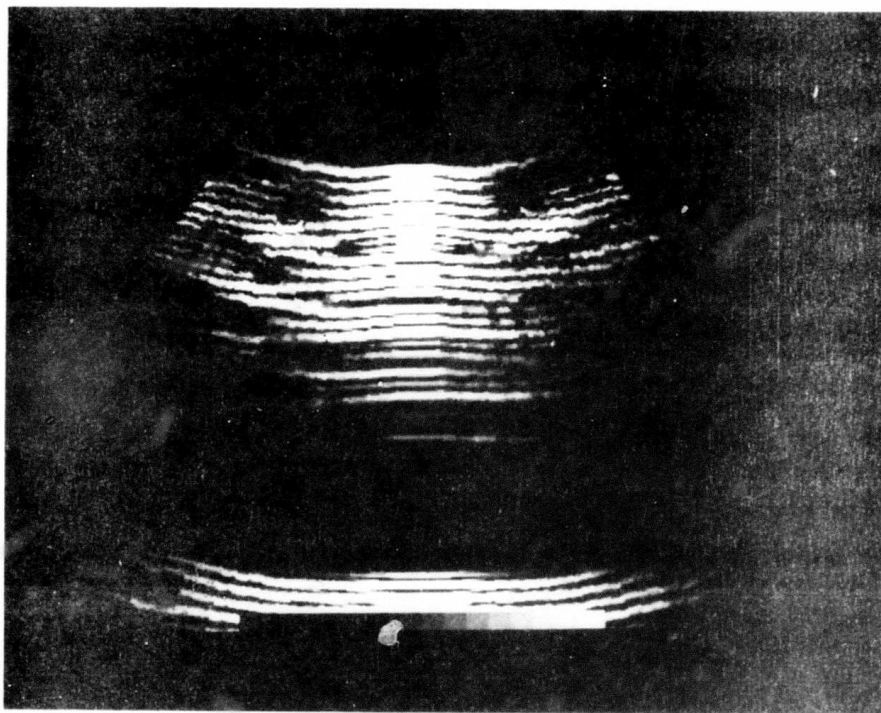


Fig. 4.29 Unprocessed image obtained from a titanium part with a flat front surface.

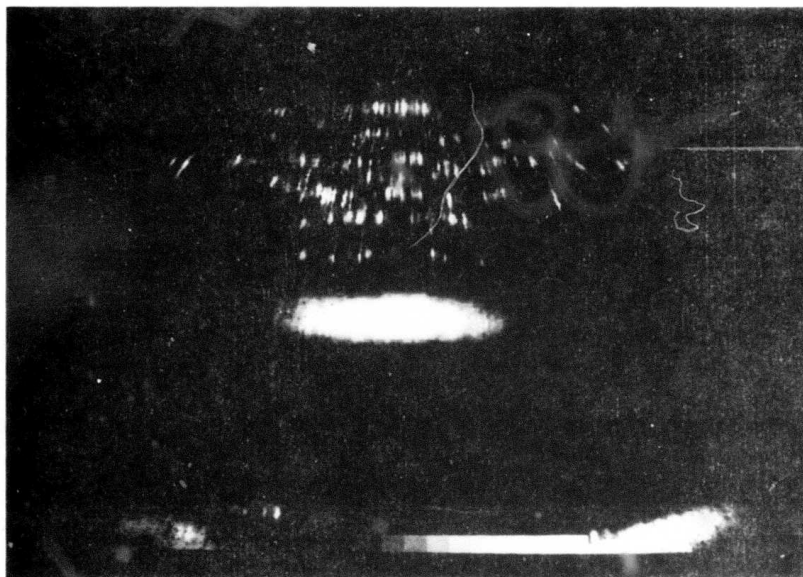


Fig. 4.30 Differential image of a 1200  $\mu\text{m}$  spherical void in a titanium disk.

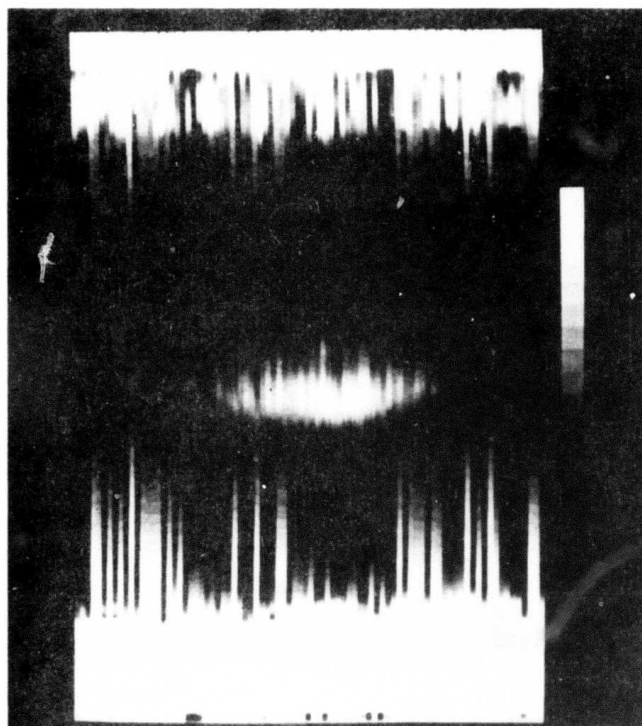


Fig. 4.31 B-scan of 1200  $\mu\text{m}$  spherical void obtained with a single element transducer having the same aperture as the array.

for the Born inversion. An unsubtracted backsurface echo was used as a reference waveform for performing the deconvolution. The bandwidth was centered at about  $ka = 1.2$  and the ratio of  $[ka]_{\max}$  to  $[ka]_{\min}$  was about 3:1. The center of the flaw was determined by extrapolating the phase at low frequencies. The Born inversion estimate of the radius was  $520 \mu\text{m}$  which is low by 13%. Considering that this is the first Born inversion data that has been obtained with an array, the agreement is excellent.

In principal the array provides a convenient technique for acquiring scattering data as a function of angle, although time has not permitted this to be done with the  $1200 \mu\text{m}$  void. Despite this potential advantage it is unlikely that an array transducer of the type described here will be useful for the detailed characterization of flaws via the Born inversion algorithm. The Born inversion work described in Section 3.2.2 established the bandwidth requirements of this algorithm as being from  $[ka]_{\min} \approx 0.75$  to  $[ka]_{\max} \approx 1.8$ . From this it is apparent that the array transducers used here are only adequate for a narrow range of flaw sizes. To measure an unknown flaw a selection of array transducers whose collective bandwidths spanned a wide range of frequencies would be necessary. The array approach is much more likely to be useful in an imaging role where various synthetic aperture techniques can be used to increase the spatial resolution.

## 5.0 SUMMARY

The Ultrasonic Test Bed Program has been an ambitious program that has had to cover a wide range of technological arenas. On the one hand there is the hardware intensive multiaxis system that has provided the scanning capability. This is coupled with the data acquisition capability that permits the digitization of entire waveforms. These units along with a color display processor work interactively under the control of a minicomputer. Most, if not all, of these units are commercially available; although the total package equals or exceeds the capabilities of most conventional NDE systems.

Using this system it is possible to study the utility and practicality of the inversion techniques that have arisen from the Interdisciplinary Quantitative NDE program.<sup>1</sup> Here the object of the work shifts to translating theoretical and experimental tools into techniques that are useful in practical NDE programs. For the first time an integrated effort has been made to combine the bits and pieces of information from a flaw that are available over a very wide frequency range. The object is to obtain a significantly better characterization of a flaw than has heretofore been possible when only straightforward measurements of the signal amplitude produced by the flaw were used.

Beyond this the Test Bed program has produced a flexible state-of-the-art phased array system that can be used to determine the feasibility of array systems in NDE applications. The system represents a hardware intensive project that involves new ultrasonic array technology at one end and digital array processor technology at the other. In between are 16 custom A/D converters and 64 hybrid pulser/receivers. The synthesis of this system requires many hardware and software skills to be focused on techniques and systems that have just become available.

The Science Center has been able to bring together in a relatively small team of people the skills required for this technologically diverse project. The major goals of the program have been met. However, as with any large program there are areas that will require more work. Further, there are some things that would be done differently in a second generation system. The

discussion below summarizes the work that has been accomplished, points out technological needs for improved capabilities, indicates desirable design changes, and discusses areas requiring additional work.

Recall that the major hardware subsystems associated with the Test Bed are the minicomputer, multiaxis controller, the data acquisition system and the display processor. Two of these units, the multiaxis controller and the A/D converter portion of the data acquisition system, represent areas of rapidly changing technology. The discussion in Section 2.0 of the report covered many of the problems encountered with these units. It should be noted that a much better mechanical system could be realized by placing each of the axes in a closed loop control system using encoders linked as closely as possible to the transducer motion. This permits a rapid assessment of the location of the transducer, permits more accurate positioning without the need of excessively rigid mechanical structures, and provides signals that are directly linked to the motion of the transducer for triggering the pulser/receiver. The multiaxis controller suffers from not having a more powerful diagnostic capability that would make it friendlier to the operator. Robustness in the operation of this unit would be a desirable goal. In a system depending on several asynchronous digital interfaces, it is desirable to link the timing of the data acquisition system tightly to the motion of the transducer to ensure that the area scanned is sampled uniformly. This objective requires some design changes in the present system but could be readily achieved in a second generation system.

The technology of high speed A/D converters is rapidly changing with the emphasis on both higher sampling speeds and higher accuracy of the sampled data. For most current NDE needs the sampling speed is adequate but the accuracy needs to be improved. It would be desirable to have an accuracy equivalent to eight bits at a data frequency of 25 MHz without the need to temporally average signals. Although newer units that have become available commercially are more accurate they still fall short of this goal. The digital data acquisition device used with an NDE system should also have a high speed bus capability to convey data to a host computer at a high bit rate. A rate of 500, 1024 point waveforms per second would satisfy many needs.

Section 3.0 on inspection procedures covered many topics. The first of these were concerned with the search mode. The Test Bed Program has not devoted too many resources to the detectability problem nor to the reliability of detection. This is recognized as an important area of study which should be pursued with the same diligence as the techniques for the characterization of the flaw. There are a number of generic detection techniques that can be included in future work as well as specific problems that relate to particular geometries. The Test Bed system uses a straightforward amplitude threshold technique to detect signals of interest. The reliability can be increased by making the threshold a function of depth within the metal. Future work should be addressed towards subsequent analysis of the detected segments of waveforms to compare them with known properties of flaw signals. In this way the reliability of detection can be improved.

The sensitivity of the detection techniques can be improved by simply using a focused transducer rather than an unfocused one. To the extent that the flaw size is less than the focal spot size, each reduction in the focal spot size by a factor of two will increase the flaw signal-to-noise ratio by a factor of 16. This implies an increase of the scanning time by a factor of four to cover the same area. Detailed studies of these important areas of detection sensitivity, scanning time, and reliability of detection have yet to be done, but the inherent scanning and signal processing capabilities of the Test Bed system will permit these studies to be carried out efficiently.

The first aspect of the detailed examination of a flaw that was considered was the imaging techniques. The techniques used were C-scan and B-scan techniques which utilized the display processor for presenting a gray scale or color coded image. Future work could improve these capabilities in two areas. First it would be desirable to display a larger dynamic range in the image than is currently possible. The limit is currently set by the available dynamic range of the A/D converter of about 48 dB. This can be extended by using nonlinear processing of the signals prior to digitization so that the dynamic range of the signals is compressed into the 48 dB range of the A/D converter. After digitization the signals must either be compressed further or color coded to fit into the approximate 30 dB dynamic range of the display



monitor. The use of these techniques would permit a viewer to simultaneously observe signals produced by both the flaws and the grain scattering. It would also permit the color coding capability of the system to be used to full advantage.

The second area that could be pursued is improved resolution of the focused transducers. At the present time commercially available transducers are used that have relatively low numerical apertures (N.A.) and consequently produce focal spot sizes that are considerably larger than the theoretical minimum of one wavelength. When the beam is focused inside a metal part they suffer additional degradation due to spherical aberration at the metal/water interface. Performance in this area can be improved with specially designed focusing lenses. It should be noted that the inspection protocol assumes that imaging can be used for  $ka$  values as low as 6, but the capabilities of commercially available transducers imposed a minimum  $ka$  value of between 20 and 30. Therefore the resolution capabilities of a QNDE system should be improved to permit the minimum imaging performance requirements to be met.

The next segment of the detailed examination procedure was concerned with the use of the Born inversion and the long wavelength techniques. The Born inversion was demonstrated to be useful for the characterization of flaws in the range of  $ka$  values that were beyond the capabilities of imaging techniques. It worked both for known flaws of ellipsoidal shape and also for naturally occurring flaws. The bandwidth requirements were shown to be within the capabilities of available transducers and the accuracy of the estimated flaw sizes was found to be robust in the face of noise. Techniques were demonstrated for determining the location of the center of the flaw using long wavelength procedures. The conclusion is that the Born inversion should be incorporated into the procedure used for conventional NDE inspection. Before this can be done the technique should be tested on a large group of representative flaw types as is being done in the Air Force program to develop a reliable QNDE module.<sup>19</sup> In addition, and this is perhaps the most important step, the procedures for applying the Born inversion to a flaw signal must be automated. This will permit the technique to be carried out with minimal input from the operator. Until this is done the technique is likely to remain a laboratory tool.

With the advent of this technique and the long wavelength techniques, the transducer requirements have changed. It is no longer essential that different but nominally identical transducers have closely matched sensitivities or bandshapes since these characteristics will be eliminated from the flaw signals during the deconvolution procedure. It is essential that the transducers have very wide bandwidths, not so much to produce short transient responses and increase longitudinal resolution, as to permit the analysis of flaws with a wide range of diameters and to obtain long wavelength data. Some work has been done on the problem of obtaining signals with two transducers having different but overlapping bandwidths; and then after deconvolution, splicing the two spectra together. This has worked in some cases but requires additional work to establish a robust procedure for matching the two spectra. Other approaches to realizing ultra wide bandwidth transducers require tradeoffs of sensitivity but may be viable for some applications. The question of transducer requirements that is raised by the need to have data over 10:1 or 20:1 bandwidths needs to be considered in a comprehensive way.

After the tools for characterizing flaws have been applied the results are combined in an algorithm that uses all the information to provide a probabilistic estimate of the flaw's character. This algorithm was used successfully to characterize flaws in ceramic materials.<sup>20</sup> Although it is available as part of the Test Bed software, it has not been used for flaw characterization. As the use of the Born inversion and long wavelength techniques becomes better established, the need for this combining algorithm will increase. At the present time the data is combined in an informal way by the operator to arrive at a complete characterization of the flaw. an example of this is provided by the characterization of the naturally occurring flaw that was provided by Rolls-Royce Ltd.

The last part of the protocol is to subject the total findings about the flaw to an accept/reject criteria. This criteria is beyond the scope of the Test Bed Program and has not been available to the program. The establishment of such a criteria is essential to a QNDE program and must arise from the results of future work.

The final aspect of the Test Bed Program to be discussed was the ultrasonic phased array system. The dominant feature of this system is its flexibility. The system utilizes two 32 element phased array transducers with a variable spacing between them. There are 16 separate receiver channels; each with its own A/D converter and buffer memory. The beam forming for the array is done by an array processor under control of the minicomputer. The scan patterns can be changed in software and a wide variety of synthetic array techniques can be investigated.

The system has been demonstrated with ellipsoidal flaws in the metal specimens and produces images with the same characteristics that would be obtained with a scanned single element transducer having the same aperture and center frequency. The quality of the signals from the array is exceptionally good. It has been possible to process these signals with the Born inversion algorithm and obtain an accurate estimate of the flaw size. Since the system just came on line at the conclusion of the Test Bed Program, there has been no opportunity to fully exploit it and exercise all of its modes of operation.

The immediate plans for the array system are to develop software for investigating its capabilities in a synthetic aperture mode of operation that will permit increased lateral resolution. In general there needs to be a systematic investigation of NDE applications that might be addressed more effectively with phased arrays. Since this system is coupled to a minicomputer, extensive post-processing of the data is possible. This permits practical difficulties related either to the transient response of the elements or to non uniformities of the single element response to be eliminated. Thus the true capabilities of the array can be evaluated and system needs can be identified.

In conclusion the Test Bed Program has addressed a wide range of topics that are important to a quantitative NDE program. As was stated in the work statement for this program it will remain set up and operating for at least one year beyond the conclusion of the program. During this period personnel from outside the Science Center are invited to use the system to address specific problems.

## 6.0 REFERENCES

1. Proceedings of the ARPA/AFML Review of Progress in Quantitative NDE, First Year Report, July 1975, Thousand Oaks, California, AFML-TR-75-212.  
  
Proceedings of the ARPA/AFML Review of Progress in Quantitative NDE, Second Year Report, July 1976, Asilomar, California, AFML-TR-77-44.  
  
Proceedings of the ARPA/AFML Review of Progress in Quantitative NDE, Third Year Report, July 1977, Ithaca, New York, AFML-TR-78-55.  
  
Proceedings of the ARPA/AFML Review of Progress in Quantitative NDE, Fourth Year Report, July 1978, La Jolla, California, AFML-TR-78-205.  
  
Proceedings of the DARPA/AFML Review of Progress in Quantitative NDE, Fifth Year Report, July 1979, La Jolla, California, AFML-TR-80-4078.  
  
Proceedings of the DARPA/AF Review of Progress in Quantitative NDE, July 1980, La Jolla, California (to be published as an Air Force Materials Laboratory Technical Report).  
  
Proceedings of the Air Force/DARPA Review of Progress in Quantitative NDE, August 1981, Boulder, Colorado (to be published as an Air Force Materials Laboratory Technical Report).
2. R.K. Elsley, "Accurate Ultrasonic Measurements with the Biomation 8100 Transient Recorder," Ultrasonic Materials Characterization, H. Berger, M. Linzer, eds., Proceedings of the First International Symposium on Ultrasonic Materials Characterization, National Bureau of Standards Special Publication 596, 1980.
3. Work on the Born inversion procedure (BIP) was sponsored by the Center for Advanced Nondestructive Evaluation, operated by the Ames Laboratory, USDOE for the Defense Advanced Research Projects Agency and the Air Force Wright Aeronautical Laboratories/Materials Laboratory under Contract No. W-7405-ENG-82.
4. Y. Murakami, B.T. Khuri-Yakub, G.S. Kino, J.M. Richardson and A.G. Evans, "An application of Wiener filtering to nondestructive evaluation," Appl. Phys. Lett. 33(8), 685-687 (October 1978).
5. J.H. Rose and J.A. Krumhansl, "Determination of Flaw Characteristics from Ultrasonic Scattering Data," J. Appl. Phys. 54(4), 2951-2952 (April 1979).
6. J.H. Rose, R.K. Elsley, B. Tittmann, V.V. Varadan and V.K. Varadan, "Inversion of Ultrasonic Scattering Data," in Acoustic, Electromagnetic and Elastic Wave Scattering - Focus on the T-Matrix Approach, V.V. Varadan and V.K. Varadan, eds., Pergamon Press, pp. 605-614 (1980).

7. R.K. Elsley and R.C. Addison, "Dependence of the Accuracy of the Born Inversion on Noise and Bandwidth," Proceedings of the DARPA/AF Review of Progress in Quantitative NDE, July 1980, La Jolla, California, AFWAL-TR-81-4080, p. 389.
8. J.H. Rose and J.M. Richardson, "Time Domain Born Approximation," (to be published in J. of Non Destructive Evaluation).
9. N. Paton, "Sample Preparation," Proceedings of the ARPA/AFML Review of Progress in Quantitative NDE, First Year Report, July 1975, Thousand Oaks, California, AFML-TR-75-212.
10. J.L. Opsal, "Time Domain Elastic Wave Scattering from Complex Flaws," Proceedings of the Air Force/DARPA Review of Progress in Quantitative NDE, August 1981, Boulder, Colorado (to be published as an Air Force Materials Laboratory Technical Report).
11. J.C. Somer, "Electronic Sector Scanning for Ultrasonic Diagnosis," Ultrasonics, July 1968, pp. 153-159.
12. F.L. Thurstone and O.T. Von Ramm, "Electronic Beam Steering for Ultrasonic Imaging," 2nd World Congress on Ultrasonics in Medicine, June 4-8, 1973, Rotterdam, Netherlands, Excerpta Medica, Amsterdam, Netherlands, 1974, pp. 43-48.
13. W.A. Anderson et al. "A New Real Time Phased Array Sector Scanner for Imaging the Entire Adult Human Heart," Ultrasound in Medicine, 3B, 1977, pp. 1547-1558.
14. C.B. Burckhardt et al. "A Simplified Ultrasound Phased Array Sector Scanner," Echocardiography, Third Symposium, Martinus Nijhoff Publishers, The Hague, 1979, pp. 385-393.
15. H.E. Karrer, J.F. Dias, J.D. Larson, R.D. Pering, "A Phased Array Acoustic Imaging System for Medical Use," 1980 Ultrasonic Symposium Proceedings, IEEE Cat. No. 80CH1602-2, pp. 757-762, 1980.
16. R.C. Addison, Jr., "Multi-element Arrays for NDE Applications," to be published in V. 11 of Acoustical Imaging, Ed. J. Powers, Plenum Press.
17. D.A. Leedom, R. Krimholtz and G.L. Matthaei, "Equivalent Circuits for Transducers Having Arbitrary Even- or Odd-Symmetry Piezoelectric Excitation," IEEE Transactions on Sonics and Ultrasonics, SU-18, pp. 128-141, July 1971.
18. C.S. DeSilets, J.D. Fraser and G.S. Kino, "The Design of Efficient Broad-Band Piezoelectric Transducers," IEEE Transactions on Sonics and Ultrasonics, SU-25, 1978, pp. 115-125.

19. "Exploratory Development for a High Reliability Quantitative Flaw Characterization Module," RFP F33615-81-R-5066. Issued by Air Force Systems Command, Aeronautical Systems Division/PMRRA, Wright-Patterson AFB, Ohio.
20. L.A. Ahlberg, R.K. Elsley, L.J. Graham and J.M. Richardson, "Long Wavelength Ultrasonic Characterization of Inclusions in Silicon Nitride," Proceedings of the DARPA/AFML Review of Progress in Quantitative NDE, Fifth Year Report, July 1979, La Jolla, California, AFML-TR-80-4078.

APPENDIX A  
DIFFUSION BONDED SAMPLE DOCUMENTATION

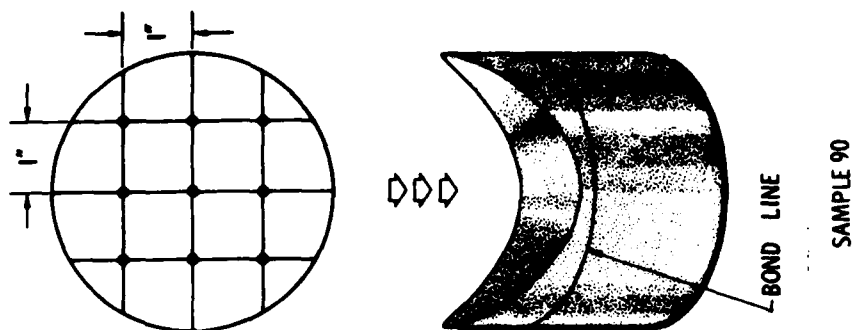
Documentation for Simulated Turbine Bore Samples

Included in this Appendix is the complete documentation for the simulated turbine disk bore samples. A complete listing of the 27 defects and the sample that contains them is given in Table A1. In Fig. A1 the three samples are shown along with the sites of the defects. In Fig. A2 through Fig. A28, the detailed documentation for each of the defects is provided. Each of these figures is laid out in a similar manner. The sketch in the upper left corner shows the configuration of the sample and also shows which diffusion bonding plane contains the defect. The drawing on the upper right shows the exact location of the defect in the plane with respect to the center line of the sample and the cylindrically curved surface. The drawings in the middle and lower left show cross sectional and plan views of the defect. The dimensions given are: 1) the nominal defect dimension, 2) the measured dimension, and 3) in the case of an inclusion, the actual dimensions of the inclusion. The photomicrograph in the lower right shows the actual plan view of the defect prior to diffusion bonding.

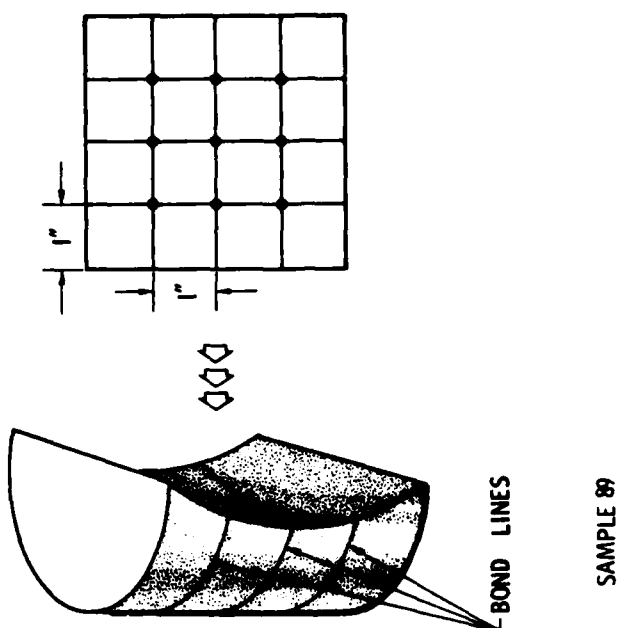
Table A1  
List of Flaws Contained In Simulated Turbine Bore Samples

Sample No.	Defect No.	Defect Type	Distance From Surface (mm)	Diameter (µm)	Height (µm)
88	1	Prolate Spheroidal Void	6.4	800	1600
88	2	Penny Shaped Crack	6.4	800	100
88	3	Oblate Spheroidal Void	6.4	800	300
88	4	Spherical Void	2.5	400	400
88	5	Penny Shaped Crack	6.4	1200	100
88	6	WC Spherical Inclusion	6.4	400	400
88	7	Simulated Fatigue Crack	6.4	1200	---
88	8	Simulated Fatigue Crack	0.4	1200	---
88	9	Al <sub>2</sub> O <sub>3</sub> Spherical Inclusion	6.4	400	400
89	1	Al <sub>2</sub> O <sub>3</sub> Spherical Inclusion	6.4	800	800
89	2	Penny Shaped Crack	6.4	1200	100
89	3	Spherical Void	6.4	800	800
89	4	Simulated Fatigue Crack	6.4	1200	---
89	5	Simulated Fatigue Crack	0.4	1200	---
89	6	Spherical Void	6.4	1200	1200
89	7	WC Spherical Inclusion	2.5	1200	1200
89	8	Penny Shaped Crack	6.4	800	100
89	9	WC Spherical Inclusion	6.4	600	800
90	1	Oblate Spheroidal Void	9.7	800	200
90	2	Simulated Fatigue Crack	6.4	1200	---
90	3	Spherical Void	9.7	400	400
90	4	Prolate Spheroidal Void	9.7	800	1600
90	5	Penny Shaped Crack	6.4	1200	100
90	6	Spherical Void	9.7	800	800
90	7	Spherical Void	9.7	1200	100
90	8	Penny Shaped Crack	6.4	800	100
90	9	Al <sub>2</sub> O <sub>3</sub> Spherical Inclusion	9.7	800	800

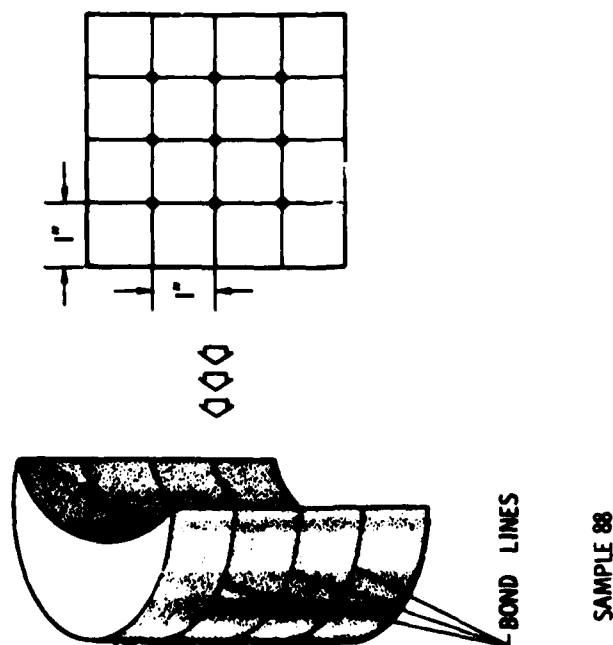




SAMPLE 90



SAMPLE 89



SAMPLE 88

Fig. A1 Simulated turbine bore samples.

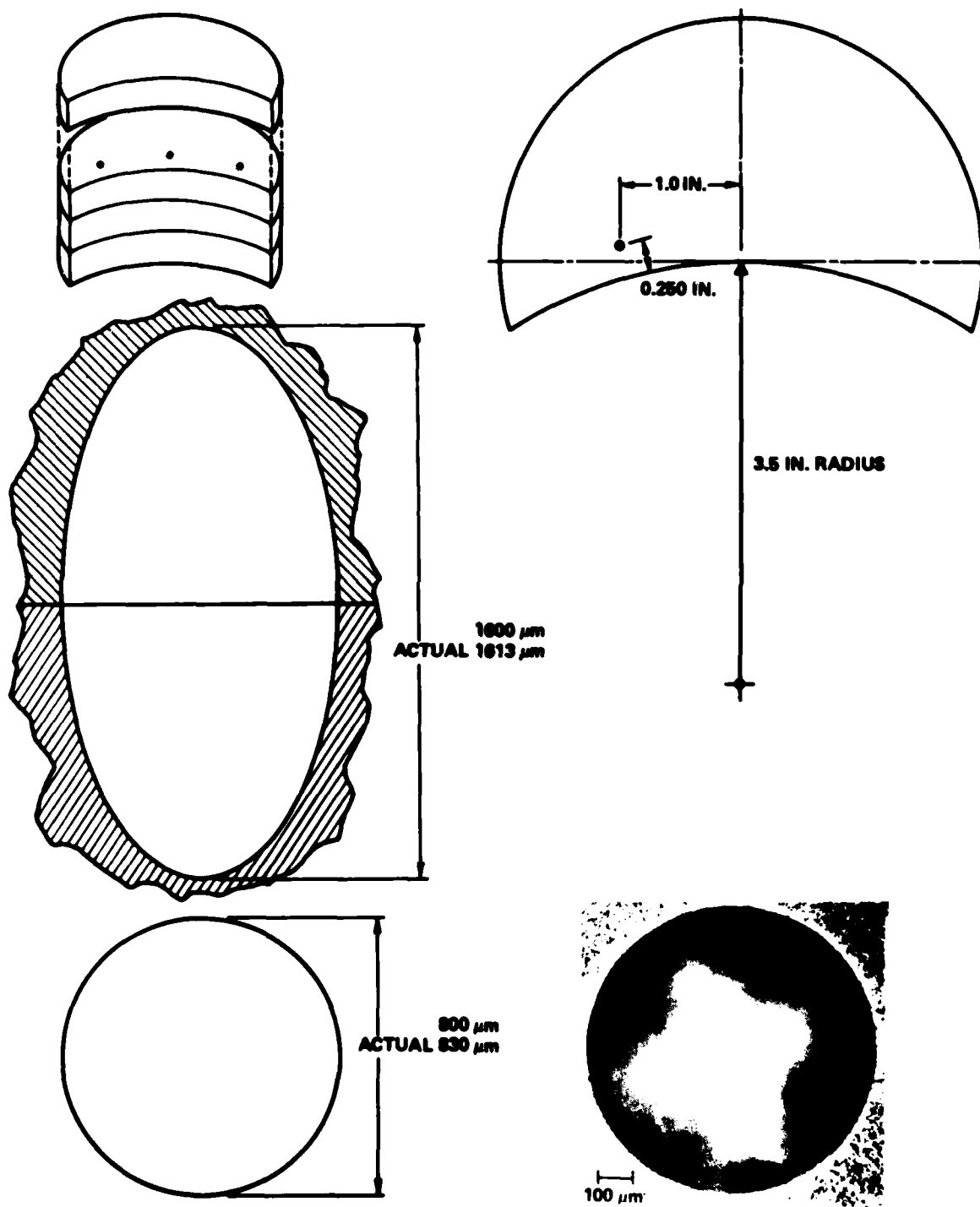


Fig. A2 Sample 88-1: 800  $\mu\text{m}$   $\times$  1600  $\mu\text{m}$  prolate spheroidal void.

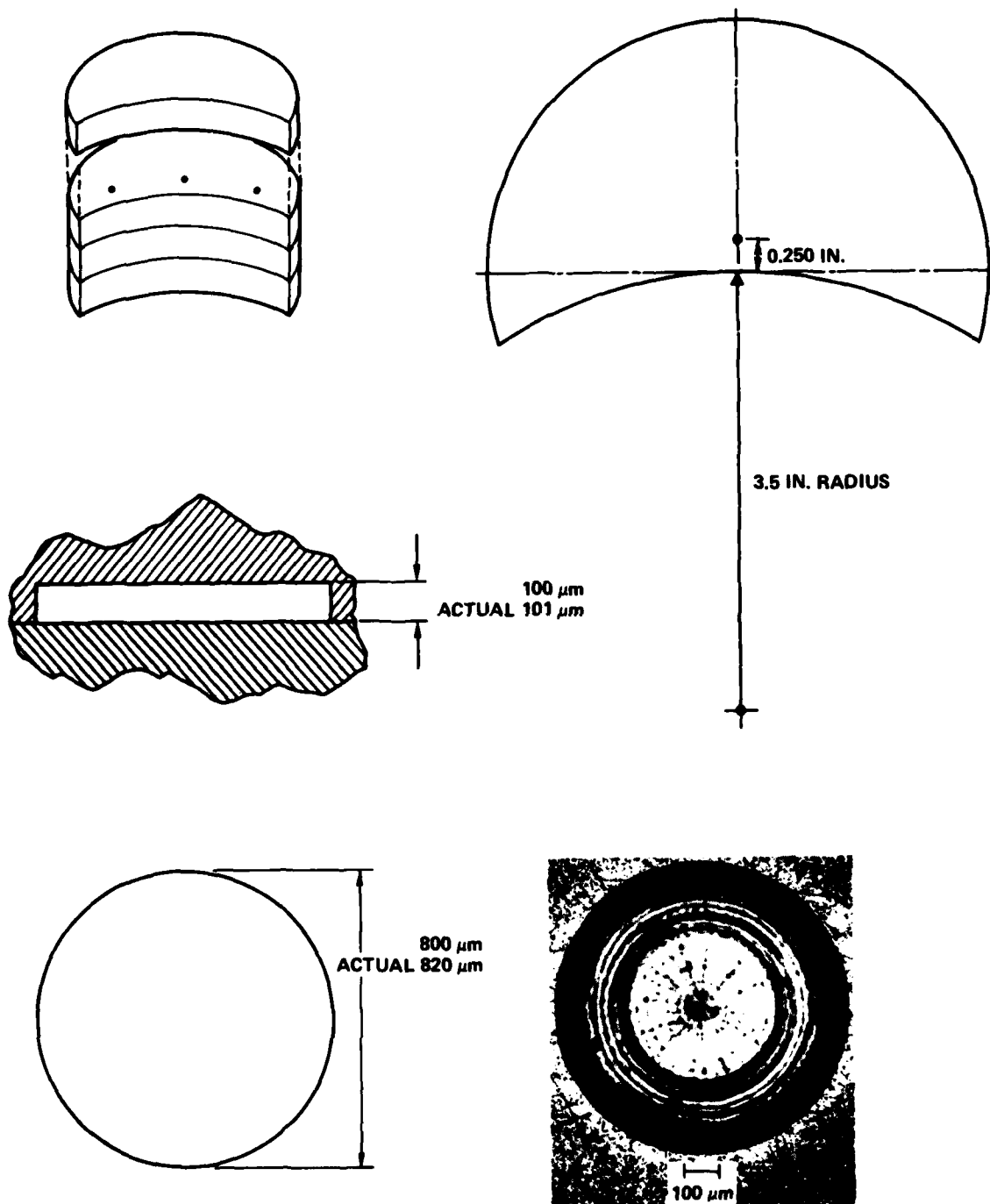


Fig. A3 Sample 88-2: 100  $\mu\text{m}$   $\times$  800  $\mu\text{m}$  penny shaped crack.

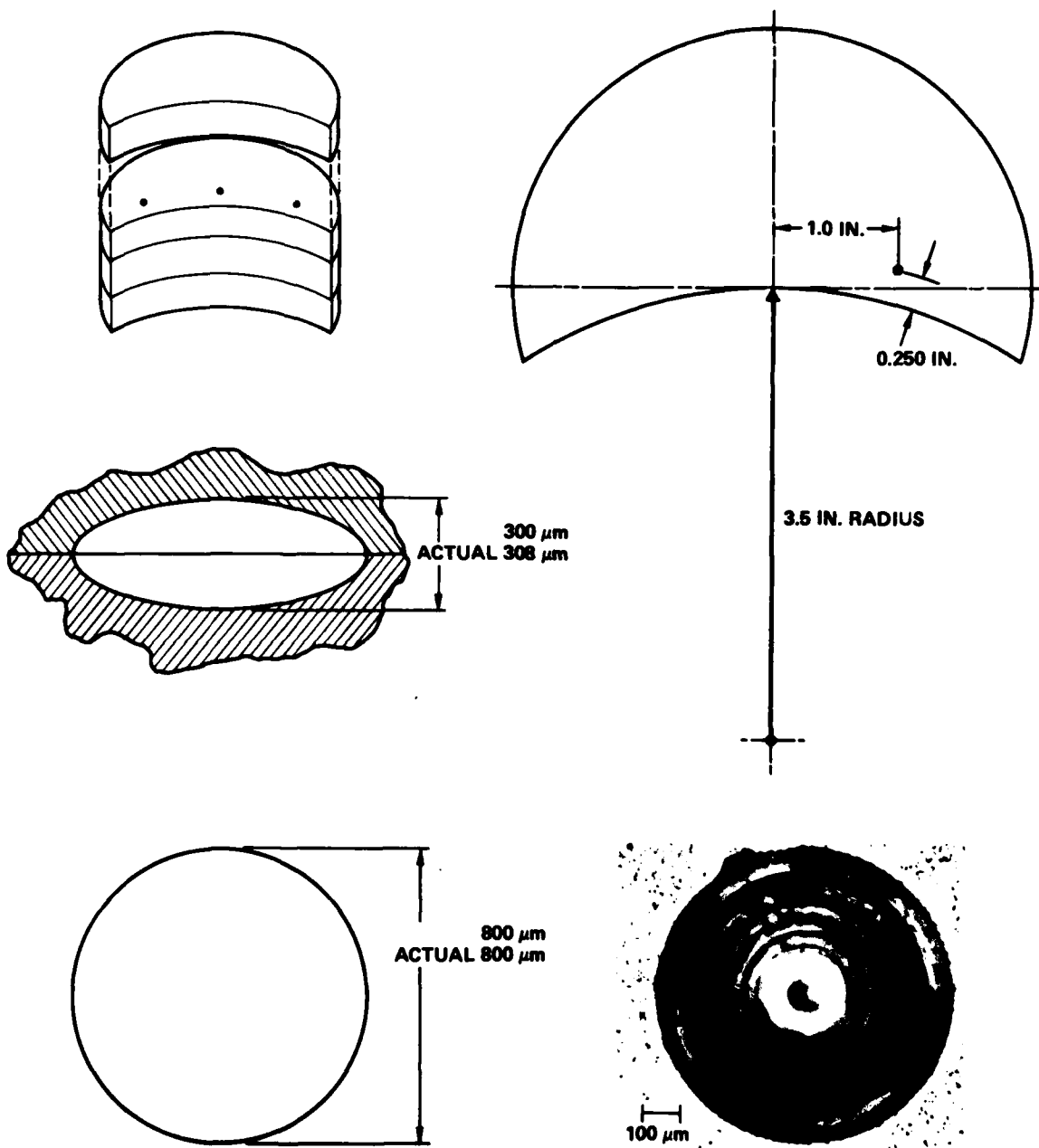


Fig. A4 Sample 88-3: 300  $\mu\text{m}$   $\times$  800  $\mu\text{m}$  oblate spheroidal void.

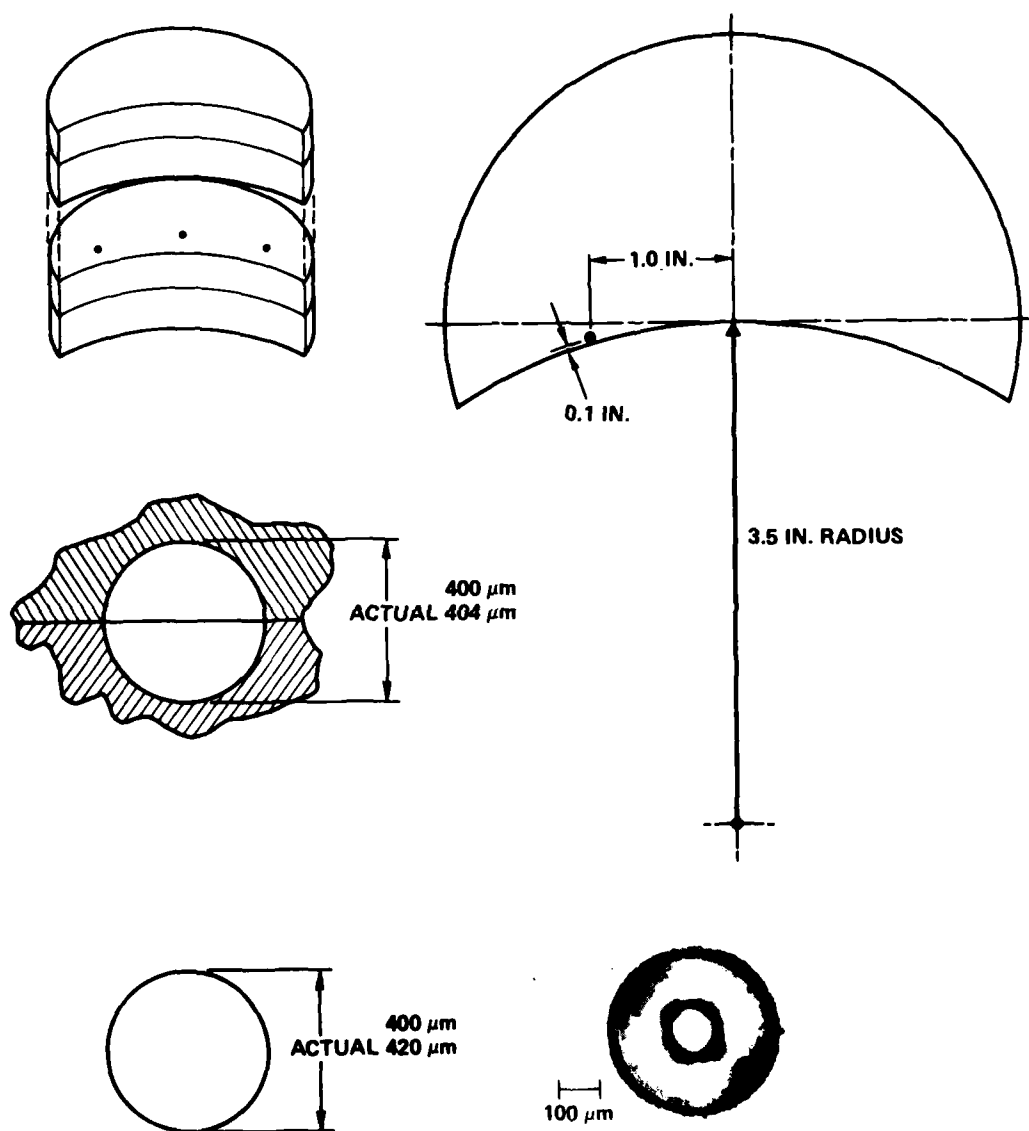


Fig. A5 Sample 88-4: 400 μm spherical void.

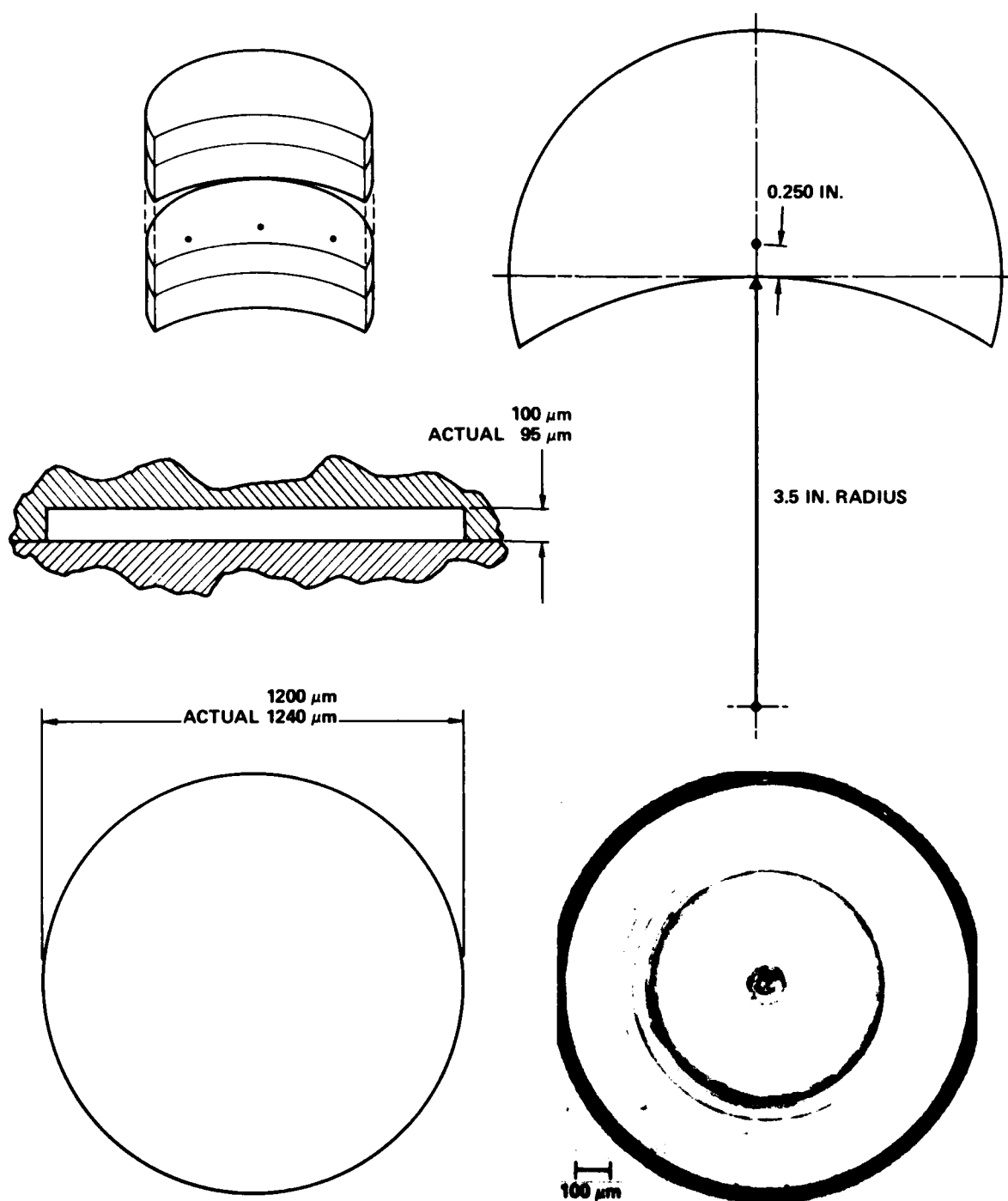


Fig. A6 Sample 88-5: 100  $\mu\text{m}$   $\times$  1200  $\mu\text{m}$  penny shaped crack.

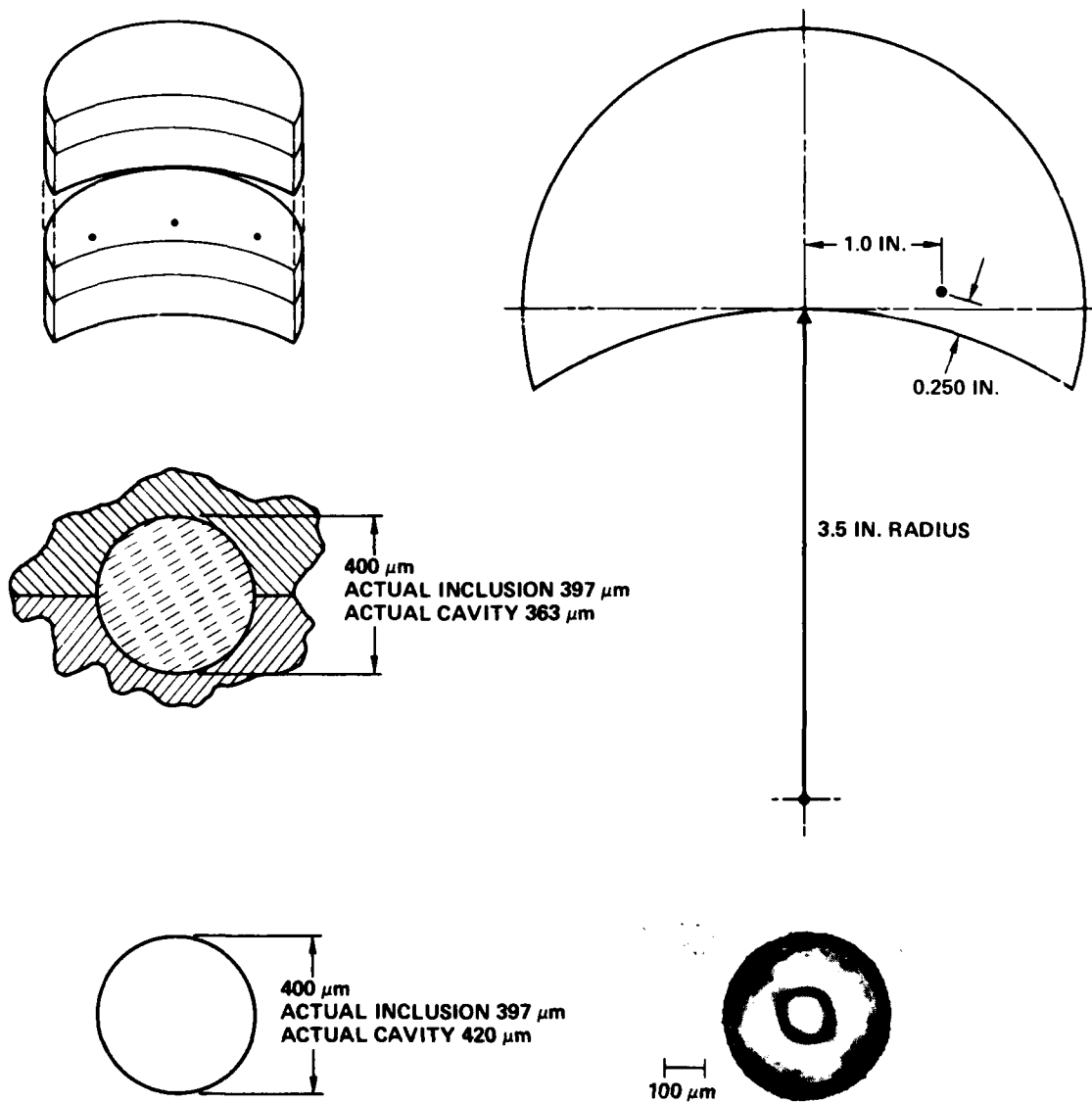


Fig. A7 Sample 88-6: 400 μm WC spherical inclusion.

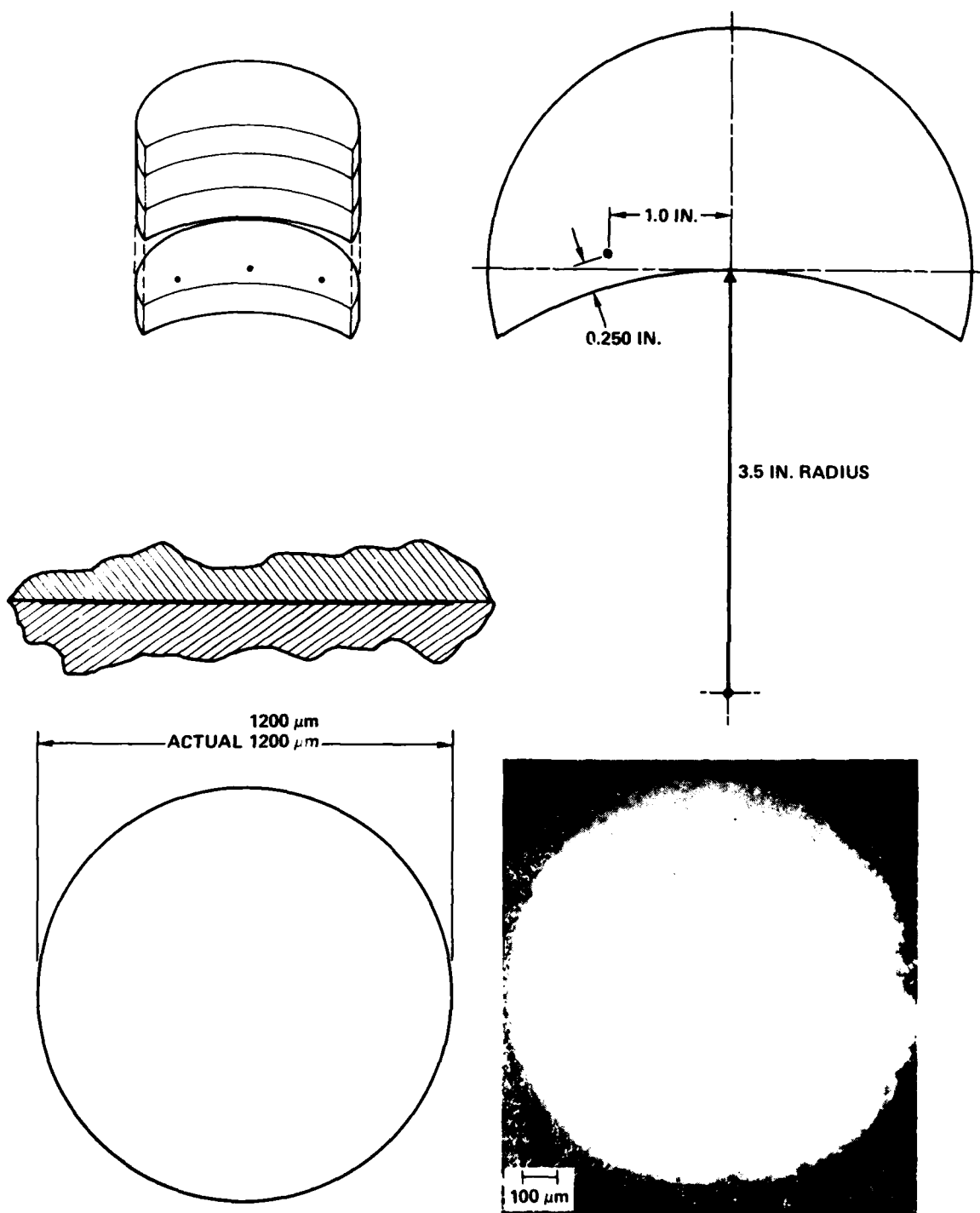


Fig. A8 Sample 88-7: 1200  $\mu\text{m}$  simulated fatigue crack.



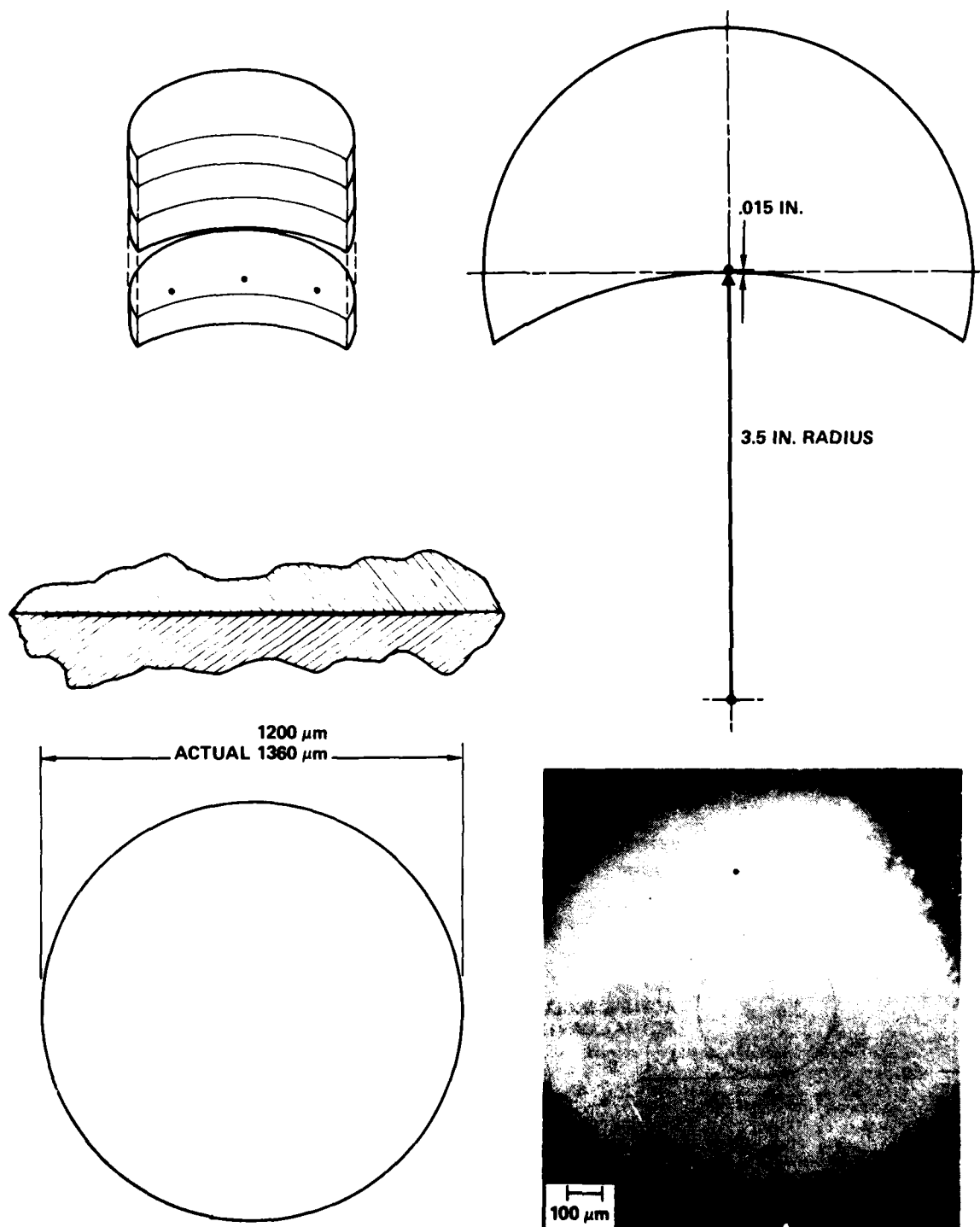


Fig. A9 Sample 88-8: 1200  $\mu\text{m}$  simulated fatigue crack.

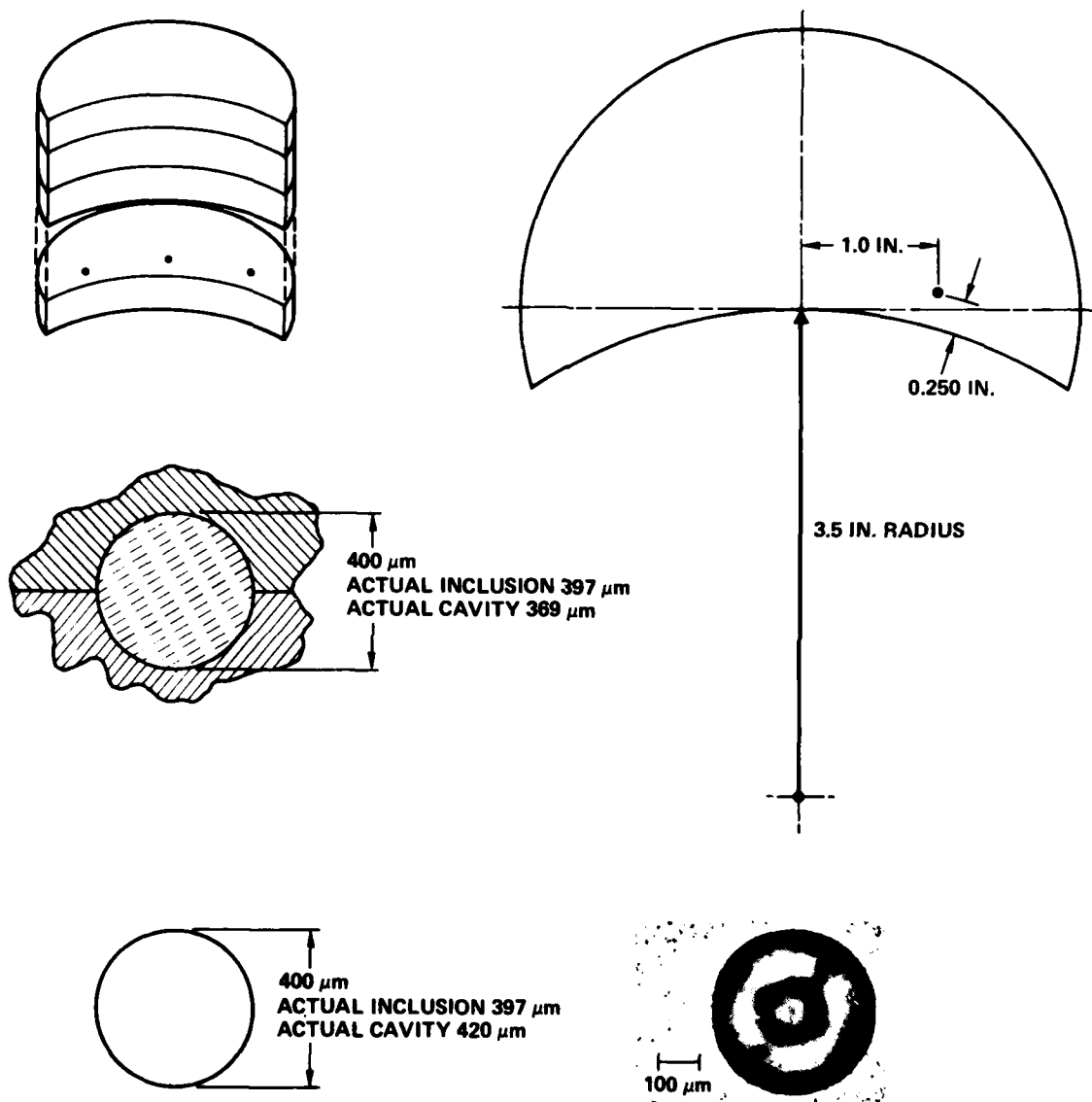


Fig. A10 Sample 88-9: 400  $\mu\text{m}$   $\text{Al}_2\text{O}_3$  spherical inclusion.

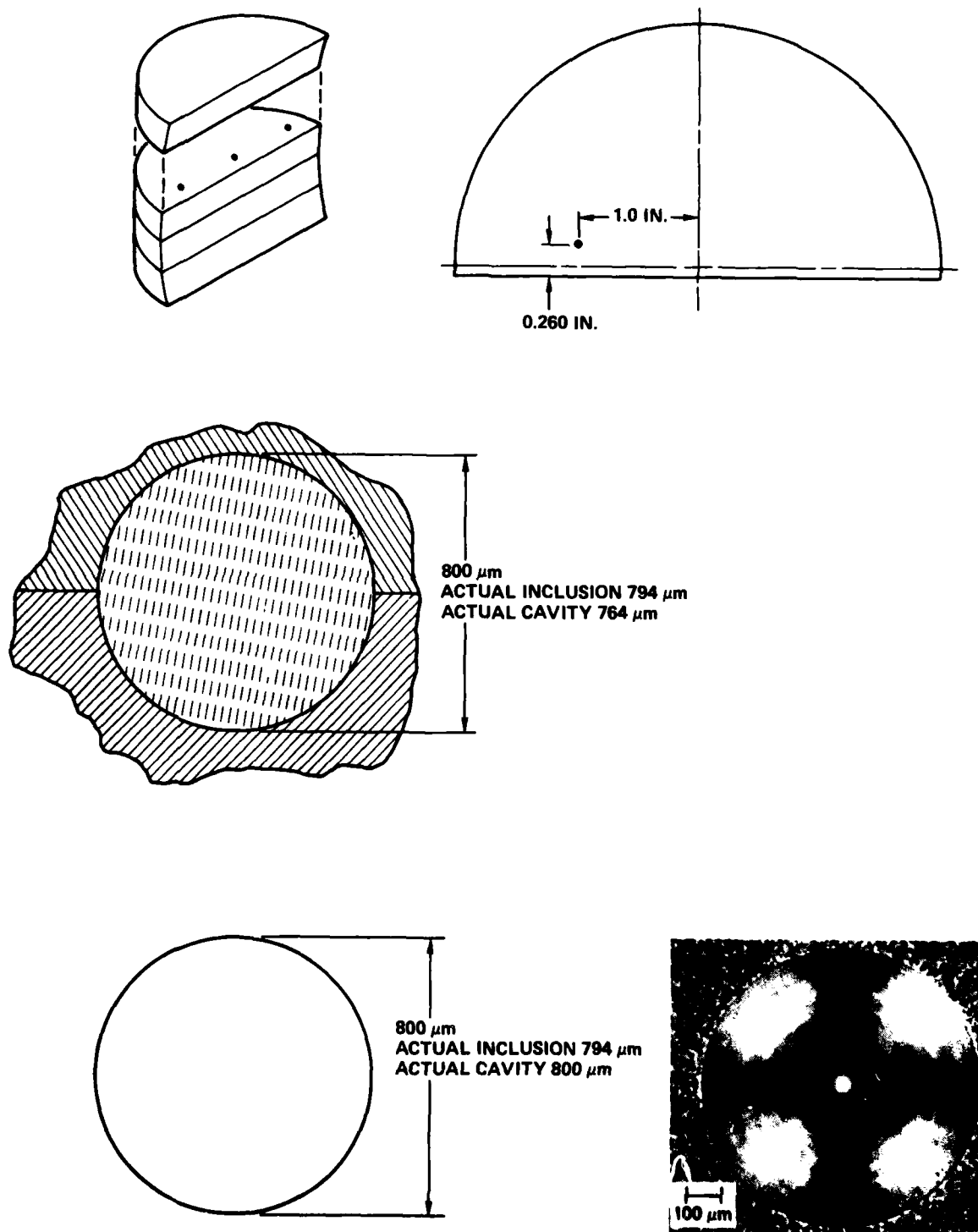


Fig. A11 Sample 89-1: 800 μm  $\text{Al}_2\text{O}_3$  spherical inclusion.

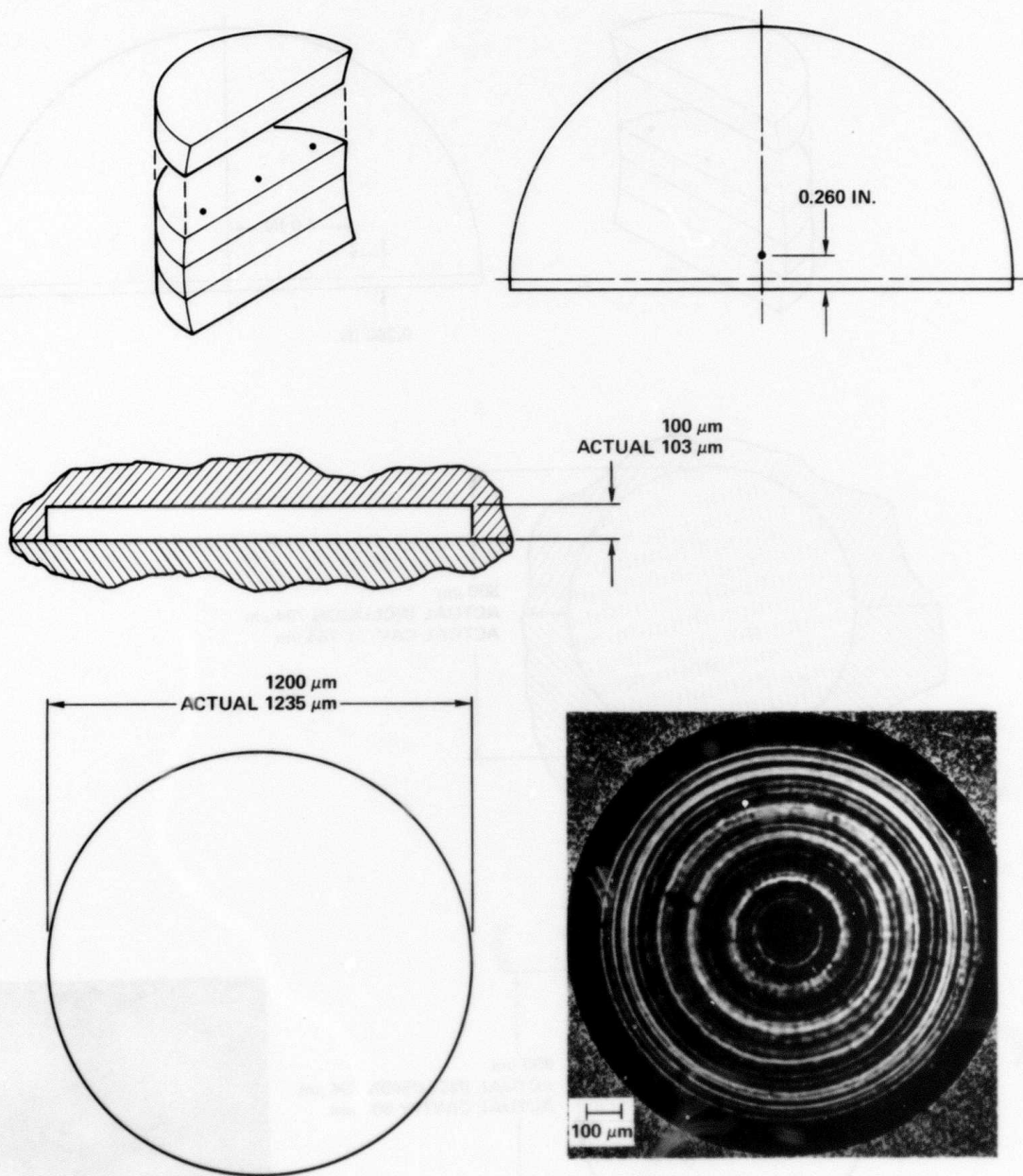


Fig. A12 Sample 89-2:  $100\text{ }\mu\text{m} \times 1200\text{ }\mu\text{m}$  penny shaped crack.

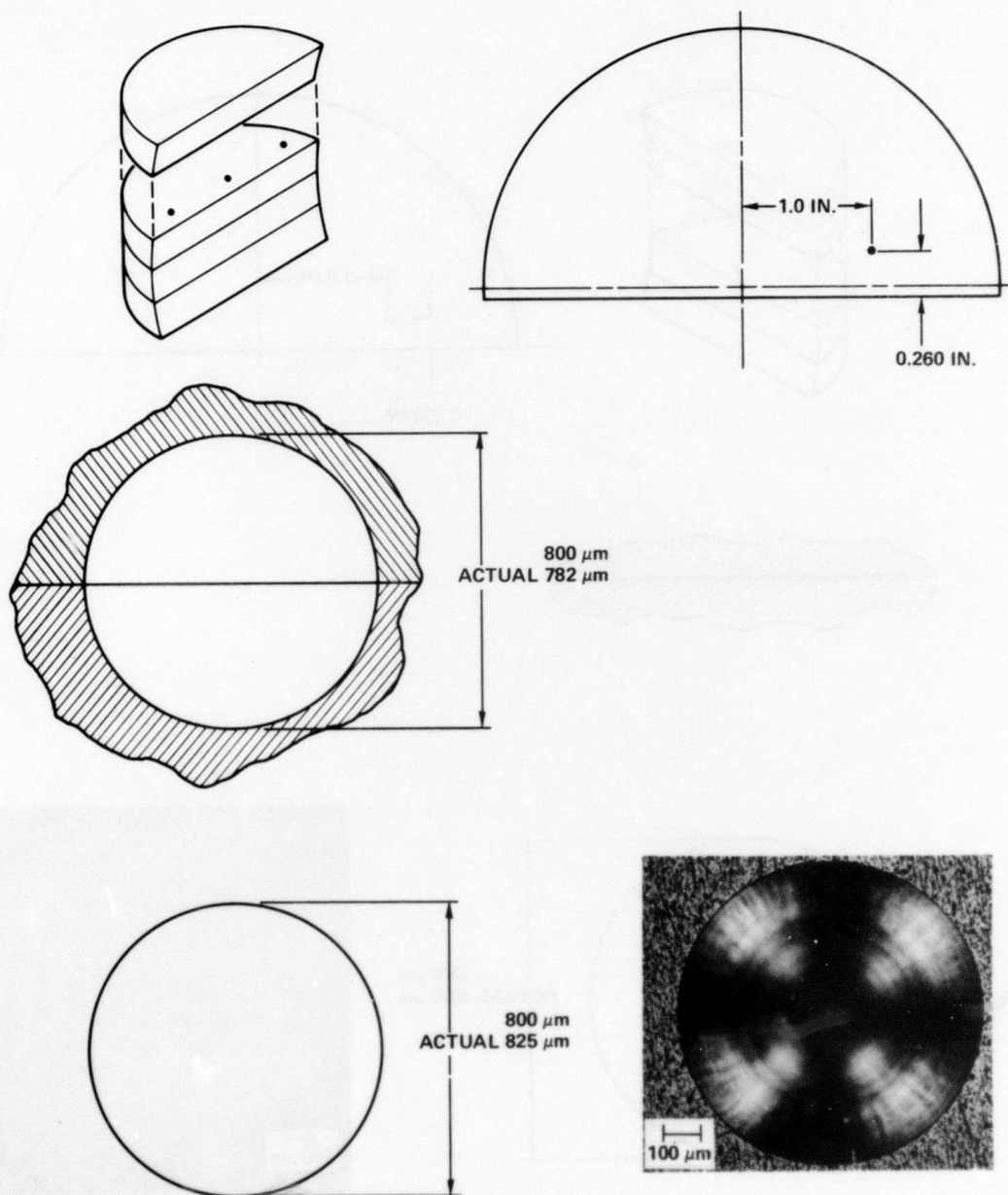


Fig. A13 Sample 89-3: 800  $\mu\text{m}$  spherical void.

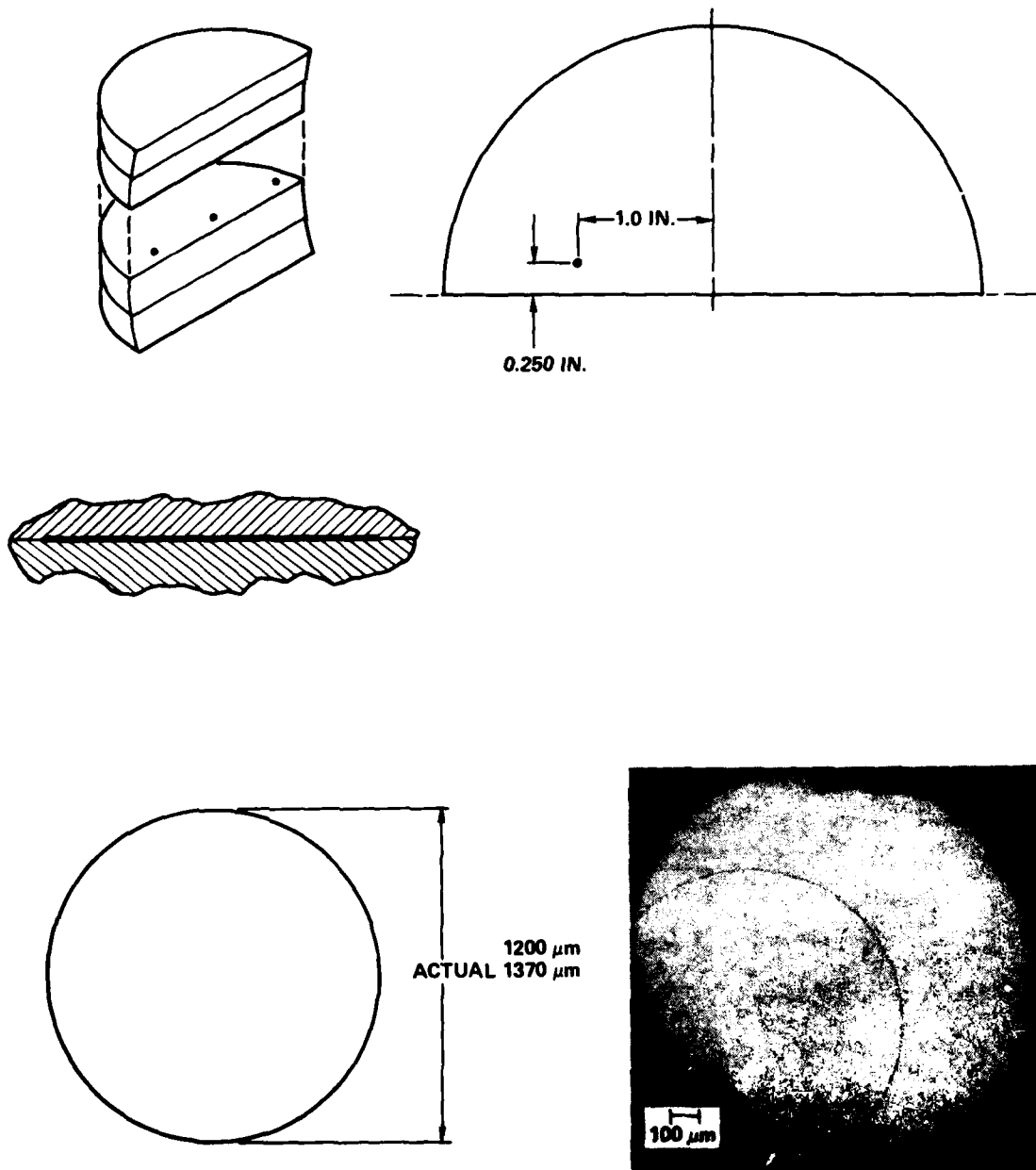


Fig. A14 Sample 89-4: 1200  $\mu\text{m}$  simulated fatigue crack.

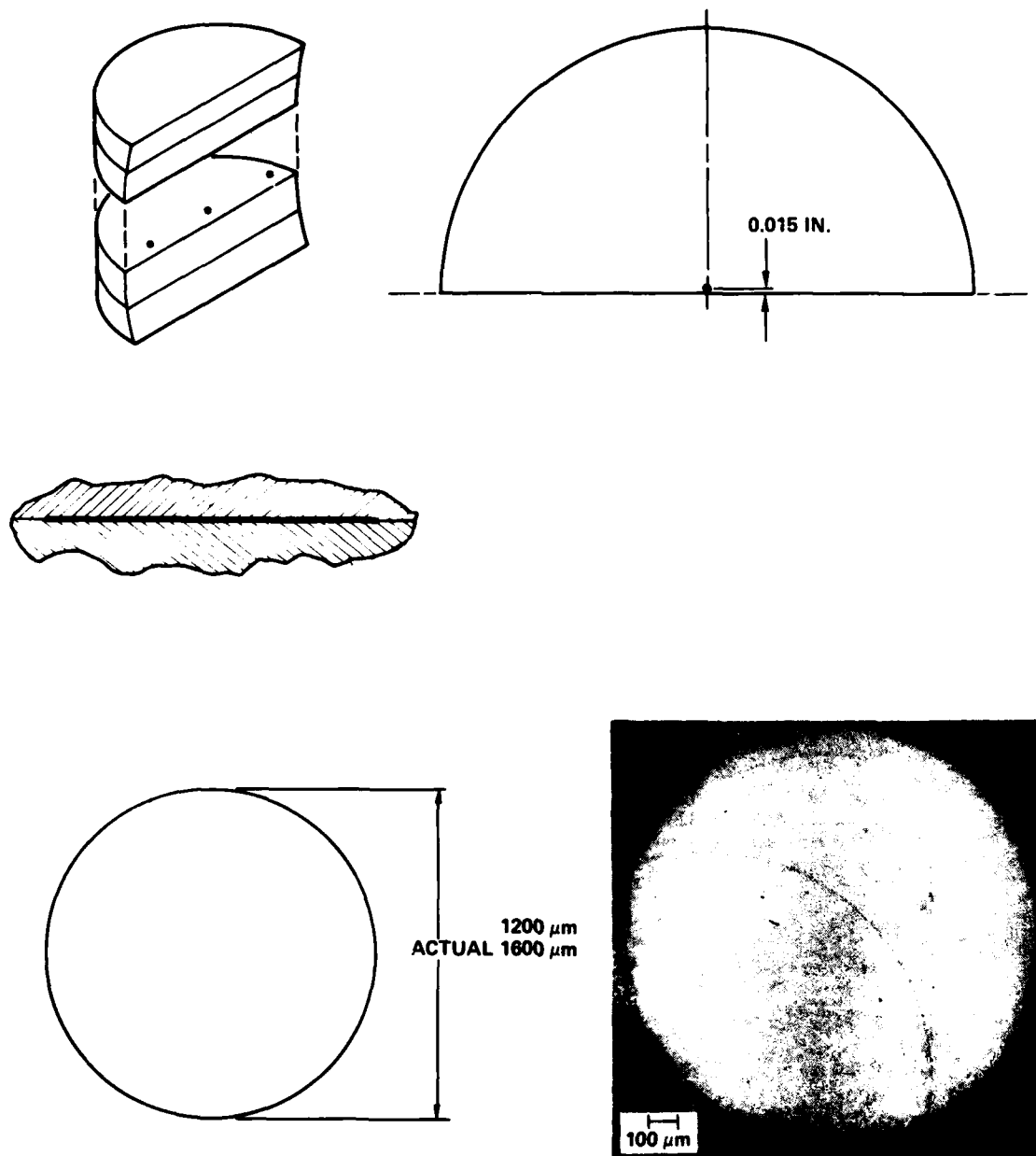


Fig. A15 Sample 89-5: 1200  $\mu\text{m}$  simulated fatigue crack.

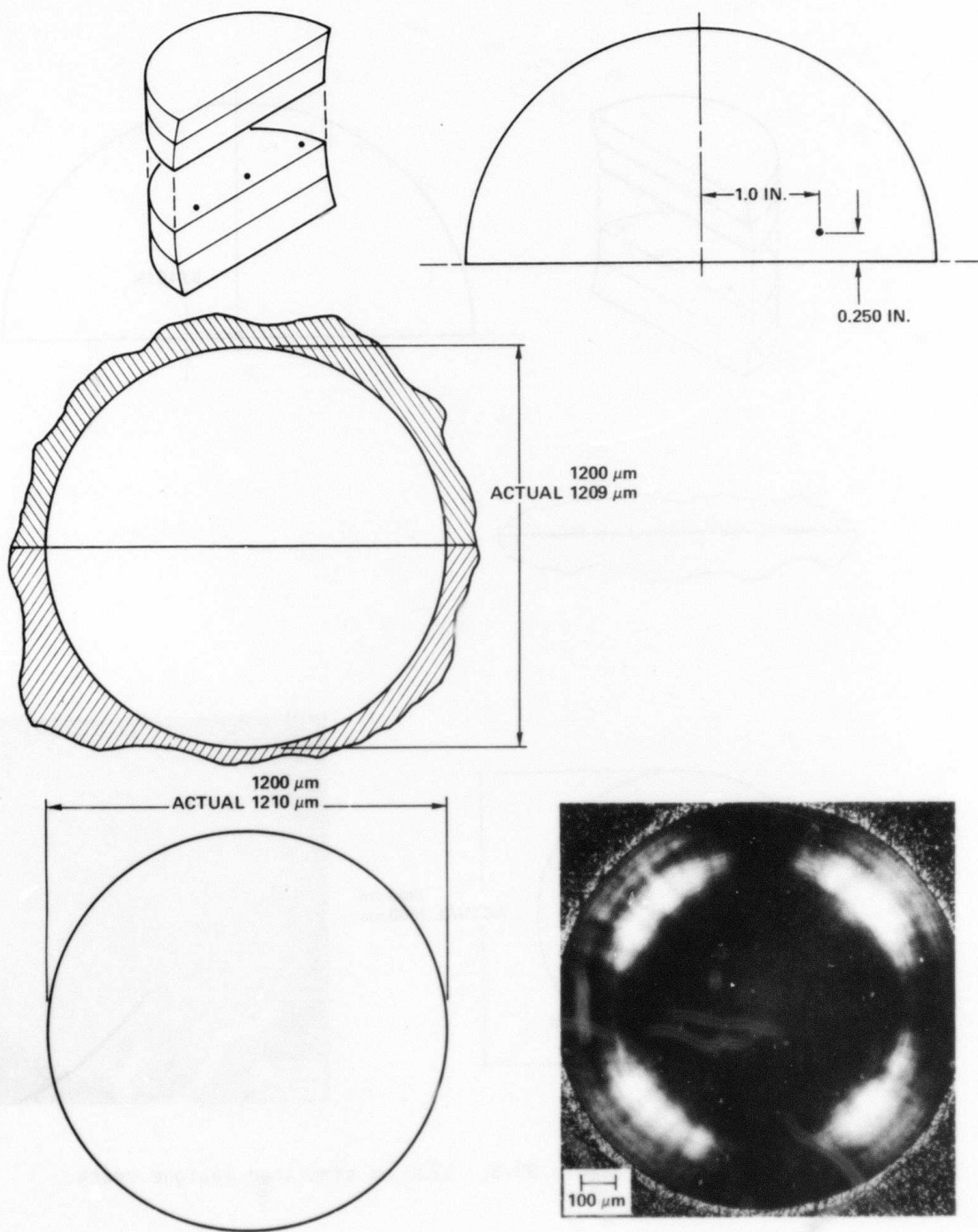


Fig. A16 Sample 89-6: 1200 μm spherical void.



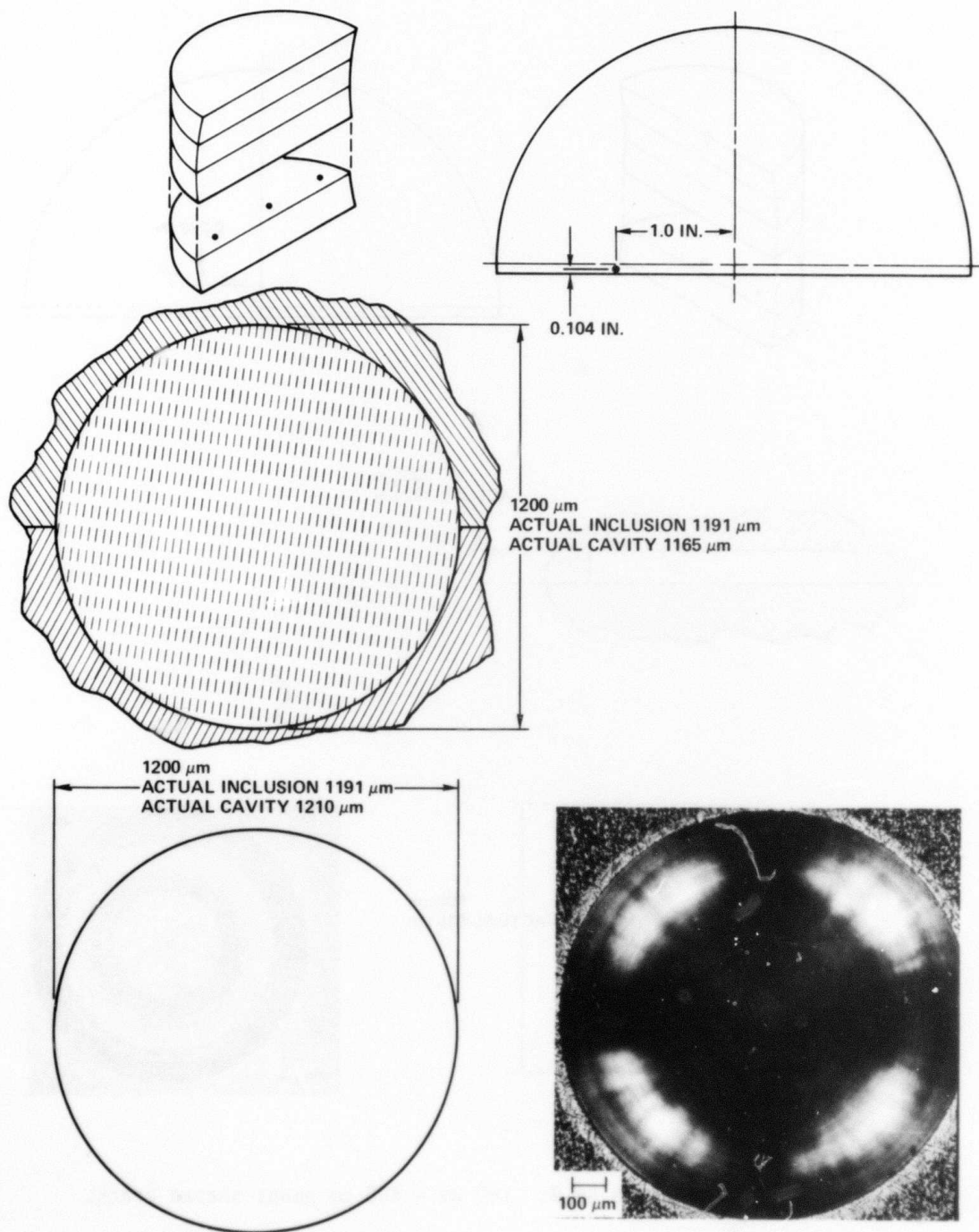


Fig. A17 Sample 89-7: 1200 μm WC spherical inclusion.

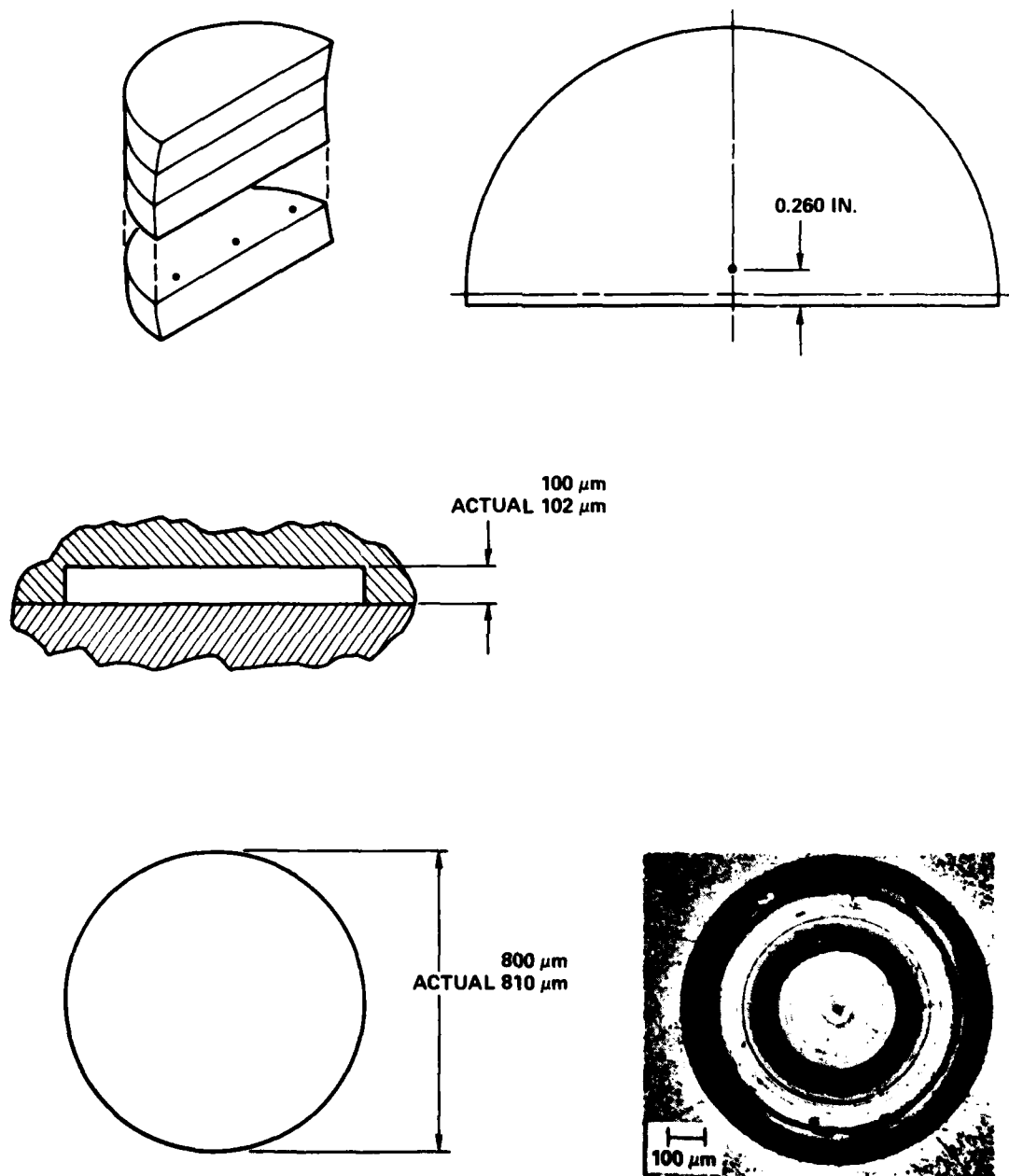


Fig. A18 Sample 89-8: 100  $\mu\text{m}$   $\times$  800  $\mu\text{m}$  penny shaped crack.

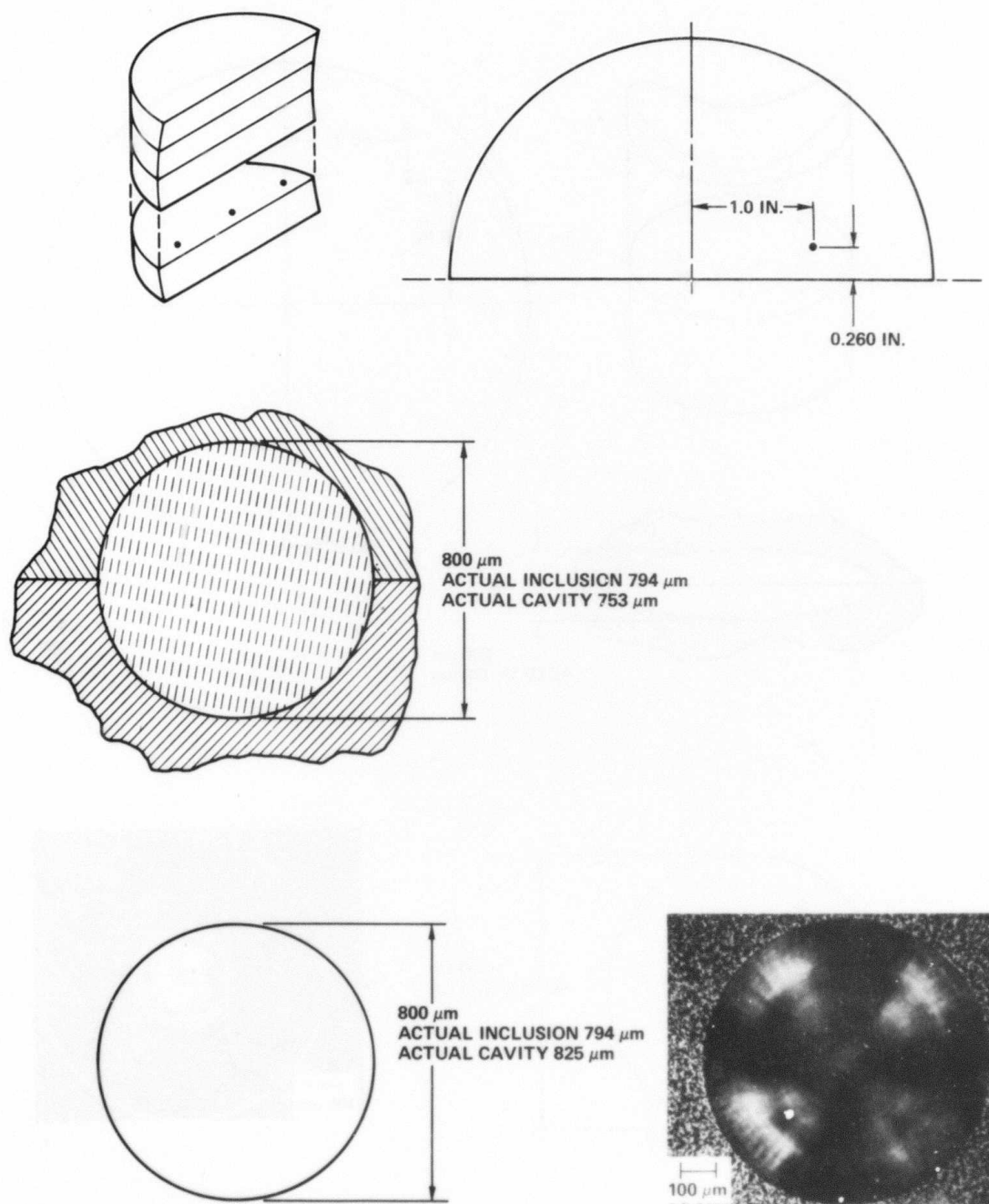


Fig. A19 Sample 89-9: 800  $\mu\text{m}$  WC spherical inclusion.

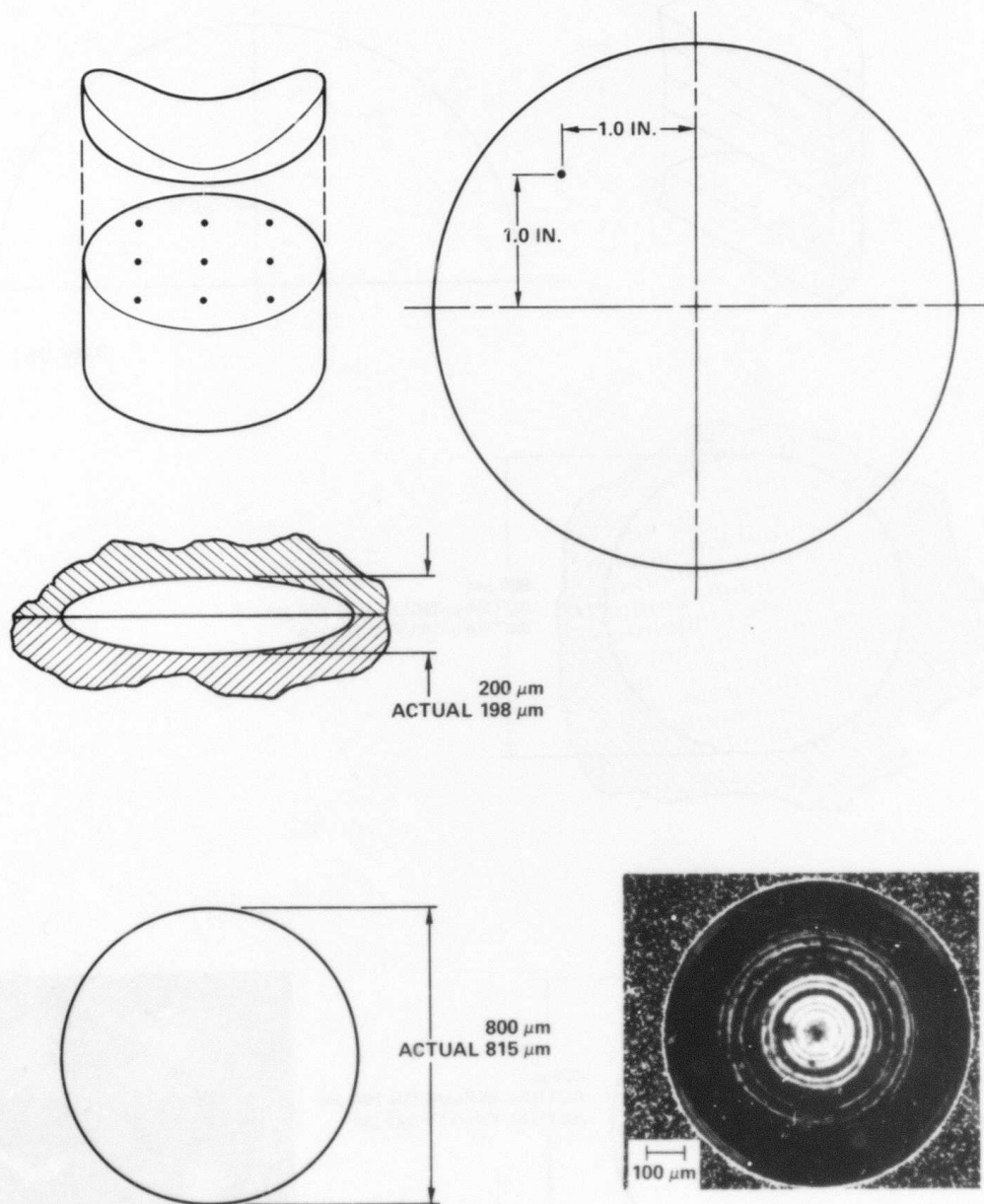


Fig. A20 Sample 90-1: 200  $\mu\text{m}$   $\times$  800  $\mu\text{m}$  oblate spheroidal void.

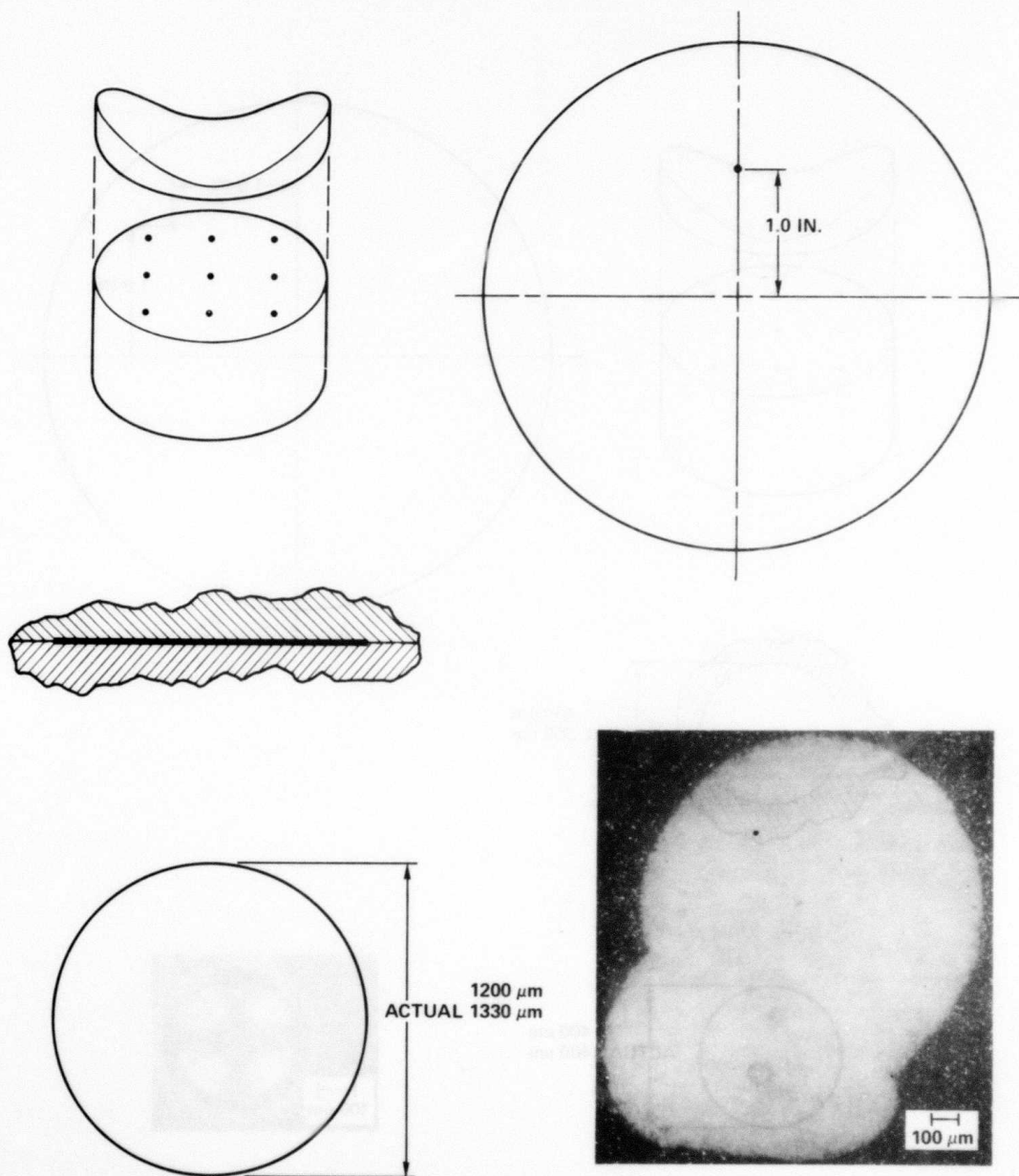


Fig. A21 Sample 90-2: 1200  $\mu\text{m}$  simulated fatigue crack.



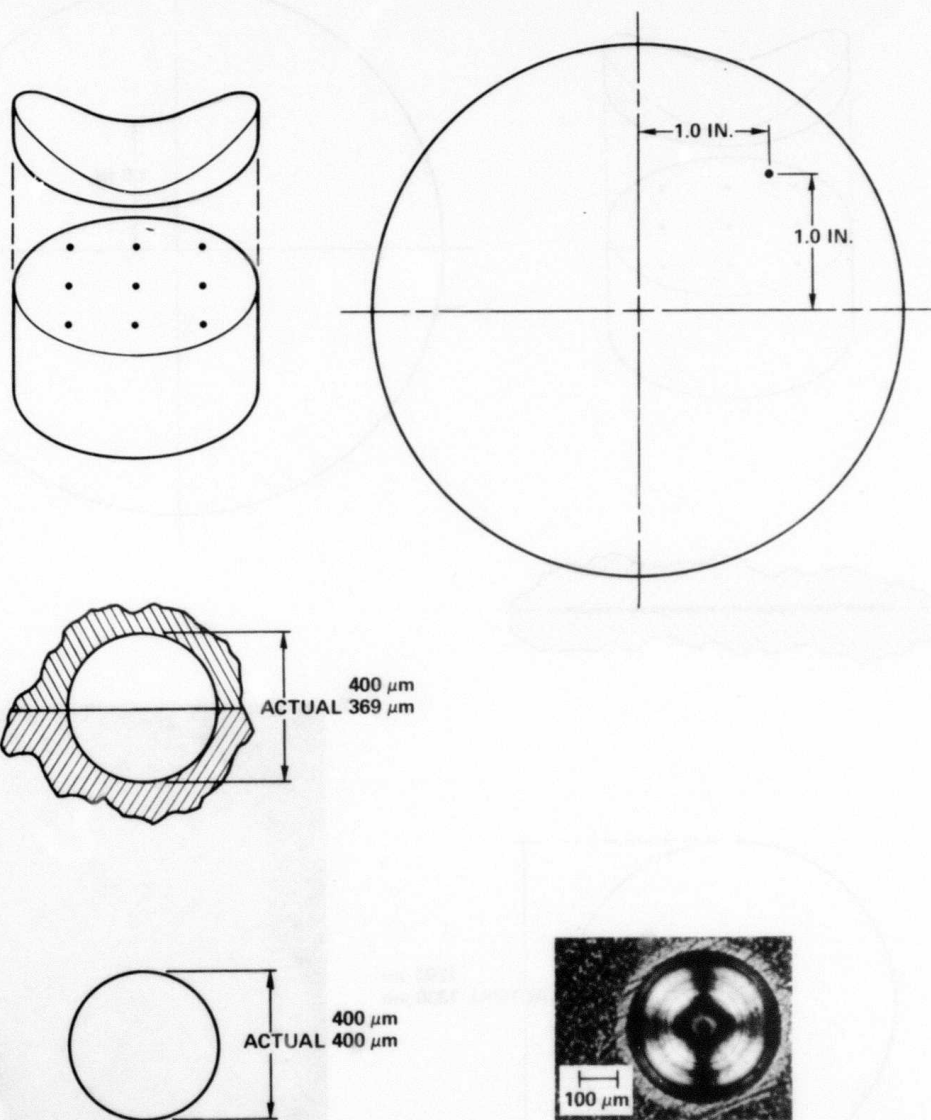


Fig. A22 Sample 90-3: 400 μm spherical void.

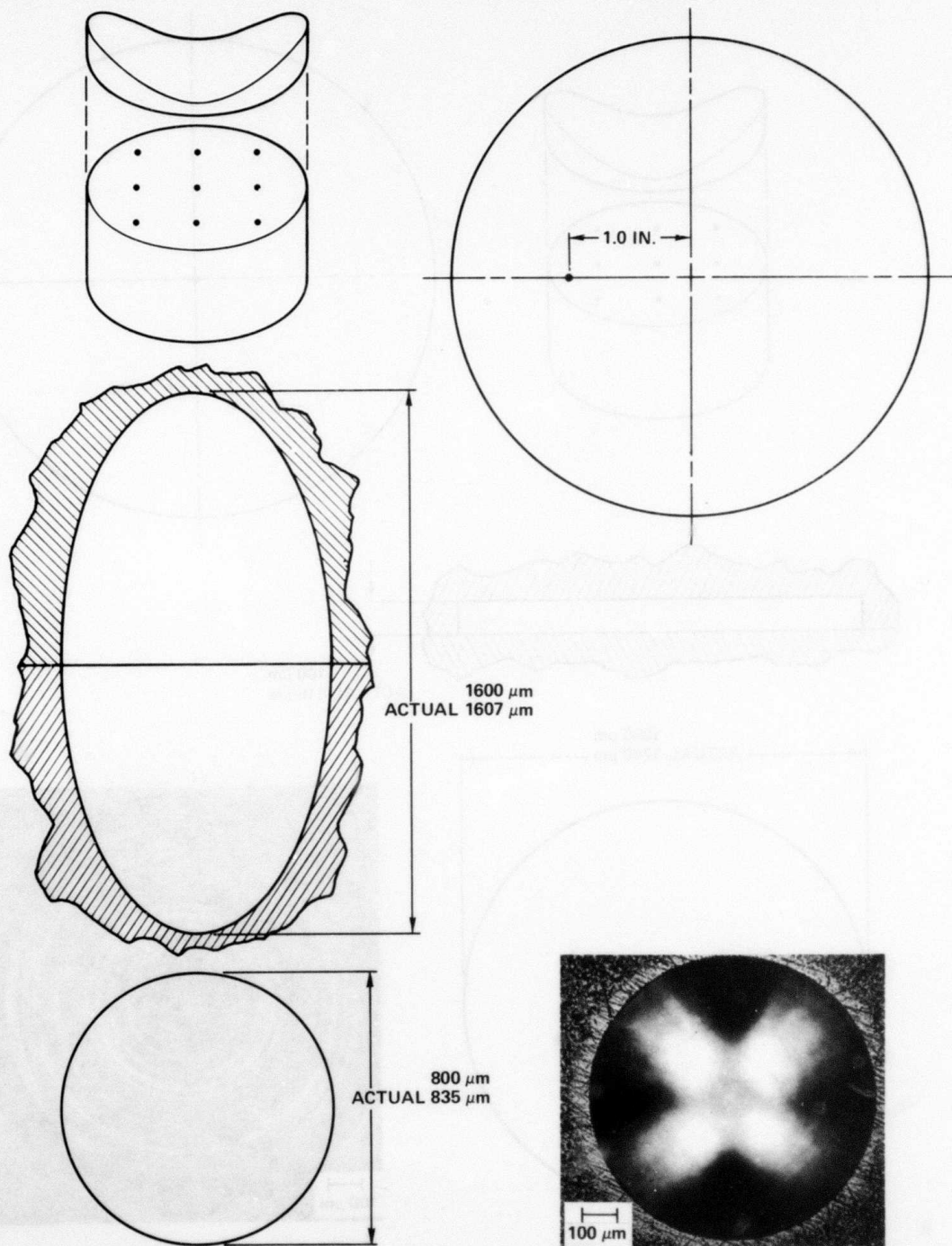


Fig. A23 Sample 90-4:  $800\ \mu\text{m} \times 100\ \mu\text{m}$  prolate spheroidal void.

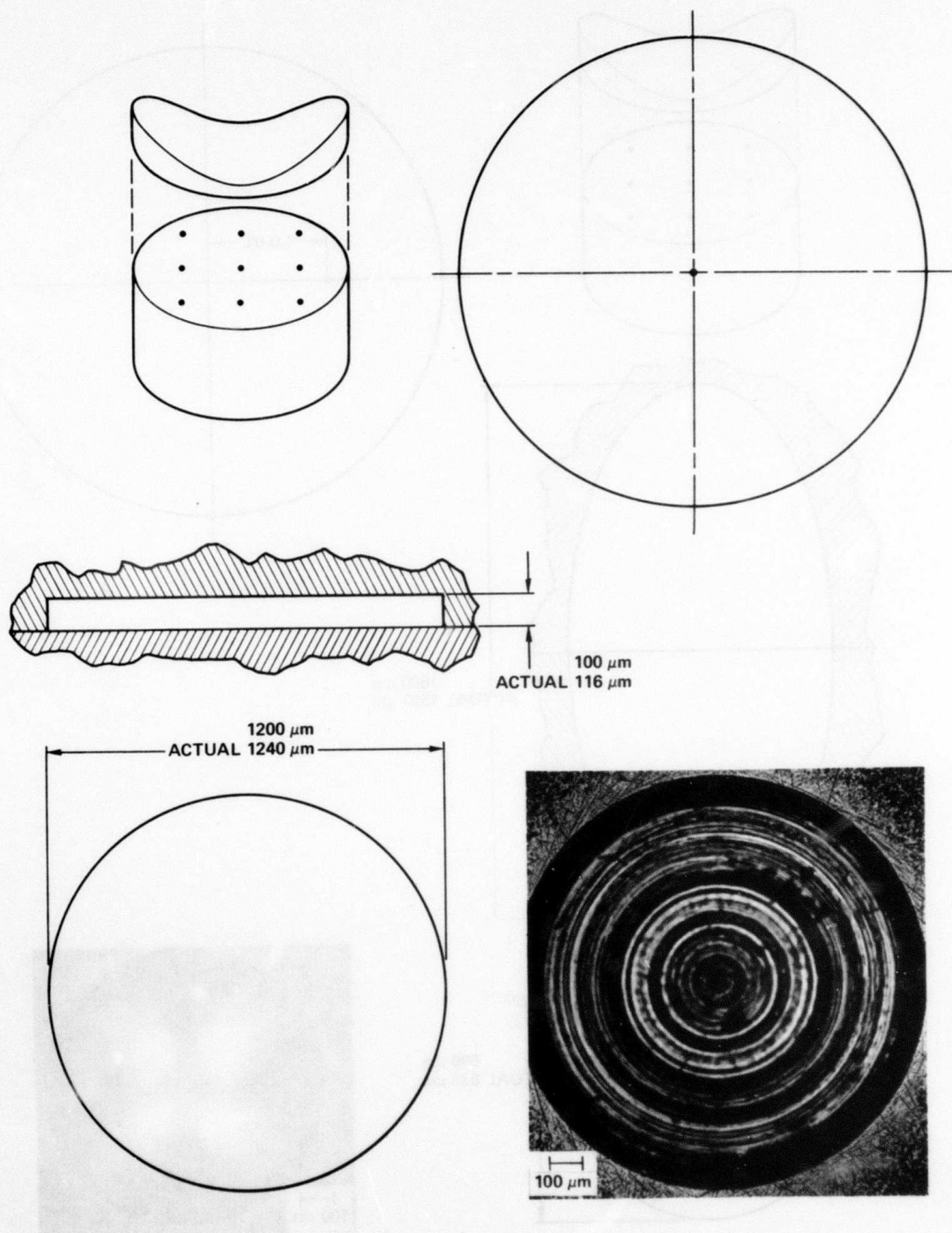


Fig. A24 Sample 90-5: 100  $\mu\text{m}$   $\times$  1200  $\mu\text{m}$  penny shaped crack.



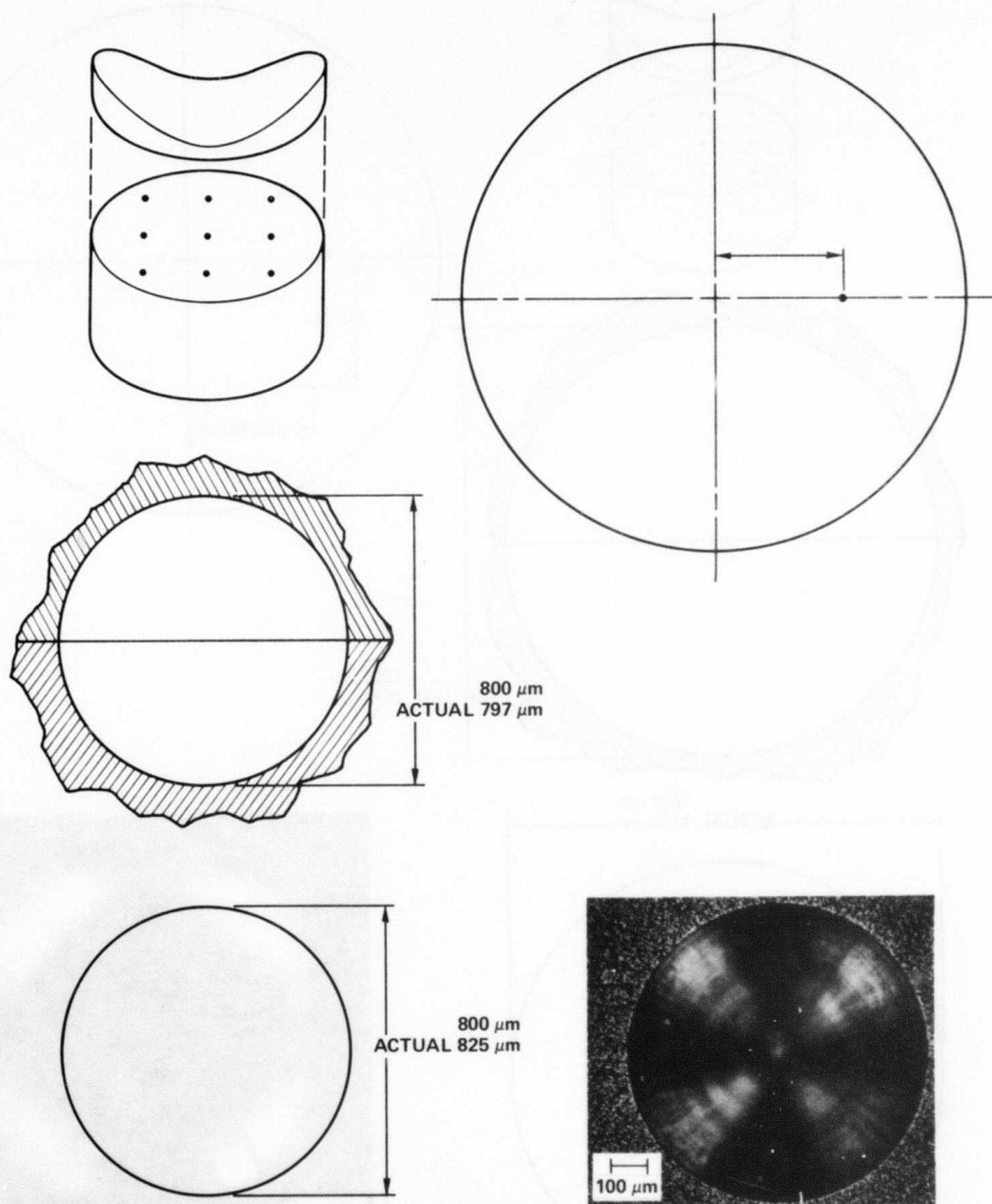


Fig. A25 Sample 90-6:  $800\ \mu\text{m}$  spherical void.

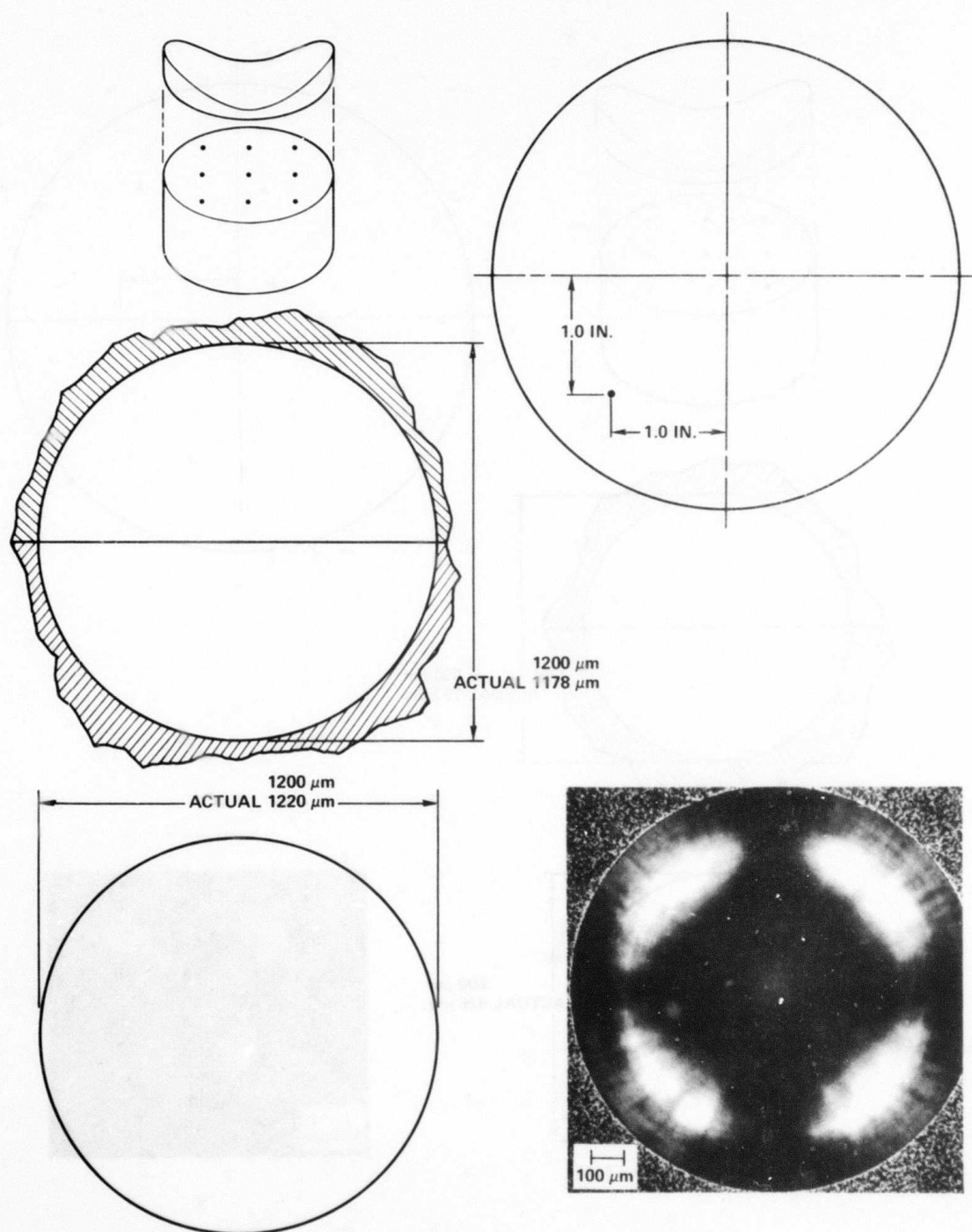


Fig. A26 Sample 90-7: 1200  $\mu\text{m}$  spherical void.

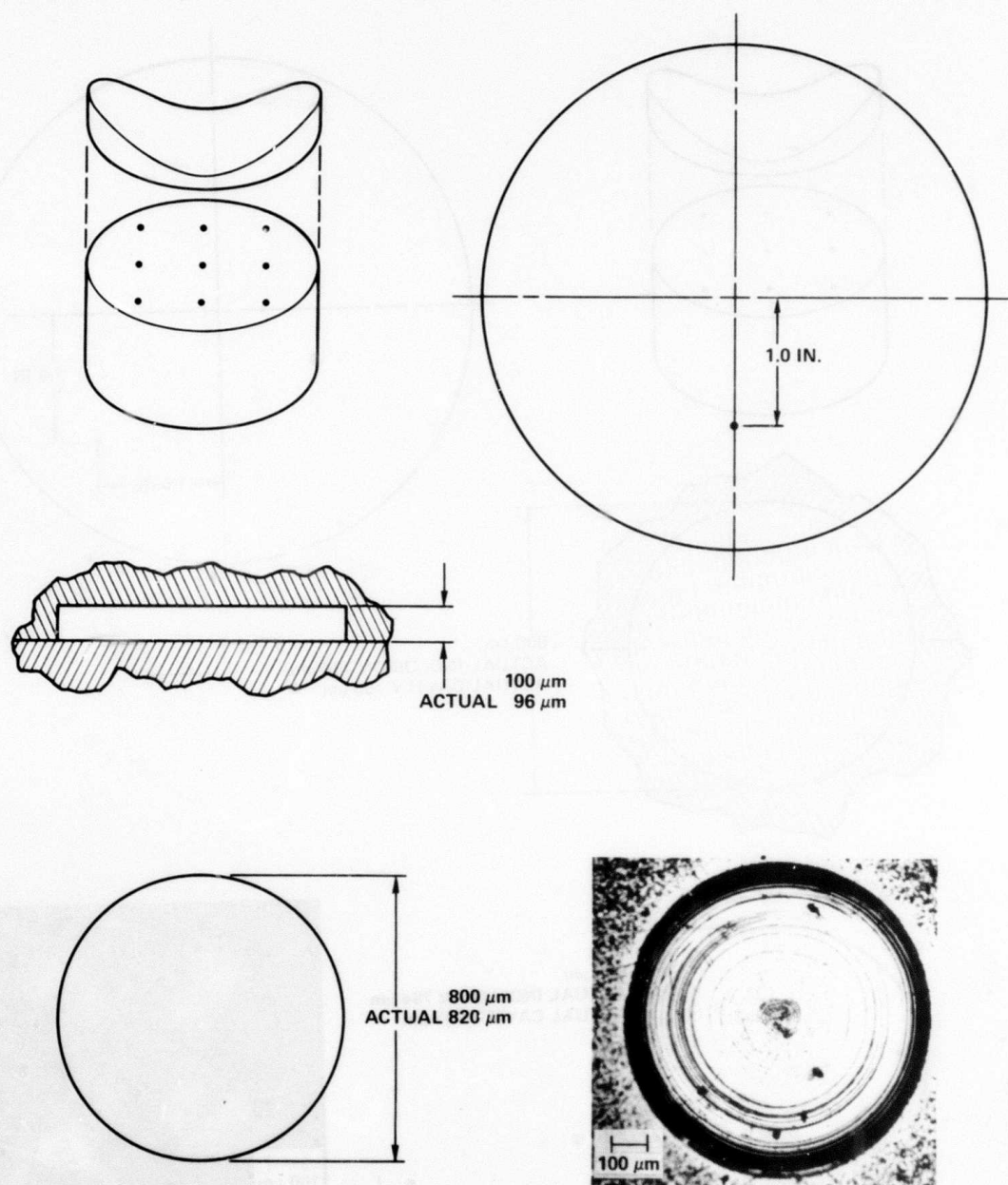


Fig. A27 Sample 90-8: 100  $\mu\text{m}$   $\times$  800  $\mu\text{m}$  penny shaped crack.

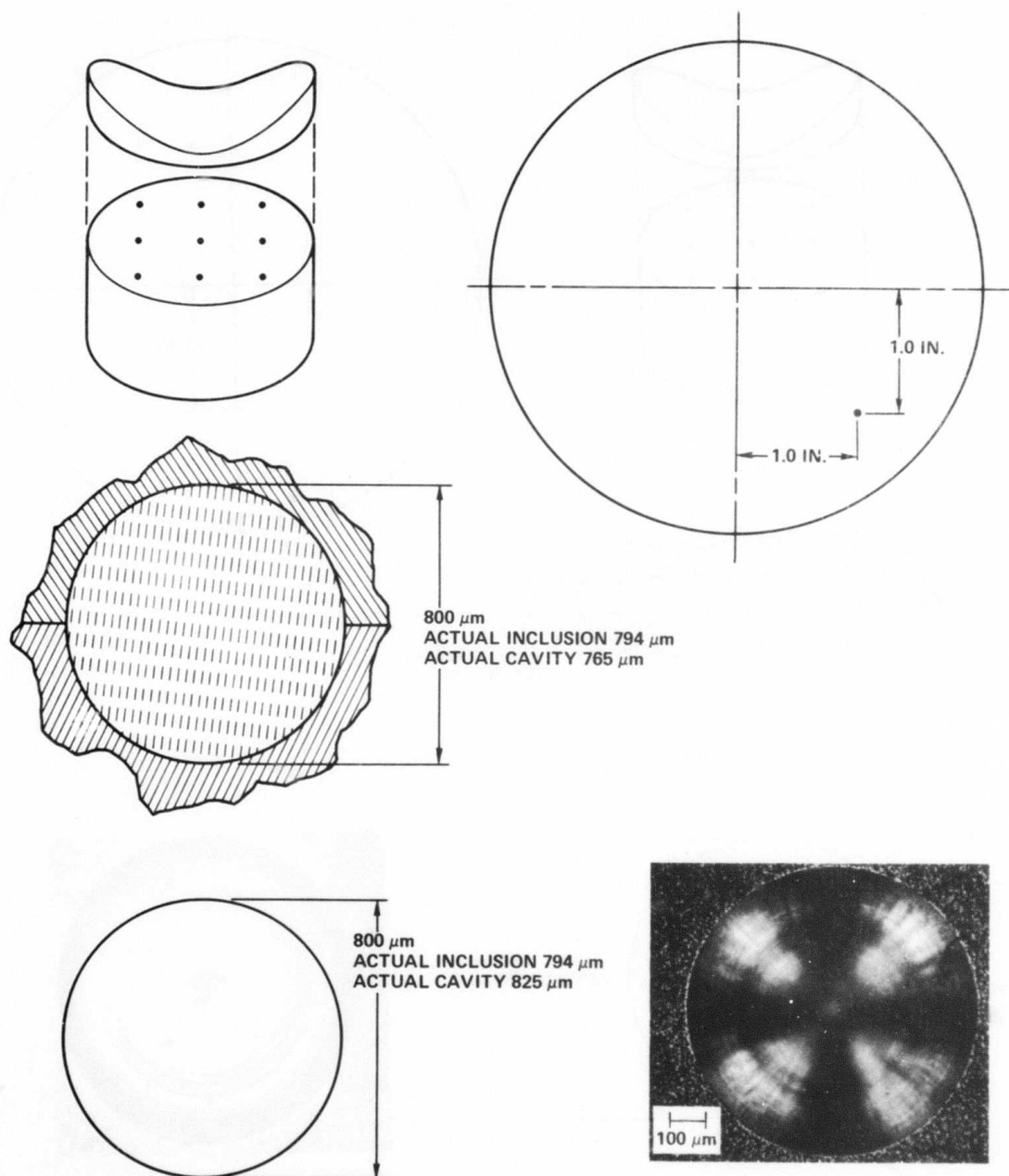


Fig. A28 Sample 90-9: 800 μm  $\text{Al}_2\text{O}_3$  spherical inclusion.

## APPENDIX B

### DOCUMENTATION FOR PHASED ARRAY HARDWARE

The documentation for the Phase Array acquisition System (PAAS) is composed of system drawings and electrical schematics. The PAAS interconnect drawing (Dwg B-1) shows the electrical paths between the main units of the system.

The Array Digitizer Electronics unit (ADE) is housed in a standard 19-in. relay rack. Two card cages contain the system control electronics and analog-to-digital conversion circuits.

Sixteen digitizer boards handle the parallel conversion and memory functions. The digitizer electrical schematic (Dwg B-2) shows the details of this board. The control functions are shared on two boards. A ten-page timing and control electrical schematic (Dwg B-3) contains the details of these boards.

The multiplexer unit (MUX) is housed in a custom Plexiglas enclosure mounted on the bridge of the scanning tank. The MUX interconnect drawing (Dwg B-4) shows the electrical connection within this assembly. The details of the buffer control board are shown in the MUX control board electrical schematic (Dwg B-5). A five-page MUX board electrical schematic (Dwg B-6) displays the details of the multiplexer/demultiplexer functions contained on two identical boards. The hybrid pulser-receiver, Pr-SCR400V-1, contains two complete circuits. The electrical schematic (Dwg B-7) and electrical parts list (Dwg B-8) contain the details for one circuit.

4

3

2

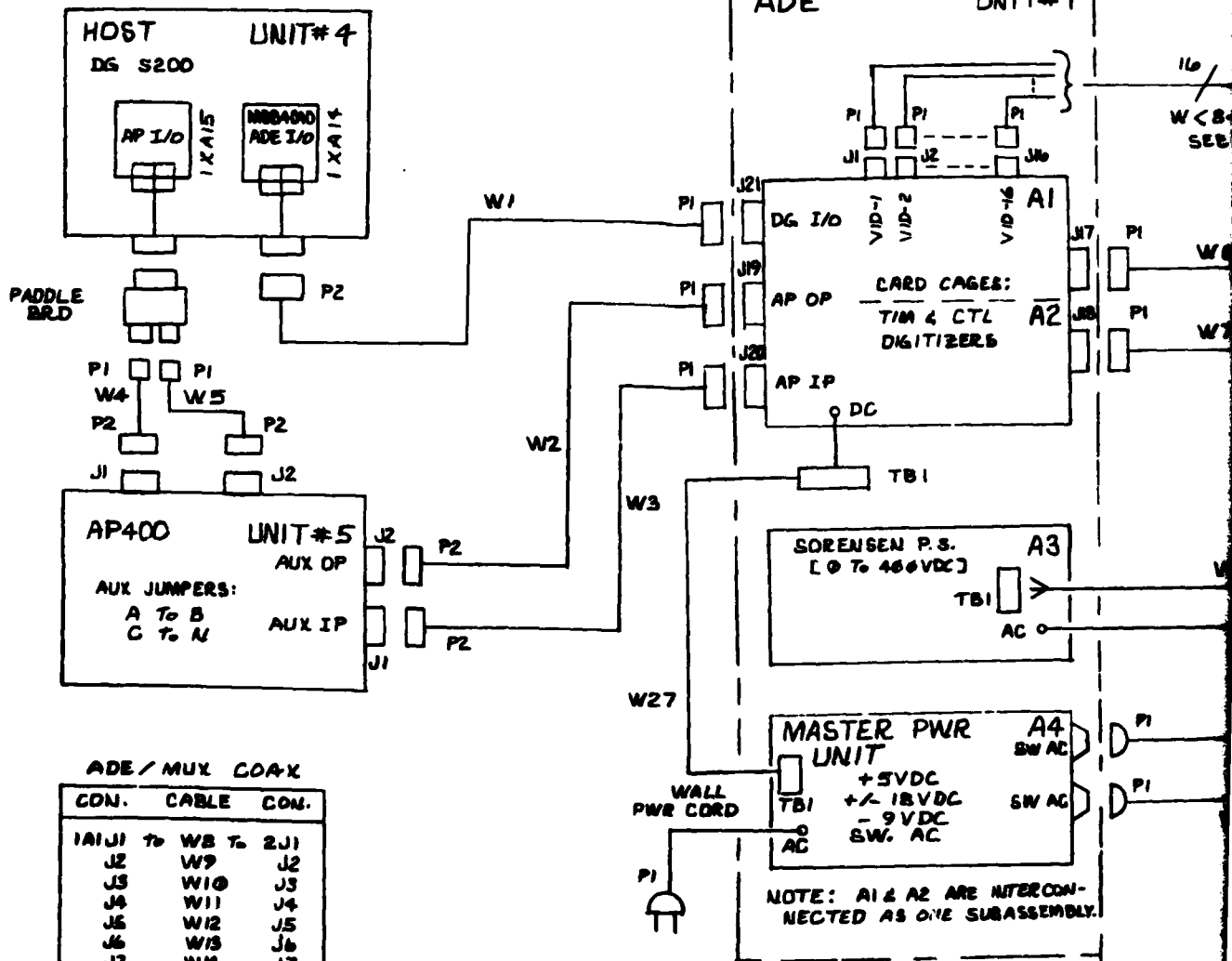
D

C

→

B

A



## ADE/MUX COAX

CON.	CABLE	CON.
1A1 J1 To	W8 To	2 J1
J2	W9	J2
J3	W10	J3
J4	W11	J4
J5	W12	J5
J6	W13	J6
J7	W14	J7
J8	W15	J8
J9	W16	J9
J10	W17	J10
J11	W18	J11
J12	W19	J12
J13	W20	J13
J14	W21	J14
J15	W22	J15
1A1 J16 To	W23 To	2 J16

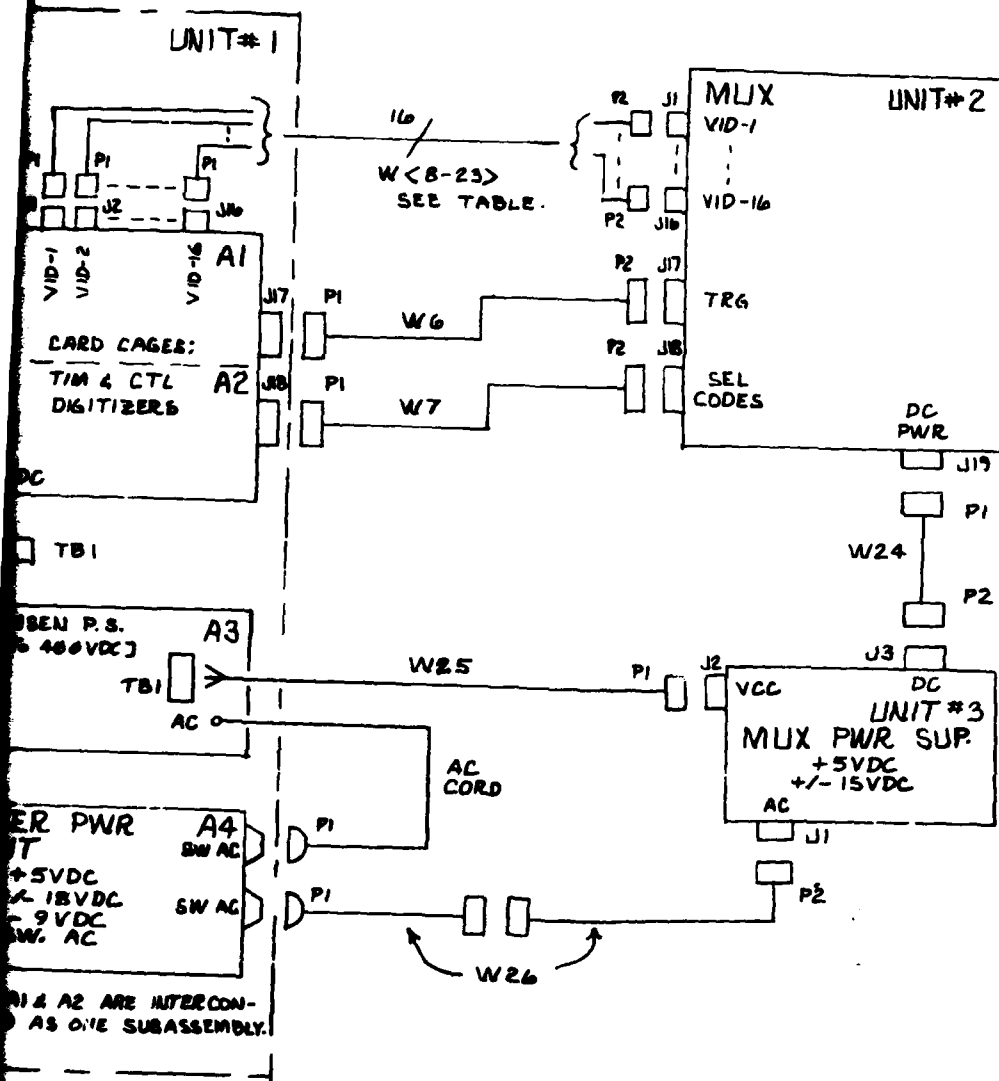
## NOTES:

- INTERCONNECT BETWEEN P1 & P2 OF SAME WIRE ASSEMBLY IS PIN 1 TO PIN 2, EXCEPT AS NOTED.

## DRAWING B-1

NO.	NEXT ASSY	USED ON
APPLICATION		
TOLERANCE: INCHES, METRIC DECIMAL JXX ± JXX ±		
✓ SURFACE ROUGHNESS		ANGLE ±
UNLESS OTHERWISE NOTED		

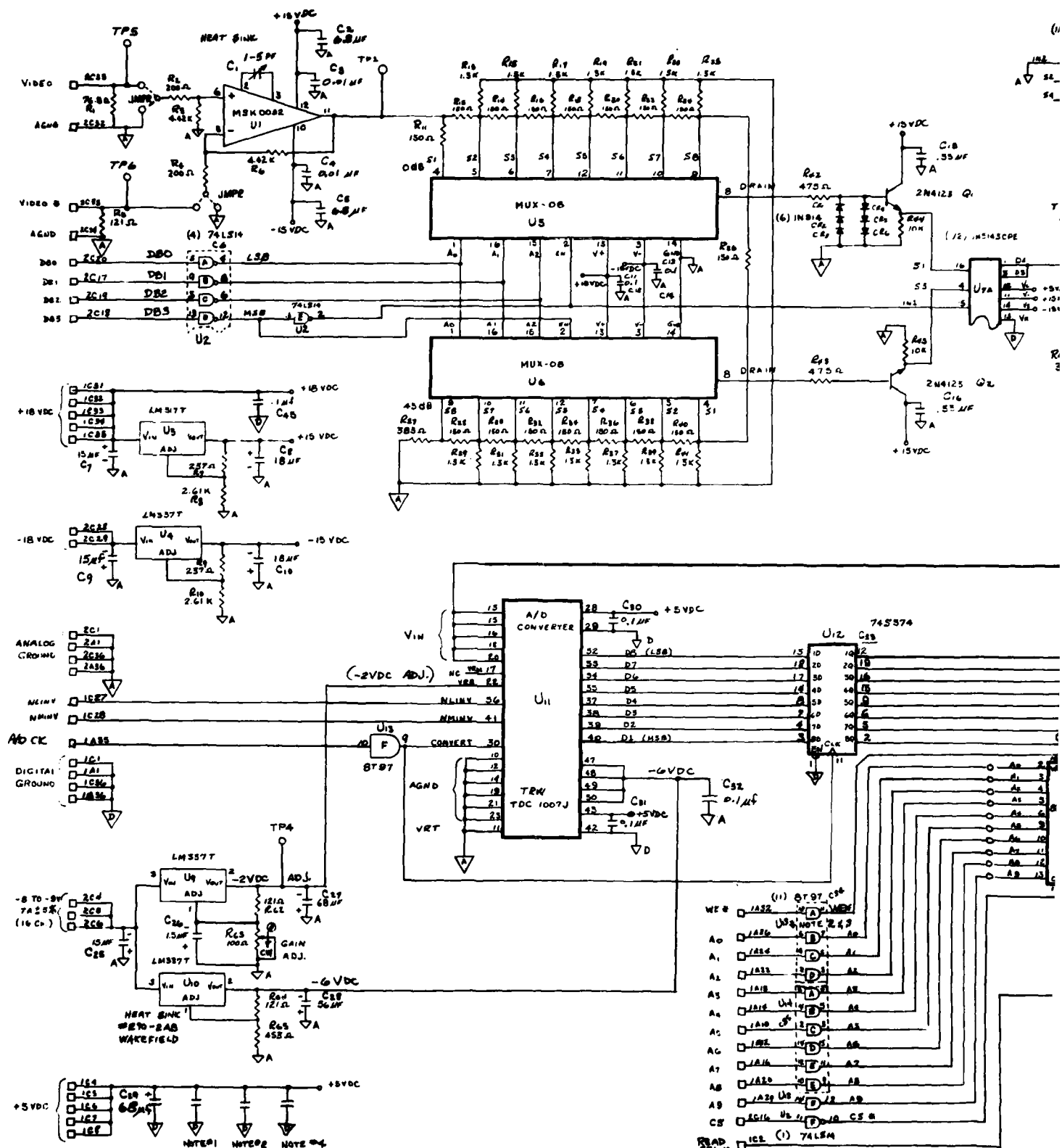
REVISIONS			
LTR	DESCRIPTION	DATE	APPROVED
A	ORIGINAL		



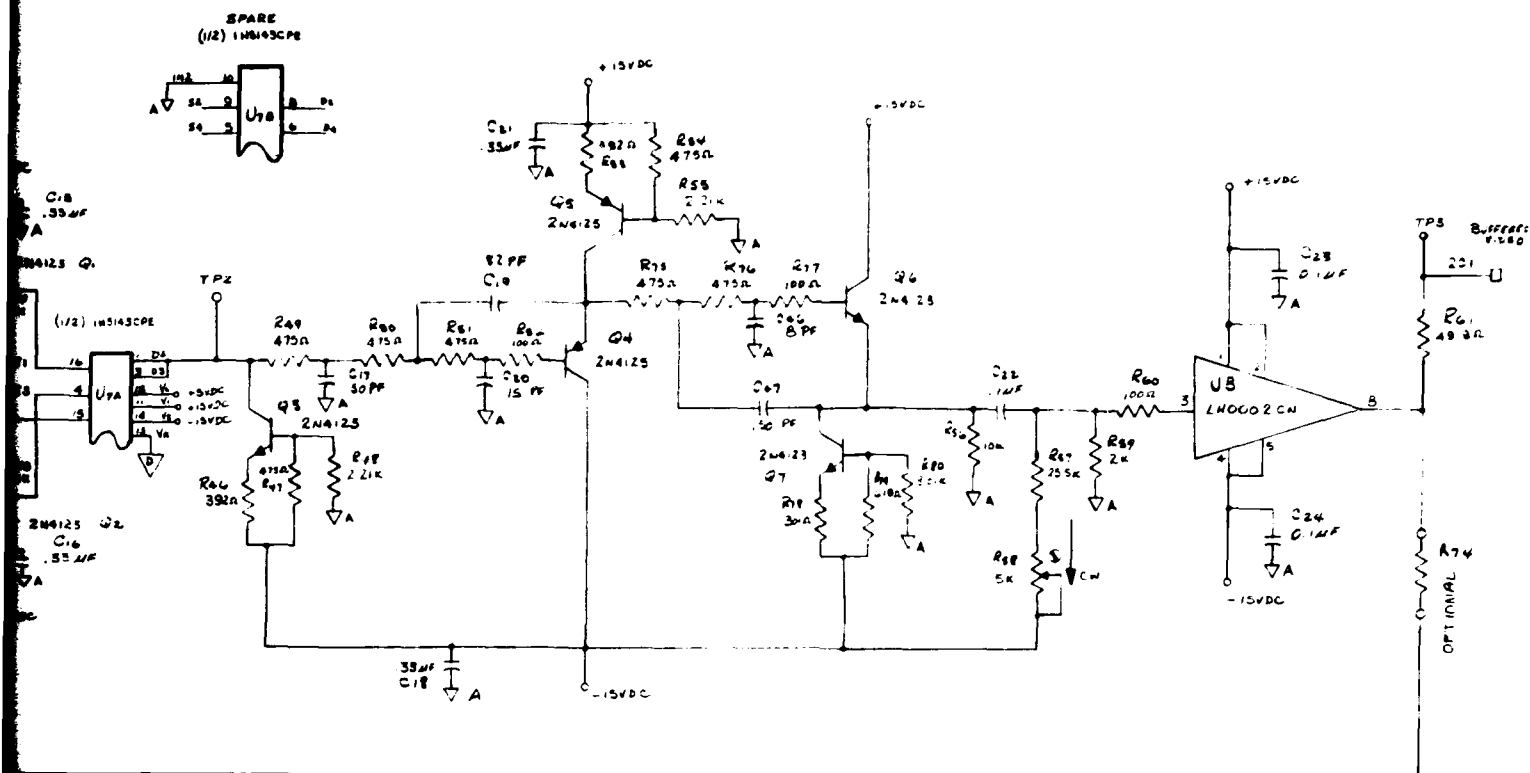
DRAWING B-1

			CONTRACT NUMBER	30016-S104		
			DRAWN			
NO.	NEXT ASSY	USED ON	DESIGN			
APPLICATION			CHECK			
TOLERANCE: INCHES, METRIC			ENGRG	CRS/Ames	11-13-81	PAAS INTERCONNECT ADE, MUX, HOST, AP
DECIMAL XX ±			MPG			
XXX ±						
✓ SURFACE ROUGHNESS		ANGLES ±	PHASED ARRAY ACQUISITION SYSTEM		SIZE C	REV. -
UNLESS OTHERWISE NOTED:					SCALE	WEIGHT
					SHEET 2 of 1	

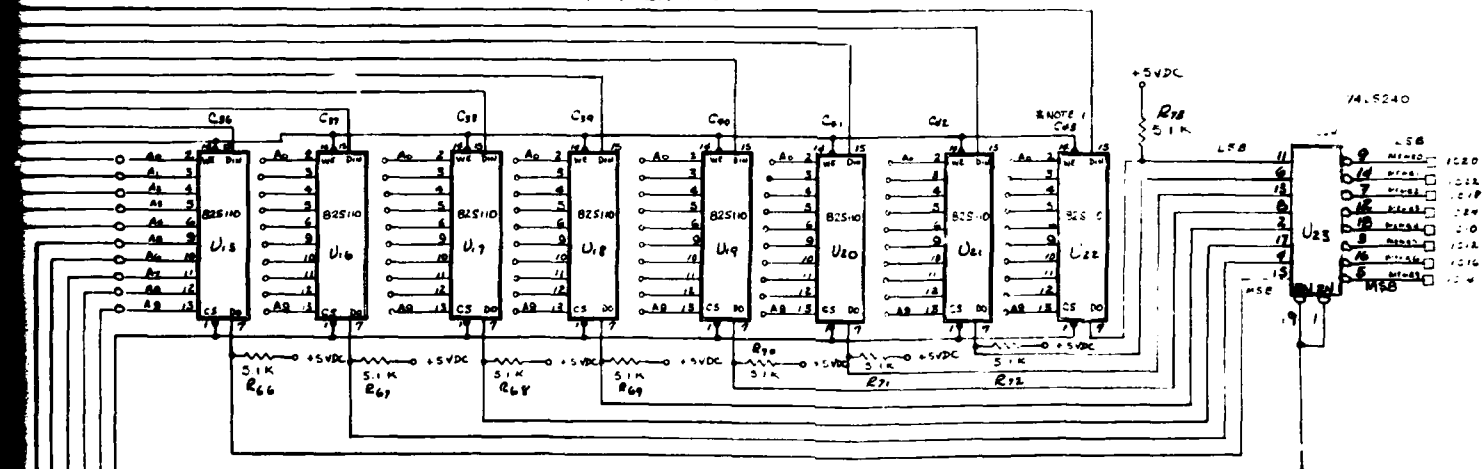








# MEMORY, 1K x 8



DRAWING B-2

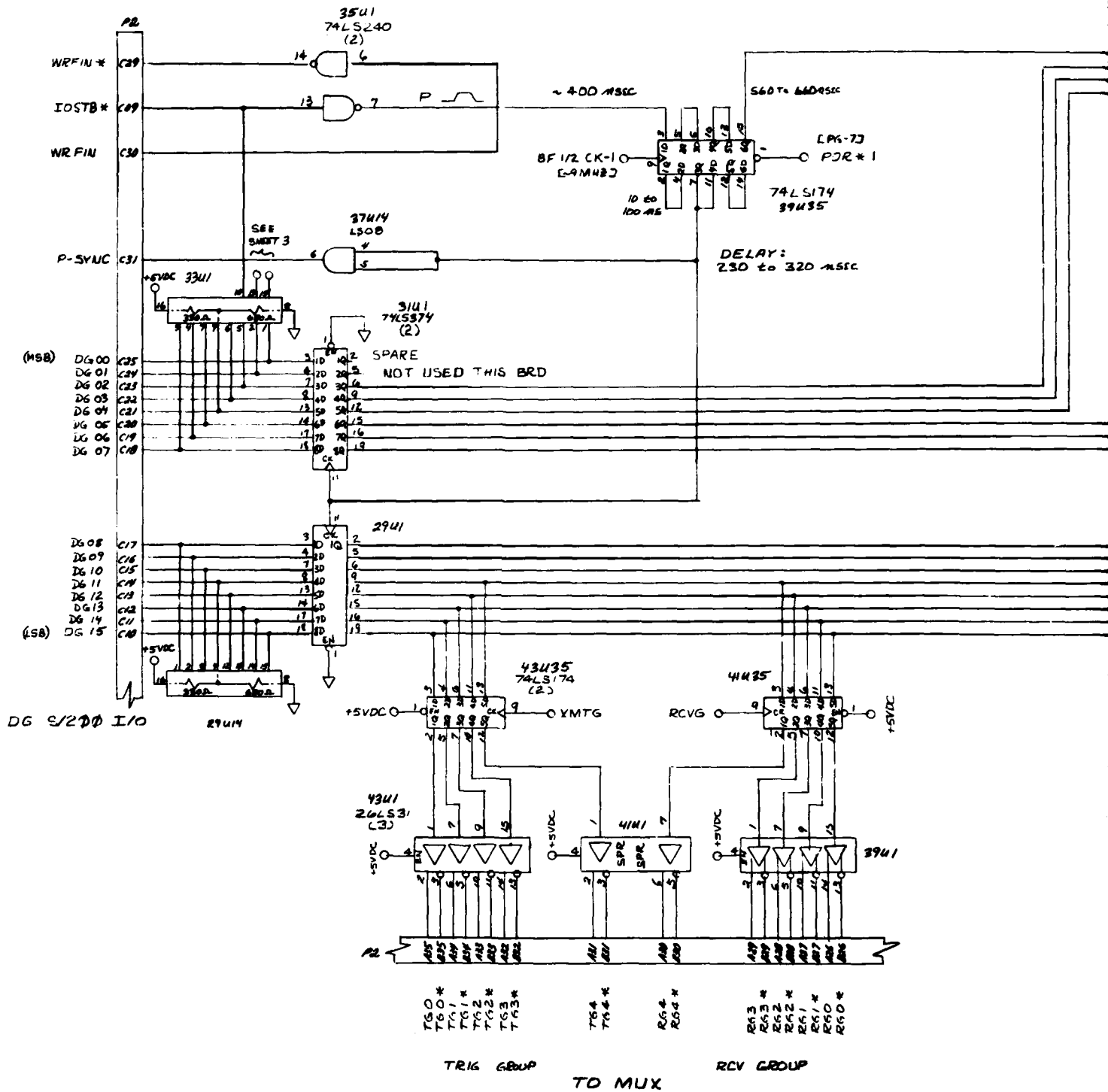
- 74124 & 74137: 0.01μF  
+5VDC ON P-20, DEND ON P-16
  - ENABLE P-15, P-16 ON 74137  
TO DEND.
  - USE 0.01μF CAP ON EACH 82510,  
+5VDC ON P-16, DEND ON P-8.
- NOTE: 1. USE 0.01μF CAP ON EACH 82510,  
+5VDC ON P-16, DEND ON P-8.
- CONNECTORS: P1 & P2

CONTINUED			05164		
DRAWN			VANCE		
DESIGN			1-11-80		
CHECK					
ENGRG					
MFG					
APPLICATION					
TOLERANCE: INCHES, METRIC					
DECIMAL XX ±					
XXX ±					
SURFACE ROUGHNESS			FINISH		
ANGLES					
UNLESS OTHERWISE NOTED:					
SIZE			REV.		
D			3		
SCALE			WEIGHT		
SHEET			1		

DIGITIZER, ADE  
SCHEMATIC, ELEC.











RD SEL#16  
RD SEL#15  
RD SEL#14  
RD SEL#13  
RD SEL#12  
RD SEL#11  
RD SEL#10  
RD SEL#9

DLY RDY

RD SEL#8  
RD SEL#7  
RD SEL#6  
RD SEL#5  
RD SEL#4  
RD SEL#3  
RD SEL#2  
RD SEL#1

XA15  
XA13

CP6-73  
CK-1B

37414  
L608

A2

IP INCR

[PW > 60 nS]

5492  
74LS174

ΔT  
2T + ΔT

NOTE:

2-12-81 OF 1. WE STILL  
NEED ONE MORE DELAY  
T = 56 nS FOR PROPER  
TIMING ALLOWANCE.

LD MEM REG

IP REG

TST RD CK

[FOR TR6/WF] \*

DRAWING B-3 SHEET 3

ADE		
TIM & CTL		
SIZE D	XA15 + XA13	A
SCALE	WEIGHT	SHEET 3

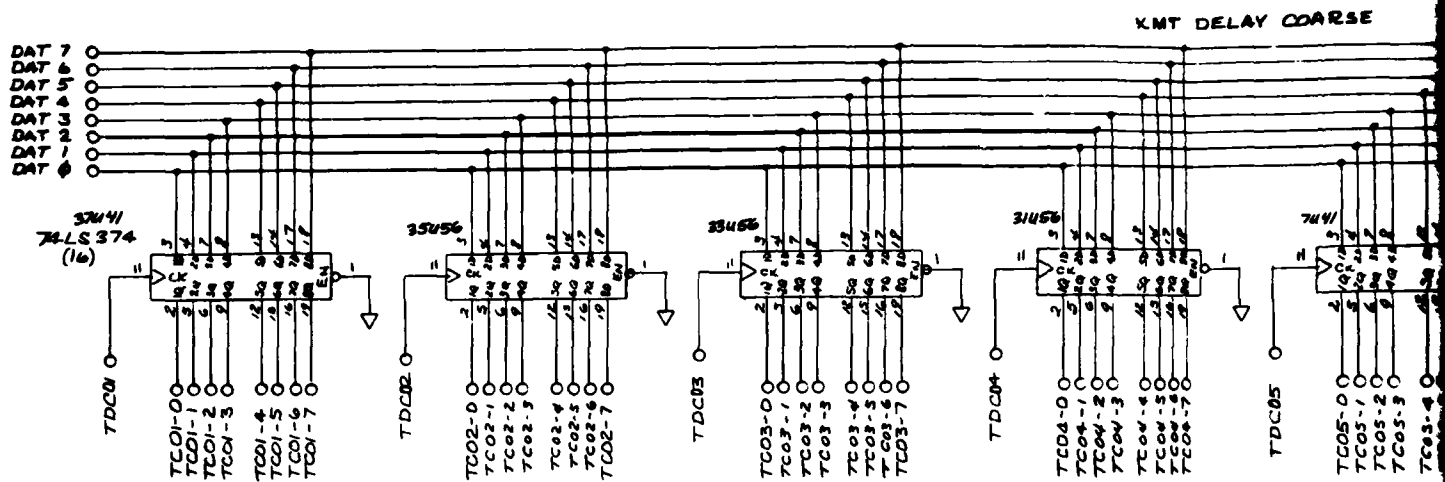
REV A 10-26-81 OF





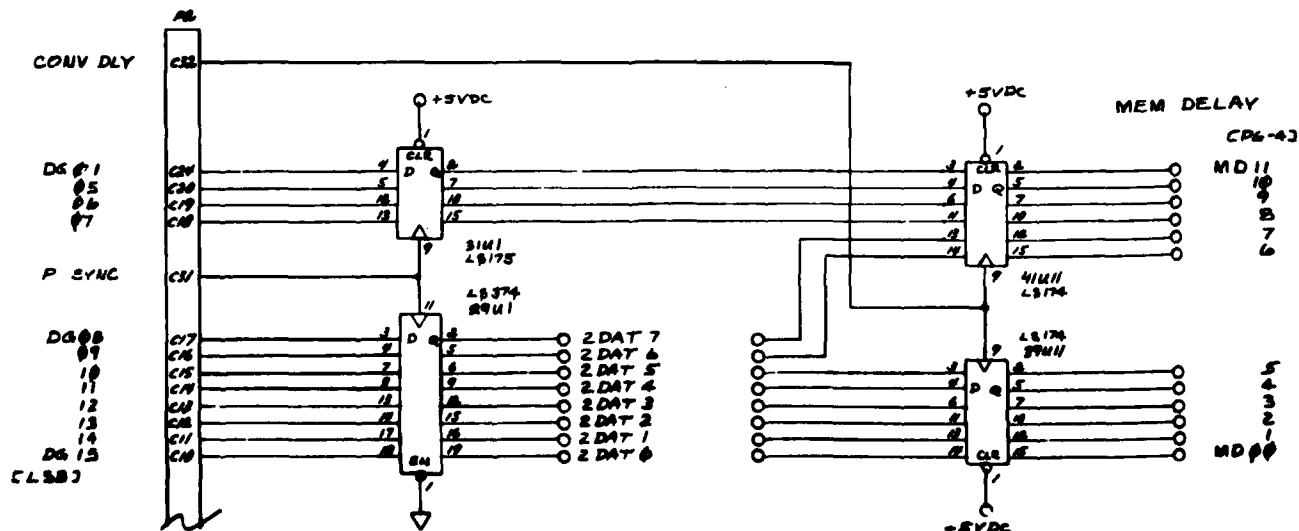
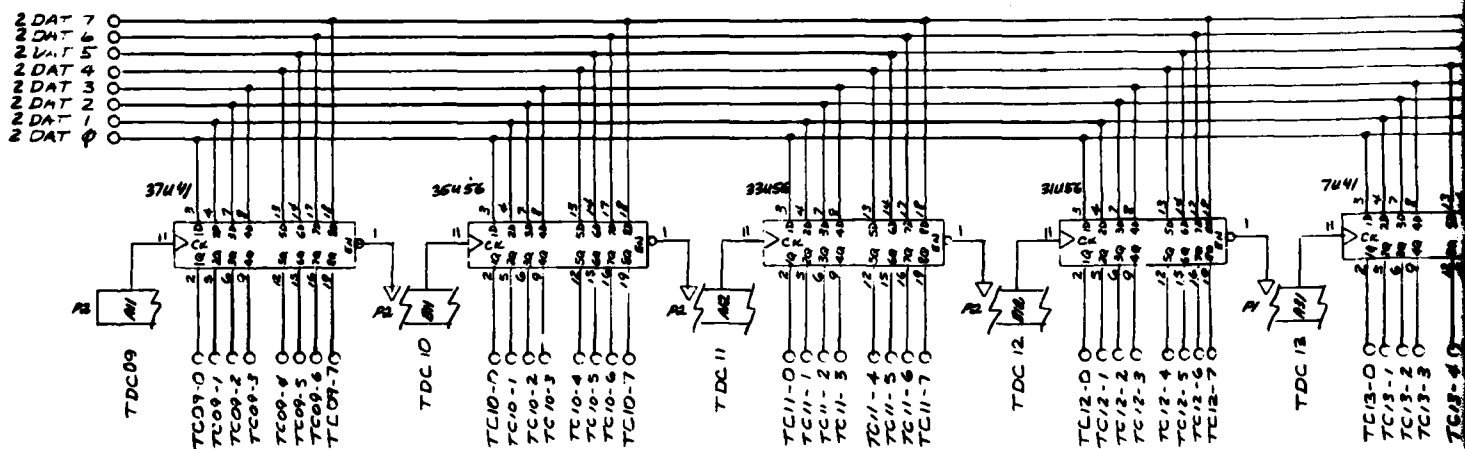


DRAWING 3-5 SHEET 4		
ADE		
TIM & CTL		
SIZE D	KAIS	REV A
SCALE	WEIGHT	SHEET 4

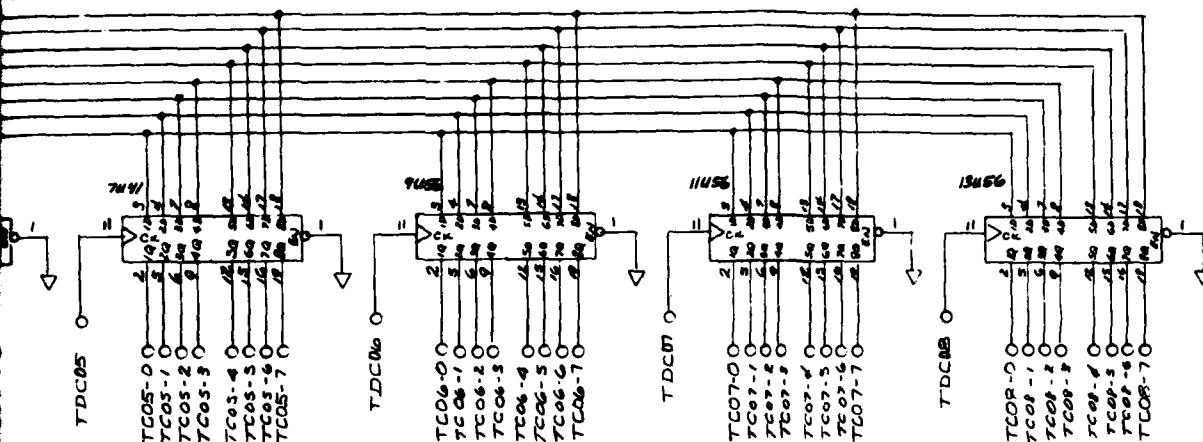


XA13

XA15

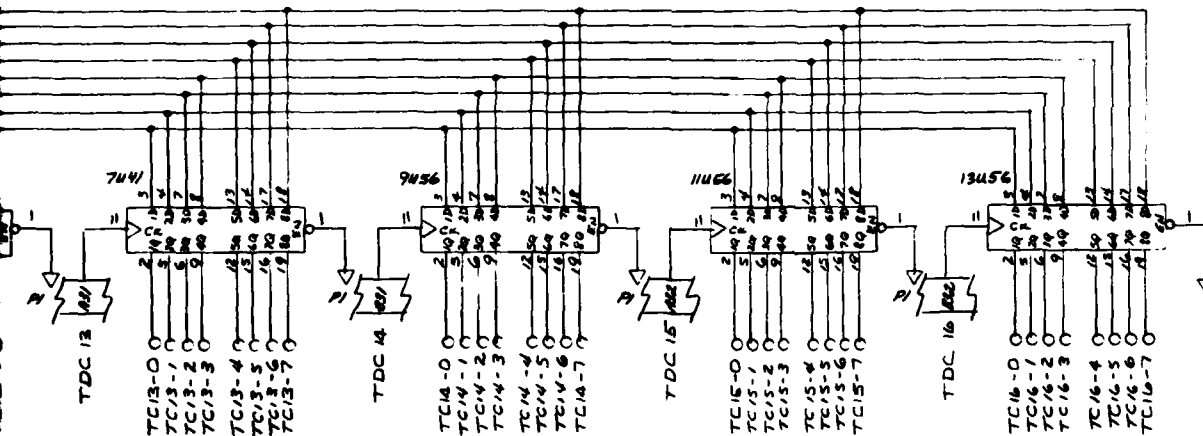


DELAY COARSE



XA 13

XA 15



DELAY

CP6-43

MD 11  
10  
9  
8  
7  
6

MD 11  
10  
9  
8  
7  
6

DRAWING B-3 SHEET 5

ADE TIM & CTL		
SIZE D	XA 13 & XA 15	REV. A
SCALE	WEIGHT	SHEET 5

REV A 10-23-81

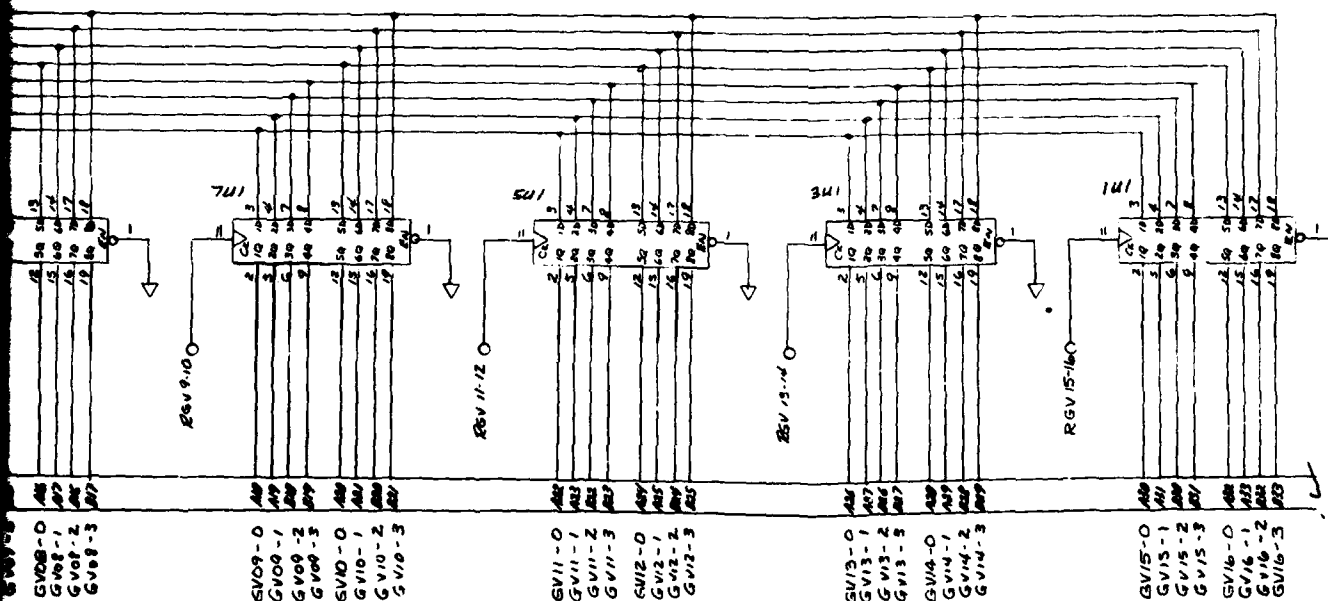


XAIS

**FINE**



YA 13



ADE  
TIM & CTL

SIZE	XA15	XA15
------	------	------

15

1

REV

**I A**

SCALE

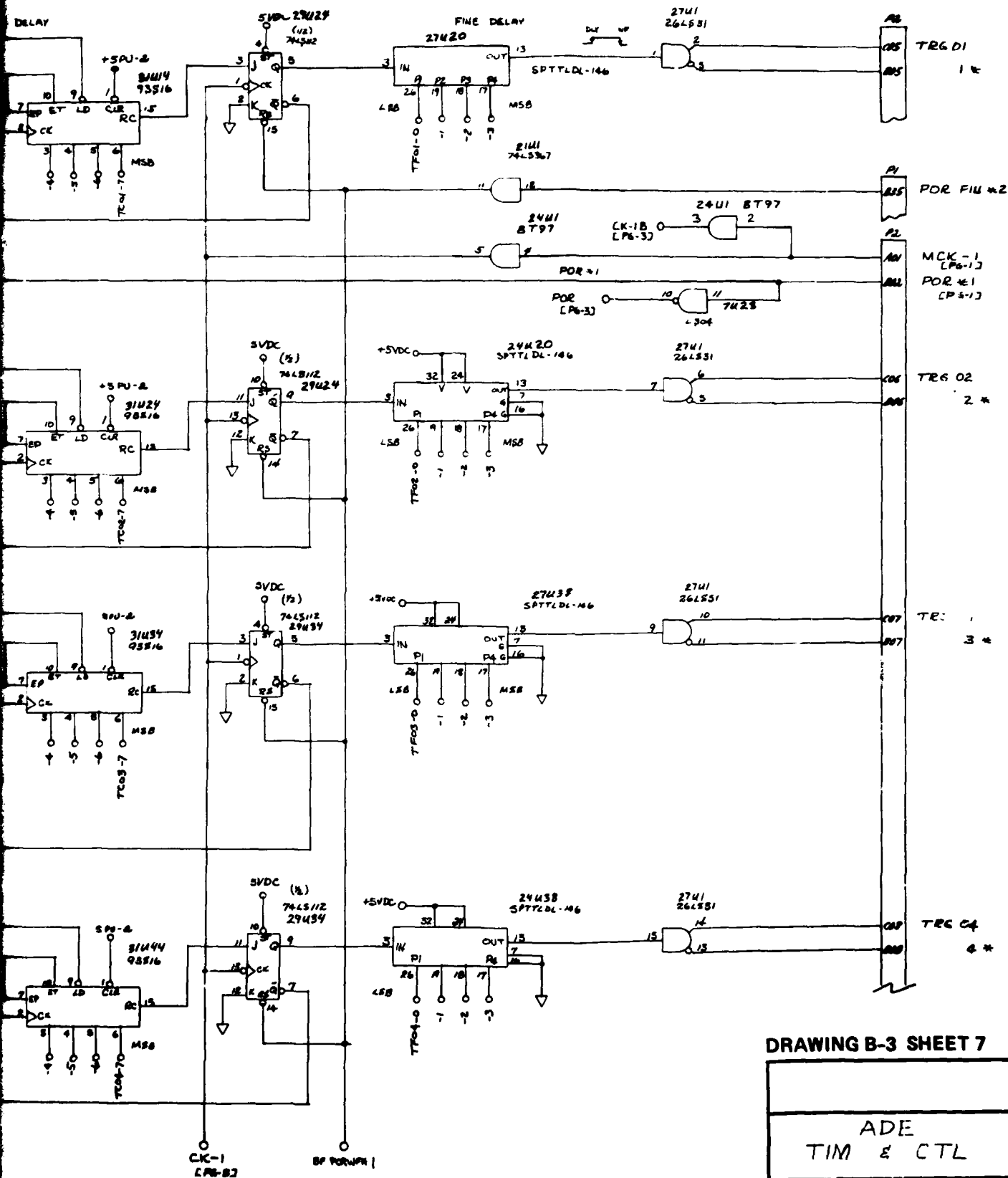
	WEIGHT
100	100
90	90
80	80
70	70
60	60
50	50
40	40
30	30
20	20
10	10
0	0

**SHEET 6**

REV A 10-23-81 

**B16/17**



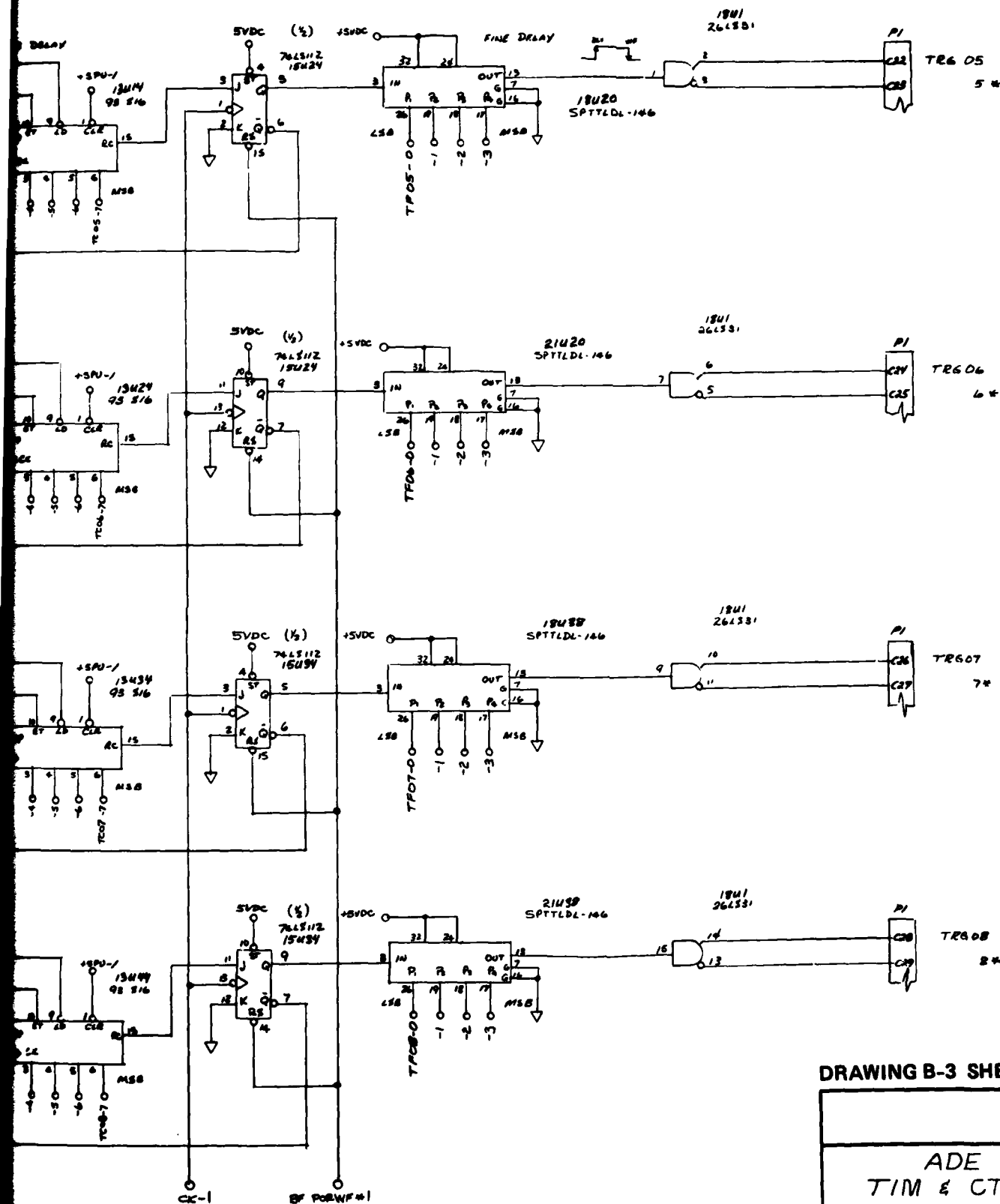


DRAWING B-3 SHEET 7

ADE TIM & CTL		
SIZE D	Y A 13	REV A
SCALE	WEIGHT	SHEET 9

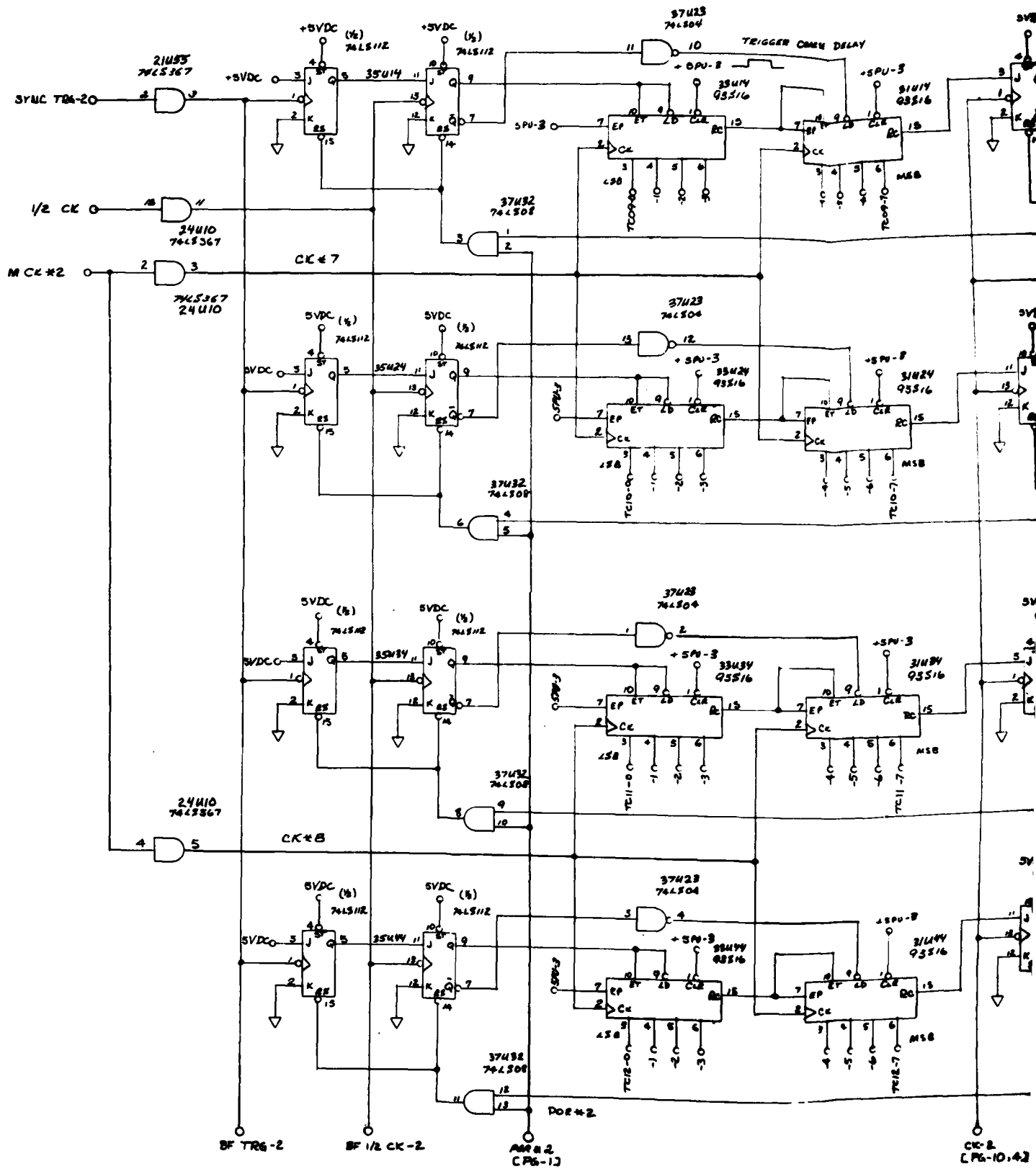


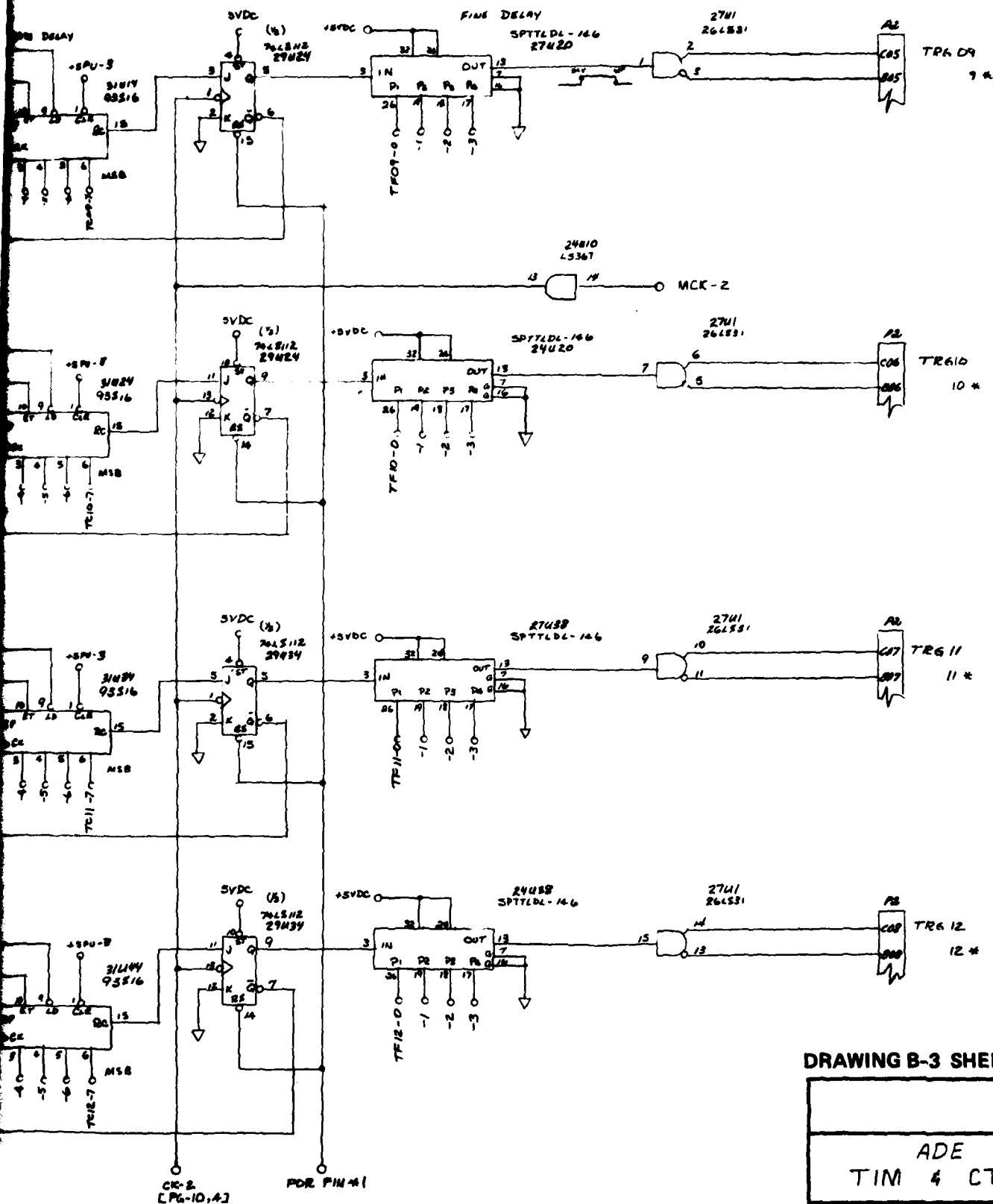




DRAWING B-3 SHEET 8

ADE TIM & CTL		
SIZE D	XA13	REV. A
SCALE	WEIGHT	SHEET 8





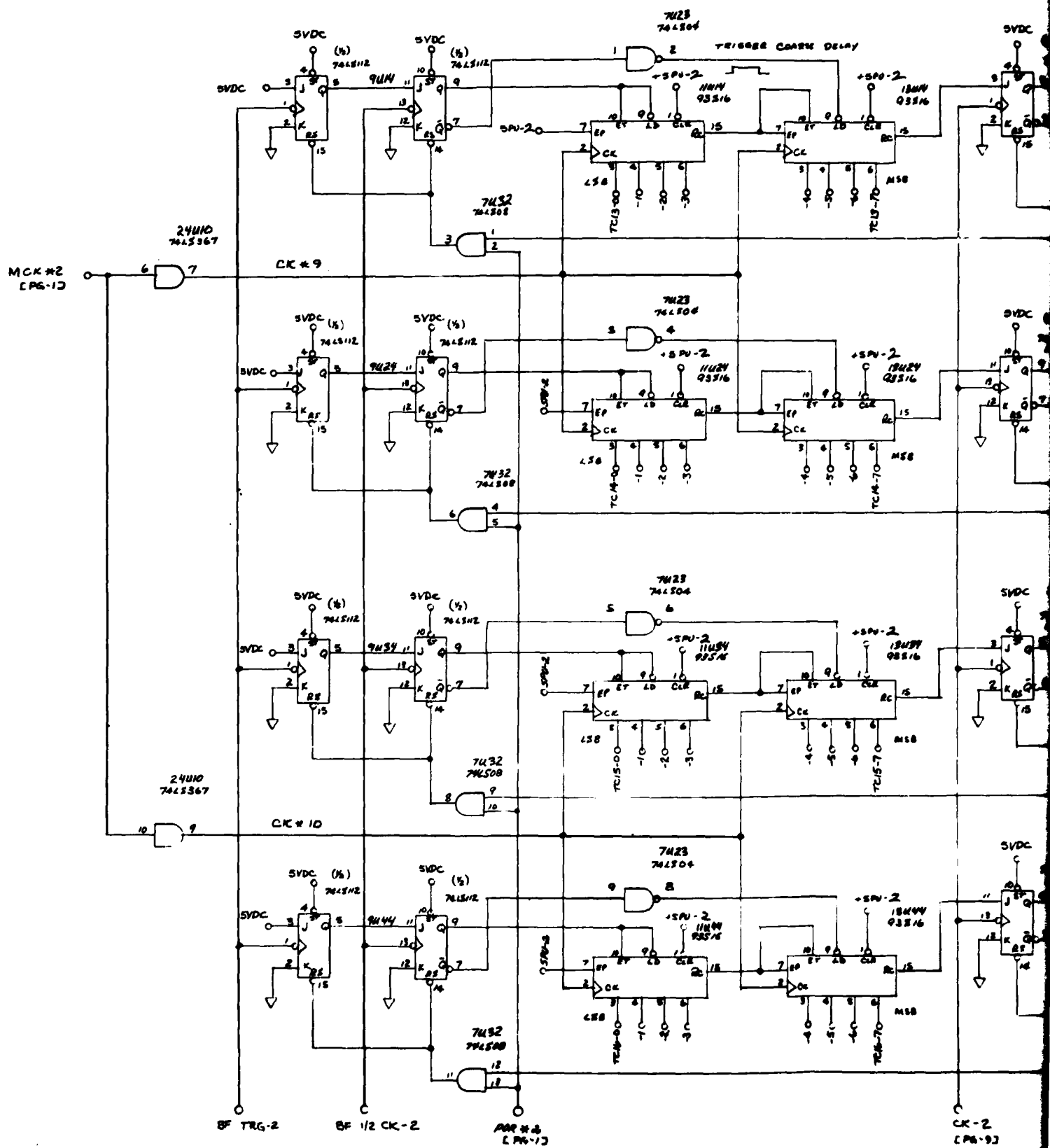
DRAWING B-3 SHEET 9

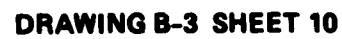
ADE		
TIM 4 CTL		
SIZE D	YAS	REV. A
SCALE	WEIGHT	SHEET 9

REV A 10-25-81 CT

B22/23

n



REV A 10-23-81 CR

4

3

2

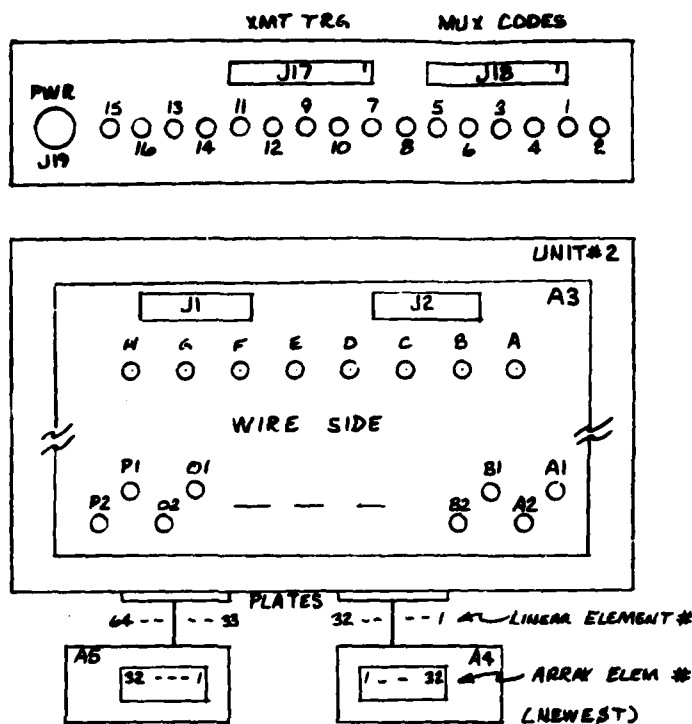
D

C

→

B

A



PIN # . MUX PWR . W19J19

1	BLU. HYBRD COM
2	BRN. COMMON
3	VIO. +15VDC. IN
4	GRY. -15VDC. IN
5	GRY. +5VDC. IN
6	-
7	-
8	GRN. +400VDC. IN

MUX COAX, SIGNAL OUTPUT

SYS W#	MUX CON	INT W#	COM BRD CON	INT W#	MUX CON	SYS W#
W9	J2	W2	A	W1	J1	W8
W11	J4	W4	B	W3	J3	W10
W13	J6	W6	C	W5	J5	W12
W15	J8	W8	D	W7	J7	W14
W17	J10	W10	E	W9	J9	W16
W19	J12	W12	F	W11	J11	W18
W21	J14	W14	G	W13	J13	W20
W23	J16	W16	H	W15	J15	W22

A2, EVEN BRD

A3, ODD BRD

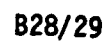
## NOTES:

- W20: PIC(1)<sup>40</sup> to P2(1)<sup>40</sup> to P3(1)<sup>40</sup>. REFER TO ELEC SCHEM, MUX CTL BRD, A1J1.
- W17: J17(1)<sup>40</sup> to P1(1)<sup>40</sup> & P1(2)<sup>40</sup> to P2(1)<sup>40</sup>, NO WIRES ON P2(1)<sup>40</sup>. REFER TO INTERCON. LIST, 1A1J17 to A1X13/15. (W6).
- W18: J18(1)<sup>40</sup> to P1(1)<sup>40</sup>. REFER TO INTERCONNECT LIST, 1A1X13 to 1A1J18 to 2J18(W7).
- W<21-26>: REFER TO ARRAY INTERCONNECT LIST, DIAGRAM, & MINIHORST'S INTERCONNECT.
- INTERNAL MUX WIRE NUMBERS, W#, ARE REFERENCED AS 2W# IN OVERALL SYSTEM NOTATION.

## DRAWING B-4

NO.	NEXT ASSY	USE
APPLICATION		
TOLERANCE: INCHES, MIL DECIMAL XX ± XXX ±		
✓ SURFACE ROUGHNESS		
UNLESS OTHERWISE NOT		

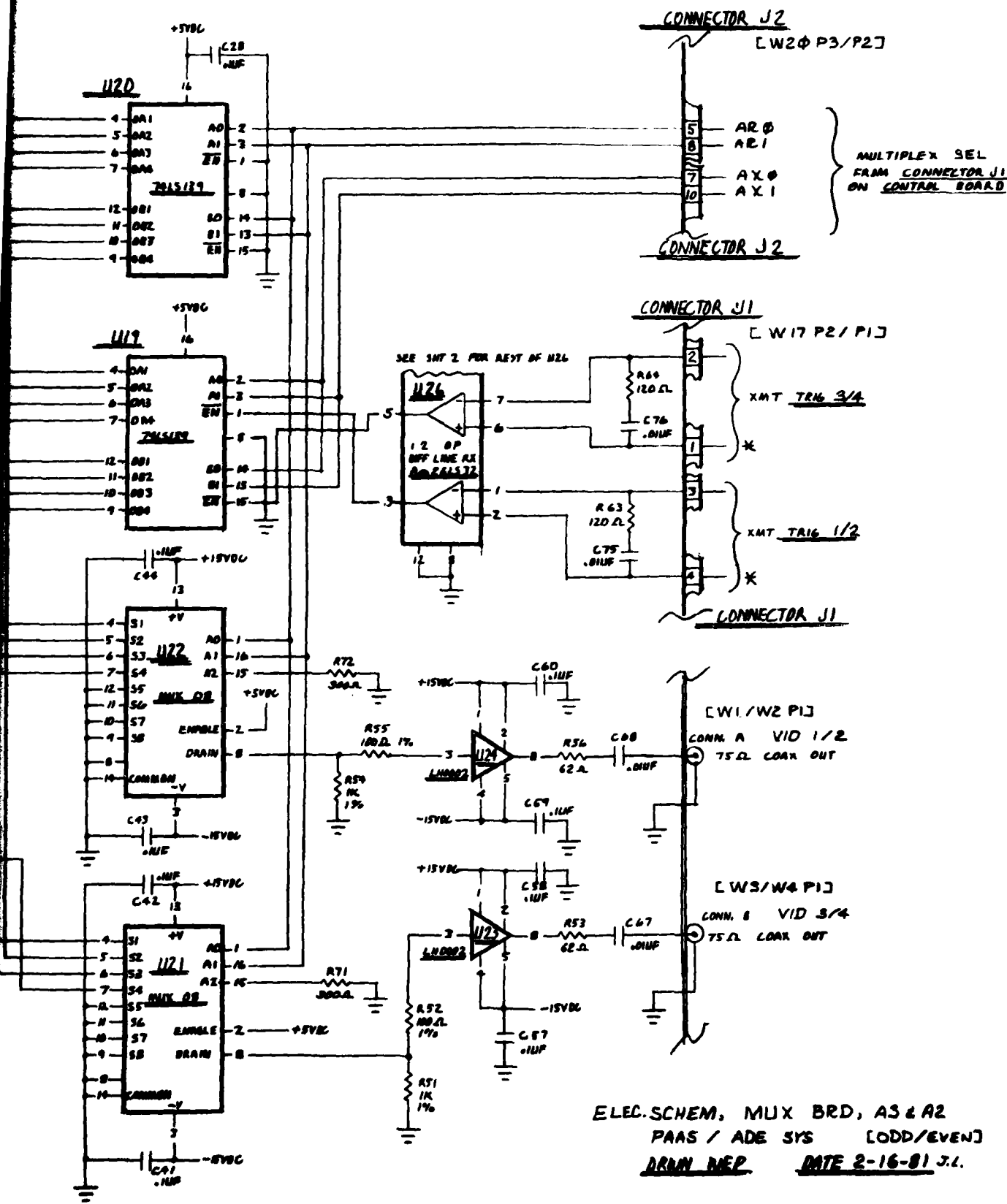












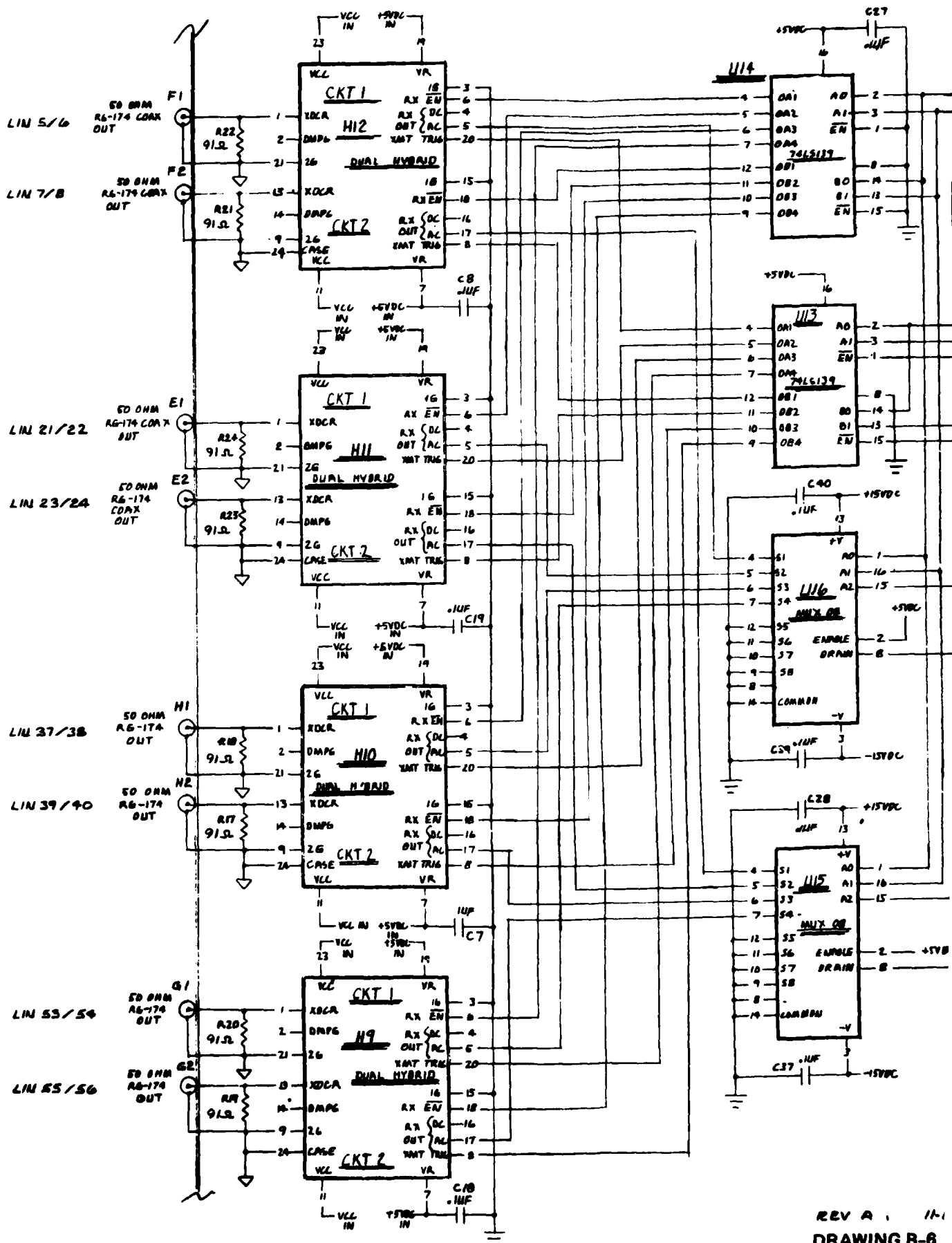
ELEC. SCHEM, MUX BRD, AS & A2  
 PAAS / ADE SYS [ODD/EVEN]  
 DRAM MEX. DATE 2-16-81 J.L.

REV A, 11-N-81, ST, NAMES UPDATE  
 DRAWING B-8 SHEET 1

SHEET 1 OF 5 SIZE C

B30/31

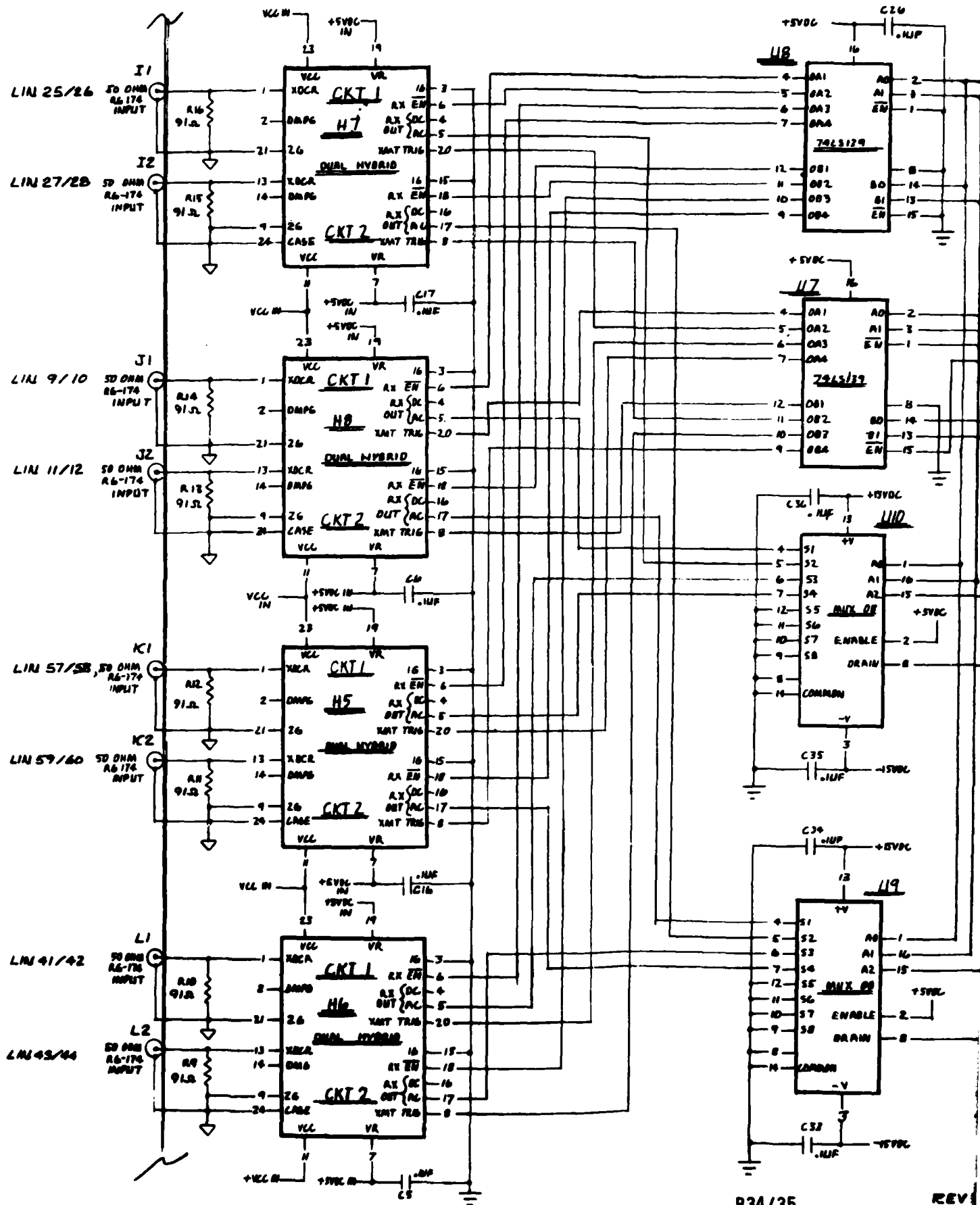
2

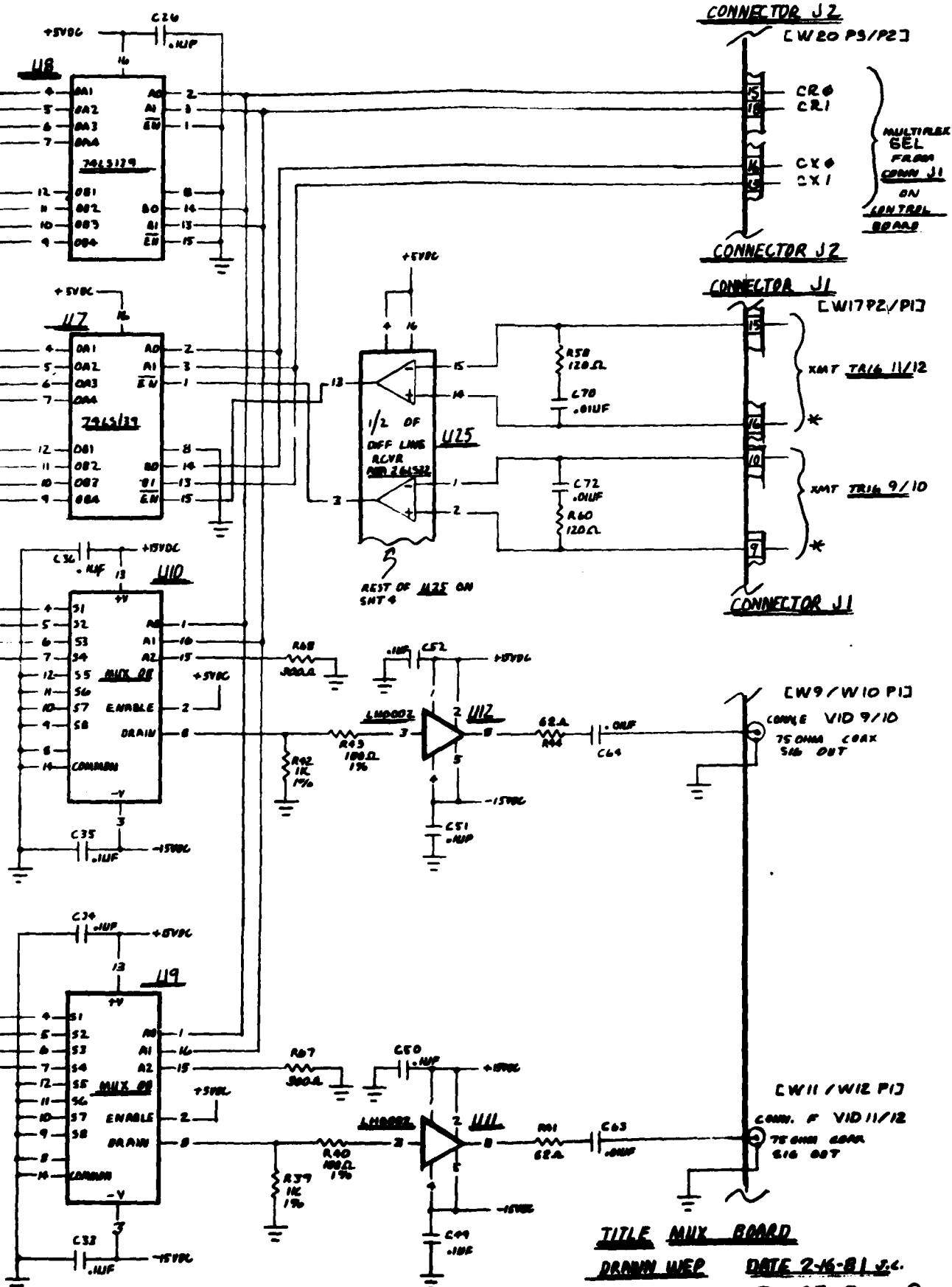


REV A 1A-1  
DRAWING B-6

B32/33

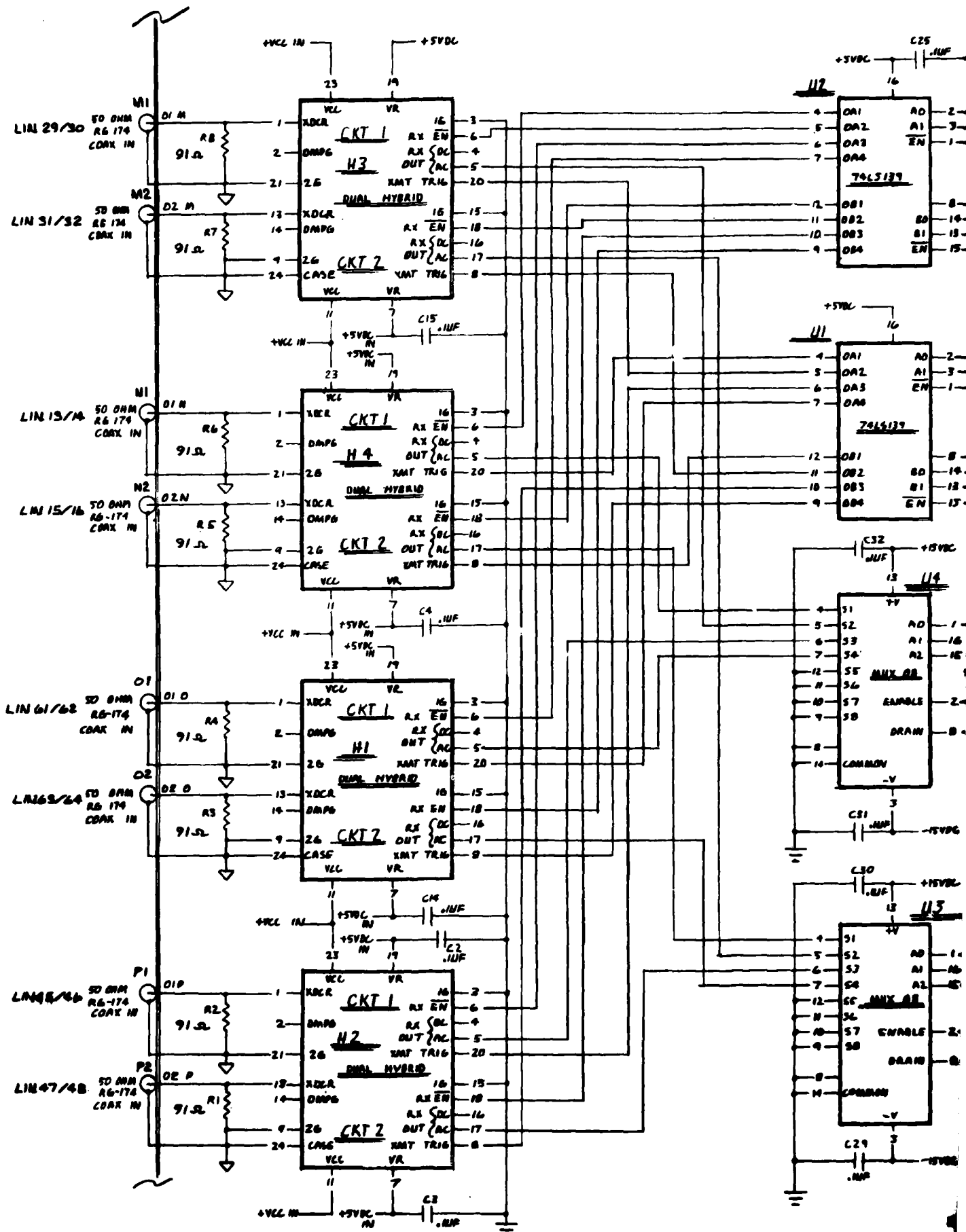




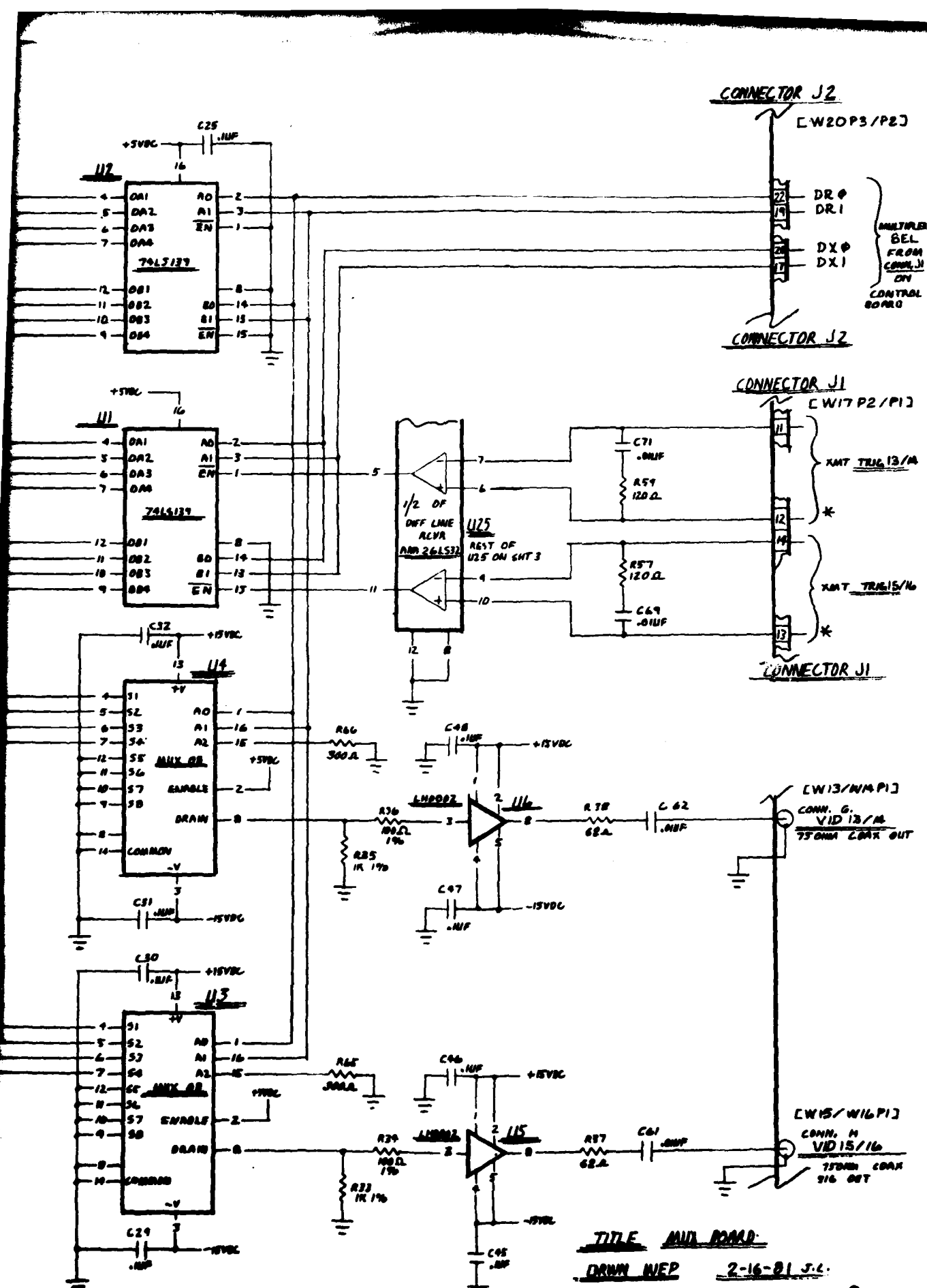


B34/35

REV A, 11-11-81 CT, NOMEN. UPDATE.  
DRAWING B-6 SHEET 3







REV A. 11-11-81. OF. NOMEN. UPDATE.  
DRAWING B-6 SHEET 4

TITLE AND BOARD  
DRAWN WEP 2-16-81 J.L.  
SHEET 4 OF 5

C

# CONNECTOR J1

CW17 P2/P17



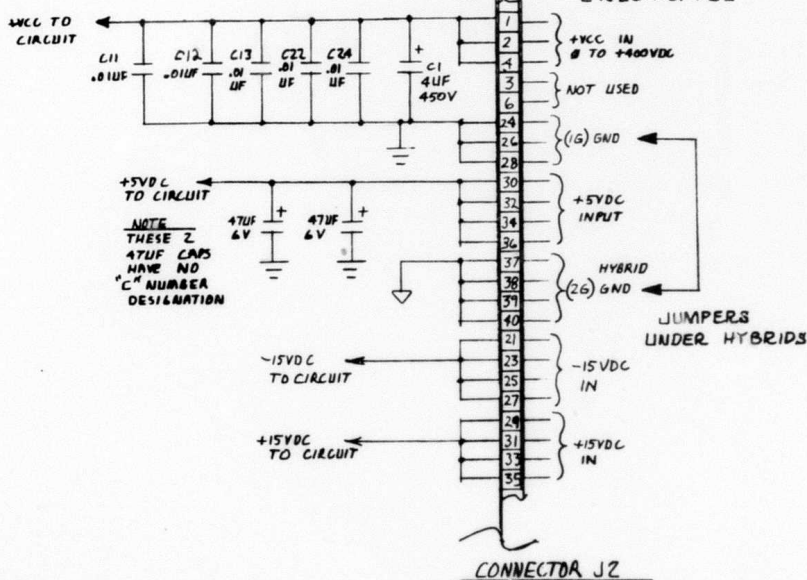
PINS DEDICATED ON WIRE HARNESS.  
EVEN BRD. A2, SIGNALS PRESENT.  
ODD BRD. A3, NO CONNECTION.

CONNECTOR J1  
PINS NOT USED  
ON PCB.

# CONNECTOR J1

# CONNECTOR J2

CW20 P3/P23



# CONNECTOR J2

# NOTES

①

# TABLE A

# CONNECTOR J1 CROSS REF

REF SMT	DESCRIPTION	CONN J1	DEF
1	* XMT TRIG 3/4	1 2	XMT
1	XMT TRIG 1/2	3 4	* XMT
2	* XMT TRIG 5/6	5 6	XMT
2	XMT TRIG 7/8	7 8	* XMT
3	* XMT TRIG 9/10	9 10	XMT
4	XMT TRIG 13/14	11 12	* XMT
4	* XMT TRIG 15/16	13 14	XMT
3	XMT TRIG 11/12	15 16	* XMT
5	NOT USED	17 18	NOT
5	NOT USED	19 20	NOT
5	NOT USED	21 22	NOT
5	NOT USED	23 24	NOT
5	NOT USED	25 26	NOT
5	NOT USED	27 28	NOT
5	NOT USED	29 30	NOT
5	NOT USED	31 32	NOT
5	NOT USED	33 34	NOT
5	NOT USED	35 36	NOT
5	NOT USED	37 38	NOT
5	NOT USED	39 40	NOT

②

# TABLE B

# CONNECTOR J2 CROSS

REF SMT	DESCRIPTION	CONN J2	DESC
5	+VCC IN	1 2	+VCC
5	NOT USED	3 4	+VCC
1	ARΦ	5 6	NOT
1	AXΦ	7 8	AR
2	BRΦ	9 10	AX
2	BX1	11 12	BR
3	CX1	13 14	BX
3	CRΦ	15 16	CX
4	DX1	17 18	CR
4	DR1	19 20	DX
5	-15VDC IN	21 22	DR
5	-15VDC IN	23 24	(16) GND
5	-15VDC IN	25 26	(16) GND
5	-15VDC IN	27 28	(16) GND
5	+15VDC IN	29 30	+5VDC
5	+15VDC IN	31 32	+5VDC
5	+15VDC IN	33 34	+5VDC
5	+15VDC IN	35 36	+5VDC
5	(26) HYBRID GND	37 38	(26) GND
5	(26) HYBRID GND	39 40	(26) GND

③

# TABLE C

# CROSS REF OUTPUT SIG

CONN	REF SMT	REF VID #	XDCR ELEM
A	1	1/2	1-17-33-4
B	1	3/4	3-19-35-4
C	2	5/6	5-21-37-4
D	2	7/8	7-23-39-4
E	3	9/10	9-25-41-5
F	3	11/12	11-27-43-5
G	4	13/14	13-29-45-5
H	4	15/16	15-31-47-5

ALL SIGNAL OUT PUTS  
XDCR ELEM SHOWN  
BRD A2 CONNEC

# NOTES

①

## TABLE A

CONNECTOR J1 CROSS REFERENCE DATA

REF SMT	DESCRIPTION	CONN J1	DESCRIPTION	REF SMT
1	* XMT TRIG 3/4	1 2	XMT TRIG 3/4	1
1	XMT TRIG 1/2	3 4	* XMT TRIG 1/2	1
2	* XMT TRIG 5/8	5 6	XMT TRIG 5/8	2
2	XMT TRIG 7/8	7 8	* XMT TRIG 7/8	2
3	* XMT TRIG 9/10	9 10	XMT TRIG 9/10	3
4	XMT TRIG 13/16	11 12	* XMT TRIG 13/16	4
4	* XMT TRIG 15/16	13 14	XMT TRIG 15/16	4
3	XMT TRIG 11/12	15 16	* XMT TRIG 11/12	3
5	NOT USED	17 18	NOT USED	5
5	NOT USED	19 20	NOT USED	5
5	NOT USED	21 22	NOT USED	5
5	NOT USED	23 24	NOT USED	5
5	NOT USED	25 26	NOT USED	5
5	NOT USED	27 28	NOT USED	5
5	NOT USED	29 30	NOT USED	5
5	NOT USED	31 32	NOT USED	5
5	NOT USED	33 34	NOT USED	5
5	NOT USED	35 36	NOT USED	5
5	NOT USED	37 38	NOT USED	5
5	NOT USED	39 40	NOT USED	5

②

## TABLE B

CONNECTOR J2 CROSS REF. DATA

REF SMT	DESCRIPTION	CONN J2	DESCRIPTION	REF SMT
5	+VCC IN	1 2	+VCC IN	5
5	NOT USED	3 4	+VCC IN	5
1	ARΦ	5 6	NOT USED	5
1	AXΦ	7 8	ARI	1
2	BRΦ	9 10	AXI	1
2	BXI	11 12	BRI	2
3	CXI	13 14	BXΦ	2
3	CRΦ	15 16	CXΦ	3
4	DXI	17 18	CRI	3
4	DRI	19 20	DXΦ	4
5	-15VDC IN	21 22	DRΦ	4
5	-15VDC IN	23 24	(16) GND IN	5
5	-15VDC IN	25 26	(16) GND IN	5
5	-15VDC IN	27 28	(16) GND IN	5
5	+15VDC IN	29 30	+5VDC IN	5
5	+15VDC IN	31 32	+5VDC IN	5
5	+15VDC IN	33 34	+5VDC IN	5
5	+15VDC IN	35 36	+5VDC IN	5
5	(26) HYBRID GND	37 38	(26) HYBRID GND	5
5	(26) HYBRID GND	39 40	(26) HYBRID GND	5

③

## TABLE C

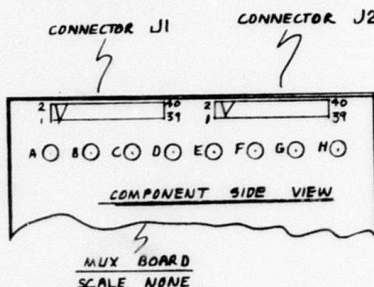
CROSS REF OUTPUT SIGNAL CONNECTORS

CONN	REF SMT	REF VID #	XDCR ELEMENTS	FROM RESPECTIVE HYBRID	CKT #
A	1	1/2	1-17-33-49	H16-H15-H14-H13	CKT1
B	1	3/4	3-19-35-51	H16-H15-H14-H13	CKT2
C	2	5/8	5-21-37-53	H12-H11-H10-H9	CKT1
D	2	7/8	7-23-39-55	H12-H11-H10-H9	CKT2
E	3	9/10	9-25-41-57	H8-H7-H6-H5	CKT1
F	3	11/12	11-27-43-59	H8-H7-H6-H5	CKT2
G	4	13/14	13-29-45-61	H4-H3-H2-H1	CKT1
H	4	15/16	15-31-47-63	H4-H3-H2-H1	CKT2

ALL SIGNAL OUTPUTS ON 75 OHM COAX.  
XDCR ELEM SHOWN FOR ODD BRD, A3;  
BRD A2 CONNECTS SIMILAR EVEN ELEM.

④

LOCATION OF CONNECTORS J1 & J2  
AND 75 OHM COAX OUTPUT CONNECTORS



⑤

CROSS REFERENCE TABLE CAPACITORS, RESISTORS,  
HYBRIDS, CHIPS

HYBRIDS	REF SMT	CHIPS	TYPE	REF SMT	R VALUE	REF SMT	C VALUE	REF SMT
H1	4	U1	74LS139	4	1	91Ω	4	1
H2	4	U2	74LS139	4	2	↑	4	2
H3	4	U3	MUX DB	4	3	↑	4	3
H4	4	U4	MUX DB	4	4	↑	4	4
H5	3	U5	LH0002	4	5	↑	4	5
H6	3	U6	LH0002	4	6	↑	4	6
H7	3	U7	74LS139	3	7	↑	4	7
H8	3	U8	74LS139	3	8	↑	4	8
H9	2	U9	MUX DB	3	9	↑	3	9
H10	2	U10	MUX DB	3	10	↑	3	10
H11	2	U11	LH0002	3	11	↑	3	11
H12	2	U12	LH0002	3	12	↑	3	12
H13	1	U13	74LS139	2	13	↑	3	13
H14	1	U14	74LS139	2	14	↑	3	14
H15	1	U15	MUX DB	2	15	↑	3	15
H16	1	U16	MUX DB	2	16	↑	3	16
		U17	LH0002	2	17	↑	2	17
		U18	LH0002	2	18	↑	2	18
		U19	74LS139	1	19	↑	2	19
		U20	74LS139	1	20	↑	2	20
		U21	MUX DB	1	21	↑	2	21
		U22	MUX DB	1	22	↑	2	22
		U23	LH0002	1	23	↑	2	23
		U24	LH0002	1	24	↑	2	24
		U25	Am26LS12	3-4	25	↑	1	25
		U26	Am26LS12	2-1	26	↑	1	26

CAPACITORS & RESISTORS CONTINUED

R VALUE	REF SMT	R VALUE	REF SMT	R VALUE	REF SMT	R VALUE	REF SMT
27 91Ω	1	45 1K 1%	2	63 120Ω	1	27 .10F	2
28 91Ω	1	46 100Ω 1%	2	64 120Ω	1	28 .10F	1
29 91Ω	1	47 62Ω	2	65 300Ω	4	29 .10F	4
30 91Ω	1	48 1K 1%	2	66 300Ω	4	30 .10F	4
31 91Ω	1	49 100Ω 1%	2	67 300Ω	3	31 .10F	4
32 91Ω	1	50 62Ω	2	68 300Ω	3	32 .10F	4
33 1K 1%	4	51 1K 1%	1	69 300Ω	2	33 .10F	3
34 100Ω 1%	4	52 100Ω 1%	1	70 300Ω	2	34 .10F	3
35 1K 1%	4	53 62Ω	1	71 300Ω	1	35 .10F	3
36 100Ω 1%	4	54 1K 1%	1	72 300Ω	1	36 .10F	3
37 62Ω	4	55 100Ω 1%	1			37 .10F	2
38 62Ω	4	56 62Ω	1			38 .10F	2
39 1K 1%	3	57 120Ω	4			39 .10F	2
40 100Ω 1%	3	58 120Ω	3			40 .10F	2
41 62Ω	3	59 120Ω	4			41 .10F	1
42 1K 1%	3	60 120Ω	3			42 .10F	1
43 100Ω 1%	3	61 120Ω	2			43 .10F	1
44 62Ω	3	62 120Ω	2			44 .10F	1

TITLE: MUX BOARD

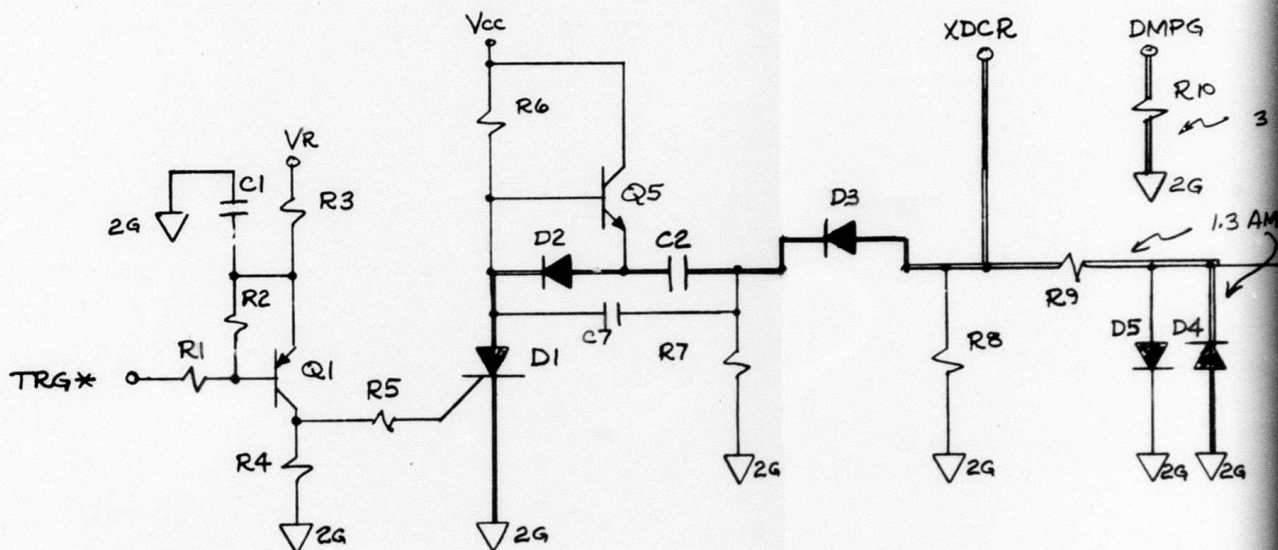
DRAWN WEP 2-77-81 J.C.

SHEET 5 OF 5

REV A, 11-11-81, 6X, NOMEN. UPDATE

DRAWING B-SHEET 5

EN \* 0



C 12-18-80 QBN ADD CB , NOTE 2.  
 B 2-18-80 QBN GENERAL NOTES.  
 A 10-1-79 QBN ORIGINAL.

REVISION STATUS:

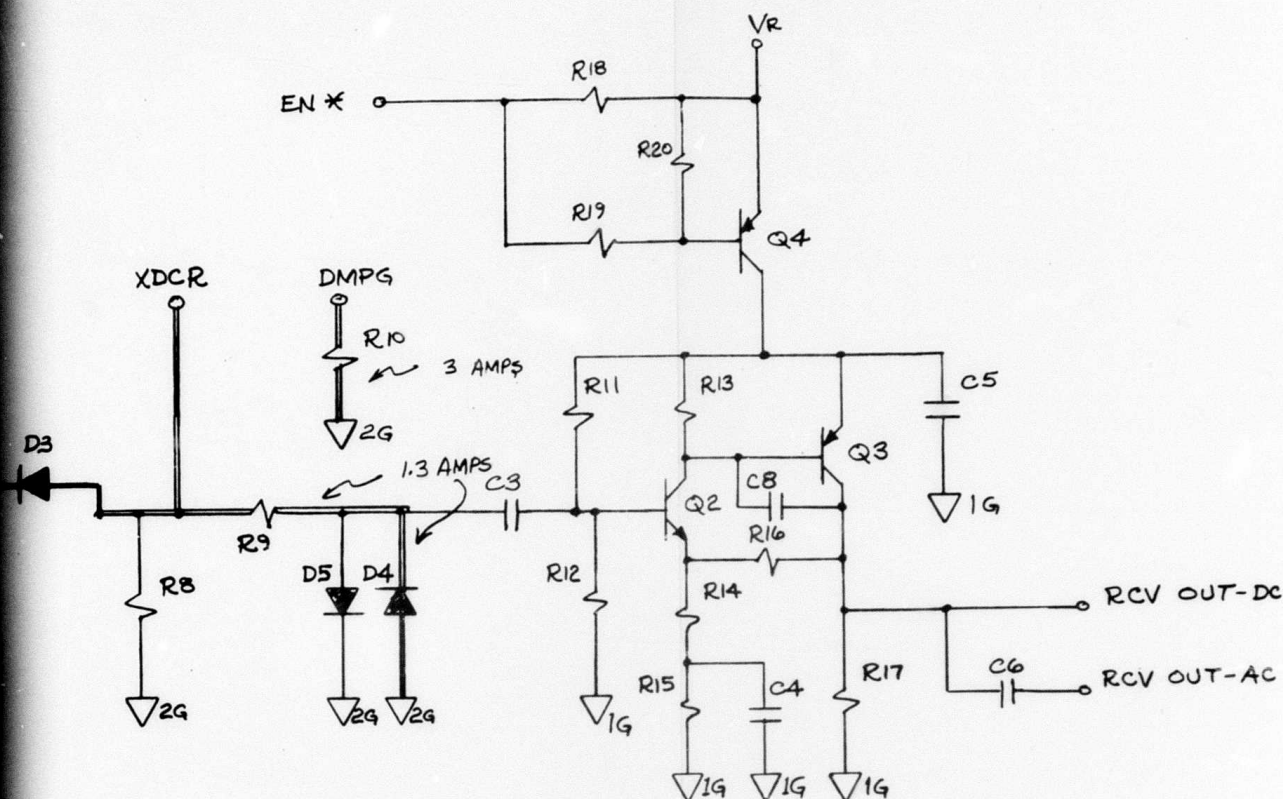
2. JUMP  
 NOTES: 1. DUAL L  
 CAPACIT

DRAWING B-7

NO.	NEXT ASSY
APPLICATION	
TOLERANCE: INCHES, DECIMAL .XX ± XXX ±	
✓ SURFACE ROUGHNESS	
UNLESS OTHERWISE	

B40/41





2. JUMPER CASE TO 1G AND 2G POSTS INTERNALLY.

NOTES: 1. DUAL LINE INTERCONNECTS ARE LOW IMPEDANCE CAPABLE OF 10 AMP PULSED, CAPACITOR DISCHARGE

DRAWING B-7

			CONTRACT NUMBER	TEST BED		
			DRAWN			
			DESIGN			
NO.	NEXT ASSY	USED ON	CHECK			
APPLICATION			ENGRG	GB Houston	10-1-79	PULSER - RECEIVER
TOLERANCE: INCHES, METRIC DECIMAL .XX ± XXX ±			MFG			HYBRID: PR-SCR40DV-1
✓ SURFACE ROUGHNESS			ANGLES	±	FINISH	SIZE C
UNLESS OTHERWISE NOTED:						REV. C
			SCALE	100%	WEIGHT	—
						SHEET 1 of 1

DRAWN BY: R.B. HOUSTON	10/2/79	TOLERANCES DECIMAL: XX = ± .010" XXX = ± .005" XXXX = ± .001" FRACTIONAL: ± 1/16" ANGULAR: ± 15'	# PR-SCR400 V-1
	CHECKED BY:		
PARTS LIST - PULSER RECEIVER	SCALE:	SHEET 2 OF 3	
	SURFACE: ☺		

DWG B-8 SHEET 1

COMMENTS

Q1	2N2907		
Q2	2N918		
Q3	2N4258		
Q4	2N2907		
Q5	UPTB540	400 V, UNITRODE	CHIP # UCT-0050, \$0.55 OR SIMILAR REPLACEMENT
D1	C106D	MOTOROLA SCR, 400 V	10 A PULSED, 500 NSEC
D2	1N5818	SBD, MOT.	10 A PULSED, 500 NSEC
D3	1N5818		10 A PULSED, 500 NSEC
D4	1N914		1.3 A PULSED, 500 NSEC
D5	1N914		
C1	0.01	μf, +/- 10%, 50 V	
C2	2000	pf, +/- 10%, 500 V	10 A PULSED (DISCHARGE)
C3	150	pf, +/- 5%, 50 V	
C4	0.033	μf, +/- 5%, 50 V	
C5	0.33	μf, +/- 20%, 50 V	
C6	3300	pf, +/- 20%, 50 V	
C7	100	pf, +/- 20%, 500 V	
C8	5.6	pf, +/- 5%, 50 V	

NOTES:

1. C2 STABLE OVER TEMPERATURE AND VOLTAGE. MUST BE LOW INDUCTANCE AND RESISTANCE.
2. D1 SCR HAS SPECIAL SPECIFICATION: IGT MAX = 200 μA, IGT MIN = 200 μA FOR TURN ON CONDITION.
3. SUBSTITUTION CRITERIA: Q5, 400 V; D2, D3, PULSED CURRENT CAPABILITY.



Science Center  
Rockwell International

DRAWN BY: R.B. HOUSTON  
CHECKED BY:

10/2/79

**TOLERANCES**

DECIMAL: XX =  $\pm .010$   
XXX =  $\pm .005$   
XXXX =  $\pm .001$   
FRACTIONAL:  $\pm \frac{1}{16}$   
ANGULAR:  $\pm 15'$

#

PR-SCR400V-1

**PARTS LIST - PULSER RECEIVER**

SCALE:

SURFACE:  $\sqrt{\text{ }}$

SHEET 3 OF 3

DWG B-8 SHEET 2

**COMMENTS**

R1	300 $\Omega$	5% , 1/8 W , 50 V	
R2	20 K $\Omega$	5% , 1/8 W , 50 V	
R3	750 $\Omega$	5% , 1/8 W , 50 V	
R4	150 $\Omega$	5% , 1/8 W , 50 V	
R5	12 $\Omega$	5% , 1/8 W , 50 V	
R6	1000 K $\Omega$	5% , 1/4 W , 500 V	
R7	1.8 K $\Omega$	5% , 1/2 W , 500 V	(300 V , 300 NSEC , T = 1 MSEC)
R8	1.8 K $\Omega$	5% , 1/2 W , 500 V	(300 V , 300 NSEC , T = 1 MSEC)
R9	300 $\Omega$	5% , 1/2 W , 500 V	(300 V , 300 NSEC , T = 1 MSEC)
R10	120 $\Omega$	5% , 1/2 W , 500 V	(300 V , 300 NSEC , T = 1 MSEC)
R11	5.1 K $\Omega$	2% , 1/8 W , 50 V	
R12	13 K $\Omega$	2% , 1/2 W , 50 V	
R13	470 $\Omega$	2% , 1/8 W , 50 V	
R14	15 $\Omega$	1% , 1/8 W , 50 V	
R15	1.2 K $\Omega$	2% , 1/8 W , 50 V	
R16	435 $\Omega$	1% , 1/8 W , 50 V	
R17	220 $\Omega$	2% , 1/8 W , 50 V	
R18	4.7 K $\Omega$	5% , 1/8 W , 50 V	
R19	4.7 K $\Omega$	5% , 1/8 W , 50 V	
R20	2.2 K $\Omega$	5% , 1/8 W , 50 V	

**NOTES:**

1. R7-R10 OPERATE IN A PULSED MODE. RESISTOR SPECIFICATIONS MUST BE COMPATIBLE WITH OVERSTRESSED CONDITION.
2. R14 AND R16 NEED TO TRACK; USE SAME MATERIAL, PLACE ADJACENT.